SYNTHESIS AND CHARACTERIZATION OF TiO$_2$ NANOCOMPOSITES VIA REVERSIBLE ADDITION FRAGMENTATION CHAIN-TRANSFER POLYMERIZATION

(Spine Title: Synthesis of TiO$_2$ nanocomposites via RAFT)

(Thesis format: Monograph)

by

Behnaz <u>Hojjati</u>

Graduate Program
in
Engineering Science
Department of Chemical and Biochemical Engineering

A thesis submitted in partial fulfillment
of the requirements for the degree of
Doctor of Philosophy

School of Graduate and Postdoctoral Studies
The University of Western Ontario
London, Ontario, Canada

THE UNIVERSITY OF WESTERN ONTARIO

SCHOOL OF GRADUATE AND POSTDOCTORAL STUDIES

CERTIFICATE OF EXAMINATIONS

Supervisor

_____
Prof. Paul A Charpentier

Supervisory Committee

_____
Prof. Sohrab Rohani

_____
Prof. Kibret Mequanint

Examiners

_____
 Prof. Michael K.C. Tam

_____
Prof. James A. Wisner

_____
Prof. Sohrab Rohani

_____
Prof. Madhumita Ray

The thesis by

Behnaz Hojjati

entitled:

Synthesis and Characterization of TiO_2 Nanocomposites via Reversible

Addition Fragmentation Chain-Transfer Polymerization

is accepted in partial fulfillment of the

requirements for the degree of

Doctor of Philosophy

Date _____   _____

Chair of Thesis Examination Board

ABSTRACT AND KEY WORDS

Polymer nanocomposites (PNCs) are materials composed of a polymeric host in which particles of nanoscale dimensions e.g. buckyballs, nanotubes, semiconductor of metallic nanocrystals, and clays are incorporated. PNCs, often termed organic-inorganic hybrids, are materials of rapidly growing interest to polymer scientists and engineers as they have properties of both the inorganic and organic components. PNCs are currently being used in a number of fields and new applications are continuously being developed including thin-film capacitors for computer chips, solid polymer electrolytes for batteries, biomaterials for bone cements and a variety of devices in solar and fuel cells.

Due to their small dimensions, nanoparticles tend to strongly agglomerate, hindering the physical and mechanical properties of the nanocomposite materials. In order to circumvent the inherent limitations associated with the agglomeration of nanoparticles in solution, the ultimate goal of this thesis is to develop an approach for growing polymer chains from the surfaces of inorganic oxides. In order to grow polymer chains, the living radical polymerization methodology, reversible addition fragmentation chain-transfer[1] was investigated. The kinetics of polymerization reactions, both in solution and in heterogeneous media was investigated. By synthesizing PNCs in organic solvents and in the green solvent, supercritical carbon dioxide ($scCO_2$), the kinetics were tested in various media. In addition, this thesis examined preparing new materials using the reversible addition fragmentation chain-transfer (RAFT) process, such as amphiphilic diblock copolymers used as templates to prepare mesoporous TiO_2.

For the methodology of growing polymers from inorganic surfaces, the inorganic oxide, titania, TiO_2 was focused on. As TiO_2 has an ability to coordinate with a

carboxylic group, in this research RAFT agents having an available carboxyl group were chosen to anchor onto TiO_2 nanoparticles and then grow chains of PAA, PMMA, and PMMA-b-PAA from these modified surfaces. The functionalization of n-TiO_2 was determined by FTIR, XPS, and partitioning studies, the livingness of the polymerization was verified using GPC and NMR, while the dispersion of the inorganic filler in the polymer was studied using electron microscopy and thermal analysis.

Methyl methacrylate was selected as the investigated monomer for the kinetic study of polymerization reactions, both in solution and in heterogeneous media. *In-situ* ATR-FTIR was employed to monitor the conversion of the monomer vs. time during polymerization. The monomer conversion and molecular weight kinetics were explored for the living RAFT polymerization, both in solution and grafted from n-TiO_2, with first-order kinetics being observed. It was found that increased graft density on n-TiO_2 led to a lower rate of polymerization, attributed to high localized concentration of RAFT agent.

The potential of supercritical carbon dioxide (scCO_2) as a green solvent was further examined to synthesize n-TiO_2/PMMA via the RAFT process and the rate of polymerization at different pressures and also in the organic solvent THF were compared. The rate of reaction in scCO_2 was found higher than that in the organic solvents.

Amphiphilic brush copolymers of PMMA-b-PAA were produced and used as a template to prepare mesoporous TiO_2. By using different chain lengths of the PAA block, the morphology of the resulting TiO_2 was investigated. These amphiphilic copolymer brushes were also grafted from n-TiO_2 to form NiO/TiO_2 particles; which can be used as nanocatalysts.

Key Words: nanocomposites, RAFT polymerization, TiO_2, grafting from, poly acrylic acid, poly methyl methacrylate, kinetics, rate of reaction, supercritical CO_2, amphiphilic copolymers, mesoporous TiO_2.

STATEMENT OF CO-AUTHORSHIP

Chapters 4, 5, 6, 7, and 8 encompass research studies that have been published or are in preparation for publication. Individual contributions of the author of each journal article are stated below.

Chapter 4: The original draft of this chapter was prepared by the author. It was reviewed by Prof. Paul A. Charpentier, who also provided a series of revision steps for improvement. The recommendations were incorporated into the chapter by the author. A version of this chapter has been published in the following journal:

- Behnaz Hojjati, Ruohong Sui., Paul A. Charpentie,. (2007), "Functionalization of TiO_2 Nanocomposites by Reversible Addition Fragmentation Chain-Transfer Polymerization." Polymer, 48, 5850-5858

The experimental work in Chapter 4 was achieved by co-operation with Dr. Ruohong Sui, a previous Ph.D. student in Prof. Charpentier's group in Chemical and Biochemical Engineering Department, the University of Western Ontario.

Chapter 5: The experimental work, analysis of data, and manuscript were prepared by the author. It was reviewed by Prof. Paul A. Charpentier, who also provided a series of revision steps for improvement. The recommendations were incorporated into the chapter by the author. A version of this chapter has been published by the following journal:

- Behnaz Hojjati, Paul A. Charpentier, (2008), "Synthesis and Kinetics of RAFT-Mediated Graft Polymerization of Methyl methacrylate on a Surface of n-TiO_2." Polymer Science Part A: Polymer Chemistry, 46, 3926-3937

Chapter 6: The original draft of this chapter was prepared by the author. It was reviewed by Prof. Paul A. Charpentier, who also provided a series of revision steps for improvement. The recommendations were incorporated into the chapter by the author. A version of this chapter has been published by the following journal:

- Behnaz Hojjati, Paul A. Charpentier, (2008) "Synthesis of TiO_2-Polymer Nano-Composite in Supercritical CO_2 via RAFT Polymerization" Submitted to Polymer Journal.

Chapter 7: The author conducted the experimental work, analyzed the data, and wrote the manuscript. Various drafts of the manuscript were reviewed by Prof. Paul A. Charpentier. This work was supervised by Prof. Paul A. Charpentier.

- Behnaz Hojjati, Paul A. Charpentier, (2009) "Synthesis of NiO/TiO_2 using Amphiphilic Diblock Copolymer brushes (PMMA-b-PAA) by RAFT Polymerization" Submitted to Langmuir Journal.

The experimental work in Chapter 7 was achieved by co-operation with Mr. Muhammad B. I. Chowdhury, a Ph.D. student in Prof. Charpentier's group in Chemical and Biochemical Engineering Department, the University of Western Ontario.

Chapter 8: The author conducted the experimental work, analyzed the data, and wrote the manuscript. Various drafts of the manuscript were reviewed by P. Charpentier. This work was supervised by P. Charpentier.

The experimental work in Chapter 8 was achieved by co-operation with Dr. Ruohong Sui, a previous Ph.D. student in Prof. Charpentier's group in Chemical and Biochemical Engineering Department, the University of Western Ontario.

To my husband, Hossein

for his love and encouragement

to my sons, Ali and Reza,

for their patience

and to my mom, brother, and sister

for their steady support

ACKNOLEDGMENT

CONTENTS

LIST OF TABLES

LIST OF FIGURES

xxv

LIST OF APPENDICES

LIST OF ABBREVIATIONS, SYMBOLS, NOMENCLATURE

Abbreviations:

AA   acrylic acid

Abs   absorbance

AIBN   2, 2′-azo Azobis (2-methylpropionitrile)

ATR-FTIR   attenuate total reflection fourier transform infrared spectroscopy

ATRP   atom transfer radical polymerization

BET   brunauer-emmett-teller

BHT   2, 6-di-tert-butyl-4-methylphenol

BJH   Barrett-Joyer-Halenda

CRP   controlled radical polymerization

DLS   dynamic light scattering

DMSO   dimethyl sulfoxide

DSC   differential scanning calorimeter

EDX   energy dispersive X-Ray spectroscopy

ESR   electron spin resonance

FRP   free radical polymerization

FTIR   fourier transform infrared spectroscopy

GPC   gel permeation chromatography

IR   infrared

LALS   low angle light scattering

MMA   methyl methacrylate

$Ni(NO_3)_2$ nickel nitrate

NMP	nitroxide mediated polymerization
NMR	nuclear magnetic resonance spectroscopy
Ni	nickel
NiO	nickel (II) oxide
$NiTiO_3$	nickel-titanium oxide
PPA	poly acrylic acid
PDI	polydispersity index = M_w/M_n
PI	polydispersity index in particle size distribution
PMMA	poly (methyl methacrylate)
RAFT	reversible addition fragmentation chain-transfer
RALS	right angle light scattering
$scCO_2$	supercritical carbon dioxide
SEC	size exclusion chromatography
SEM	scanning electron microscope
SFRP	stable free-radical polymerization
SiO_2	silica
TCD	thermal conductivity detector
TGA	thermogravimetric analysis
THF	tetrahydrofuran
TiO_2	titania
TTIP	titanium tetraisopropoxide
TPR	temperature program reduction
XRD	x-ray diffraction

Symbols:

A_2 second virial coefficient

C concentration ($mol \cdot L^{-1}$)

CTA chain transfer agent

d number of radicals formed from the initiator

D_{pore} adsorption average pore diameter (nm)

f initiator efficiency

E_b binding energy of the core electron

E_k kinetic energy of photoelectron

$h\nu$ photon energy (eV)

$[I]_0$ initial concentration of initiator ($mol \cdot L^{-1}$)

$[I]$ concentration of initiator ($mol \cdot L^{-1}$)

K optical constant

k_d decomposition rate constant (s^{-1})

k_p propagation rate constant ($mol \cdot L^{-1} \cdot s^{-1}$)

K_{ad} addition rate coefficients

K_β fragmentation rate coefficients

M monomer

$[M]_o$ initial concentration of monomer ($mol \cdot L^{-1}$)

$[M]$ concentration of monomer ($mol \cdot L^{-1}$)

M_n number average molecular weight (*g/mol*)

M_w weight average molecular weight (*g/mol*)

n	refractive index of a polymer solution
n_o	refractive index of a solvent
P	pressure
P_n	concentration of active growing polymer chains ($mol \cdot L^{-1}$)
P_θ	static structure factor
R	gas constant ($8.314\ J \cdot K^{-1} \cdot mol^{-1}$)
R_h	hydrodynamic radius
R_p	rate of reaction
R_θ	Raleigh ratio
S_{bet}	Brunauer-Emmett-Teller (BET) surface area
T	temperature ($^\circ C$ or K)
Tg	glass transition temperature ($^\circ C$)
V_h	hydrodynamic volume
Wt%	weight percent
x	conversion (%)

Greek letters:

μ	viscosity (cp)
τ	torque ($N \cdot M$)
$[\eta]$	intrinsic viscosity (dL/g)
θ	incident angle
n	layer of planes
λ	wave length (m)
ϕ	work function (eV)

CHAPTER 1

INTRODUCTION

1.1   Polymer Nanocomposites

Nanotechnology is the study of the science and technology of nanostructured materials at the dimensions from roughly 1 to 100 nanometers (10^{-9}). Due to their small dimensions, the physical properties of nano structured materials differ fundamentally from those of the corresponding bulk materials. One of the main reasons for using nanomaterials is the large surface to volume ratio. The resulting large surface area increases the number of particle-matrix interactions, thus increasing the effects on the overall material properties. These dispersed particle systems are mainly used to enhance or improve the properties of the composite material, such as conductivity, strength, energetics, wear resistance, and optical properties.[2]

Nanoscale metal oxides, such as TiO_2, SiO_2, are materials with high surface areas that exhibit exceptional chemical reactivity compared with commercial metal oxides. Metal oxide nanoparticles may potentially be inexpensive alternatives to carbon nanotubes with superior properties for many applications including catalysis, separation, gas storage, energy conversion, drug release, sensing and environmental protection, and biocompatible nanocomposites.[3-9] Among these, nanotitania (n-TiO_2) is of significant scientific and industrial interest for several applications, such as semiconductor electrodes in photo electrochemical cells,[10] photoconductive agents,[11] and photocatalysts.[12] As an example, TiO_2/polyelectrolyte composites such as TiO_2 /poly (ethyleneimine) /poly(acrylic acid) (PAA) are materials of interest for their potential application for the solid electrolytes in dye-sensitized solar cells.[13] TiO_2 powder is chemically inert, stable under sunlight, and is very opaque.[14]

2

However, there are several limitations for using these materials such as the difficult handling of these incredibly small objects (1-100 nm), which tend to agglomerate due to their high surface free energy. As shown in Figure 1.1, the attractive force between two particles is a function of the distance between them, where kT is the difference in energy of a solvent with particles compared with that in pure solvent, and f is the free energy per unit area. As the distance between the two particles decreases, the attraction force between them increases, which can result in agglomeration. Conversely, as the distance between the two particles increases, the particles experience lower and lower attraction for one another. Therefore, if the particles can be prevented from getting close enough to one another, agglomeration can effectively be prevented. The overall result is an energy barrier which must be overcome if the two particles are to agglomerate, as depicted by the solid line in Figure1.1.[15]
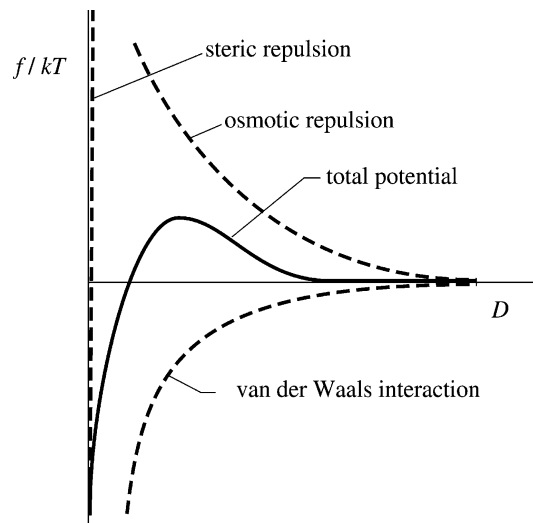
Figure 1. 1 Three interaction potentials acting on a particle in contact with a grafted layer (dashed lines) and the total interaction potential (solid line) as a function of the distance between them.[16]

Many efforts have been undertaken in order to overcome this aggregation problem and to enhance the filler-matrix interactions. One approach is breaking down the agglomerated nanoparticles using a mechanical method such as ultrasonic irradiation which has been used for dispersion of SiO_2, TiO_2, and Al_2O_3 nanoparticles during synthesizing inorganic/polymer nanocomposite materials.[17] However, this approach is restricted due to the limited interaction between the inorganic fillers and the organic matrix, compared with the very strong interaction between individual nanoparticles, as demonstrated by Figure 1.1.

An improved approach is modifying the surface of the inorganic filler and covalent attachment of stabilizing polymer ligands by either the "grafting from" or "grafting to" methods. The "grafting from" technique involves growing the polymer chains from the inorganic backbone, while the "grafting to" technique involves the attachment of preformed polymer chains to the backbone, minimizing agglomeration while strengthening the interaction between the nanofiller and polymer matrix, as illustrated schematically in Figure 1.2.[18, 19, 20]

Matrix Polymer

Nanoparticle

(a)

Grafting Polymer   Matrix Polymer

Nanoparticle

(b)
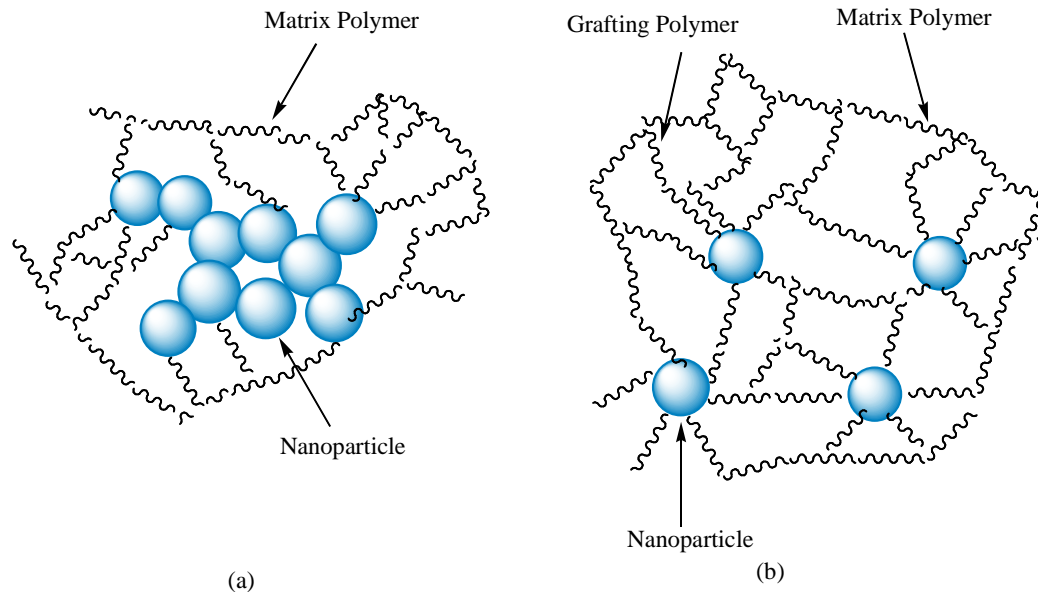
Figure 1. 2 Schematics of: (a) agglomerated nanoparticles in the matrix polymer in the case without grafting polymer and (b) separation of particles due to the grafting polymer.[19, 20]

The simplest method of grafting involves the chemical attachment of preformed polymer chains to the surface and is a common method for the creation of brushes,[21] self assembled monolayers,[22] and similar graft systems (Figure 1.3). This technique is based on the reaction of an appropriate polymer end group with an appropriate substrate such as carbon black, graphite, gold and silicon or reactive substrates as well as some polymeric substrates. Currently "click" chemistry is a popular approach to polymer chain attachment.[23]
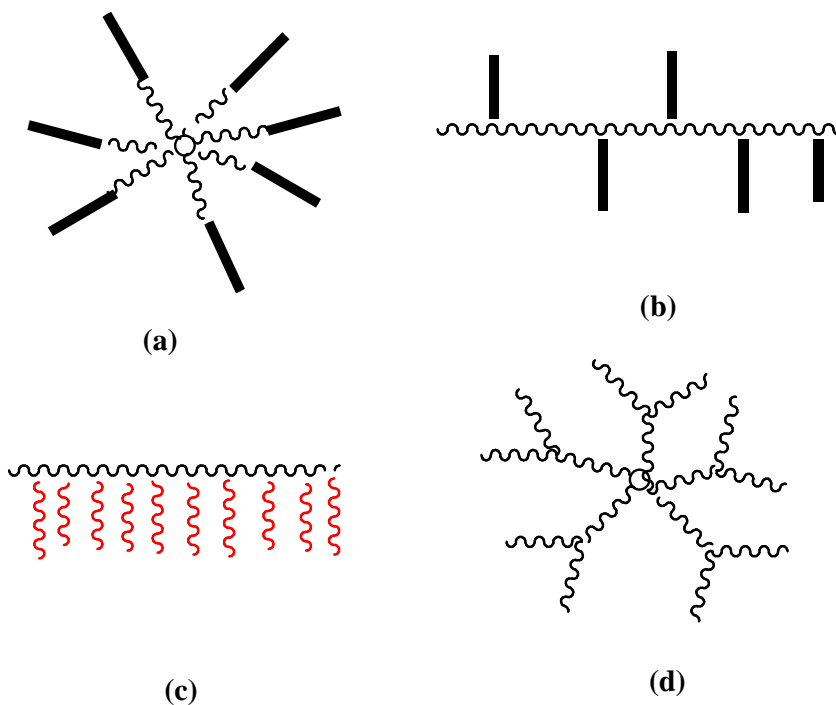
Figure 1. 3 Examples of branched polymers: (a) Star polymer, (b) Graft polymer, (c) Comb polymer, (d) Dendritic polymer.

In the "grafting to" method, the surface is first functionalized with an organic component, labeled "A" in Figure 1.4. Then, the polymer chains synthesized by any of a number of standard polymerization methods are grafted to the surface using one end group of the chain such as "B". Using this approach, the number of polymer chains that one can graft to the surface is generally small because the free volume occupied by each grafted chain acts as a barrier to the attachment of subsequent chains. This means that the "grafting to" approach is increasingly difficult as more chains are added to the surface, limiting the degree of control over the molecular weights and polydispersity.

Nanoparticle surface

A   A   A   A   A   A

A   A   A   A

B

A
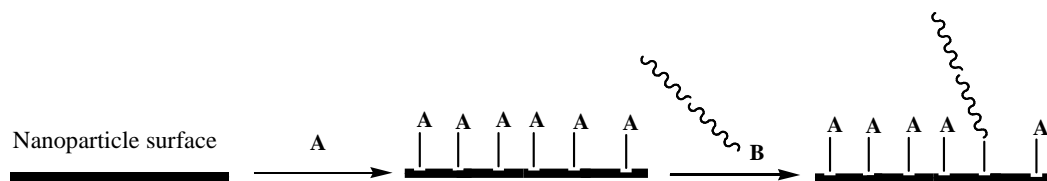
Figure 1. 4 Mechanism of "grafting to".

On the other hand, using the "grafting from" approach that uses initiators anchored to the surface, labeled "I", this approach allows chain growth from the surface of a substrate with the chains propagating outward into the solution (Figure 1.5). Low molar mass monomer molecules can easily diffuse to the surface, allowing chain growth to occur. As in solution or bulk polymerizations, the initiator is able to polymerize any of a broad array of vinyl monomers. Using the "grafting from" approach, the surface density can be controlled by varying the amount of initiator immobilized on the surface. For these reasons, "grafting from" has emerged in the literature as the most promising route to synthesize polymer brushes in a controlled manner, and is the general strategy utilized in this thesis.

I   I   I   I   I   I

I

Monomer

M   M   M   M

I   I   I   I   I

*
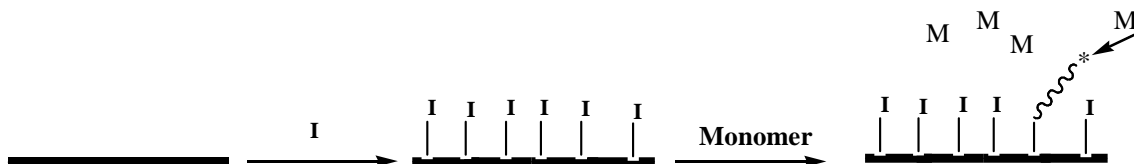
Figure 1. 5 Mechanism of "grafting from".

Very late in the twentieth century several new methods were discovered which allowed the development of living polymerization using free radical chemistry. Reversible addition fragmentation chain transfer (RAFT) technique is a new type of living radical polymerization which allows the synthesis of well-defined macromolecular architectures with relatively low polydispersity indices. RAFT polymerizations achieve

their controlled character due to a reversible chain transfer to reduce the amount of radicals and thus to reduce the occurrence of termination reactions. The main advantage of this controlled radical polymerization technique is its compatibility with a wide range of monomers. [24]

In the last decade, the synthesis of polymer nanocomposite materials has been intensely studied due to their extraordinary properties and wide-spread potential applications. A wide variety of polymers have been explored for the matrices of nanocomposites, while a diversity of crystalline materials, i.e., three-dimensional nano metal oxides,[25] two-dimensional layered silicates such as nanoclays,[26] and one-dimensional carbon nanotubes[27] have been used for reinforcement of the polymer matrices.[28,29]

The ultimate goal of this thesis is to develop a living radical polymerization methodology that can circumvent the inherent limitations associated with the agglomeration of nanoparticles in solution, and by doing so, to synthesize nanocomposites of controlled dimensions and properties. As well, in order to understand the role of the solvent and mechanism of polymerization, the kinetics of polymerization will be investigated, both in solution and in heterogeneous media. This knowledge will be used to synthesize block copolymers for use as templates to prepare novel mesoporous TiO_2 nanostructures.

To achieve these goals, the following specific objectives are sought in various chapters of the thesis:

- Chapter 1 : Introduction

This chapter provides an outline of the objectives and the layout of the thesis.

- Chapter 2: Theoretical background

    This chapter presents a general review of living radical polymerization techniques and polymer nanocomposites.

- Chapter 3: Experimental and Characterization methods

    In this chapter, the experimental setup and the major characterization methods employed in this research are introduced.

- Chapter 4: Synthesis of n-TiO$_2$/PAA Nanocomposite by RAFT Polymerization

    In this chapter, a new method for synthesizing n-TiO$_2$/polymer nanocomposites is presented with a good dispersion of the nanofillers by using the bifunctional RAFT agent, 2-{[(butylsulfanyl)carbonothioyl]sulfanyl}propanoic acid. This RAFT agent has an available carboxyl group to anchor onto TiO$_2$ nanoparticles, and an S=C (SC$_4$H$_9$) moiety for subsequent RAFT polymerization of acrylic acid (AA) to form n-TiO$_2$/PAA nanocomposites.

- Chapter 5: Synthesis and Kinetics of Graft Polymerization of Methyl methacrylate from the RAFT Coordinated Surface of n-TiO$_2$

    Polymer chains of PMMA are grown from n-TiO$_2$ by the RAFT polymerization process. The mechanism and kinetics of MMA polymerization from both solution and ''grafted from'' n-TiO$_2$ are studied in this chapter. The RAFT agent, 4-cyano-4-(dodecylsulfanylthiocarbonyl) sulfanyl pentanoic acid, with an available carboxyl group is used to anchor onto the n-TiO$_2$ surface, with the S=C (SC$_{12}$H$_{25}$) moiety used for subsequent RAFT polymerization of MMA to form n-TiO$_2$/PMMA nanocomposites. The monomer conversion and molecular weight kinetics are explored for the living RAFT

polymerization, both in solution and grafted from n-TiO_2, with first-order kinetics being observed.

- Chapter 6: Synthesis of n-TiO_2-Polymer Nanocomposite in Supercritical CO_2 via RAFT Polymerization

In this chapter, PMMA chains are grown from n-TiO_2 by the RAFT polymerization process using supercritical carbon dioxide (scCO_2) as a green solvent. The rates of polymerization at different pressures and also in organic solvent (THF) are compared.

- Chapter 7: Synthesis of NiO/TiO_2 using Amphiphilic Diblock Copolymer Brushes (PMMA-b-PAA) by RAFT Polymerization

In this chapter, amphiphilic diblock polymer brushes of PMMA-b-PAA are grown from n-TiO_2 by the RAFT polymerization process. In the nanocomposite, NiO particles are attached to the surface of TiO_2 nanoparticles using n-TiO_2/PMMA-b-PAA as PAA is hydrophilic allowing Ni^{2+} ions to be attached to TiO_2 nanocomposites. After removing the copolymer chains by heat treatment, NiO/TiO_2 still remains which can be used as a nanocatalyst.

- Chapter 8: Synthesis of Mesoporous TiO_2 using Amphiphilic Diblock Copolymer (PMMA-b-PAA) as a Self-Assembling Agent by RAFT Polymerization

The synthesis of mesoporous TiO_2 using a template method is presented in this chapter. Amphiphilic diblock copolymer (PMMA-b-PAA) produced via RAFT polymerization and titanium (IV) isopropoxide (TTIP) are used as the template and the

starting material, respectively. The effect of the chain length of PAA in the diblock copolymer template on the morphology of the mesoporous synthesized TiO_2 is studied.

- <u>Chapter 9: Summery and Conclusions</u>

This chapter provides a general conclusion of the above studies and recommendations for future work on the synthesis of the nanocomposites and mesoporous materials via the RAFT technique.

CHAPTER 2

THEORETICAL BACKGROUND

Polymer is a composite Greek word of ***poly*** and ***meros*** meaning "many parts". Polymers are generally considered to be substances containing a large number of structural units joined by the same type of covalent linkage. These substances often form into 1-dimensional chain-like structures. Natural polymers are found in many forms such as horns of animals, tortoise shells, rosin (from pine trees), and asphalt.[30] Man-made polymers have been studied since 1832, with the formation of vulcanized rubber. Today, the polymer industry has grown to be larger than the aluminum, copper and steel industries combined.[31] Polymers have found numerous applications as materials and plastics, in the construction, automobile, and packaging industries by virtue of their mechanical and thermal properties, their easy processability, and low cost.

Depending on the particular needs for a given application, new polymeric materials must satisfy certain requirements in terms of resistance to the environment, cost, and specific performance aspects, such as mechanical, optical, surface, electrical, and thermal properties. Therefore, increasingly demanding new technologies are requiring new polymerization tools to prepare advanced polymeric structures and architectures. Particularly, the ability to control the macromolecular architecture becomes increasingly important, by controlling the molar masses, polydispersities, tacticities, and terminal functional groups of the polymer.

One of the classifications of polymers is based on their polymerization mechanisms; step-growth (condensation) and chain-growth (free radical) polymerization. Chain-growth polymerization requires the presence of an initiating molecule, such as a free radical, that can be used to add a monomer molecule to form a growing polymer

chain. The generation of the radical usually takes place by the homolytic dissociation of a thermally unstable compound (azo-compound, peroxide, etc.).

Free radical polymerization (FRP) is one of the most widely used industrial processes for the commercial production of high molecular weight polymers because of its wide ranging applicability and versatility.[32] Firstly, it can polymerize a very wide range of monomers under a wide variety of experimental conditions compared to other chain growth polymerization techniques such as anionic or cationic polymerization. Secondly, it does not require expensive catalysts and operates at relatively mild conditions, such as near ambient temperatures, and because of the lack of highly active catalysts in the system, it is generally less sensitive to impurities and contaminants. It can either be performed in a homogeneous system, such as bulk or solution polymerization, or in a heterogeneous system such as emulsion or suspension polymerization.[33]

Free radical polymerization is a chain growth polymerization technique that can be roughly broken down into 4 steps: (Figure 2.1)

• Initiation: Radicals are formed.

• Propagation: The formed radicals react with the double bonds in the vinyl monomer effectively growing the polymer chains.

• Termination: The radical species are destroyed through various means to make dead polymer.

• Chain Transfer: The radical species is moved from one molecule to another without terminating the radical. In this way the active radical concentration remains constant, not affecting the rate of polymerization, R_p.

In FRP, the molecular weights of chains formed in the early stages of polymerization are relatively high, which subsequently decreases with increasing monomer conversion. FRP gives relatively broad polydispersity indexes (PDI= $M_w/M_n >$ 2, where M_w is the weight average molecular weight and M_n is the number average molecular weight). In addition, FRP techniques are limited in their ability to synthesize complex architecture polymers such as block copolymers, star copolymers or dendrimers.[32]

$$Monomer \xrightarrow{\text{Initiation}} P^{*}_{n} \xrightarrow{\text{Termination}} Polymer$$

$$k_p$$
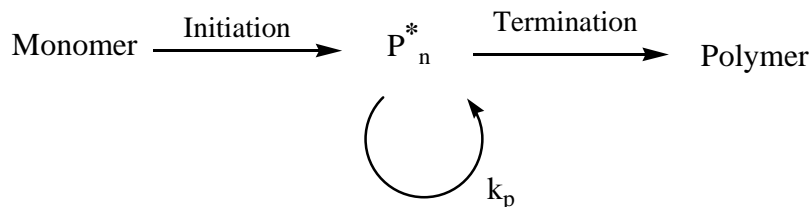
Figure 2.1 Conventional Free Radical Polymerization.[34]

Therefore, the academic and industrial interest for so-called living polymerizations has shown tremendous growth. The bimolecular termination step is the major limiting factor for the control of all chain polymerization techniques, which if it can be eliminated, would allow superior control of the polymerization system. The concept of living polymerization was first described in 1956 by Szwarc for producing low polydispersity index polymers.[35, 36] The original living polymerization system was used to produce rubber from styrene and 1,3- butadiene that is still used commercially today.[37] Living polymerization behavior has been defined as:[38]

 a) The polymerization proceeds to complete conversion, and further monomer addition leads to continued polymerization to produce homopolymers with longer chains, or when using a different monomer, block copolymers.

b) The number average molecular weight (M_n) directly increases with conversion/time.

c) The polydispersity of the molecular weight distribution is low (PDI~1.2).

d) Polymers with chain end functionality can be obtained quantitatively.

Ionic polymerization is the traditional example of a living polymerization process, which gives the possibility to synthesize complex macromolecular architectures in a controlled way. However, problems that have not been overcome with this technique include the relatively limited range of monomers that can be used, the extreme polymerization conditions that are required (often around -30°C or even lower), and the high sensitivity to impurities.[39]

In 1982, Otsu *et al.* extended the idea of living polymerization to the free radical system by combining advantages of both free radical and ionic polymerization techniques.[40] For a living polymerization, the termination reactions must be negligible compared with the propagation and activation/deactivation steps.[41, 42] On the other hand, the term "controlled" refers to whether the process can be used to synthesize well-defined architectures, such as block copolymers.[43]

In an ideal living polymerization, all chains are initiated at the beginning of the polymerization, grow at the same rate, and have no termination step. To confer living character on a radical polymerization, it is necessary to eliminate all processes that terminate chains irreversibly. Thus, living radical polymerization only becomes possible in the presence of reagents that react with the propagating radicals (P_n^*) by reversible deactivation (Figure 2.2) or reversible chain transfer (Figure 2.3) so that the majority of chains are maintained in a dormant form (P—X).

16

$$P^*_n \; + \; X^* \rightleftharpoons P_n{-}X$$
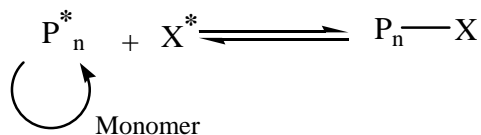
(Monomer)

Figure 2. 2 Reversible deactivation.[34]

$$P^*_n \; + \; P_m{-}X \rightleftharpoons P^*_m \; + \; P_n{-}X$$
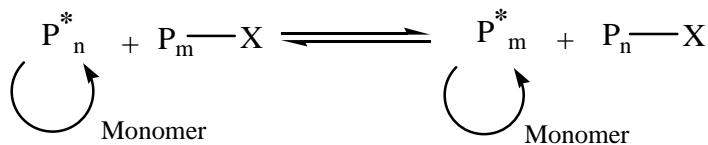
(Monomer) (Monomer)

Figure 2. 3 Reversible chain transfer.[34]

A rapid equilibrium between the active and dormant forms of the polymer chain ensures that all chains will grow until all monomer is consumed. Under these conditions, the molecular weight increases linearly with time (conversion) and the molecular weight distribution can be narrow (e.g. $M_w/M_n \sim 1.2$) (Figure 2.4).

(a)
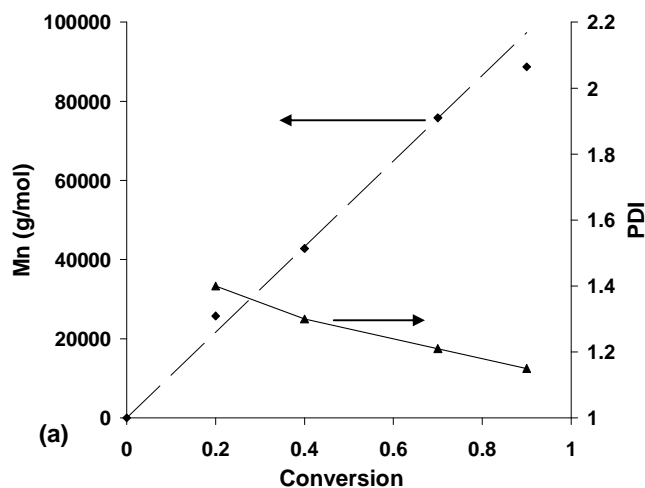
Figure 2. 4 Typical molecular weight and PDI vs. conversion for a living radical polymerization.[44]

As described above, living behavior is achieved by minimizing the normal bimolecular termination, and prolonging the lifetime of propagating radicals into hours or longer. This kind of polymerization has excellent commercial potential for material

synthesis as many more monomers undergo radical polymerization compared to ionic polymerization. In addition, living radical polymerization techniques are used to produce very well-defined polymers and also complex architectures and novel molecules. However, the kinetics of these systems are slow, and normally not known when grown from surfaces.

2.1.   Methods in Living Radical/Controlled Polymerization (LCP)

As mentioned above, living radical/controlled polymerization (LCP) is based on two principles: reversible deactivation (Figure 2.2), and reversible chain transfer (Figure 2.3).[34] The essence of this mechanism is that any radical species can be rapidly deactivated; maintaining a low radical concentration and thus limiting the bimolecular termination step which greatly affects normal free radical polymerizations.

Based on this principle, three controlled free radical polymerization techniques have been investigated:

a)   Stable Free-Radical Polymerization (SFRP)

a)   Atom Transfer Radical Polymerization (ATRP)

b)   Reversible Addition-Fragmentation Chain Transfer (RAFT)

SFRP and ATRP polymerization techniques control chain growth by reversible deactivation in which deactivation is provided by reversible group transfer with transition-metal complexes or coupling with aminoxyl radicals. The RAFT technique controls chain growth through reversible chain transfer. As the dormant species is a stable compound, it is a simple process to stop the polymerization and reinitiate it to produce block copolymers and other more complicated structures such as stars[45], combs[46] and graft[47] polymers (Figure 1.3). The three LCP techniques are briefly described below.

18

2.1.1. Stable Free-Radical Polymerization (SFRP)

In the 1990s the groups of Rizzardo and Georges reported a stable free radical polymerization process (SFRP) allowing the preparation of polystyrene with a narrow polydispersity.[48,49] Later, the polymerization of acrylates was catalyzed by cobalt porphyrin alkyls[50] and more recently a wide range of monomers were polymerized via the preparation of monomer specific initiators.[51] SFRP uses a stable radical to reversibly terminate the polymerization, thus limiting the radical concentration and the chance of non-reversible termination reactions (Figure 2.5). This reversible termination reaction allows the polymer chains to grow incrementally with conversion, producing a linear relationship between molecular weight and conversion as well as quite low polydispersity indexes (~1.5).

$$R^1 - ONR^2R^3 \rightleftharpoons R^1 \cdot + \cdot ONR^2R^3$$

$$\downarrow M$$

$$R^1M_n \cdot$$

$$\updownarrow \bullet ONR^2R^3$$

$$R^1M_n - ONR^2R^3$$
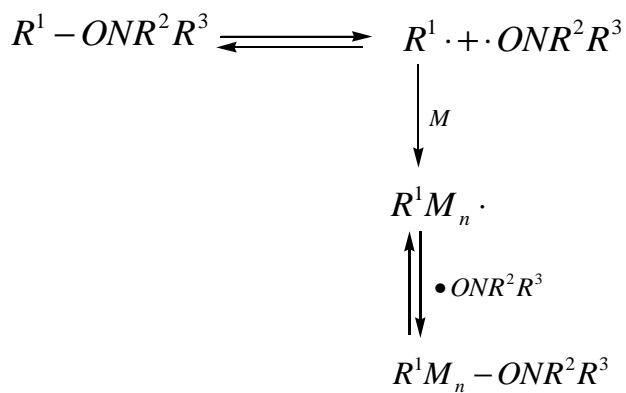
Figure 2. 5 SFRP polymerization mechanism.

SFRP requires high temperatures (125-140 °C) and relatively long reaction times (1-3 days). Only a few initiators are commercially available, which normally need to be synthesized. Various stable radicals such as nitroxide, triazolinyl, and dithiocarbomate have been used as the mediating agents for SFRP. Cyclic nitroxide radicals such as

2,2,6,6-tetramethyl-1-piperidinyloxy (TEMPO) has been studied for this technique (Figure 2.6). SFRP with nitroxides is called nitroxide mediated polymerization (NMP).
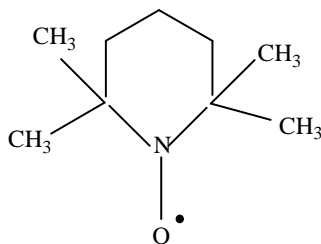
Figure 2. 6 Schematic of 2,2,6,6-tetramethyl-1-piperidinyloxy (TEMPO).

2.1.2. Atom Transfer Radical Polymerization (ATRP)

ATRP was originally reported by Matyjaszewski in the USA[52] and Sawamotob in Japan[53] almost simultaneously. It has been used to polymerize styrenic,[54] acrylamides, [54]acrylates, acrylonitrile, and diene monomers with controlled molecular weights and low polydispersities.[55] Radical generation in ATRP involves an organic halide undergoing a reversible redox process catalyzed by a transition metal compound, with Cu, Fe, and Ni commonly used as the catalysts. Activation of the initiator involves the CuBr metal center undergoing an electron transfer with simultaneous halogen atom abstraction and expansion of its coordination sphere (Figure 2.7). $R^\bullet$ is the reactive radical that initiates polymerization. $CuBr_2(L)$ is called the deactivator and is the persistent radical that reduces the steady-state concentration of propagating radicals and minimizes normal termination of living polymers.[56] In ATRP, radicals are generated by the redox reaction of alkyl halides (R-Br in Figure 2.7) with transition-metal complexes. Radicals can then propagate with monomer but are rapidly deactivated by the oxidized form of the transition-metal catalyst ($CuBr_2$ (L) in Figure 2.7).[57]

The main limitation of ATRP is the employment of a relatively high amount of transition metal complex (0.1-1% in the reaction mixture) that has to be removed from the final polymer.

$$R-Br+CuBr \xrightleftharpoons{\hspace{0.3cm}k_a\hspace{0.3cm}} R^{\bullet}+CuBr_2$$

$$\big\downarrow M$$

$$RM_n^{\bullet}$$

$$\updownarrow CuBr_2(L)$$

$$RM_n-Br+CuBr(L)$$
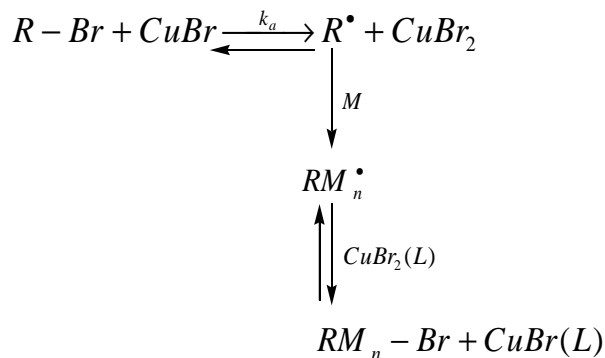
Figure 2.7 ATRP polymerization mechanism.

ATRP is reversible and lies fairly heavily on the dormant side (RM_n-Br), thus reducing the concentration of radicals and minimizing bimolecular termination. The advantage of ATRP is in its wide applicability for the production of advanced and novel polymeric structures.

2.1.3. Reversible Fragmentation Chain-Transfer Polymerization (RAFT)

Reversible Addition Fragmentation Chain Transfer Polymerization or RAFT is a recent living radical polymerization technique developed in Australia by Ezio Rizzardo's team at CSIRO in 1998.[58] In recent years, RAFT polymerization has emerged as a very attractive method of living free radical polymerization.[58,59] RAFT has been found to polymerize a wide range of monomers compared to ATRP and SFRP, including styrenic, acrylamides,[54] acrylates, acrylonitrile, vinyl acetates, vinyl formamide, vinyl chlorides as well as a range of other vinyl monomers,[60] and has been found to be highly versatile.[61]

RAFT has been shown to control molecular weight and molecular weight distributions, providing PDI's in the range of 1.03-1.25.[17] As mentioned above, in an ideal living radical polymerization, the molecular weight directly increases with monomer conversion/time.[62]

Another advantage of the RAFT process is that it can be carried out in the same conditions as a classical free radical polymerization, except for the addition of a chain transfer agent (CTA), which is also referred to as the RAFT agent. These RAFT agents include macromonomers,[63] allyl sulfides,[64] allyl bromides,[65] allyl peroxides,[66] and thionoesters.[67] As a result, RAFT polymerizations have been carried out in bulk, aqueous solutions,[68] organic solutions, suspensions, emulsions, mini and micro emulsions, and ionic liquids.[60] As mentioned in Ch.1, complex macromolecular architectures, (Figure 1.3), can be generated ranging from block to star copolymers by using the RAFT technique.[59, 69-71]

RAFT living polymerizations control chain growth through reversible chain transfer. The RAFT polymerization achieves "living" growth starting from the initial chain transfer agent, dithioesters or trithiocarbonates, which are activated by radicals generated from a traditional initiator (*e.g.* AIBN).[17] A chain-transfer agent such as cumyldithiobenzoate reversibly transfers a labile end group to a propagating chain (Figure 2.8). The R group initiates the growth of polymeric chains, while the Z group activates the thiocarbonyl bond toward radical addition and then stabilizes the resultant adduct radical.[60]
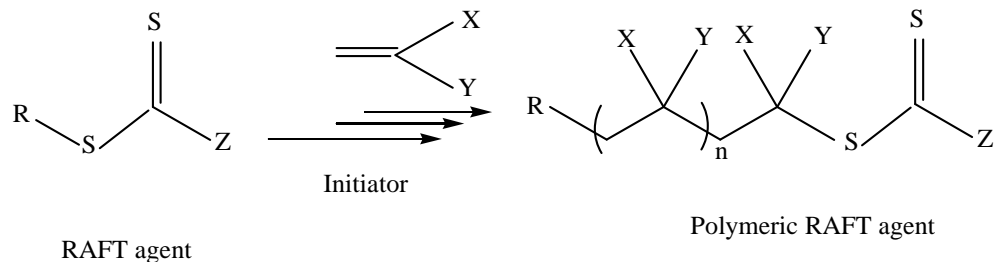
Figure 2.8 Overall reaction in RAFT polymerization. [34]

2.1.4. Mechanism of RAFT polymerization

The mechanism for achieving control in RAFT polymerization differs significantly from that involved in SFRP and ATRP, as they involve reversible deactivation of propagating radicals by radical—radical reaction (SFRP) or atom transfer (ATRP). In RAFT polymerization, the deactivation—activation equilibria are chain-transfer reactions, as described below. Radicals are neither formed nor destroyed in these steps, with an external source of free radicals required to initiate and maintain polymerization.[34]

The mechanism of RAFT polymerization was suggested by Vana[72](Figure 2.9). This kinetic scheme consists of the: (I) initiation processes, (II) pre-equilibrium involving the initial RAFT agent (CTA),[73] (III) propagation and re-initiation processes, (IV) core-equilibration (the core of the RAFT process), and (V) termination processes. In the early stages of the polymerization, the initiating radical is generated from degradation of an initiator species (I). These radicals then react with the RAFT agent (**1**) in a step of initialization (step II). If appropriately selected, all RAFT agents are consumed in this step before any propagation commences. This is due to the highly reactive C=S bond of the RAFT agent, which means that radical addition is favored over the addition to any of the double bonds that are present on the monomer.[60] The radical intermediate (**2**) can

23

fragment back to the original RAFT agent (**1**) and a polymer radical P_m^*, or fragment to a polymeric thiocarbonylthio compound ($P_mSC-(Z) =S$) (**3**) and a reinitiating R radical. The structure of R should be such that it is a good reinitiating group, which can subsequently initiate the monomer.[73]After re-initiating the monomer, a new propagating radical (P_n^*) is produced that can be exchanged by P_m in the compound $P_mSC-(Z) = S$ to produce a new polymeric thiocarbonylthio compound ($P_nSC (Z) =S$). Rapid equilibrium between P_m^* and P_n^* and compound (**3**) is the key to this living polymerization process, which allows all chains to grow at approximately the same rate, leading to a linear evolution of the molecular weight with conversion, and a low PDI. Some dead polymer chains will be formed via termination events in the reaction. This may occur through either a combination or disproportionation event depending on the monomer.

(I) Initiation

$$\text{Initiator} \longrightarrow \text{I}^* \xrightarrow{\ \text{M}\ } \xrightarrow{\ \text{M}\ } \text{P}^*_m$$

(II) Pre-Eqilibrium

(1)　　　　　　　(2)　　　　　　　(3)
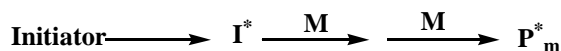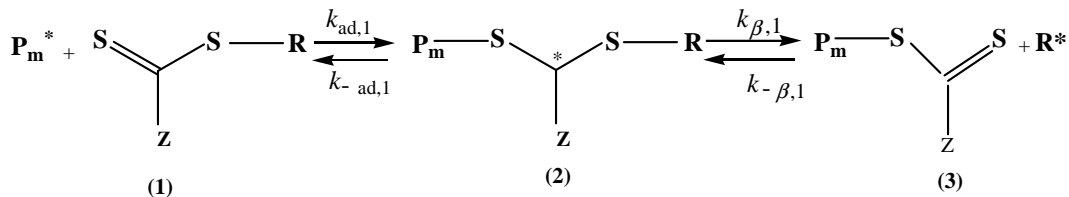
(III) Propogation

$$\text{R}^* \xrightarrow[k_i]{\text{Monomer}} \text{P}^*_n$$
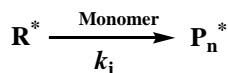
(IV) Core-Equilibrium

(3)　　　　　(4)

(V) Termination

$$\text{P}^*_n + \text{P}^*_m \longrightarrow \text{P}_{n+m}$$
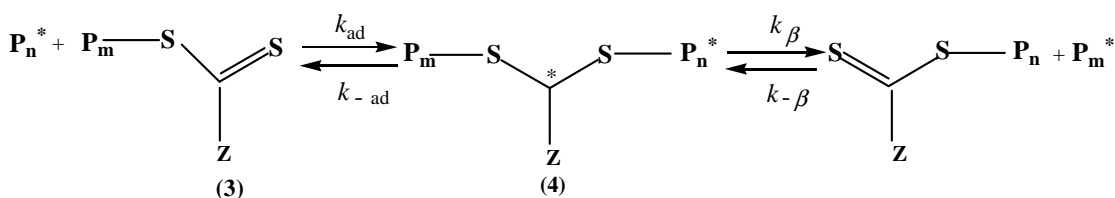
Figure 2.9 Mechanism of RAFT polymerization.[72]

2.1.5. Choice of RAFT Agents

The key that makes RAFT a living polymerization technique is the choice of the RAFT agent (CTA). For an efficient RAFT polymerization (Figure 2.9):[74]

• The initial RAFT agents (**1**) and the polymer RAFT agent (**3**) should have a reactive C=S double bond (high $k_{ad,1}$)

• The intermediate radicals (**2**) and (**4**) should fragment rapidly (weak S–R bond in intermediate) and give no side reactions.

• The intermediate (**2**) should partition in favour of products ($k_{\beta,1} \geq k_{-ad,1}$).

• The expelled radicals (R^*) must efficiently re-initiate polymerization.

The effectiveness of the RAFT agent depends on the monomer being polymerized and the properties of the free-radical leaving group R and the group Z, which can be chosen to activate or deactivate the reactivity of the C=S bond towards addition (Figure 2.10).[74]
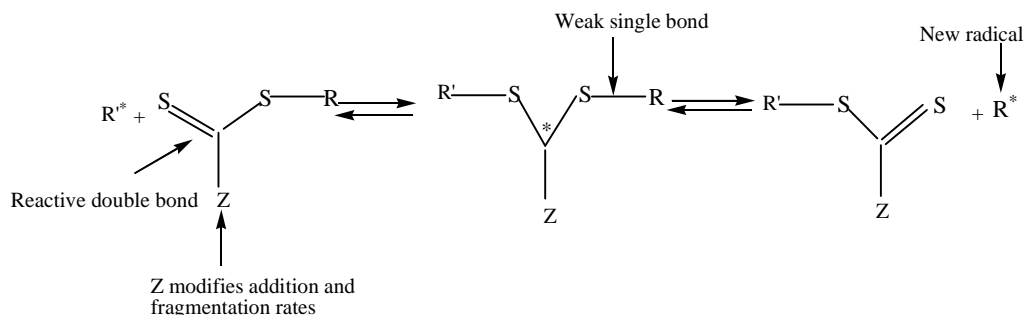
Figure 2. 10 Schematic of general RAFT polymerization.

A wide variety of RAFT agents with different Z and R groups have been synthesized and evaluated for their effectiveness in controlling the polymerization of vinyl monomers which are most commonly dithioesters such as benzyl phenylethane (dithioate), or trithiocarbonates such as (2-{[(butylsulfanyl) carbonothioyl] sulfanyl}-propanoic acid) (Figure 2.11).[58, 71]
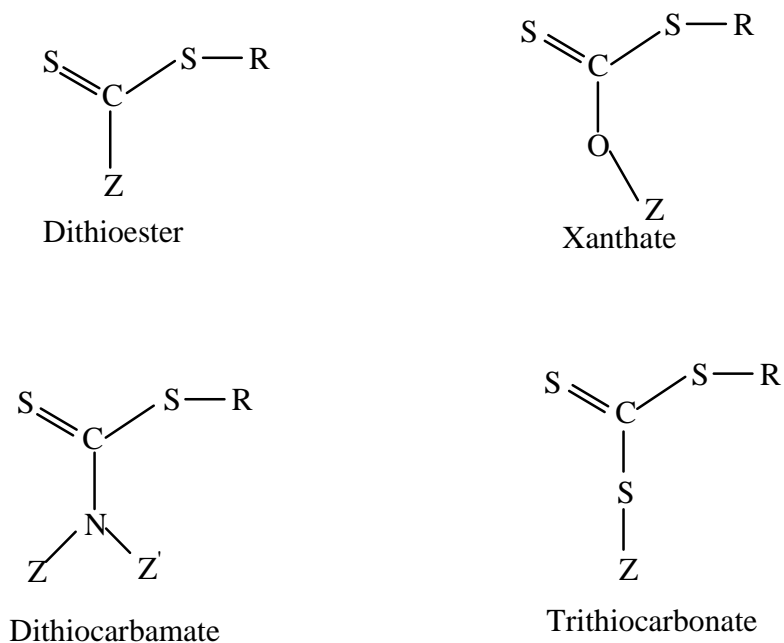
Figure 2. 11 Structure of different classes of reagents currently used as RAFT agents.

The Z group is the functional group that remains attached to the RAFT agent throughout the polymerization, and acts to stabilize the radical intermediates. This group should be chosen so that it will activate the C=S bond toward radical addition and then impart minimal stabilization of the adduct radical formed. For example, the rate of activation is higher when Z = aryl, alkyl (dithioesters), or S-alkyl (trithiocarbonates), and lower when Z = *O*-alkyl (xanthates) or *N,N*-dialkyl (dithiocarbamates). This is due to the interaction between O or N lone pairs and the C=S double bond, resulting in delocalization of this bond; the phenomenon in which electrons in some molecules are not fixed to specific atoms or bonds but are spread out over several atoms or bonds (Figure 2.12).[74]
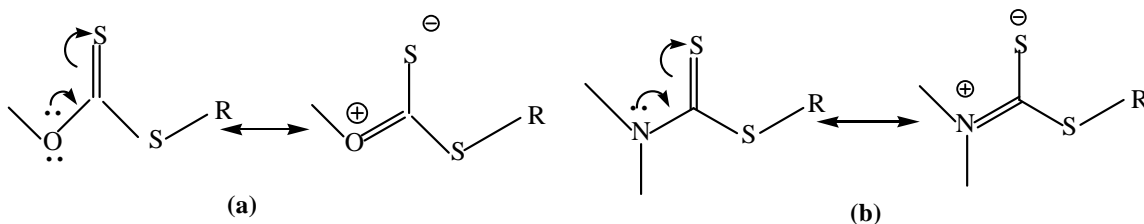
Figure 2. 12 Canonical form of (a) xanthates and (b) dithiocarbamates.

The R group or leaving group departs from the RAFT agent during the fragmentation step to re-initiate polymer chains, and also must form a stable free radical. Steric factors, radical stability, and polar effects are significant in determining the leaving/reinitiating ability of the R group.[75] Increased radical stability enables the R group to be a good leaving group; however, if the radical is too stabilized, it may not effectively add monomer and reinitiate polymerization. Increased steric bulk is likely to increase the leaving groups ability, but is also likely to have a detrimental effect on the reinitiating capability due to steric hindrance. Electron withdrawing substituents within the R group affect the electrophilicity of the derived radical. For example, the RAFT agent where R = CH$_2$Ph (e.g. benzyl dithiobenzoate) functions as a suitable chain-transfer agent in polymerization with styryl and acrylyl propagating radicals, but not in those with methacrylyl propagating radicals. This can be explained as the benzyl radical is a reasonable leaving group with respect to the styryl and acrylyl propagating radicals, but is a poor leaving group with respect to the methacrylyl propagating radical.[74] The ability of the homolytic leaving group R is tertiary>> secondary> primary (Figure 2.13).[76]

Tertiary   >>   secondary   >   primary
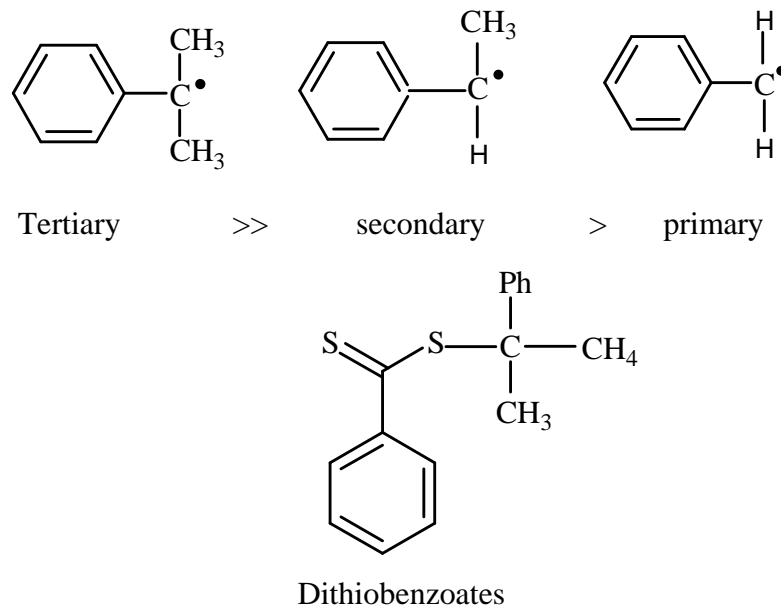
Dithiobenzoates

Figure 2. 13 Structure of some R groups and Dithiobenzoates.

Rizzardo et al. suggested guidelines based on the monomer structure, leaving group R, and group Z in RSC-(Z) =S (Figure 2.14).[34] For Z, the addition rate decreases and the fragmentation rates increase from left to right. In general, the stability of Z group of the RAFT agents decreases in the order dithiobenzoates > trithiocarbonates ~ dithioalkanoates > dithiocarbonates (xanthates) > dithiocarbamates which that can be attributed to the electron-withdrawing Z substituents. However, the RAFT agents with electrophilic Z substituent with lone pairs directly conjugated to the C=S double bond (O-, N-) have low stability (Figure 2.14).[58] For R, the fragmentation rates decreases from left to right. Dashed lines in the below figure indicates partial control of molecular weight but poor polydispersity.

R:

CN ~ Ph >> CO$_2$R >> alkyl

Chain length n > 2 >> 1 (strong penultimate unit effect)

Z:

Ph >> SCH$_3$ ~ CH$_3$ ~ [pyrrole] >> [pyrrolidinone] > OPh ~ OEt ~ N(Ph)(CH$_3$) > N(Et)$_2$

← MMA →

← VAc →

← S,MA,AM,AN →
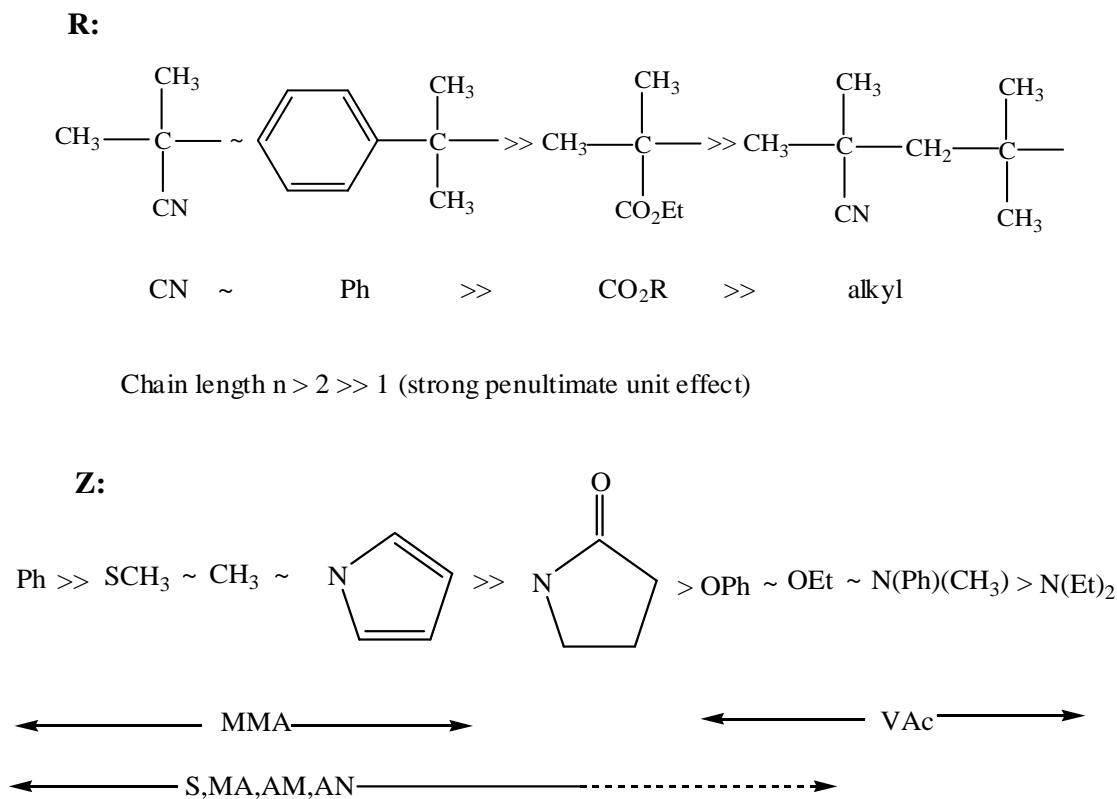
Figure 2. 14 Guideline for selection of RAFT agents.[34]

2.1.6. Side reactions in RAFT polymerization

In many RAFT polymerizations, an inhibition period is obtained where no polymerization activity is observed in the initial phase of the polymerization.[77] As well, rate retardation may occur i.e. where R_p decreases slightly with increasing concentration of the RAFT agent.[62] It has been found that the stability and thus the average lifetime of the intermediate RAFT radicals (**2**) and (**4**) (Figure 2.9) are of key importance for rate retardation and inhibition effects in RAFT polymerization. It was observed that when using polymeric RAFT agents (**3**) in RAFT polymerization, that an inhibition period did not occur, which means that inhibition effects can be attributed to the individual reactions of the pre-equilibrium.[78] On the other hand, rate retardation may either be explained by

slow fragmentation of the intermediate radicals (**2**, **4**), or by additional side reactions, such as cross-termination; irreversible termination reactions of the intermediate RAFT radical (**2**), (**4**) with growing macroradicals, P_m^* (Figure 2.15a-b) [62] or self-termination; irreversible termination of the intermediate RAFT radical (**4**) with itself (Figure 2.15c).[79]
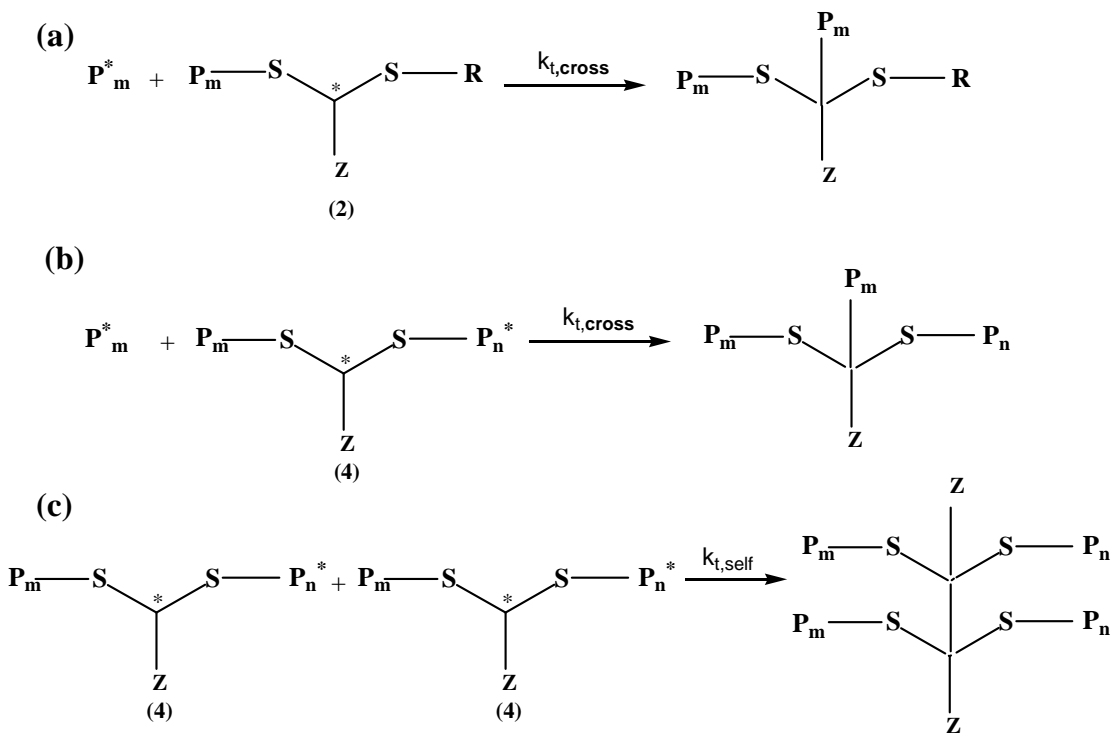
Figure 2. 15 Schematic of (a) cross-termination between propagating and intermediate radicals of the pre-equilibrium, (b) the core-equilibrium, and (c) self-termination reaction between intermediate radicals of the core-equilibrium.

2.1.7. Block Copolymerization

When two different types of monomers are joined in the same polymer chain, the polymer is called a copolymer. Copolymers can be classified based on how these units are arranged along the chain.

Alternating copolymers $\longrightarrow$ -A-B-A-B-A-B-A-B-A-B-

Random copolymers $\longrightarrow$ -A-A-B-B-B-A-B-A-A-B-B-A

Block copolymers ⟶ -A-A-A-A-A-A-A-B-B-B-B-B-B-
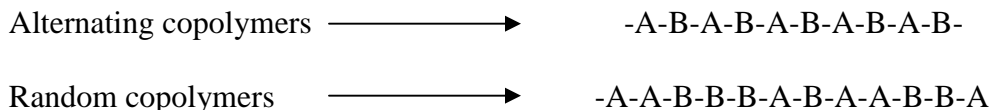
Block copolymers are polymeric materials consisting of sequences or blocks of identical repeating units. Block copolymers with their unique properties, are not only of tremendous academic importance but also of commercial interest. The applications of block copolymers range from surfactants, dispersants, coatings, and adhesives to materials for pharmaceuticals and microelectronics.[80] The linear AB block copolymer is the simplest block copolymer structure where two blocks of different chemical structures are linked together through a common junction point. In this method, the first monomer is polymerized and after its complete consumption, the second monomer is added and the polymerization is allowed to proceed to completion.

It is generally impossible to produce block copolymers by free radical polymerization. Therefore, living radical polymerization is used to synthesize block copolymers of desired chemical composition and molar mass, with a narrow PDI. This technique allows the preparation of functional polymers with pre-determined molecular weight and complex structures, such as block, graft, and star polymers.[81]

Living radical/controlled polymerization (LCP) techniques have been used for the synthesis of block copolymers. As examples, Hua *et al.* synthesized poly (ethylene oxide-*b*-styrene) via SFRP,[82] while Sun *et al.* synthesized poly (ethylene oxide-*b*-methyl methacrylate) via ATRP.[83] Chen *et al.* copolymerized *N*-(2-Acetoxyethyl)maleimide (AEMI) with styrene via ATRP,[84] while styrene was copolymerized with maleimide via SFRP by Cianga *et al.*[85]

However, the RAFT polymerization technique is recognized as one of the most versatile methods for block copolymer synthesis.[34,86] The obtained polymer initially

32

polymerized (monomer A) in the presence of RAFT agent, consists of polymer chains with the RAFT end group attached to its end. (Figure 2.16)[34]
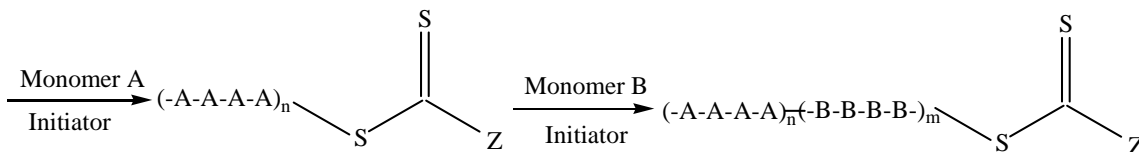
Figure 2. 16 Schematic of linear diblock copolymerization via RAFT.

This RAFT-functional polymer can further act as a polymeric RAFT agent (referred to as macro-CTA) in the presence of a desired monomer.[87] A fresh amount of initiator can be added to reinitiate the polymerization, leading to block copolymer formation. As shown in Figure 2.16, the second monomer is inserted between the thiocarbonyl thio (S(S)C) moiety, and the last inserted monomer of the first block, while the RAFT-functionality remains at the block copolymer chain end during polymerization. Potentially, this RAFT functionality can be used for attachment of the block copolymer to surfaces.

In RAFT block copolymerization, the order of monomer addition is critical.[34] It is important that the starting block acts as a better leaving group than the block formed in the second step.[71, 88] For example, in the synthesis of poly(methacrylate-styrene) diblock, the methacrylate block should be prepared first. The styrene propagating radicals are very poor leaving groups compared to methacrylate propagating radicals.[89] Using this technique, synthesis of AB, ABC, etc blocks are possible.

Among the block copolymers, there has been great interest in amphiphilic block copolymers in academic and industrial research in the past decade. Amphiphilic block copolymers consist of at least one hydrophilic and one hydrophobic polymer chain which

are covalently linked.[90] Amphiphilic block copolymers can self-assemble into a large variety of micro and nano structures in selective solvents that are good for one block and poor for the other block (Figure 2.17).[91,92,93]
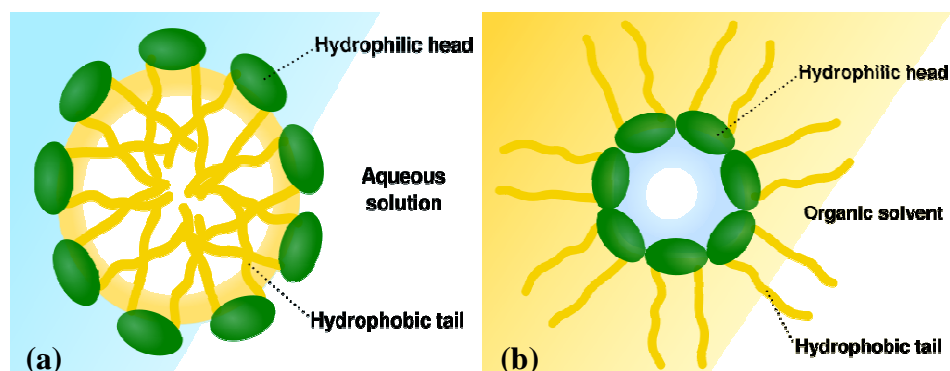
Figure 2. 17 Scheme of a micelle formed by an amphiphilic copolymer in (a) aqueous solvent, (b) organic solvent. [93]

Amphiphilic copolymers find applications in various industrial fields, such as detergents, personal care, paints, pharmaceuticals, oil recovery, environmental protection, agrochemicals, food industry, etc.

2.1.8. Block Copolymer Self-Assembly

Self-assembly is a supramolecular approach which relies on complementary non-covalent interactions, such as electrostatic interactions, hydrogen bonds, van der Waals forces, coordination interactions and solvophobic effects. In self-assembled structures, these temporary intermolecular forces connect the molecular scale building blocks in a reversible, controllable and specific way.[94]

The microphase separation which occurs in block copolymers upon self-assembly is mainly due to the chemical incompatibilities between the different blocks forming the copolymer molecules. The blocks of amphiphilic copolymers tend to separate in order to

lower the enthalpy of mixing. As the blocks are covalently bonded to one another, the separation of blocks is restricted, giving rise to a variety of unique microstructures (Figure 2.18). The particular morphology is a function of the composition, interaction and molecular weights of the constituent blocks.
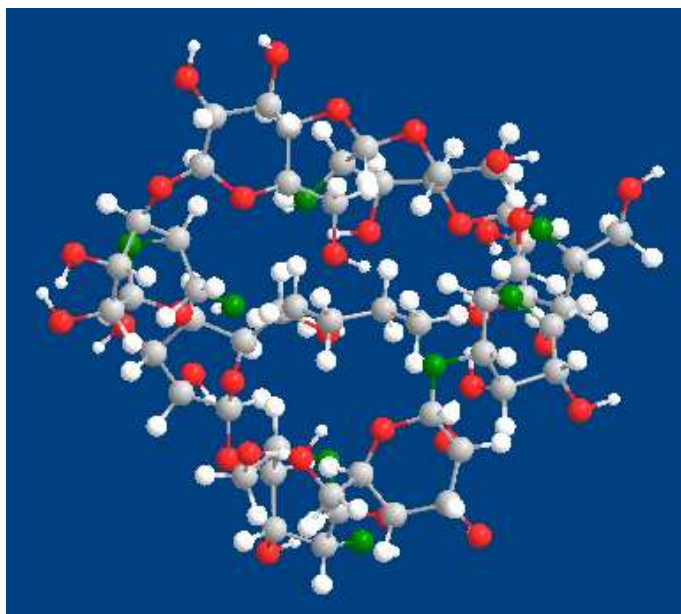
Figure 2. 18 Schematic of a supramolecular structure.

2.2. Surface Modification via Living Radical/Controlled Polymerization

Surface modification has seen rapid expansion over the past two decades, due to a surge in interest in nanotechnology, and because of the growth and development of reliable surface characterization techniques. The chemical modification technique, such as grafting of macromolecules onto a surface alters the physical behavior of the composite in the system to more desired properties for end-use applications.[95]

To minimize the agglomeration of the nanoparticles and to enhance the filler–matrix interactions, living techniques have been employed in which the grafting polymer chains separate and bridge the nanoparticles and entangle with the polymer matrix. In

35

order to have surface-initiating graft polymerization on nanomaterials, various polymers such as PS, PMMA, and PnBuA have been successfully grafted from nanoparticles via living/ radical controlled polymerization techniques.[19, 96, 97]

By applying ATRP, Ejaz *et al.*[98] grew polymer chains of methyl methacrylate from solid surfaces including silicon wafers, silica particles, and glass filters. Using RAFT polymerization, Baum *et al.* and Nguyen *et al.* [99, 100] polymerized St and MMA from silica nanoparticles, Hong *et al.* [101] and Cui *et al.* [102] functionalized multi-walled carbon nanotubes with poly(N-(2-hydroxypropyl)methacrylamide) and polystyrene, respectively, Chen *et al.*[103] grafted PMMA and poly(poly(ethylene glycol) monom-ethacrylate) (PPEGMA) from poly(vinylidene fluoride) (PVDF) surfaces, while Barner *et al* [104] grafted copolymerization of styrene and m-isopropenyl-α,α'-dimethylbenzyl isocyanate [105] from polypropylene (PP) by using γ-initiated RAFT polymerization. Core (polyvinyl neodecanoate-ethylene glycol dimethacrylate)-shell (polyvinyl alcohol) microspheres were developed by seeded polymerization with the use of conventional free radical and RAFT/MADIX mediated polymerization.[106]

Using RAFT to control grafting reactions adds some level of complexity to the polymerization kinetics and mechanism. In a radical polymerization mediated with either free RAFT agents or surface anchored RAFT agents, the chain propagation steps are almost unaffected by the immobilized RAFT agent on the surface. However, the chain transfer reactions are more complicated as the RAFT agent is distributed homogenously in solution polymerization, while in the case of being surface anchored, the local concentration of RAFT agent on the nanoparticle surfaces is very high due to immobilization of the RAFT agent. Once a radical in solution is transferred to the

36

nanoparticle surface via a chain transfer reaction, a new radical on the particle will be

created (Figure 2.19a), which can react either with a RAFT agent on another particle

surface or with a neighboring RAFT agent on the same particle surface (Figure 2.19b).

The first mode could be very slow as it requires interpenetration of the polymer chains on

the two particles which will incur a large barrier. Therefore, the radicals prefer to transfer

to a nearby RAFT agent rather than propagate, due to the high local RAFT agent

concentration, therefore leading to polymerization retardation.[107]

(a)   (b)
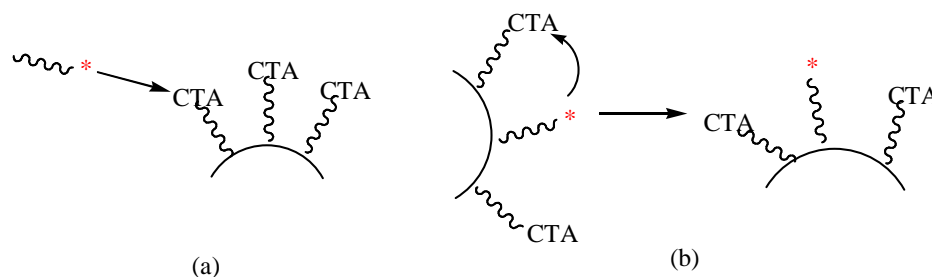
Figure 2. 19 Chain transfer reaction for the radicals (a) in solution and (b) on the particle surface.

CHAPTER 3

EXPERIMENTAL AND CHARACTERIZATION METHODS

In this chapter, the experimental setup characterization techniques and evaluation procedures used to analyze the synthesized materials followed for this thesis are described. The synthesis of the nanocomposites was carried out either in glassware reactors or using *in-situ* FT-IR. The glassware reactors were connected to N_2 or argon, while the high-pressure reactors were connected with CO_2, along with having temperature and pressure controllers.

Characterization methods of the synthesized materials include: gel permeation chromatography (GPC), *in-situ* attenuate total fourier transform infrared spectroscopy (ATR-FTIR), thermo gravimetric analysis (TGA), differential scanning calorimeter (DSC), transmission electron microscopy (TEM), and scanning electron microscopy (SEM).

3.1.   Gel Permeation Chromatography (GPC)

Gel Permeation Chromatography (GPC), also known as Size Exclusion Chromatography (SEC), is a popular analytical tool for characterizing natural and synthetic polymers and proteins. GPC is a chromatographic technique that employs specialized columns to separate natural and synthetic polymers on the basis of their size (Figure 3.1). The polymer solution is injected into a column which it is packed with porous particles of fairly defined pore sizes (*i.e.* glass beads or polymer gels) that are comparable to the size of the polymer molecules. The SEC mobile phase, *i.e.* the eluent, is generally the same solvent as used to dissolve the polymer. Furthermore, the eluent should be strong enough to prevent any adsorption of the polymer molecules on the stationary phase. As the polymer elutes through the column, the molecules that are too

large to penetrate into the pores of the column elute first, while smaller molecules can penetrate or diffuse into the larger pore volumes and elute at a later elution volume.

As the sample is separated and elutes from the GPC column, it can be characterized by a single or series of detectors. The GPC analysis depends on the number of detectors used in the experiment. The triple detector GPC system used for this thesis employs the following three kinds of detectors: refractive index (RI) detector (conventional calibration), viscometer detector (universal calibration), and light scattering detector (triple detector GPC).
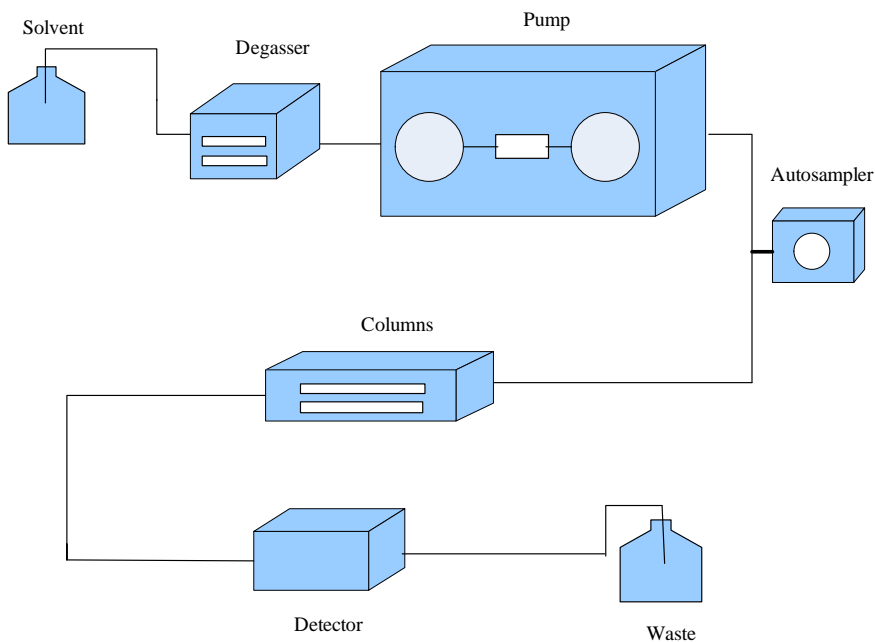
Figure 3. 1 Schematic diagram of GPC.

3.1.1. Refractive Index (RI) Detector

The RI detector is based on the deflection of a beam of the light as it passes through a dual compartment flow cell containing the reference solvent, with refractive index n_o in one part, while the solution sample, with refractive index n, in the other part.

The beam is refracted at the liquid-glass interfaces separating the two compartments (Figure 3.2). The area under the RI peak is proportional to $\frac{dn}{dc}$, the refractive index increment, and C, the concentration of the sample (Eq. 3.1).[108]

$$RI_{Area} \propto C \frac{dn}{dc} \qquad (3.1)$$

where:

$$\frac{dn}{dc} = \frac{n - n_0}{C} \qquad (3.2)$$
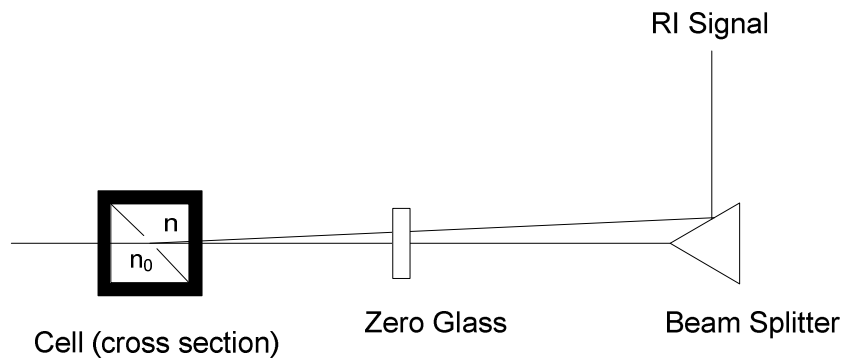
Figure 3. 2 Schematic of deflection type refractometer.

One of the applications of this detector is conventional calibration. The conventional method for calibration of the GPC columns uses commercially available polymer standards with low polydispersity indexes. The molecular weight is plotted versus the elution volume (Figure 3.3). The molecular weight of an unknown sample is then calculated by dividing the area below the curve in small fractions (slices) and projecting the retention volume of each slice on the calibration curve.

41
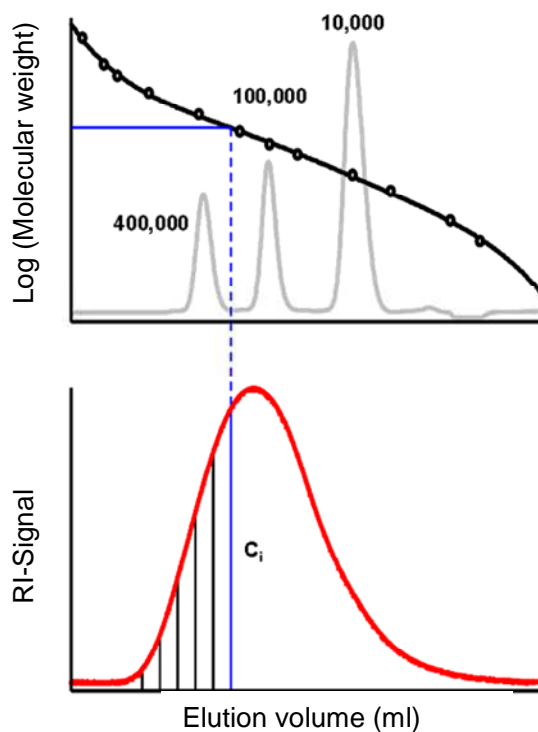
Figure 3. 3 Principle of conventional calibration.[108]

3.1.2. Viscometer Detector

The viscometer detector is based upon the measurement of a differential pressure between the pure solvent and the polymer solution. In the early 1980s, Max Haney proposed the Four-Capillary Bridge Viscometer (Figure 3.4).[108] Four capillary tubes R1–R4 with internal diameters of approximately 0.25 mm are arranged in a balanced bridge configuration. Differential pressure transducers measure the pressure difference DP across the midpoint of the bridge and the pressure difference IP from inlet to outlet. A delay volume is inserted in the circuit before capillary R4, in order to provide a reference flow of solvent through R4 during elution of the polymer sample.
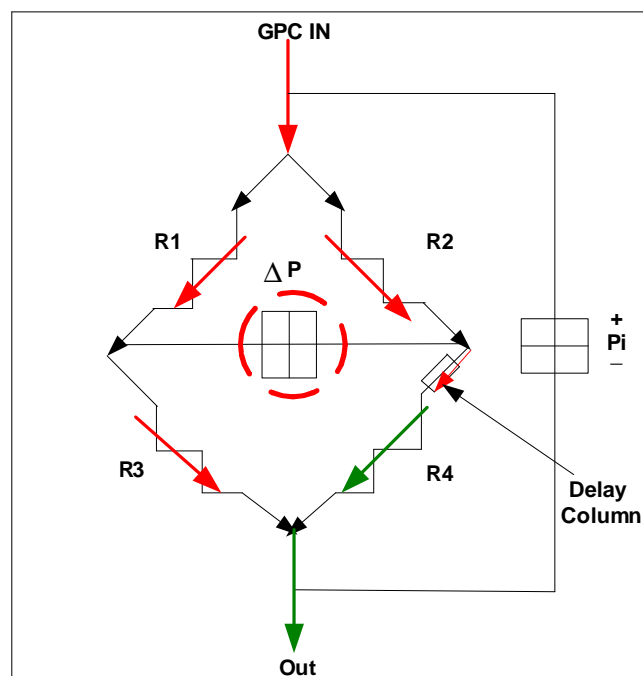
Figure 3. 4 Schematic of Differential Viscometer. [108]

For many polymers where narrow standards are not available, a standard calibration such as MMA or polystyrene can be used. It is then assumed that the calibration curve is universal and thus different polymers can be analyzed by using the intrinsic viscosity/molecular weight relationship referred to as the Mark-Houwink-Sakurada equation (Eq. 3.3)

$$[\eta] = K \cdot M_v{}^a \tag{3.3}$$

This equation relates the intrinsic viscosity $[\eta]$ to the molecular weight of the analyzed polymer through two constants, K and a, which are specific to a polymer-solvent system at a given temperature. Although this technique is widely used, it has been criticized for errors induced by the fact that the Mark-Houwink-Sakurada relationship is not strictly linear over a wide molecular weight range. (Figure 3.5)

43
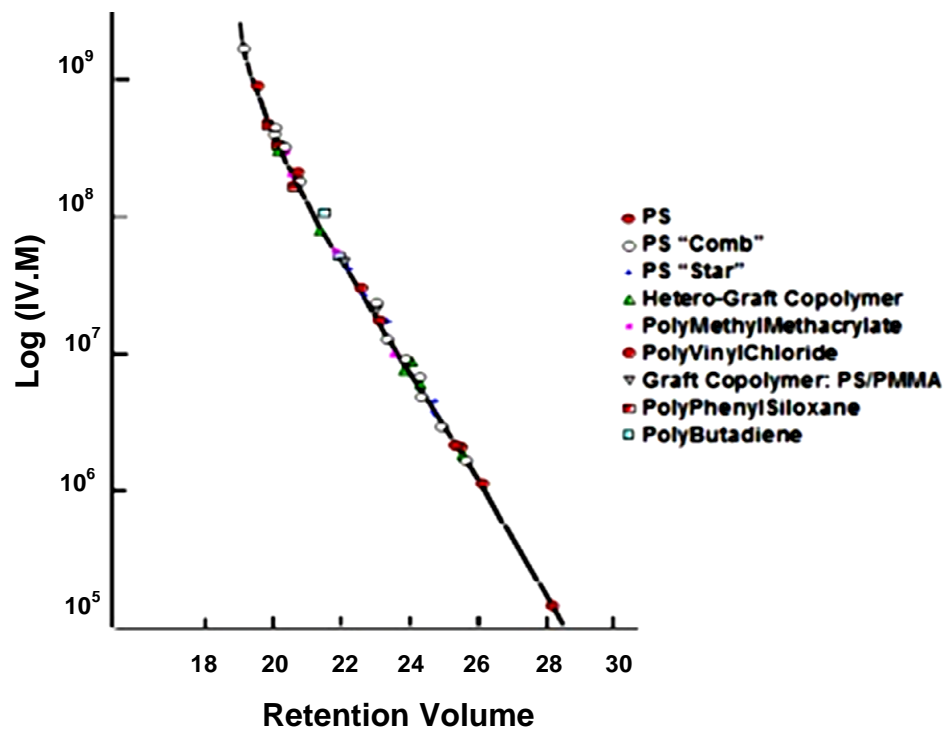
Figure 3. 5 Universal calibration curve.[108]

3.1.3. Light Scattering Detector

Dynamic Light Scattering (DLS) is a batch technique that provides a direct measurement of molecular size or hydrodynamic radius (Rh), as well as information on polydispersity and molecular weight. Static light scattering detectors measure the average intensity of light scattered by macromolecules in solution (Figure 3.6).

Scattered Signal

Laser   Cell   Lens   Mirror
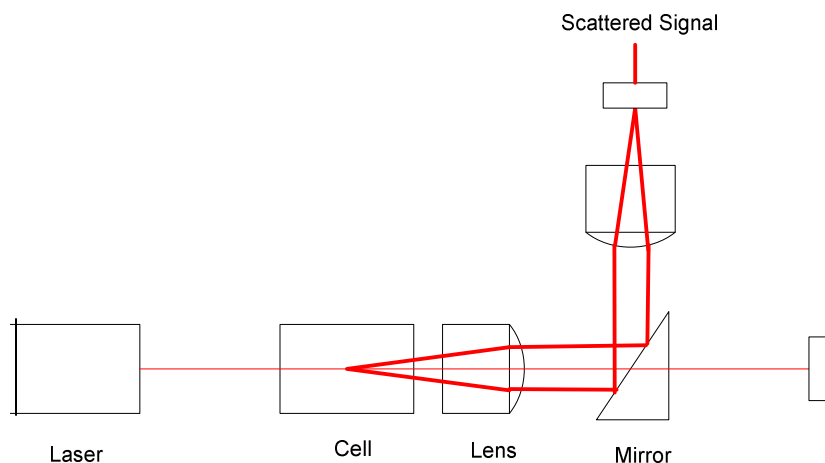
Figure 3. 6 Schematic of Light Scattering Detector.

The light scattering detector is used to determine the weight average molecular weight (M_w) by GPC. The molecular weight is measured without the need for a calibration curve because of the direct proportionality of the light scattering signal to the molecular weight. The Rayleigh Equation (Eq. 3.4) describes the relation of the scattered light of the dissolved polymer molecules by the so-called Rayleigh ratio, R_θ, the polymer concentration C and the weight average molecular weight, M_w.

$$\frac{K \cdot C}{R_\theta} = \frac{1}{M_w \cdot P_\theta} + A_2 \cdot C \qquad (3.4)$$

where K is an optical constant, A_2 is the second virial coefficient and P_θ is the static structure factor. At normal GPC/SEC concentrations, the second virial coefficient is typically insignificant compared to the first term in the denominator, so Eq. 3.4 can be simplified by neglecting the A_2 term. Also P_θ depends on the measuring angle, which is exactly equal to unity for all molecules when θ is zero, so to measure the right molecular weight the scattered light at $\theta = 0°$ must be measured (Eq.3.5). This is experimentally

45

impossible because of the primary beam of the laser. One way to solve this problem is to measure the scattered light at an angle as close as possible to 0°. This approach is called low angle light scattering (LALS).

$$R(\theta)\big|_{\theta \to 0} \cong K \cdot C \cdot M_w \qquad (3.5)$$

The GPC used in this study is Triple Detection, which employs a Concentration detector, Viscometer detector, and Low Angle Light Scattering detector acting in concert, with each detector providing complementary but different information.

- Concentration is measured with an RI detector, and is necessary for the determination of both molecular weight and Refractive index.

- The viscometer detector provides a direct measurement of intrinsic viscosity or molecular density, and allows the determination of molecular size, conformation and structure.

- The light scattering detector provides a direct measurement of molecular weight and eliminates the need for column calibration.

The molecular weight can be calculated using the following equations:

$$RI \cdot sig \propto C \cdot \frac{dn}{dc} \qquad (3.6)$$

$$Vis \cdot sig \propto C \cdot [\eta] \qquad (3.7)$$

$$LS \cdot sig \propto C \cdot K \cdot M_w \propto C \cdot \left(\frac{dn}{dc}\right)^2 \cdot M_w \qquad (3.8)$$

There are four unknown variables, however only three equations can relate them together. Knowing the accurate value of concentration enables us to determine the other unknown variables of Eq.3.6 to 3.8.

In Triple detection, simply running a single narrow standard will enable calibration of all three detectors as well as performing corrections for inter-detector shift and inter-detector peak broadening effects.

3.2.   Infrared (IR) Spectroscopy

Infrared (IR) spectroscopy is one of the most common spectroscopic techniques used for functional group characterization. Infrared waves have wavelengths longer than visible and shorter than microwaves, and have frequencies which are lower than visible and higher than microwaves. Infrared is broken into three categories: far ($4 \sim 400cm^{-1}$), mid ($400 \sim 4,000cm^{-1}$), and near-infrared ($4,000 \sim 14,000cm^{-1}$).[109] Near-infrared refers to the part of the infrared spectrum which is closer to visible light, while far-infrared refers to the part that is closer to the microwave region. Mid-infrared is the region between these two regions which is the most useful part of the electromagnetic spectrum useful for measuring organic compounds. The basic concept behind this spectroscopic technique is the absorption measurement of different IR frequencies by a sample positioned in the path of an IR beam to determine the chemical functional groups in the sample. When an infrared light interacts with the matter, chemical bonds will stretch, contract and bend. As a result, a chemical functional group tends to adsorb infrared radiation in a specific wavenumber range regardless of the structure of the rest of the molecule. An IR spectrum is produced by absorption of energy ($400 \sim 4000$ cm^{-1}) due to vibrations of polar covalent bonds.

Fourier Transform Infrared Spectroscopy provides specific information about chemical bonding and molecular structures, making it useful for analyzing organic materials and certain inorganic materials. FTIR is an improved technique to make the IR

measurements easier and faster, in which the IR beam is guided through an interferometer. A FTIR spectrum is obtained from performing a mathematical Fourier Transform on the interferogram. Figure 3.7 shows the FT-IR which was used in this study for in-situ studies, under ambient and high pressure conditions.
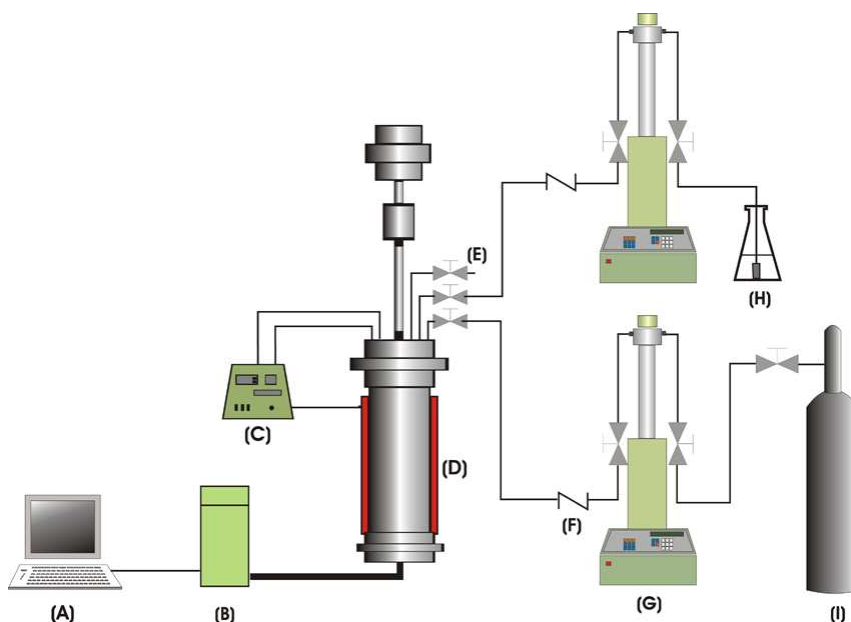
Figure 3. 7 Schematic of FT-IR: autoclave with online FTIR and GC-MS. (A) computer; (B) FTIR; (C) temperature and RPM controller with pressure display; (D) 100 ml autoclave equipped with diamond IR probe; (E) needle valves; (F) check valves; (G) syringe pump; (H) container for carboxylic acid; (I) CO_2 cylinder.

ATR-FTIR is a method for analyzing solid samples using infrared spectroscopy. It is also suitable for characterization of materials which are either too thick or too strongly absorbing to be analyzed by transmission spectroscopy. The basis of this method is that an infrared beam is reflected off the sample, with the absorption measured from the reflected beam. Unfortunately the reflected radiation has a very low intensity. To get around this limitation, the infrared beam is bounced through a crystal such as ZnSe or Ge

at an angle such that the beam is totally internally reflected. The solid sample sits on the crystal, and the result is that the beam will be reflected off the sample (Figure 3.8).
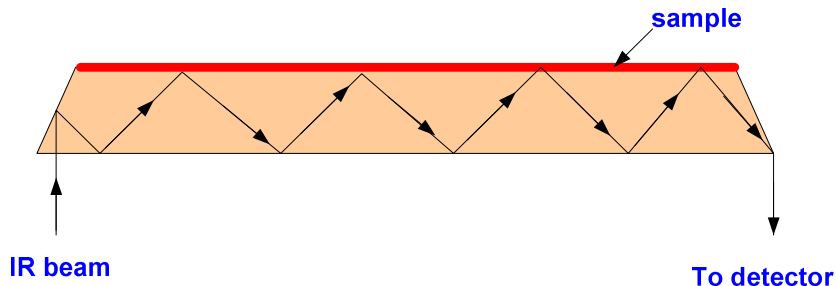
Figure 3. 8 Schematic of ATR-FTIR operation.

3.3.   Thermal Analysis

Thermal analysis is a form of analytical technique most commonly used in the branch of materials science where changes in the properties of materials are examined with respect to the temperature, using differential scanning calorimetry and thermogravimetric analysis.

3.3.1. Differential Scanning Calorimetry (DSC)

Differential scanning calorimetry (DSC) is a technique for measuring the energy necessary to establish a nearly zero temperature difference between a substance and an inert reference material, as the two specimens are subjected to identical temperature regimes in an environment heated or cooled at a controlled rate. The main application of DSC is in studying qualitative and quantitative information about physical and chemical changes that involve endothermic processes such as melting, and exothermic processes such as crystallization, or changes in heat capacity such as at the glass transition temperature [110]. These transitions involve energy changes or heat capacity changes that

can be detected by DSC with great sensitivity. In this study, Mettler Toledo DSC822^e was used to measure T_g of polymer and polymer nanocomposites, and it was shown that T_g of polymer nanocomposites is higher than that of polymer as there is a strong interfacial bonding between the functionalized nanoparticles and polymer chains.

3.3.2. Thermogravimetric Analysis

Thermogravimetric analysis is an analytical technique used to determine a material's thermal stability and its fraction of volatile components by monitoring the weight change that occurs as a specimen is heated. The measurement is normally carried out in air or in an inert atmosphere, such as Helium or Nitrogen, and the weight is recorded as a function of increasing temperature. TGA is widely used for characterization of solid materials including polymer, organic, inorganic, and composite materials. Especially, TGA can be used to determine the percentage of inorganic fillers in inorganic/polymer composites, as utilized in this thesis. In this study, Mettler Toledo TGA Q500 (at a heating rate of 10 °C/min under a nitrogen atmosphere from room temperature to 800°C) was used to measure the percentage of functionalized organic materials and polymer in inorganic/polymer composites. Nitrogen atmosphere was used to prevent oxidation or other undesired reactions.

3.4. Electron Microscopy

Electron microscopes are scientific instruments that use an electron gun to generate the beam of energetic electrons. Whereas the light microscope uses glass lenses to magnify and focus images, the electron microscope uses magnetic lenses to magnify and focus images. Since electrons cannot travel freely in air, electron microscopes are

built into airtight metal tubes or "columns" and use vacuum pumps to remove all the air from within the microscope. The wavelength of electrons is 100,000 times smaller than that of light, so the resolution that they can provide is much higher. There are two main types of electron microscope: (1) the transmission electron microscope (TEM) and (2) the scanning electron microscope (SEM). In general, the TEM image provides high-resolution information on the internal structure of a specimen while the SEM provides a detailed image of the surface structure of a sample.

3.4.1. Transmission Electron Microscopy (TEM)

TEM is a technique used to investigate the morphology, crystallographic structure, and composition of a specimen. Transmission electron microscopy is similar to optical microscopy, except that the photons are replaced by electrons. By propelling electrons at a thin sample, and detecting those transmitted through it, one is able to obtain a map of the local densities of the sample, as well as diffraction information when there are ordered structures such as crystals involved. TEM utilize very thin (0.5 µm or less) samples illuminated by an electron beam. Images are recorded by detecting the electrons that pass though the sample to a system of electromagnetic lenses which focus and enlarge the image on a fluorescent screen, photographic film or digital camera. Figure 3.9 shows a schematic diagram of a TEM instrument. An "Electron source" at the top of the microscope emits the electrons that travel through vacuum in the column of the microscope. Instead of glass lenses focusing the light in the light microscope, the TEM uses electromagnetic lenses to focus the electrons into a very thin beam which travels through the specimen. Depending on the density of the material present, some of the electrons are scattered and disappear from the beam. At the bottom of the microscope the

unscattered electrons hit a fluorescent screen and light is generated, allowing the user to see the image with camera.

STEM is a special TEM technique, in which an electron transparent sample is bombarded with a finely focused electron beam (typically of a diameter of less than 10 nm) which can be scanned across the specimen or rocked across the optical axis and transmitted. STEM (bright and dark field imaging in transmission mode) essentially provides high resolution imaging of the inner microstructure and the surface of a thin sample (or small particles). In dark field (DF) images, the direct beam is blocked by the aperture while one or more diffracted beams are allowed to pass the objective aperture, while in the bright field (BF) mode; an aperture is placed in the back focal plane of the objective lens which allows only the direct beam to pass. In this study, nanocomposites were examined with TEM (Phillips CM 10 electron microscope at 80 kV) to investigate the dispersion of nanoparticles in polymer matrix, and to study the nanocrystalline phases of synthesized TiO_2, while the "grafting from" polymer surrounding the nanoparticles was shown by using STEM (Hitachi HD2000 at 200 kV), in both bright and dark field modes.

Electron source

Electron beam

Pecimen

Electron Magnetic lense

Viewing screen
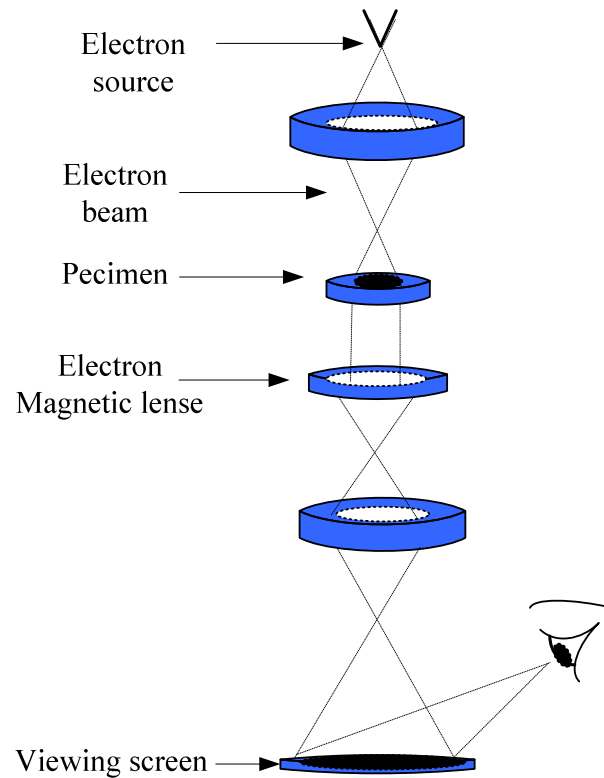
Figure 3. 9 Schematic diagram of a TEM instrument.

3.4.2. Scanning Electron Microscopy (SEM)

The layout of the SEM is very different from a TEM, as shown schematically in Figure 3.10. The SEM column consists of the electron gun and then several magnetic lenses, which are used to focus the electron beam onto a small spot on the sample surface. Unlike the TEM, there are no lenses after the specimen in a SEM. Scan coils are used to deflect the finely focused electron beam to create a tiny rectangular grid of parallel lines over the area of interest, while detectors measure the number of electrons that are displaced from each point on the surface and read both the electrons scattered by the object and the secondary electrons produced by it. Specimens for conventional SEM need to be electrically conducting so that charge built up in the surface from the incident

electron beam can be conducted away. Usually, the magnification range of the SEM is between 10 to 222,000 times.

Energy Dispersive X-Ray Analysis (EDX), also referred to as EDS, is an X-ray technique used to identify the elemental composition of a specimen. EDX is the measurement of X-rays emitted during electron bombardment in an electron microscope (SEM or TEM) to determine the chemical composition of materials on the micro and nano scale. By determining the energies of the X-rays emitted from the area being excited by the electron beam, the elements present in the sample are determined (qualitative analysis). If the electron beam is rastered over an area of the sample, then EDX systems can also acquire X-ray maps showing variation of elements in the sample.

Electron gun

Scanning coil

Magnetic lens

Secondary Electron Detector

Specimen
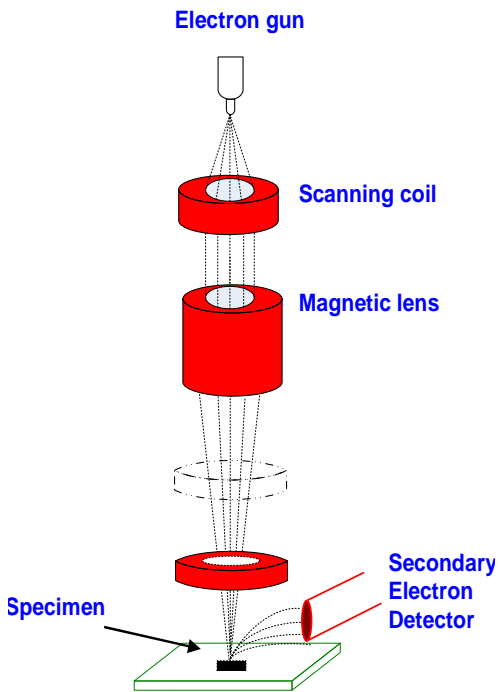
Figure 3. 10 Schematic diagram of a SEM instrument.

In this study, Scanning electron microscopy (SEM) images and energy dispersive X-Ray (EDX) were recorded using either Hitachi S-2600N or LEO 1530 instrument without gold coating at 10 kV. SEM was employed to study the morphology of nanoparticles before and after functionalization, and also after grafting polymer chains from the surface of nanoparticles. EDX was used to measure the percentage and also the dispersion of the specific elements, such as sulfur in functionalized n-TiO_2 or Ni in NiO/TiO_2 composites.

CHAPTER 4

SYNTHESIS OF n-TiO$_2$/PAA NANOCOMPOSITES BY RAFT POLYMERIZATION

Due to the strong agglomeration tendency of nanoparticles such as metal oxides, homogeneous dispersion of these materials throughout a polymeric matrix is extremely challenging. In order to overcome this problem and to enhance the filler polymer interaction, this chapter focuses on living polymerization initialized from the surface of titania nanofillers. A new method of synthesizing n-TiO$_2$/polymer nanocomposites was found with a good dispersion of the nanofillers by using the bifunctional RAFT agent (**1**), 2-{[(butylsulfanyl)carbonothioyl]sulfanyl}propanoic acid). This RAFT agent has an available carboxyl group to anchor onto TiO$_2$ nanoparticles, and the S=C (SC$_4$H$_9$) moiety for subsequent RAFT polymerization of acrylic acid (AA) to form n-TiO$_2$/PAA nanocomposites.
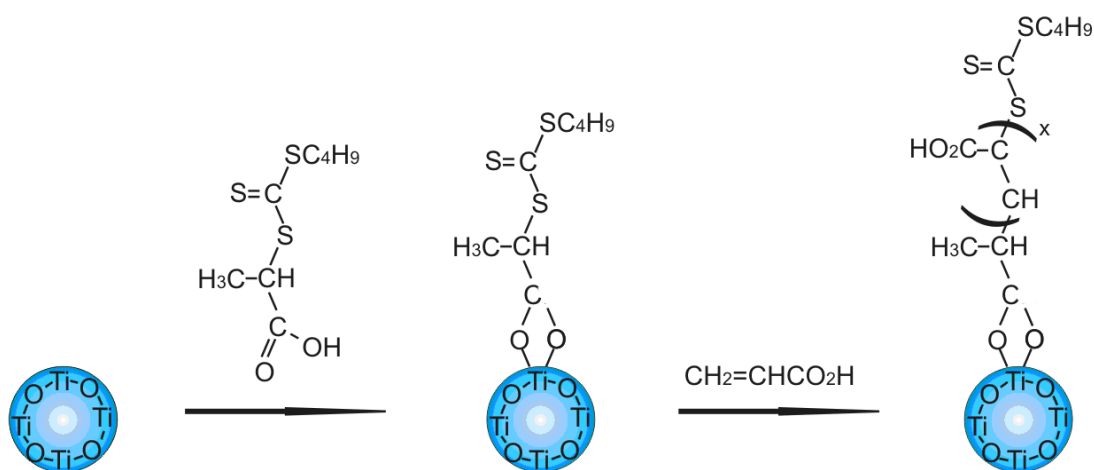
4.1 Introduction

Due to their extremely large surface-area/volume ratio, nanoscale metal oxides, such as TiO_2, SiO_2, tend to strongly agglomerate, hence reducing the resultant mechanical properties of the nanocomposite materials.[111] Many efforts have been taken in order to minimize agglomeration and to enhance the filler-matrix interaction, such as using a mechanical method (ultrasonic irradiation), or chemical method ("grafting from" or "grafting to" methods). Living radical/controlled polymerization techniques (ATRP, NMP, and RAFT) have been employed in order to have surface-initiating graft polymerization on nanomaterials. RAFT polymerization is of significant current interest, because it enables the control of the final polymer product with respect to molecular weight, polydispersity, and macromolecular architecture.[17] Immobilizing the RAFT agent on a solid support e. g. silica or titania may therefore be an attractive pathway for designing inorganic-organic hybrids.

Nanotitania (n-TiO_2) is of significant scientific and industrial interest for several applications, such as semiconductor electrodes in photo electrochemical cells and dye sensitized solar cells (DSSCs).[10] Titanium dioxide (TiO_2) when irradiated with a light whose energy is greater than the band gap of TiO_2 produces reactive oxygen species such as hydroxyl radicals,[112] hydrogen peroxide,[113] and super oxide anions oxygen in water.[114] Nanotitania (n-TiO_2) can also be used as anticancer agents with the goal of increased selectivity towards cancer tissues.[115] For this application the nanoparticles need to disperse homogeneously. These dispersions require colloidal stability and should be resistant to high salt concentrations or protein adsorption to avoid thrombus formation.[116, 117]

The isoelectric point of TiO_2 is close to neutral pH, making the practical use of TiO_2 particles very difficult in aqueous solution. A general approach for improvement of particle dispersion is adsorption of hydrophilic polymer dispersants such as polyethylene glycol [118], polyacrylamide[119] and polyacrylic acid (PAA) on the n-TiO_2 surface.[120, 121] In general, the TiO_2 dispersion system in the presence of PAA, hydrogen bonding and chemical interactions occur at the n-TiO_2 surface and electrostatic repulsion of the carboxylic acid groups of PAA on different particles provides colloidal stabilization in an aqueous medium.[116] n-TiO_2/PAA also is used in UV-Light-Induced Swelling and Visible-Light-Induced Shrinking of a TiO_2-Containing Redox Gel.[122]

Ti(IV) is known to be able to form carboxylate complexes. In the complex, the acetate can potentially coordinate with the metal as a chelating, bridging bidentate or monodentate formation (Figure 4.1).[123] FTIR is an established technique for analyzing the complexes of metal carboxylate species.[124]

monodentate   chelating bidentate   bridging bidentate
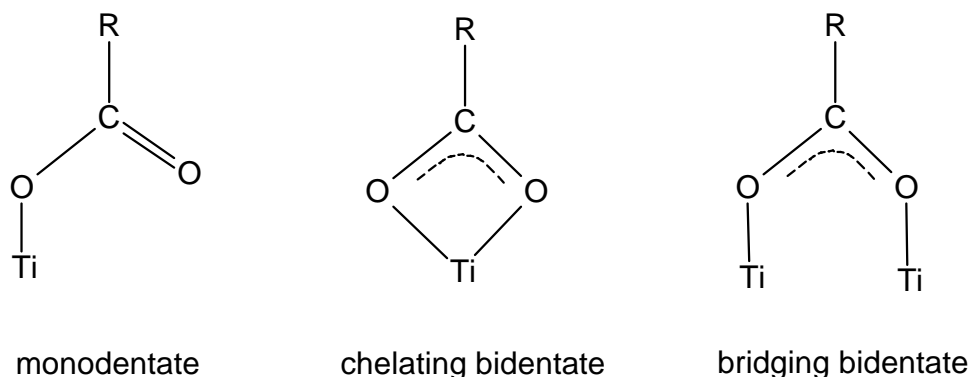
Figure 4. 1 Coordination modes of RCOO⁻ with titania surface.[62]

Our approach in selecting the RAFT initiator agent is to choose the R structure with a free carboxylate group that can coordinate to Ti (IV) on the titania surface. Anchoring of a RAFT agent to a surface can be accomplished via either the Z or R

group[62, 125] (Figure 4.2) however most studies have chosen the R group approach, which leads to a scenario more closely resembling ''grafting from'' polymerization. The mechanism of attachment of the Z group to the nanoparticle surface is similar to that of the ''grafting to'' approach. As described in Ch.2, the "grafting to" approach, is inherently limited in its ability to create high density grafted polymer as crowding of chains at the surface prevents further attachment.[62] On the other hand, using the ''grafting from'' approach, low molar mass monomer molecules can easily diffuse to the functionalized surface of the particles to start polymerization and grow the polymer chains.

Z group approach

R group approach
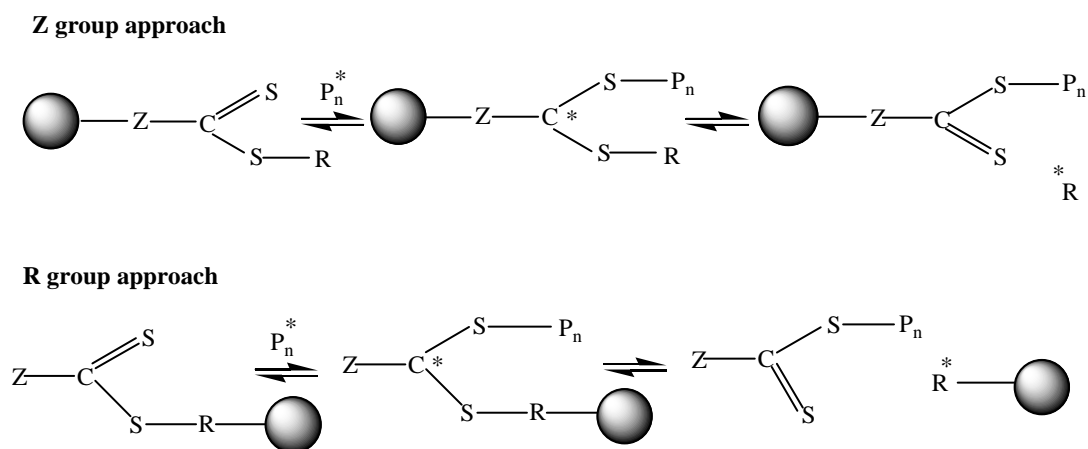
Figure 4. 2 Schematic diagram of RAFT polymerization from a trithiocarbonate RAFT agent anchored to the surface of nanoparticles via Z and R groups.[62]

In this study, two kinds of RAFT agents (**1**) and (**2**) (Figure 4.3) were synthesized to determine which one is appropriate for the acrylic acid monomer.

$$\underset{Z}{\overset{S}{\parallel}}C\overset{}{\underset{S}{\diagdown}}\overset{R}{}$$

(**1**) Z = C$_4$H$_9$S (**2**) Z = OEt

R = CH(CH$_3$)CO$_2$H R = C(CH$_3$)(CO$_2$Et)$_2$
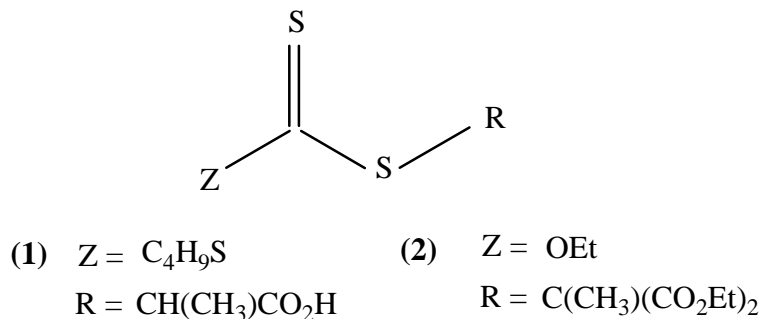
Figure 4. 3 Structures of RAFT agents (1) and (2).

Then the bifunctional RAFT agent (**1**), 2-{[(butylsulfanyl)carbonothioyl] sulfanyl}- propanoic acid) is used to coordinate to n-TiO$_2$, while the S=C(SC$_4$H$_9$) moiety is used for subsequent RAFT polymerization of acrylic acid (AA). Coordination of the RAFT agent onto the n-TiO$_2$ surface is confirmed using ATR-FTIR analysis, livingness of the solution polymerization of AA is demonstrated by solution polymerization using (**1**) with subsequent ^{1}H NMR and GPC analysis, while the resulting nanocomposites are characterized by electron microscopy, FTIR, and thermal analysis.

4.2 Experimental

4.2.1. Materials

Titania nanospherical particles (n-TiO$_2$) (99.5%, Sigma-Aldrich, avg. part. size 25-70 nm), 2, 2′-azo Azobis (2-methylpropionitrile) (AIBN) initiator (Toronto Research Company), methanol (HPLC grade, Sigma-Aldrich), hydrochloric acid (39%, Sigma-Aldrich), and radical inhibitor BHT (2, 6-di-tert-butyl-4-methylphenol, 99%, Sigma-Aldrich) were used as received. Acrylic acid (AA) monomer (99%, Sigma-Aldrich, inhibited with 200 ppm BHT) was passed through an inhibitor remover column (Sigma-Aldrich) before use. The RAFT agents (2-{[(butylsulfanyl) carbonothioyl] sulfanyl}propanoic acid) (**1**) and 2-((Ethoxythiocarbonyl)-2-Methyl Malonate (**2**) (Figure

4.2) were prepared as described elsewhere (for more detailed description see Appendices 1 and 2).[126]

4.2.2. Functionalization of n-TiO$_2$

0.5 g of the RAFT agent (**1**) and 3.5 g of n-TiO$_2$ were dispersed in 60 mL methanol with the aid of ultrasound for 1 hour. The dispersed solution was then transferred to a 100 mL round bottom flask equipped with a condenser and a magnetic stirrer under nitrogen. The solution temperature was maintained at 65 ℃ under stirring for 24 hours. The particles were recovered by centrifugation at 7000 rpm for 10 min. The particles were then re-dissolved in the solvent and re-precipitated by centrifugation which was repeated until the solution was clear. The solid product was dried overnight under vacuum at 50 °C.

4.2.3. Synthesis of n-TiO$_2$/Poly acrylic acid (PAA) Nanocomposite

0.6 g of acrylic acid monomer, 0.06 g of functionalized TiO$_2$-RAFT agent (**1**) (10:1 wt:wt), and 0.004 g of AIBN were dispersed in 60 mL methanol with the aid of ultrasonication. Then the solution was transferred to a 100 mL three-neck flask equipped with nitrogen supply, a thermometer, and a condenser under constant stirring for 24 hours. The particles were recovered by following the same procedure mentioned for functionalization of n-TiO$_2$ (Figure 4.4).
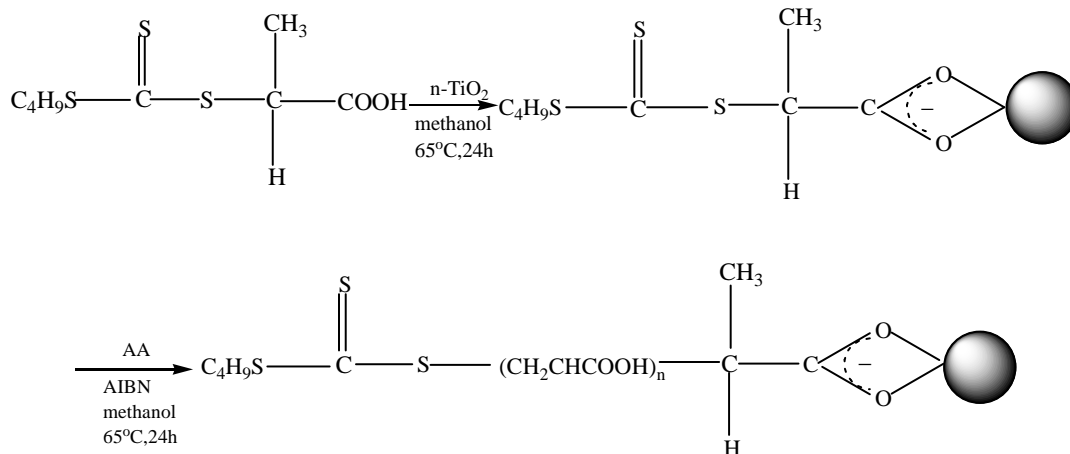
Figure 4. 4 Functionalization of TiO$_2$ and formation of n-TiO$_2$/PAA nanocomposite.

4.2.4. Cleaving Grafted Polymer from Particles

30 mg of PAA "grafted from" TiO$_2$ nanoparticles were dissolved in 1 mL of HCl (2 M) and 30 mL of deionized water. The solution was allowed to stir at 80°C under reflux for 24 hours. After centrifuging at 2500 rpm for 2 hours, the solution was poured onto a glass plate and allowed to stand in a fume hood overnight. The recovered polymers were dissolved in an aqueous buffer (NaHCO$_3$ 0.05 M, NaNO$_3$ 0.1 M, NaN$_3$ 0.02 M) for subsequent GPC analysis.

4.2.5. RAFT Polymerization of Acrylic Acid

A 0.0229 mol/L solution of RAFT agent (**1/2**) and a 2.29 mol/L solution of acrylic acid ([AA]/ [RAFT agent] = 100) were dissolved in 150 mL methanol in a 250 mL three-neck flask equipped by a line of nitrogen supply, a thermometer, a stirrer for gentle mixing, and a condenser (with silica gel at the top for moisture removing). The solution was first heated to 65 $^{\circ}$C, then 0.00229 mol/L of AIBN was added, which acted as an initiator ([RAFT agent]/ [AIBN] = 10). During the reaction at various time intervals,

GPC samples were prepared by removing small samples of the reaction mixture, inhibiting polymerization by BHT as radical inhibitor, solvent stripping in vacuum at 40 ^{o}C, and then re-dissolving in an aqueous buffer (NaHCO$_3$ 0.05 M, NaNO$_3$ 0.1 M, NaN$_3$ 0.02 M) before molecular weight analysis.

4.3.   Characterization

The molecular weight and PDIs of PAA were measured by gel permeation chromatography (GPC) with a Viscotek instrument using triple detectors (RI, LS, and V) referenced to PS standards (1 ml/min, at 30 ^{o}C). ^{1}H NMR spectroscopy was operated on a Varian Mercury 400 while FTIR spectra were collected from a KBr pellet on a Bruker IFS 55 FTIR instrument attached with a MCT detector, with a resolution of 2 cm^{-1} and 128 scans for each sample. Scanning electron microscopy (SEM) images and energy dispersive X-Ray (EDX) were recorded using a Hitachi S-2600N without gold coating at 10 kV, transmission electron microscopy (TEM) was performed on a Phillips CM 10 electron microscope at 80 kV, and STEM was performed using a Hitachi HD2000 at 200 kV. Thermo gravimetric analysis was performed using a TGA Q500 at a heating rate of 10 °C/min under nitrogen.

4.4.   Results and Discussion
4.4.1. ^{1}H NMR

As described in Ch.2, RAFT polymerization achieves living growth starting from the initial dithioester or trithiocarbonate RAFT agent, which is activated by the radicals generated from a traditional initiator [17] e.g. AIBN in this case. The synthesized RAFT agent (**1**) and PAA in methanol d-4 were examined using ^{1}H NMR (Figure 4.5). In Figure

4.5a, the peaks B, C and E-H are assigned to the RAFT agent,[127] and peaks I, J in Figure 4.5b are attributed to the repeating unit of PAA.[128] Peak A is due to CD_3OH that is generated through substitution of methanol-d4 and carboxylic acid, and peak D is from the solvent. The NMR spectrum in Figure 4.5b shows that the functional groups of the RAFT agent are retained in the polymer, which provides strong evidence for the RAFT reaction occurring.
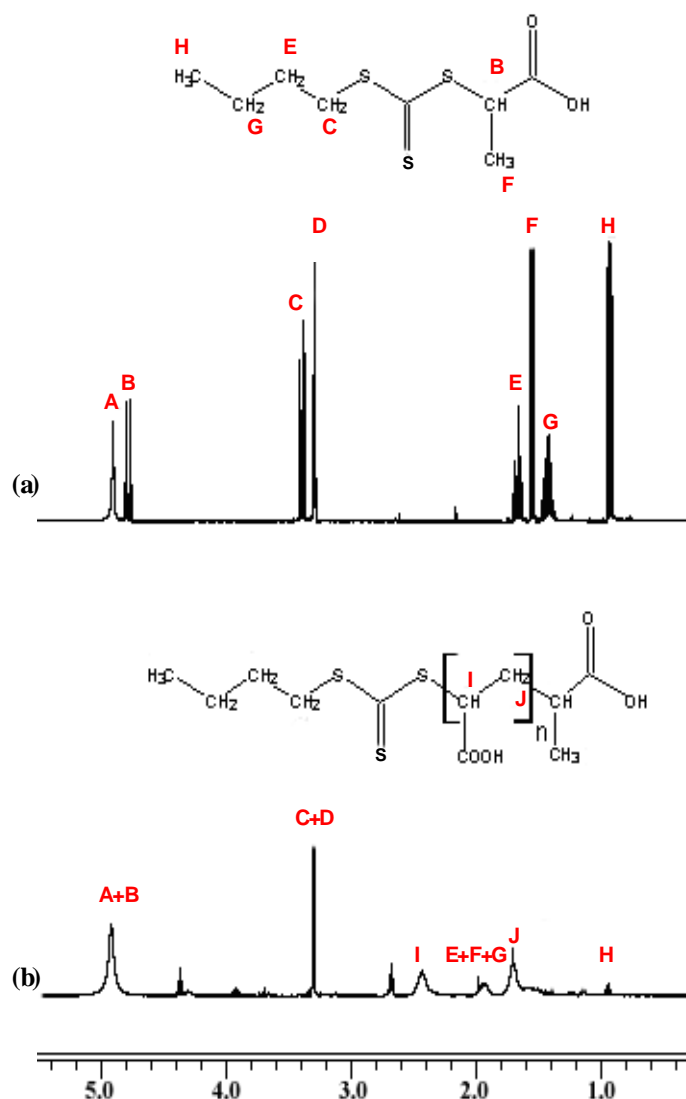
Figure 4. 5 ^{1}H NMR spectra of (a) RAFT agent (1), 2-{[(butylsulfanyl) carbonothioyl] sulfanyl} propanoic acid, and (b) PAA.

65

4.4.2. Molecular Weight Determination of PAA in Solution

Living polymerization is characterized by a linear increase of the molecular weight with conversion and reaction time, and a narrow molecular weight distribution as evidenced by a polydispersity index ($PDI=M_w/M_n$) approaching 1(see section 2.3). Table 4.1 shows the M_n of acrylic acid synthesized by using two kinds of RAFT agents (**1**) and (**2**) at different concentration ratios. By using (**2**), after one hour the M_n of the polymer is relatively unchanged with polymerization time and the PDIs are broad, which is in contrast with the data obtained by Ladaviere *et al.*[129] , where the M_n increased with time and the PDIs were narrow. As mentioned earlier, the effectiveness of the RAFT agent depends on both the monomer structure, and the R and Z groups. Moad *et al.* [34] showed that RAFT agents having O or N atoms (*e.g*. O-alkyl xanthate and N, N-dialkyl dithiocarbamate derivatives) are not very effective RAFT agents, because of the interaction between O or N lone pairs and the C=S double bond, resulting in delocalization of this bond (Figure 4.6). This helps to explain why RAFT agent (**2**) controlled the molecular weight poorly.
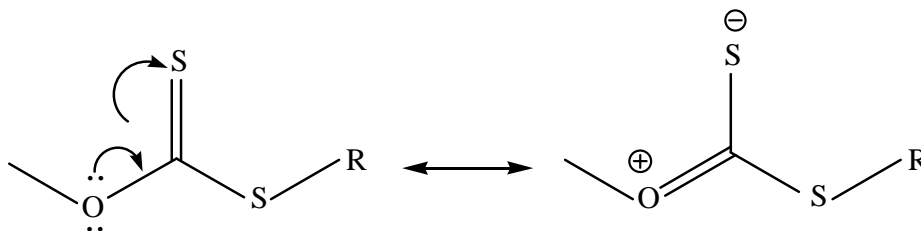
Figure 4. 6 Canonical form of xanthates and dithiocarbamates.[34]

On the other hand, the molecular weights of polyacrylic acid made by (**1**) increased linearly with time, and gave very narrow PDIs. As well, the polymer obtained with (**2**) was white, while that obtained from (**1**) had a yellow tinge, indicating the

presence of the RAFT agent, which was also confirmed by the ^{1}H NMR results. Figure 4.7 shows the GPC elution profiles of the PAA obtained using solution polymerization with RAFT agent (**1**), where additional experiments were carried out for longer periods of time. The molecular weights of PAA increased directly with reaction time, and the PDIs were in the range of 1.12 –1.06. These results confirmed that the RAFT agent (**1**) was involved in a living polymerization reaction.

Table 4. 1 Polymerization of AA at different [AA] / [RAFT agent] in methanol as a solvent, at 65°C, and AIBN as an initiator, [RAFT agent]/[AIBN] = 10, [AA] = 2.29 mol/L.

Time (h)	1				2			
	[AA]/[1]				[AA]/[2]			
	50		100		50		100	
	M_n	PDI	M_n	PDI	M_n	PDI	M_n	PDI
1	1700	1.12	3600	1.11	6000	1.82	6500	1.79
2	2900	1.10	4700	1.10	5600	1.68	6300	1.76
3	3200	1.07	6300	1.06	5000	2.18	6100	1.87
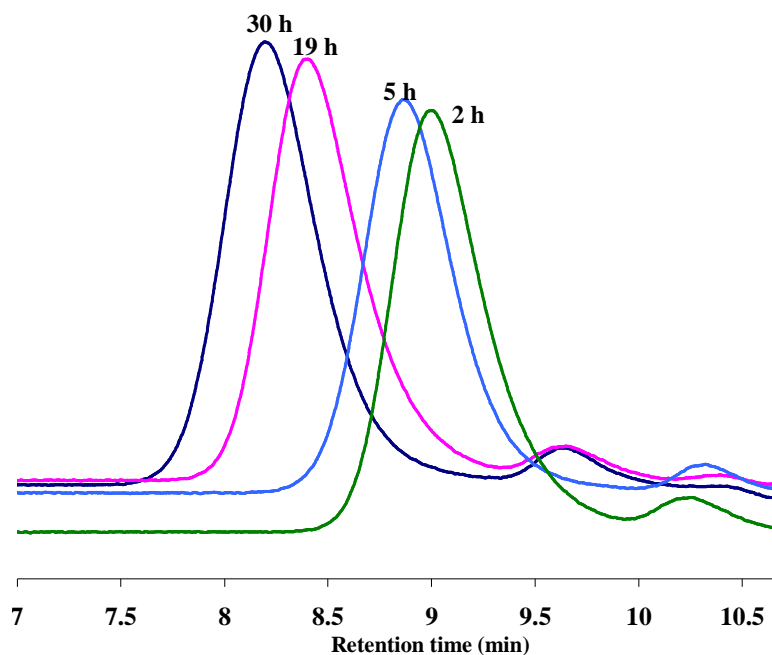
Figure 4. 7 GPC elution profiles for RAFT polymerization of acrylic acid using RAFT agent (**1**) at 65 °C, for 2 h (M_n=2900 g/mol, PDI= 1.10), 5 h (M_n= 3980 g/mol, PDI= 1.12), 19 h (M_n= 8000 g/mol, PDI= 1.13), 30 h (M_n=10000 g/mol, PDI= 1.14).

4.4.3. FTIR Study

In order to verify the functionalization of n-TiO$_2$ as well as the formation of the nanocomposite, FTIR analysis was carried out as FTIR is an established technique for analyzing the complexes of metal carboxylate species.[123, 124, 130, 131] The spectrum of the RAFT agent (**1**) in Figure 4.8a exhibits peaks at 1707 cm^{-1} (carboxylic group), 1375 - 1450 cm^{-1} (alkane groups), and no obvious peak in the region from 1475 to 1650 cm^{-1}. The new peaks at 1547, 1568, and 1626 cm^{-1} of the functionalized n-TiO$_2$ are assigned to the bridging or chelating bidentate coordination between titanium atoms and the carboxyl groups (Figure 4.8b). The weak peaks at 1708 and 1746 cm^{-1} are attributed to residual un-coordinated RAFT agent and carboxylate monodentate, respectively. In the spectrum of a typical n-TiO$_2$/PAA composite, the strong peaks at 1724 cm^{-1} and 1653 cm^{-1} are

attributed to the presence of the carboxylic group of PAA,[132] and the broad peaks in the range of 1500 –1625 cm^{-1} shows the remaining of Ti-acetate bidentate (Figure 4.8c). The FTIR spectra confirm that the TiO_2 nanoparticles were successfully functionalized with the carboxylic group of the RAFT agent.
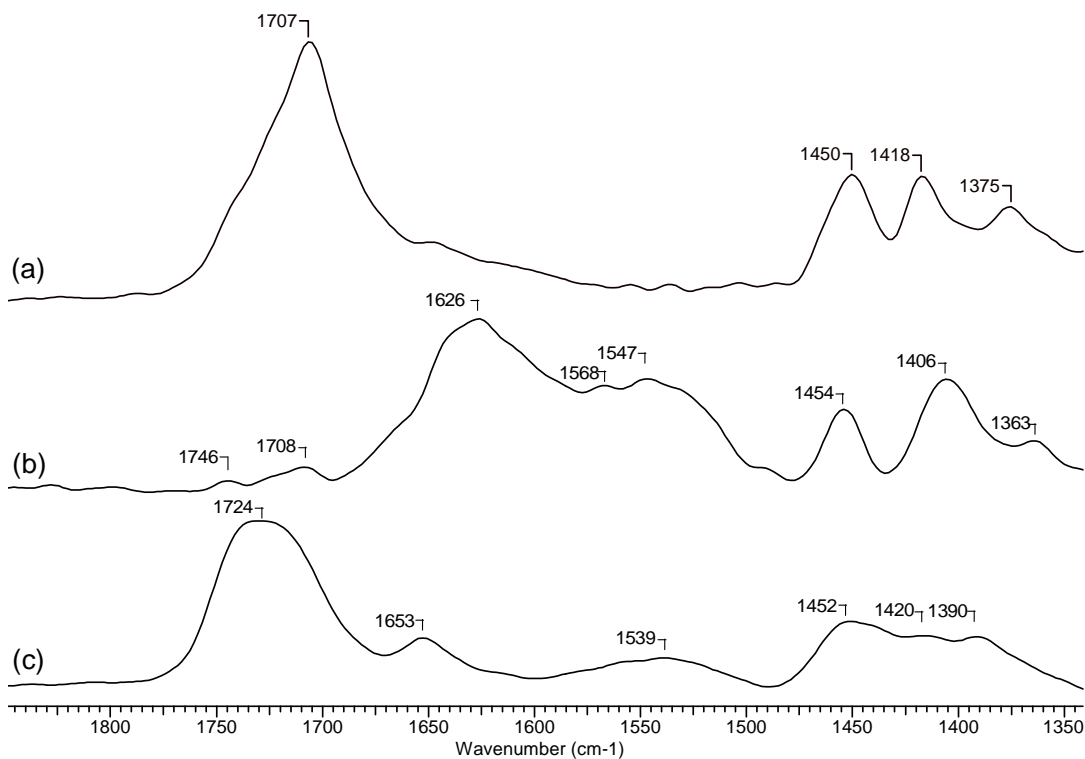
Figure 4. 8 FT-IR Spectra of (a) the RAFT agent (1), (b) the functionalized n-TiO$_2$ and (c) the n-TiO$_2$/PAA composite.

4.4.4. Organic/water partitioning study

In addition to FTIR, the resulting materials were studied by organic phase/water partitioning experiments. As one would expect after functionalization by an organic group, n-TiO$_2$'s hydrophilicity changes. Figure 4.9a shows the n-TiO$_2$ dispersed in ethyl acetate/water bilayers, where the n-TiO$_2$ is suspended in the water phase (lower phase), indicating that it is hydrophilic. The n-TiO$_2$ functionalized with the RAFT agent,

however, partitions into the organic phase (upper), due to the existence of the organic moiety, mainly contributed by -Bu groups (Figure 4.9b). Due to many carboxylic groups and a few -Bu groups in the PAA molecules, the n-TiO$_2$/PAA composite is mainly hydrophilic in nature, as evidenced by partitioning into the water phase (Figure 4.9c).
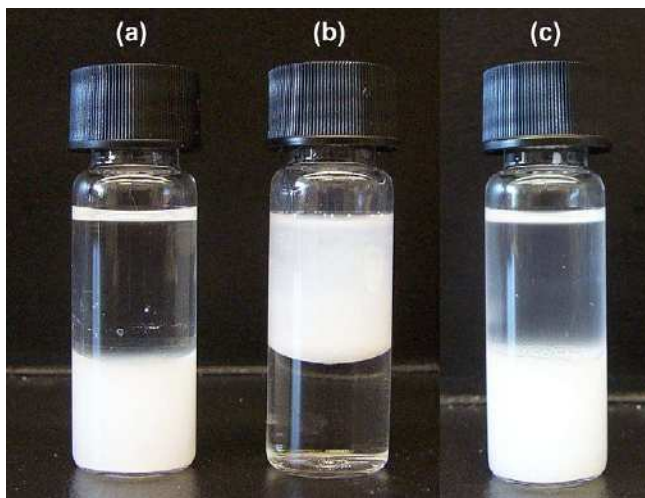
Figure 4. 9 In the vials, the upper layer is ethyl acetate and the lower layer is water phase. (a) The non-functionalized n-TiO$_2$ is well dispersed in the water phase, (b) while the functionalized n-TiO$_2$ is suspended in the organic phase, and (c) n-TiO$_2$/PAA composite stays in water phase.

4.4.5. Molecular Weight Determination of Cleaved PAA

In order to determine whether the polymerization was still living when the RAFT agent had been attached to the n-TiO$_2$, the PAA was cleaved after various polymerization times using acidic conditions. As shown in Table 4.2, the number average molecular weight increased directly with reaction time, and the PDIs were relatively low. For the n-TiO$_2$/PAA composites, thermo gravimetric analysis showed an increase in PAA polymer content with increased polymerization time. These results indicate that the anchored RAFT agent participated in the living polymerization of acrylic acid.

Table 4. 2 Molecular weight and PDIs (GPC) of cleaved PAA at different reaction times and fraction of grafted PAA (wt %).

Time (hour)	M_n (GPC) (gmol^{-1})	PDI	Fraction of grafted PAA (TGA) (wt %)
6	5000	1.23	9
19	10000	1.17	41.6
24	10800	1.50	47.8

4.4.6. TGA Analysis

The functionalized n-TiO$_2$ and n-TiO$_2$/PAA nanocomposites were dried and subjected to TGA. The sample of RAFT agent complexed to n-TiO$_2$ displayed a weight loss of 4%, which was removed during heating in the range of 150-450 °C (Figure 4.10a). Similarly for the n-TiO$_2$/PAA at different polymerization times (Figure 4.10b), the weight loss occurred in the range of 150-450 °C. Higher fractions of PAA were formed as the polymerization time increased; indicating the successful graft polymerization of AA from the RAFT functionalized n-TiO$_2$.
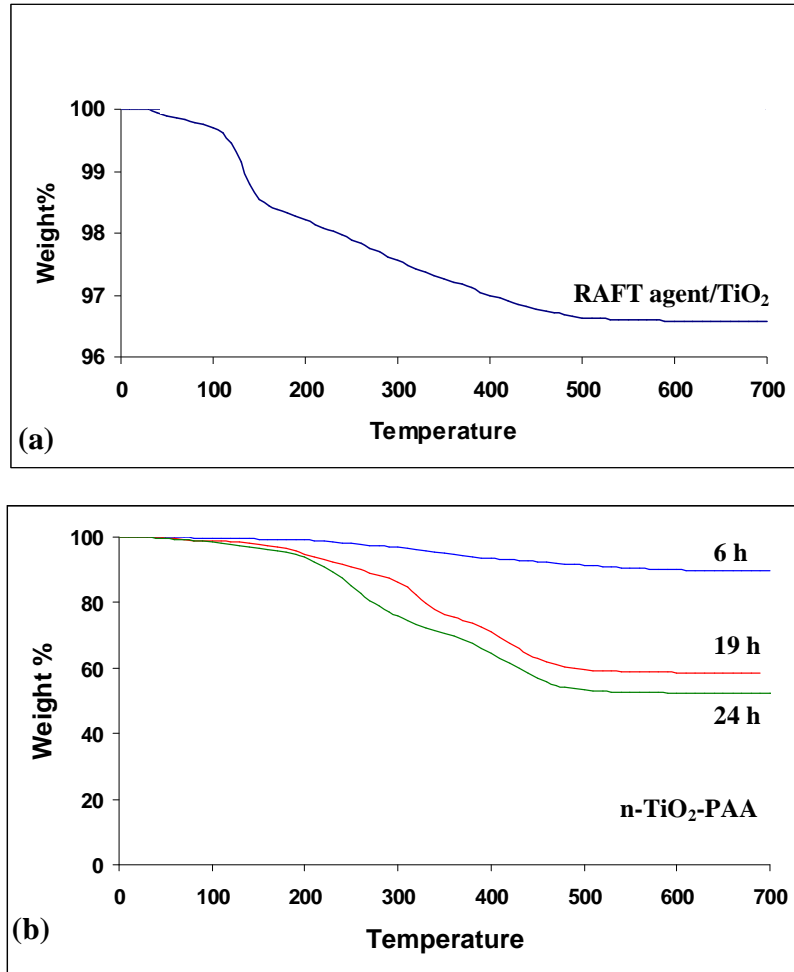
Figure 4. 10 TGA curves of the (a) functionalized n-TiO$_2$, and (b) n-TiO$_2$/PAA at different times.

4.4.7. Electron microscopy

In order to examine the microstructures and nanofiller distribution in the polymer, SEM equipped with EDX, and TEM electron microscopy were used.

SEM was used to study the morphology of n-TiO$_2$ before and after functionalization, as well as the polymer-nanocomposites. Figure 4.11a shows the SEM image of the commercial n-TiO$_2$ consisting of agglomerated spherical particles, whereas Figure 4.11b shows the n-TiO$_2$ after functionalization. No obvious morphology change can be observed from the functionalization step. Figure 4.11c shows the EDX sulfur mapping of

RAFT functionalized n-TiO$_2$, showing well-distributed sulfur in the nanomaterials, indicating successful functionalization. Figure 4.11d shows the n-TiO$_2$/PAA nanocomposite formed after "grafting from" polymerization with AA in which many nanoparticles with a diameter of ca. 20-400 nm can be observed. These are attributed to the polymer chains that can only grow from the RAFT agent attached to the n-TiO$_2$ surface, resulting in the formation of n-TiO$_2$/PAA nanocomposite, which were also characterized by TGA (above).
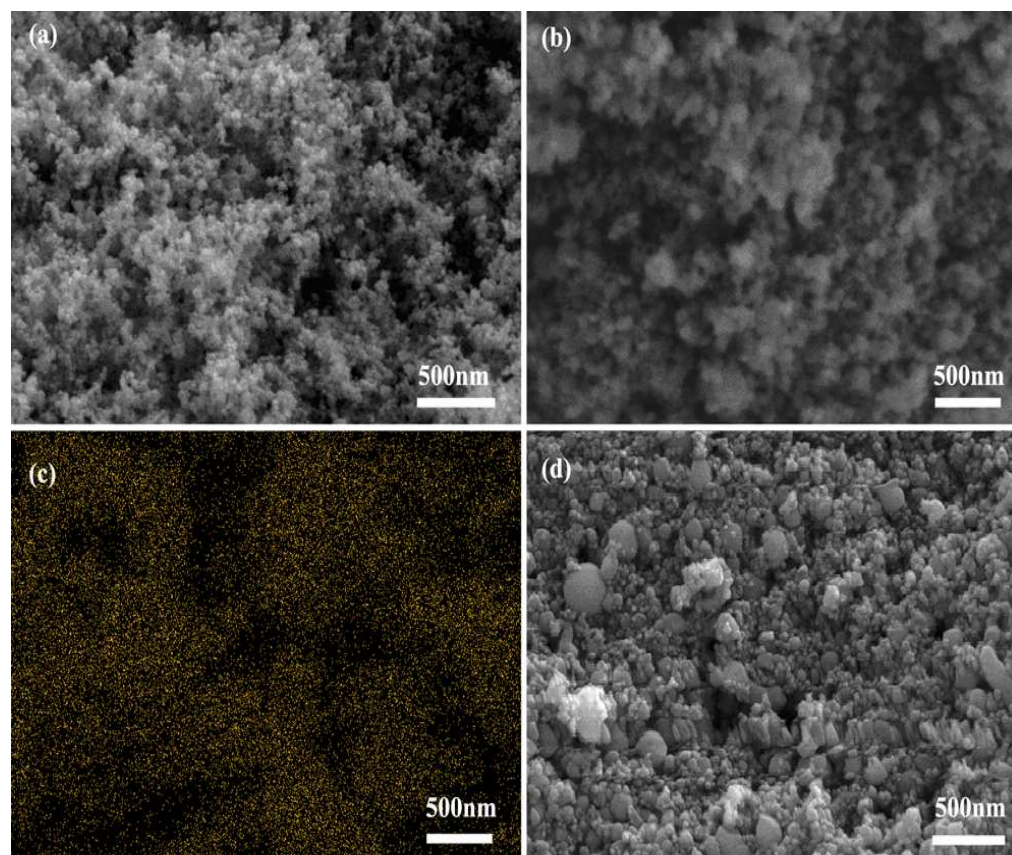
Figure 4. 11 (a) SEM of the non-functionalized n-TiO$_2$, (b-c) SEM and EDX sulfur mapping of RAFT functionalized n-TiO$_2$, and (d) SEM of n-TiO$_2$/PAA composite.

The n-TiO$_2$/PAA composites were examined with TEM and STEM (Figure 4.12a-d). Figure 4.12a-b show the well-dispersed n-TiO$_2$ at low magnification, while Figure

4.12c shows the n-TiO$_2$ at higher magnification. Under high magnification using both bright and dark field electron microscopy, the "grafting from" polymer surrounding the n-TiO$_2$ can be clearly observed (Figure 4.12d-e). The excellent separation of n-TiO$_2$ particles in this work is attributed to the grafting of AA polymer, which separates the previously agglomerated TiO$_2$ nanoparticles. In addition, as PAA is known as a polyelectrolyte, this may also contribute to the excellent dispersion of the n-TiO$_2$ particles.[131, 133]
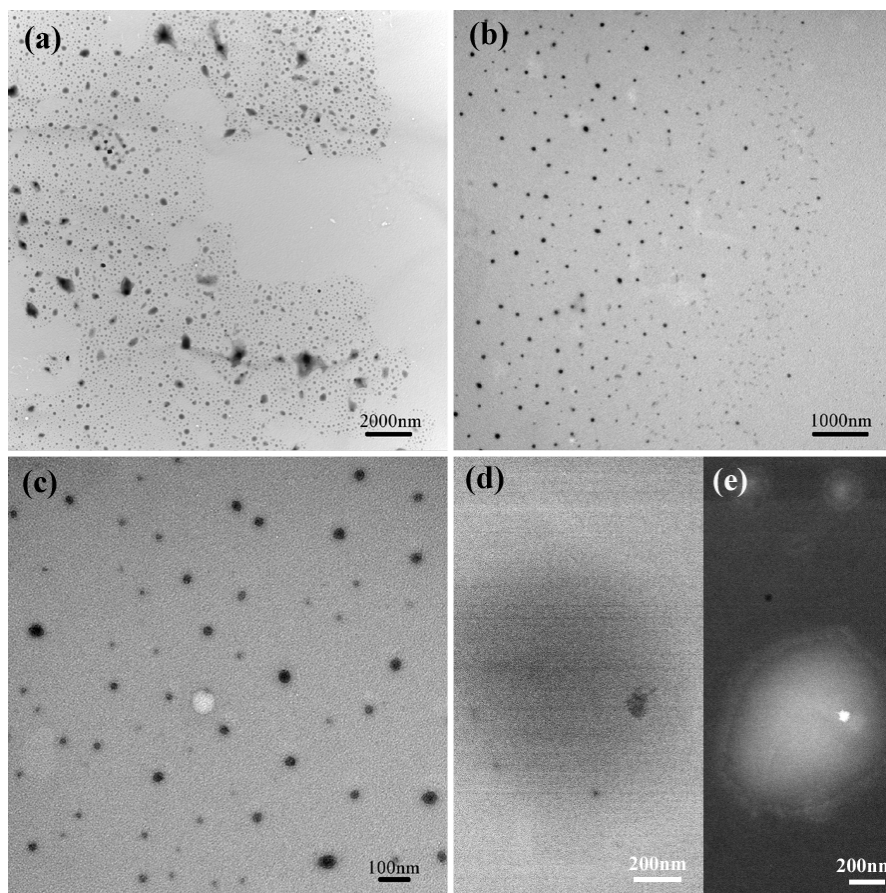
Figure 4. 12 (a-c) TEM of the n-TiO$_2$/PAA at different magnification, and (d-e) STEM of n-TiO$_2$/ PAA at high magnification with bright and dark field.

4.5. Conclusions

For the first time, n-TiO$_2$ was functionalized with a RAFT agent, followed by living grafting-from polymerization, with resultant n-TiO$_2$/PAA hybrid materials being synthesized. The RAFT agent, 2-{[(butylsulfanyl) carbonothioyl] sulfanyl} propanoic acid, was shown to be both a functionalization and living polymerization agent. The FTIR analysis and organic phase/water phase partitioning studies provided the evidence of the functionalization of n-TiO$_2$ by the RAFT agent, while GPC results of cleaved polymer after various reaction times showed that the polymerization was still living, even after the RAFT agent was coordinated to n-TiO$_2$. Electron microscopy images revealed the growth of the "grafted-from" polymers around n-TiO$_2$, and the nanofillers were well separated and distributed in the polymer matrix. This research demonstrated that living polymerization initialized from functional groups on n-TiO$_2$ surfaces is promising to synthesize hybrid materials with an excellent dispersion of the nanofillers for the solid electrolytes in dye-sensitized solar cells.[13]

CHAPTER 5

SYNTHESIS AND KINETICS OF GRAFT POLYMERIZATION OF METHYL METHACRYLATE FROM THE RAFT COORDINATED SURFACE OF n- TiO$_2$

In this chapter polymer chains of PMMA were grown from n-TiO$_2$ by the RAFT polymerization process. The mechanism and kinetics of MMA polymerization from both solution and ''grafted from'' n-TiO$_2$ were studied. The RAFT agent (**3**), 4-cyano-4-(dodecylsulfanylthiocarbonyl) sulfanyl pentanoic acid, with an available carboxyl group was used to anchor onto the n-TiO$_2$ surface, with the S=C(SC$_{12}$H$_{25}$) moiety used for subsequent RAFT polymerization of MMA to form n-TiO$_2$/PMMA nanocomposites.
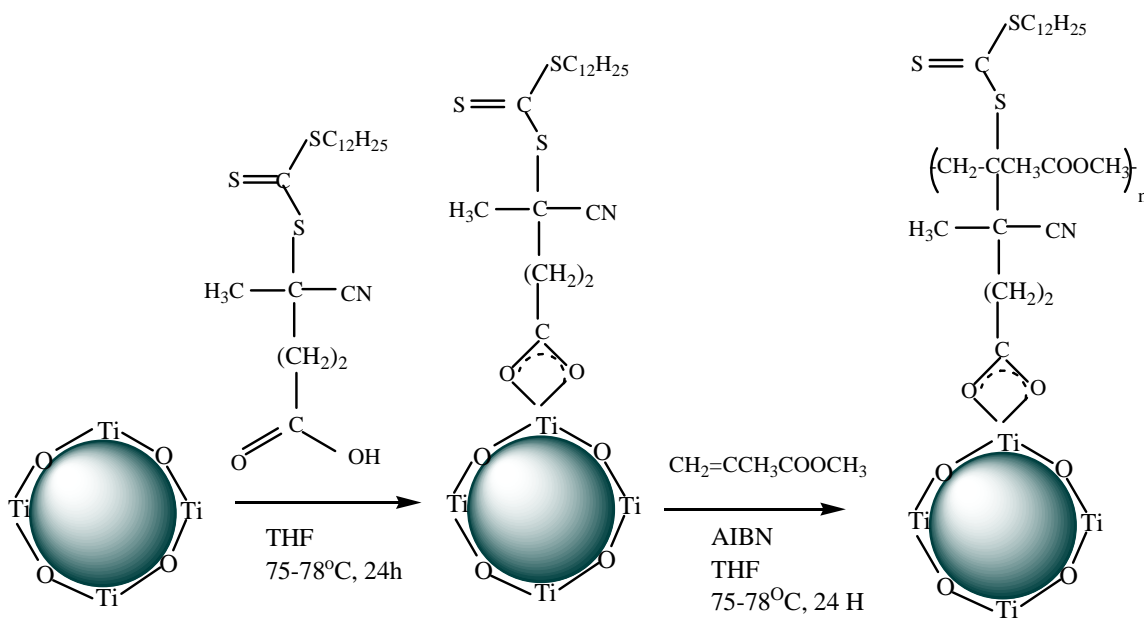
5.1.   Introduction

Living radical polymerization has received significant attention in recent years, as it allows production of polymers with controlled molecular weight, narrow polydispersity, and complex macromolecular architectures.[72] As mentioned in Ch.2, three main types of controlled radical polymerizations have been investigated: NMP, ATRP, and RAFT.[62] Among them, the RAFT process utilizes classical free radical initiators, monomers, and also includes the presence of a RAFT agent. The use of RAFT polymerization methods has shown significant potential to control grafting of polymers from inert substrates.[89, 134]

TiO_2 is excellent in shielding ultraviolet radiation and has been used as a pigment to improve its thermal and photic stability (in the rutile crystal phase).[135] In addition, some titania nanocomposites such as n-TiO_2/PMMA nanocomposites have potential applications for dental and orthopedic use, for example, as bone cements, where the n-TiO_2 will provide both increased strength, and act as a radiopacifier.[136] It is well known that n-TiO_2 particles typically possess a strong tendency to aggregate, which is detrimental for retaining their size dependent properties. In nanocomposites, nanofillers must be finely dispersed in polymers so that the heterogeneous nature of the material is evident only when sampling on a nanometer scale. Due to the high reflecting ability of these micrometer-sized agglomerates, the transparency of the polymeric material is significantly decreased,[137] hence making it important to eliminate the agglomeration of n-TiO_2 particles in PMMA. For this reason a critical challenge in the design of these inorganic–organic systems is to control the mixing between the two dissimilar phases, with several approaches being utilized to overcome this problem, as described in Ch.2.

This chapter explores a living polymerization technique using the bifunctional RAFT agent, 4-cyano-4-(dodecylsulfanylthiocarbonyl) sulfanyl pentanoic acid (**3**) which is used to directly coordinate to n-TiO$_2$, while the S=C(SC$_{12}$H$_{25}$) moiety is used for subsequent RAFT polymerization of MMA.

Coordination of the RAFT agent onto the n-TiO$_2$ surface is confirmed using both XPS and FTIR analysis, livingness of the solution polymerization of MMA using (**3**) is demonstrated with ^{1}H NMR and GPC analysis, while the resulting nanocomposites are characterized by electron microscopy, FTIR, and thermal analysis. The kinetics of the RAFT polymerization using the direct attachment procedure is then investigated comparing solution phase to surface growth.

5.2.   Experimental

5.2.1.   Materials

Titania nanospherical particles (99.5%, Sigma-Aldrich, avg. part. size D= 23.2 nm), 2, 2′-azobis (2-methylpropionitrile) (AIBN) initiator (Toronto Research Company), THF (anhydrous, ≥99.9%, inhibitor-free, Sigma-Aldrich), and radical inhibitor BHT (2, 6-di-tert-butyl-4-methylphenol, 99%, Sigma-Aldrich) were used as received. Methyl methacrylate monomer (MMA) (99%, Sigma-Aldrich, inhibited with 200 ppm BHT) was passed through an inhibitor removal column (Sigma-Aldrich) before use. The RAFT agent 4-cyano-4-(dodecylsulfanylthiocarbonyl) sulfanyl pentanoic acid (**3**) was prepared as described elsewhere (for more detailed description see Appendix 3).[126]

5.2.2. Functionalization of n-TiO$_2$

n-TiO$_2$ was functionalized with RAFT agent (**3**) based on the procedure described in section 4.2.2.

5.2.3. Synthesis of n-TiO$_2$/Poly methyl methacrylate (PMMA) Nanocomposite

45 mL of MMA monomer, 1.8 g of functionalized n-TiO$_2$-RAFT agent (**3**) (high and/or low surface density), and 0.010 g of AIBN were dispersed in 120 mL THF with the aid of sonication. Then the solution was transferred to a 250 mL three-neck flask equipped with nitrogen supply, a thermometer, and a condenser under constant stirring for 24 hours at 75-78 ^{o}C. To ensure that no un-grafted polymer remained in the product, the particles were re-dissolved in THF and re-precipitated by centrifugation at 7000 rpm for 10 min. The solid product was dried overnight under vacuum at 50 °C and the amount of free (non-grafted) PMMA formed during the polymerization was obtained gravimetrically by drying the supernatant in vacuum at 70 ^{o}C overnight (Figure 5.1).
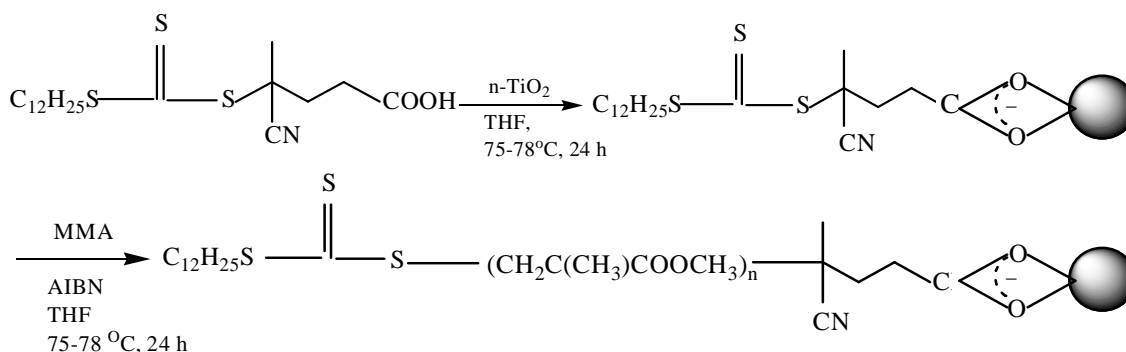
Figure 5. 1 Functionalization of n-TiO$_2$ and formation of n-TiO$_2$/ PMMA nanocomposite.

5.2.4. Cleaving Grafted Polymer from Particles

Grafted PMMA from n-TiO$_2$ nanoparticles was cleaved based on the procedure described in section 4.2.4.

5.2.5. RAFT Polymerization of Methyl methacrylate

A solution consisting of RAFT agent (**3**), 0.24 g (0.0032 mol/L), and methyl methacrylate, 60 g (6 mol/L), was dissolved in 100 mL degassed and dry THF in a 250 mL three-neck flask equipped by a line of argon supply, a thermometer, a stirrer for gentle mixing, and a condenser (with silica gel at the top for moisture removing). The solution was first heated to 70 ^{o}C, then 0.0116 g of AIBN was added, which acted as an initiator ([RAFT agent]/[AIBN] = 4) (Figure 5.2). At various time intervals during the polymerization, GPC samples were prepared by inhibiting polymerization by adding a radical inhibitor (BHT), solvent stripping under vacuum at 50 ^{o}C, and then re-dissolving in THF before injection.
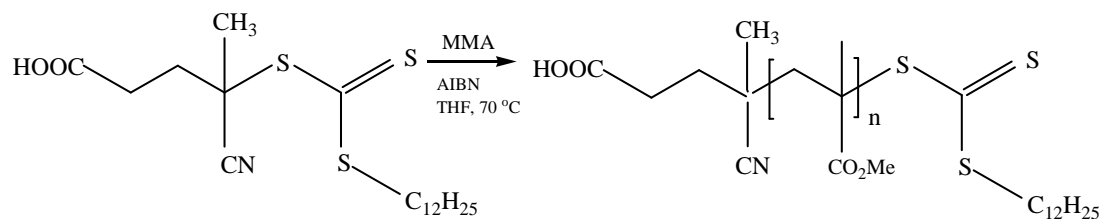
Figure 5. 2 Synthesis route of the RAFT polymerization of methyl methacrylate in solution using (3).

5.3. Characterization

The molecular weight and PDIs of PMMA were measured by gel permeation chromatography (GPC) with a Viscotek instrument using triple detectors (RI, LS, and V) referenced to PS standards (1 ml/min, at 30 ^{o}C). ^{1}H NMR spectroscopy was carried out on a Varian Mercury 400 while FT-IR spectra were collected using both KBr pellet on a Bruker IFS 55 FTIR instrument attached with a MCT detector, and an *in-situ* FT-IR (ASI Mettler Toledo), with a resolution of 2 cm^{-1} and 128 scans for each sample. The X-ray Photoelectron Spectroscopy (XPS) analysis was carried out with a Kratos Axis Ultra

spectrometer using a monochromatic Al Ka source (15mA, 14kV). The instrument work function was calibrated to give a binding energy (BE) of 83.96 eV for the Au $4f_{7/2}$ line for metallic gold and the spectrometer dispersion was adjusted to give a BE of 932.62 eV for the Cu $2p_{3/2}$ line of metallic copper. Scanning electron microscopy (SEM) images were recorded using a LEO 1530 instrument without gold coating at 10 kV, and transmission electron microscopy (TEM) was performed on a Phillips CM 10 electron microscope at 80 kV. Differential scanning calorimetry (DSC) and thermo gravimetric analysis were performed using a Mettler Toledo DSC822^e and TGA Q500, respectively, at a heating rate of 10 °C/min under a nitrogen atmosphere.

5.4. Results and Discussion

5.4.1. ^{1}H NMR

The synthesized RAFT agent (**3**) and PMMA in CDCl$_3$ were examined using ^{1}H NMR (Figure 5.3). The spectra showed that the functional groups of the RAFT agent were retained in the purified polymer, providing strong evidence for the RAFT reaction occurring.

^{1} H NMR: RAFT agent (**3**) (^{1} H, CDCl$_3$): 0.9 (3H, C**H**$_3$), 1.3-1.8 (20 H, C**H**$_2$), 1.9 (3H, SC (CN)-C**H**$_3$), 2.5-2.7 (4H, CH$_3$-(CN)-S-C-(C**H**$_2$)), 3.3 (2H, S-C**H**$_2$).

PMMA (^{1} H, CDCl$_3$): 0.7, 0.9, 1.2 (3H, C**H**$_3$), 1.6 (2H, C**H**$_2$), 3.5 (3H, COOC**H**$_3$)
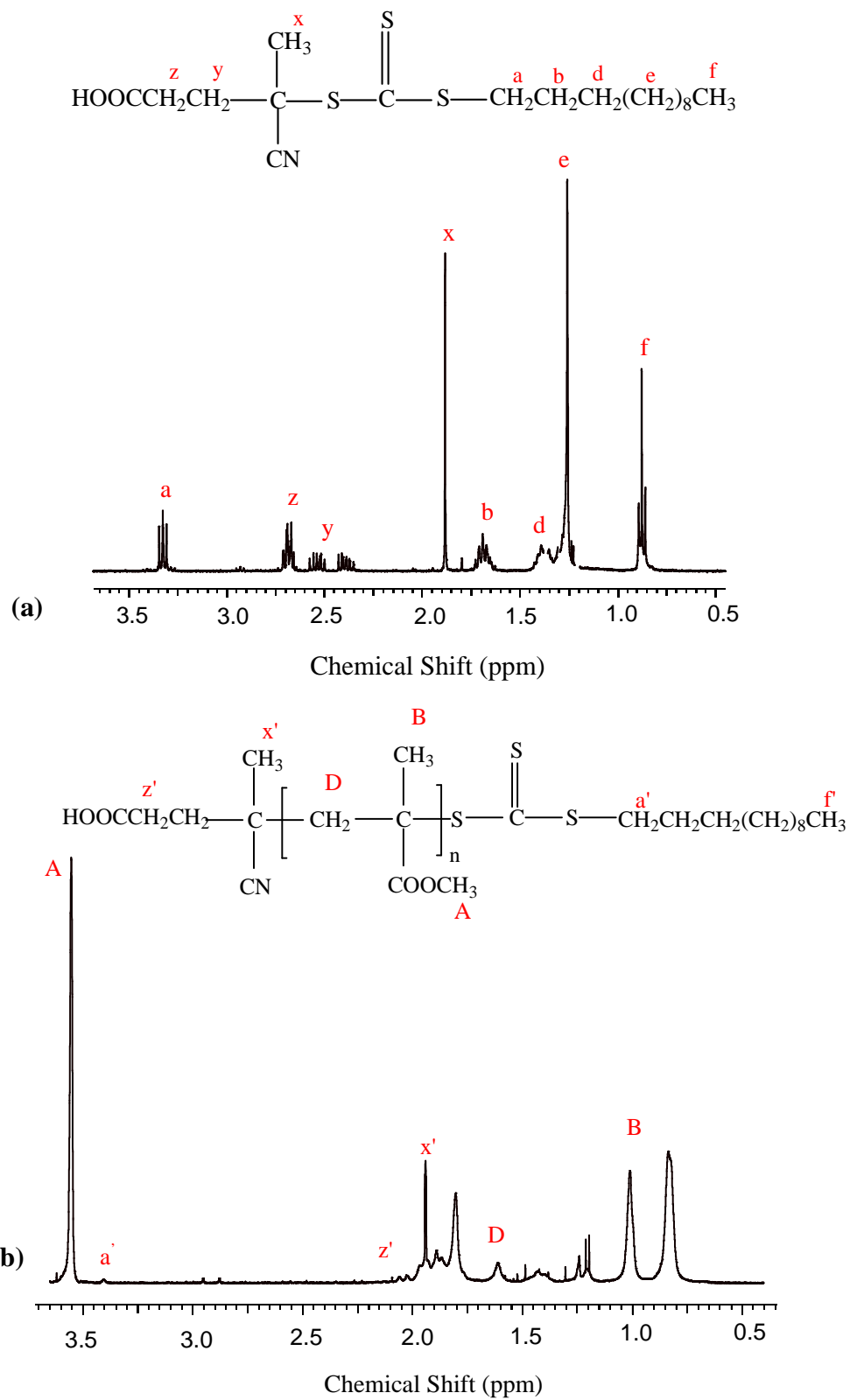
Figure 5. 3 **¹HNMR spectra of (a) 4-cyano-4-(dodecylsulfanylthiocarbonyl) sulfanyl pentanoic acid, and (b) PMMA.**

5.4.2. Kinetics of RAFT Polymerization of MMA in Solution

In a radical polymerization, the growth of chains by addition of monomers to the radicals (P_n) can be represented by reaction (5.1):

$$P_n + M \xrightarrow{k_p} P_m \tag{5.1}$$

where M is monomer, P_n and P_m are propagating radicals, and k_p is the propagation rate constant.

In living free radical polymerization, unlike conventional free radical polymerization, the rate of initiation must be greater than the rate of propagation for all the polymer chains to grow in parallel. Due to the limited termination and chain-transfer events, we can greatly simplify our reaction model and thus R_p can be given by:

$$R_p = -\frac{d[M]}{dt} = k_p \cdot [P_n] \cdot [M] \tag{5.2}$$

where $[P_n]$ is the concentration of active growing polymer chains, and $[M]$ is the concentration of monomer at time $= t$. This is approximately equal to the initial initiator concentration in an ideal case.

Integrating Eq. 5.2 we get:

$$\ln\left(\frac{[M]_o}{[M]}\right) = k_p \cdot [P_n] \cdot t \tag{5.3}$$

where $[M]_o$ is the initial concentration of monomer at time $= 0$. The ratio $\frac{[M]_o}{[M]}$ is linked to the monomer conversion x as shown by Eq.5.4:

$$\frac{[M]_0}{[M]} = \frac{1}{1-x} \tag{5.4}$$

$$\ln\left(\frac{1}{1-x}\right) = k_p \cdot [P_n] \cdot t \qquad (5.5)$$

If we plot $\ln\left(\frac{1}{1-x}\right)$ vs. time to give a straight line, we have evidence of a

constant concentration of active species P_n and this also gives the apparent rate of

polymerization $k_p \cdot [P_n]$.

The number average molecular weight, M_n, can be calculated by the concentration

of monomer converted to polymer divided by the concentration of polymer chains and is

given by Eq. 5.6:

$$M_n = \frac{[M]_0 \cdot x \cdot M_{n,monomer}}{[I]_0} \qquad (5.6)$$

where x is the monomer conversion and $M_{n,monomer}$ is the molecular weight of the

monomer.

In RAFT polymerization, we assume that all the polymer chains will be initiated

by the liberated R-groups from the RAFT agent to form the start of a polymer chain. The

initiator in this situation determines the concentration of active radicals in solution, not

the number of polymer chains. Hence, we need to modify Eq. 5.6 to take this into

consideration.

$$M_n = \frac{[M]_0 \cdot x \cdot M_{n,monomer}}{[RAFT]} \qquad (5.7)$$

As described in Ch.2, the molecular weight increases linearly with

conversion/reaction time in a living polymerization and a narrow molecular weight

distribution is obtained.[34] Figure 5.4a summarizes how M_n (experimental and calculated)

and the PDI's change with conversion, with the conversions being determined

gravimetrically. It is clear that M_n using RAFT agent (**3**) increases directly with conversion, along with having low PDIs, further proving the livingness of this polymerization. [71]

As shown in Figure 5.4a, model Eq. 5.7 works rather well for our plotted experimental data, in the studied experimental region. Figure 5.4b shows the GPC elution profiles of the PMMA obtained using solution polymerization with RAFT agent (**3**) for 1-15 hours of polymerization time. The molecular weight distributions are relatively unimodal, with low PDIs. At low conversion, the PDI has relatively high values, and it gradually decreases as M_n increases. It can be explained that in RAFT polymerization PDI usually decrease with time because of the chain equilibration process.[138]
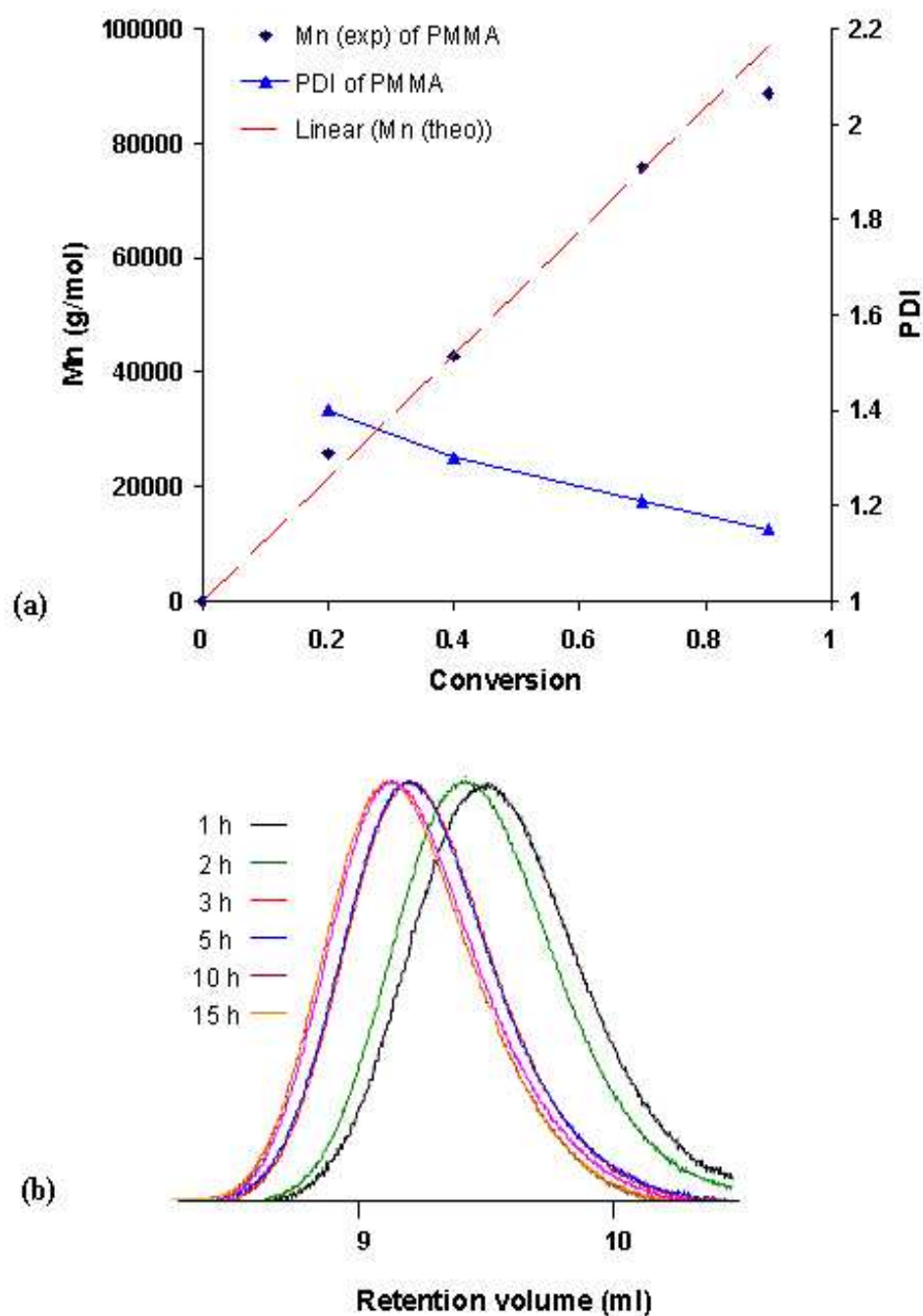
Figure 5. 4 (a) Molecular weight and PDI/conversion data for RAFT polymerization of MMA using RAFT agent (3) (0.0061 M); Mn calculated with Eq. 5.7 (----),and (b) GPC elulion profiles for RAFT polymerization of MMA (655 M in THF) with AIBN (0.0018 M) as initiator and RAFT agent (3) (0.0061 M) at 70 °C, for 1 h (M_n=42,800 g/mol, PDI= 1.48), 2 h (M_n= 75,000 g/mol, PDI= 1.31), 3 h (M_n= 85,100 g/mol, PDI= 1.19), 5 h (M_n =88,700 g/mol, PDI= 1.20), 10 h (M_n= 91,600 g/mol, PDI= 1.34), 15h(M_n= 101,300 g/mol, PDI= 1.09).

Figure 5.5a shows the conversion-time plots for varying concentrations of RAFT agent (**3**) in the solution polymerization of MMA, while Figure 5.5b shows that these polymerizations follow first order kinetics in monomer concentration. These plots show that the rate of reaction decreases slightly with increasing concentration of RAFT agent, which is a well known occurrence in RAFT polymerization.[77] This retardation effect can be influenced by the structure/concentration of the RAFT agent, or the structure/concentration of monomer,[139] although the retardation effect with the studied trithiocarbonate is significantly lower than those studied using dithiobenzoate RAFT agents.[34] In the RAFT mechanism shown in Figure 2.9, the retardation has been attributed to either: (a) slow fragmentation of the intermediate radicals (**2**, **4**),[140] or (b) irreversible termination of these intermediate radicals.[141] The intermediates **2** and/or **4** have been observed by electronic spin resonance spectroscopy (ESR), however these intermediates were not detectable during MMA polymerization or in polymerizations with trithiocarbonates as the RAFT agent, attributed to the high rate of fragmentation (high k_β and low equilibrium constant, $K = k_{ad}/k_\beta$) and short lifetime of these intermediates during polymerization.[34] Hence, it is likely that irreversible termination is responsible for the retardation rate.
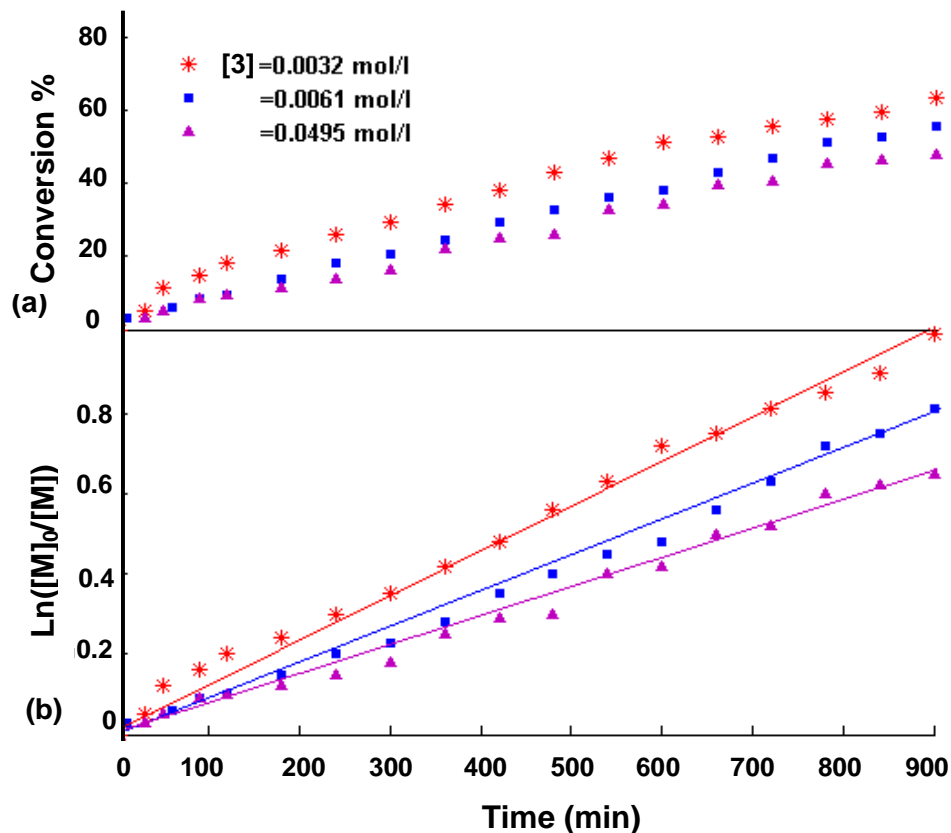
Figure 5. 5 (a) Conversion-time and (b) First-order kinetic plots for the RAFT polymerization of MMA (6.55 M in THF) at 75°C with AIBN initiator at different concentration of RAFT agent (3).

5.4.3. Organic/Water partitioning study

The n-TiO$_2$ both before and after functionalization with the RAFT agent (**3**) was studied by organic phase/water partitioning experiments. As one would expect after functionalization by an organic group, n-TiO$_2$'s hydrophilicity changes. Figure 5.6 shows two vials containing equal volumes of MMA and water, and equal masses of non-functionalized titania (Figure 5.6a) and functionalized titania (Figure 5.6b). The functionalized titania exhibited good dispersion in MMA, while the non-functionalized one partitioned into the water phase, indicating the success of the incorporation of the organic group to the titania surface.
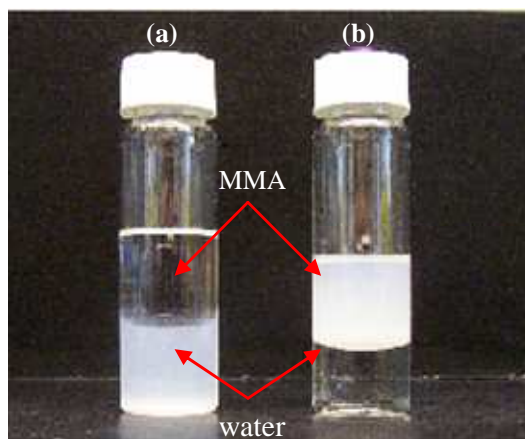
Figure 5. 6 In the vials, the upper layer is Methyl methacrylate and the lower layer is water phase. (a) The non-functionalized n-TiO₂ is well dispersed in the water phase, (b) while the functionalized n-TiO₂ is suspended in the organic phase.

5.4.4. FTIR and XPS Study

In order to verify the functionalization of n-TiO$_2$ as well as the formation of the nanocomposite, FTIR analysis is conducted. The spectrum of the RAFT agent (**3**) in Figure 5.7a exhibits peaks at 1703 cm^{-1} (carboxylic group), 1400 -1460 cm^{-1} (alkane groups), and no obvious peak in the region from 1470 to 1650 cm^{-1}.   In Figure 5.7b for the RAFT functionalized n-TiO$_2$, new peaks at 1563 and 1646 cm^{-1} are assigned to the bridging or chelating bidentate coordination between titanium atoms and the carboxyl group of the RAFT agent. The absence of a peak at 1703 cm^{-1} indicates that there is no free RAFT agent after functionalization. The FTIR spectra confirm that the TiO$_2$ nanoparticles were successfully functionalized with the carboxylic group of the RAFT agent.
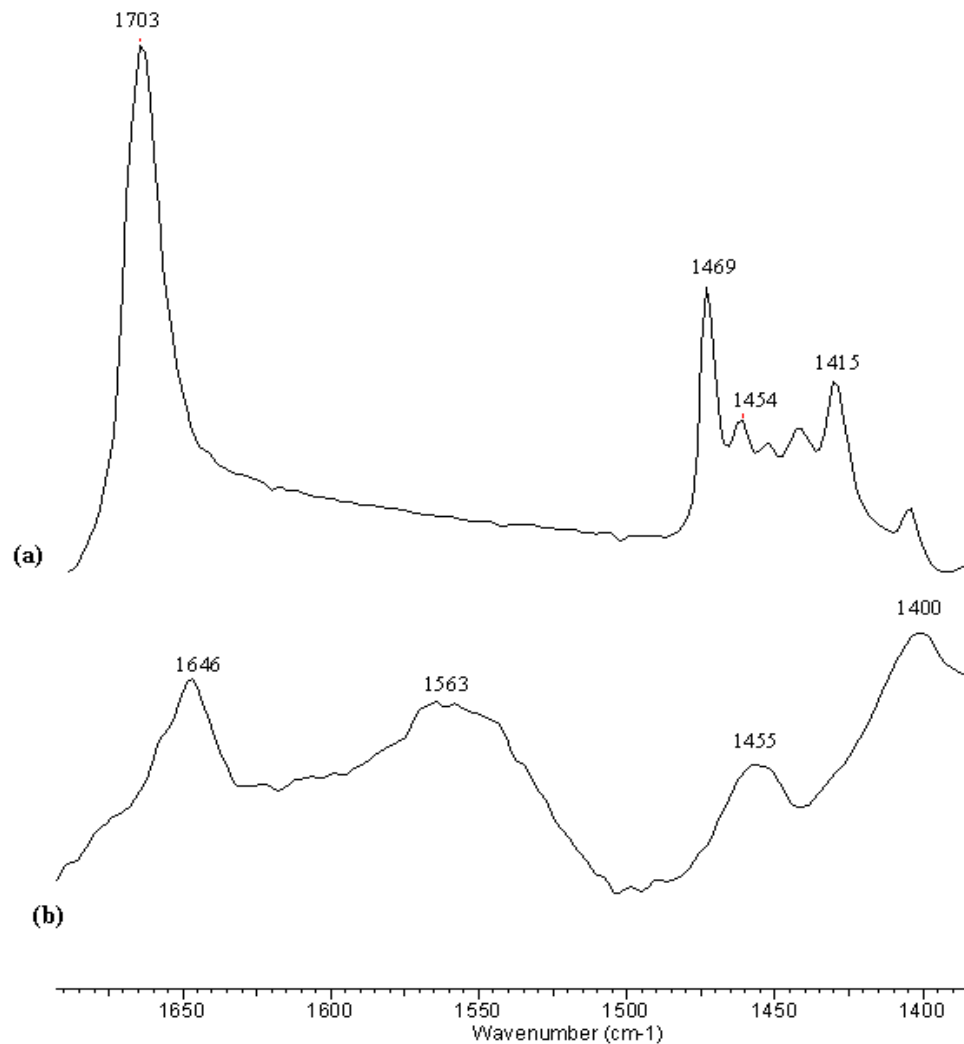
Figure 5. 7 FT-IR spectra of (a) the RAFT agent (3), and (b) the functionalized n-TiO$_2$.

In addition, the chemical composition of the RAFT agent functionalized onto the n-TiO$_2$ surface was also examined using the XPS technique. The XPS full spectrum of the functionalized TiO$_2$ illustrates the existence of S, N, C elements beside O and Ti (Figure 5.8a). The content of S is about 0.2% with respect to Ti.

High resolution XPS scan of O 1s region (Figure 5.8b) shows peaks at ~ 529.9 eV, 531.1 eV and 532 eV which are assigned to the O atom in TiO$_2$, the carbonyl group and OH (hydroxyl) groups, respectively.[142] XPS record of the C1s region (Figure 5.8c)

represents three major sources of carbon peaks. The first peak at ~284.8 eV binding energy corresponds to the C-C bond (alkyl group) of the RAFT agent while the appearance of the second peak at ~286.3 eV can be assigned to the CN bond of the RAFT agent.[143] The third peak at ~ 288.4 eV is attributed to the carbonyl group of the RAFT agent.[144]
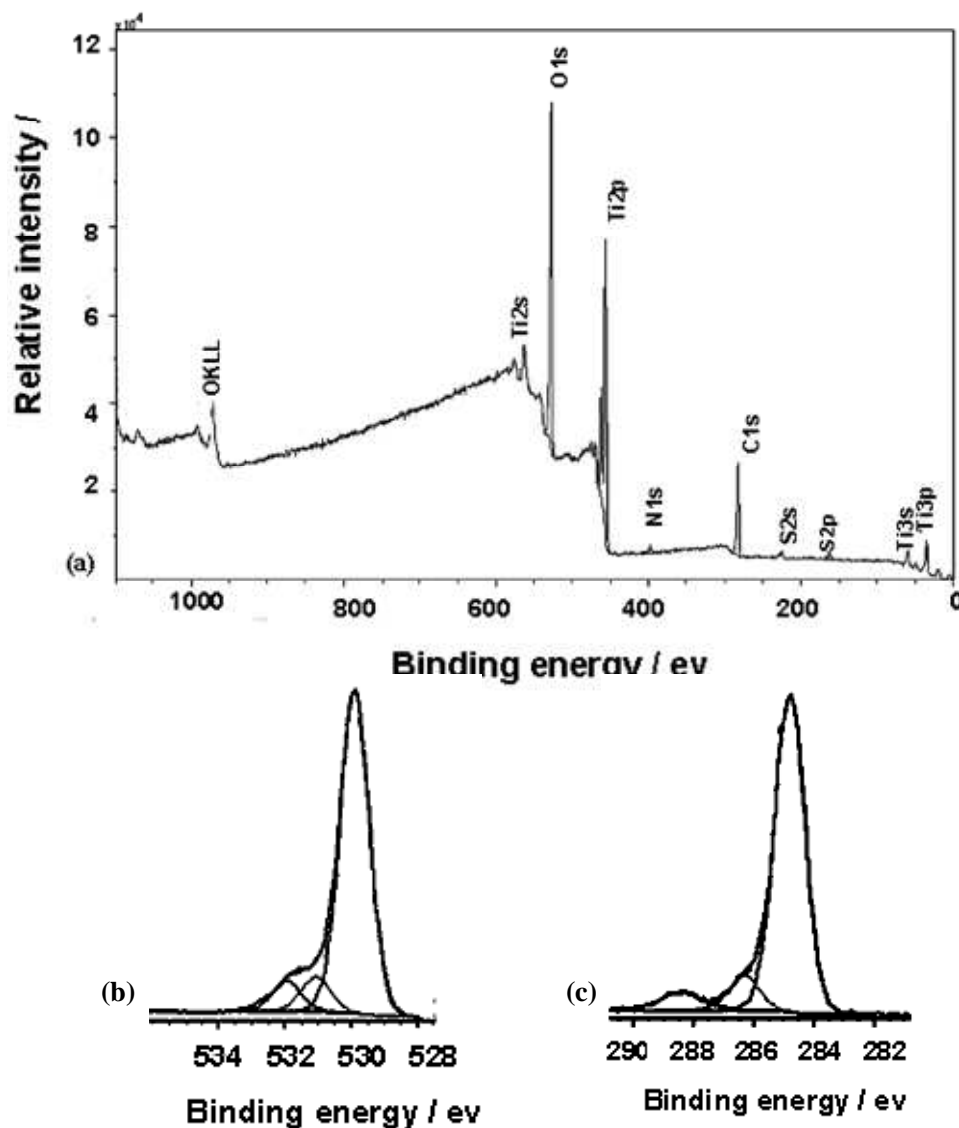
Figure 5. 8 (a) XPS full scan spectrum of the RAFT functionalized TiO$_2$, high resolution spectrum of (b) O, and (c) C.

5.4.5. Electron microscopy

In order to examine the microstructures and nanofiller distribution within the polymer, SEM and TEM electron microscopy were used. SEM was used to study the morphology of n-TiO$_2$ before and after living polymerization. Figure 5.9a shows the SEM image of the commercial n-TiO$_2$ consisting of agglomerated spherical particles, whereas Figure 5.9b shows the n-TiO$_2$ after "grafting from" polymerization using MMA monomer in which many particles with a diameter of ca. 100-1000 nm can be observed. These are attributed to the polymer chains that can only grow from the RAFT agent attached to the n-TiO$_2$ surface as the materials were re-dissolved in THF and re-precipitated by centrifugation at 7000 rpm for 10 min, resulting in the formation of n-TiO$_2$/PMMA nanocomposite. These nanocomposites were also examined with TEM (Figure 5.9c-d), which show well-dispersed n-TiO$_2$ at high magnification. Some agglomeration of n-TiO$_2$ still exists, although the generally excellent separation of n-TiO$_2$ particles is attributed to the growing of "grafting from" PMMA polymer, which separates the previously agglomerated TiO$_2$ nanoparticles.
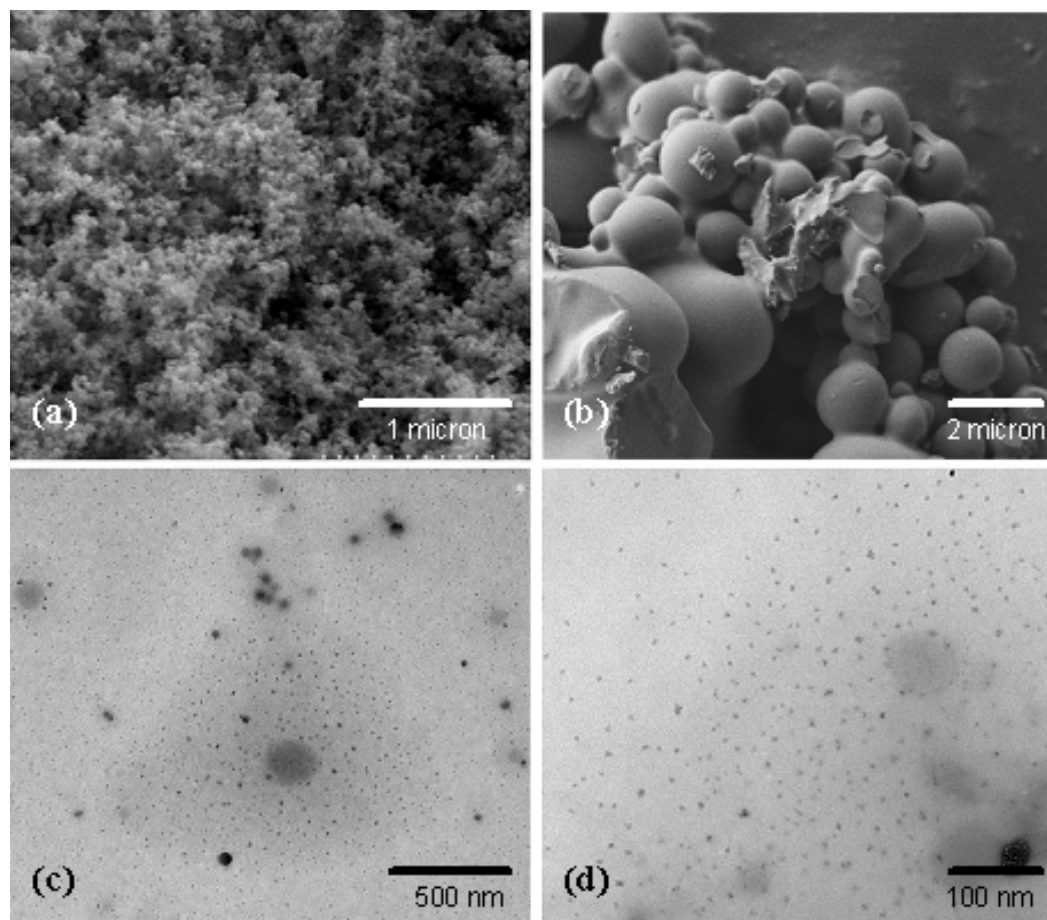
Figure 5. 9 SEM of the (a) non-functionalized n-TiO$_2$, (b) n-TiO$_2$/PMMA composite, and (c-d) TEM of the n-TiO$_2$/PMMA at different magnification.

5.4.6. DSC and TGA

The functionalized n-TiO$_2$, n-TiO$_2$/PMMA nanocomposites, and cleaved n-TiO$_2$ were dried and subjected to dynamic scanning calorimetry (DSC) and thermal gravimetric analysis. An enhanced thermal stability of the n-TiO$_2$-PMMA nanocomposites was observed using both DSC and TGA. As shown in Table 5.1, the unfilled PMMA exhibited a glass transition temperature at 106 °C, while the PMMA-titania nanocomposites exhibited elevated T$_g$ values ranging from 125-133 °C. Strong interfacial bonding between the functionalized nanoparticles and polymer chains leads to an increase of the T$_g$ of composites by impeding the chain flexibility.[136] However, upon

increasing the time of polymerization; the length of the polymer chains grown from the nanoparticles increases, causing more flexible polymer chains, and a decrease of the T_g of the nanocomposites.

Table 5. 1 TGA and DSC Results of RAFT Polymerizations at Different Reaction Times Sample.

Sample	Time	T_g (^{o}C)	Fraction of grafted (wt %)	Fraction of un-grafted polymer (wt%)
PMMA	_	106	_	_
TiO$_2$-RAFT agent	_	_	4.1	_
TiO$_2$-RAFT agent PMMA	1.5	133	13.9	28
TiO$_2$-RAFT agent-PMMA	9	129	26.1	31
TiO$_2$-RAFT agent-PMMA	15	125	58.7	35

In addition to DSC, the functionalized n-TiO$_2$ and n-TiO$_2$/PMMA nanocomposites were dried and subjected to TGA (Figure 5.10). For the n-TiO$_2$/PMMA sample, the first weight loss region below ~200°C can be assigned to evaporation of the entrapped water or solvent from the surface of n-TiO$_2$, while the second region (200-600°C) can be attributed to the decomposition of PMMA grafted from n-TiO$_2$ particles. Higher fractions of PMMA were formed as the polymerization time increased (shown quantitatively in Table 5.1); indicating the successful graft polymerization of MMA from the RAFT functionalized n-TiO$_2$. After cleaving under acidic conditions for 24 hours, TGA analysis of the n-TiO$_2$ fraction showed 1.5-2% weight loss, indicating that more

than 98% of the polymer chains were cleaved from the n-TiO$_2$ under the explored experimental conditions.
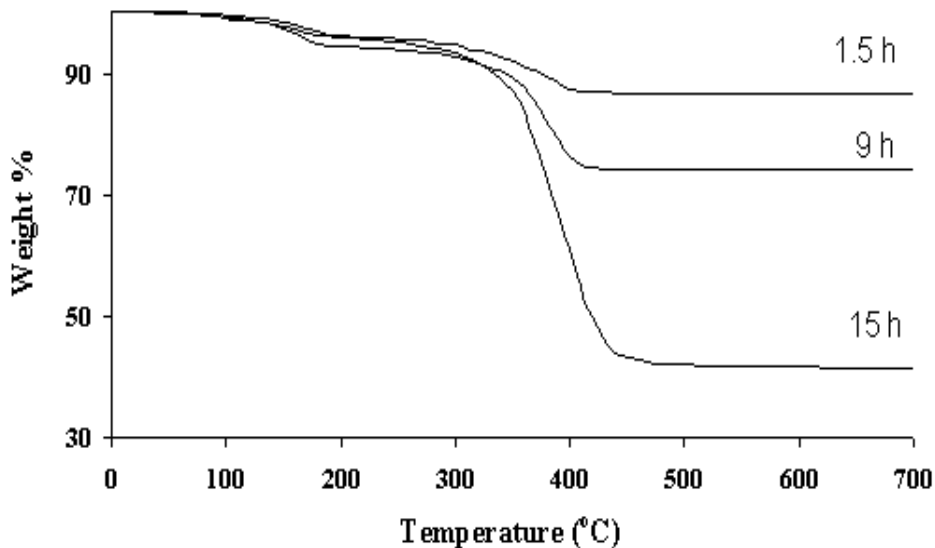
Figure 5. 10 TGA curves of the n-TiO$_2$/PMMA at different polymerization times.

5.4.7. Kinetics of Surface Graft Polymerization of MMA on the n-TiO$_2$

To investigate the kinetics of MMA polymerization from the direct attachment of RAFT agent (**3**) to the n-TiO$_2$ surface, and to determine if the polymerizations were still "living", two different surface densities of RAFT agents were prepared by varying the ratio of RAFT agent to n-TiO$_2$ (Figure 5.11). The amount of RAFT agent anchored to the nanoparticles was determined by TGA (5.4% and 4.1%, i.e. 134μmol/g and 102μmol/g, which is equivalent to 1.4 and 1.0 #RAFT agents/nm^2, respectively) using the procedure of Li *et al.* [107] while assuming the density of RAFT agent/n-TiO$_2$ is comparable with the density of n-TiO$_2$ (4.26 g/cm^3) (for more detailed description see Appendix 4).

High surface density   Low surface density
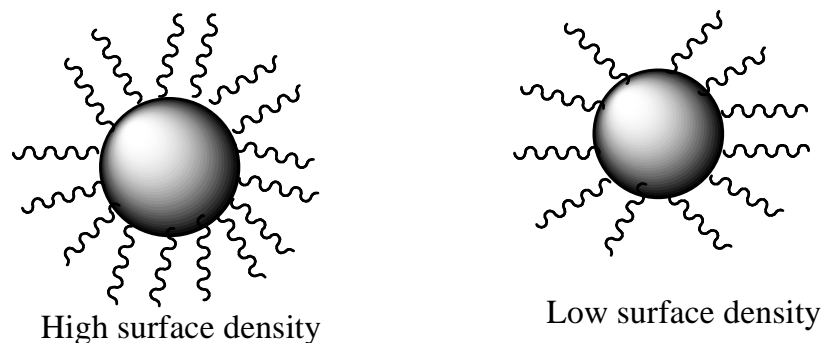
Figure 5. 11 High and Low surface density schematic.

The results of the kinetic studies for graft polymerizations of MMA from n-TiO$_2$ with these two different surface densities of RAFT agent are shown in Figure 5.12. As described by Eq.5.3, if we plot $\ln\left(\dfrac{[M]_0}{[M]}\right)$ vs. time to give a straight line we have evidence of constant concentration of active species P_n, indicating that the polymerization kinetics are first-order in regards to monomer concentration.

When comparing Figure 5.12 to Figure 5.5, it is clear that the rates of polymerization from n-TiO$_2$ were considerably lower than those found in solution. In explanation, these lower rates can be attributed to the high local concentration of functionalized RAFT agent on the surface of n-TiO$_2$. For the 102 μmol/g and 134 μmol/g prepared samples of anchored RAFT agent, the concentration of RAFT agent in the volume of the surface layer extending 1 nm from the surface of n-TiO$_2$ was calculated to be 0.30 M and 0.41 M, respectively, which is significantly higher than the RAFT agent concentration in solution (0.32 x 10^{-2} M). In the standard RAFT mechanism, radicals are initiated by conventional initiators which attack the C=S bond of the RAFT agent anchored to the surface, and homolytic cleavage of the C-S bond leaves the incoming chain capped with the dithioester containing the Z group (see Figure 4.2). The radical on

97

the surface can then propagate by transferring monomer from solution, with chain transfer occurring with the polymeric RAFT agent. In addition, Figure 5.12 shows the inhibition rate for both high and low surface density; no polymerization for almost 20 min. A similar phenomenon of rate retardation has been observed with growing styrene, methyl methacrylate, and n-butyl acrylate polymer chains from silica nanoparticles, which was attributed to the high local density of RAFT agent on the surface of silica.[107]
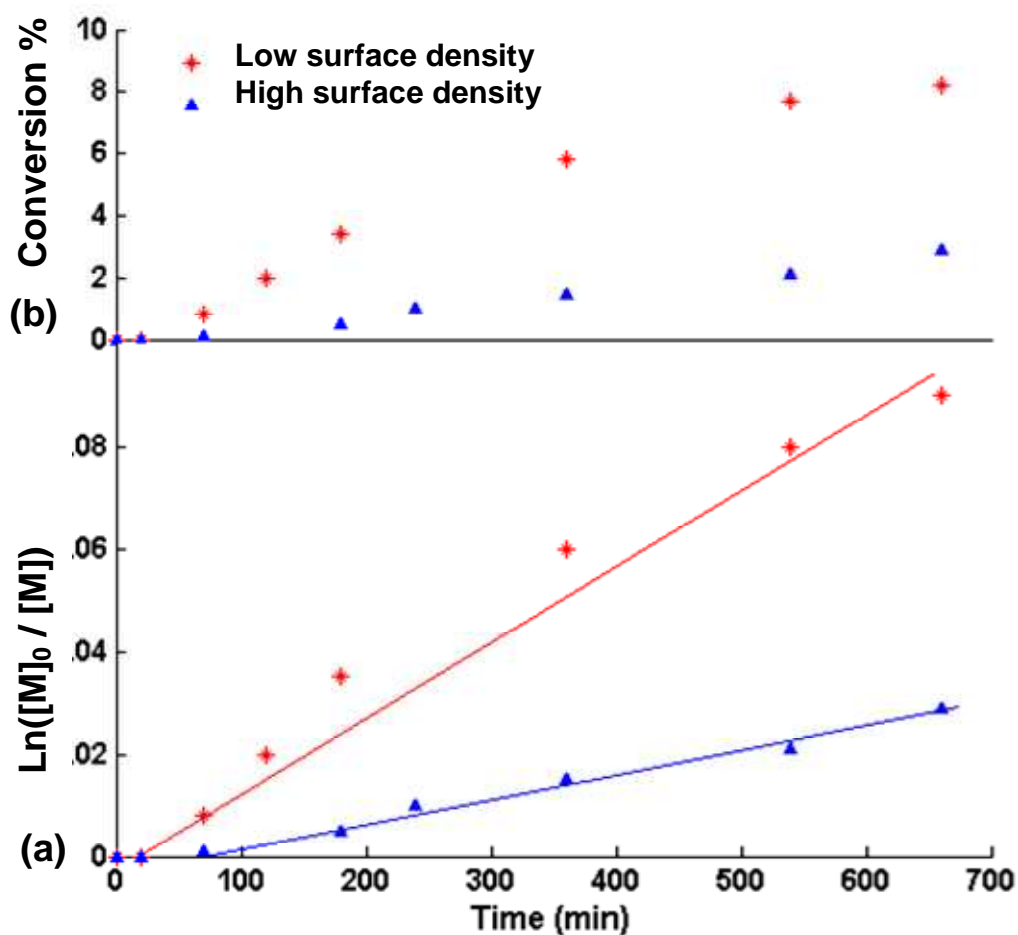
Figure 5. 12 (a) Conversion-time, and (b) First-order kinetic plots for the graft polymerization of MMA (655 M in THF) at 80°C with AIBN initiator mediated with functionalized n-TiO₂; low surface density (102 μ mol/g) and high surface density(134 μ mol/g).

Figure 5.13 shows the living character of the direct RAFT attachment on growing PMMA from the modified surface of n-TiO$_2$. Figure 5.13a summarizes how M_n (experimental and theoretical (Eq.5.7)) and the PDI's change with conversion, while Figure 5.13b shows the GPC elution profiles of the PMMA obtained after cleaving from the nanocomposite. It is clear that this direct coordination method for attaching the RAFT agent onto the n-TiO$_2$ surface provides a living polymerization with reasonably high molecular weights following first order kinetics. However, the PDIs were higher than those obtained from solution, possibly due to the heterogeneous surface of the n-TiO$_2$ and incomplete separation of nanoparticles.
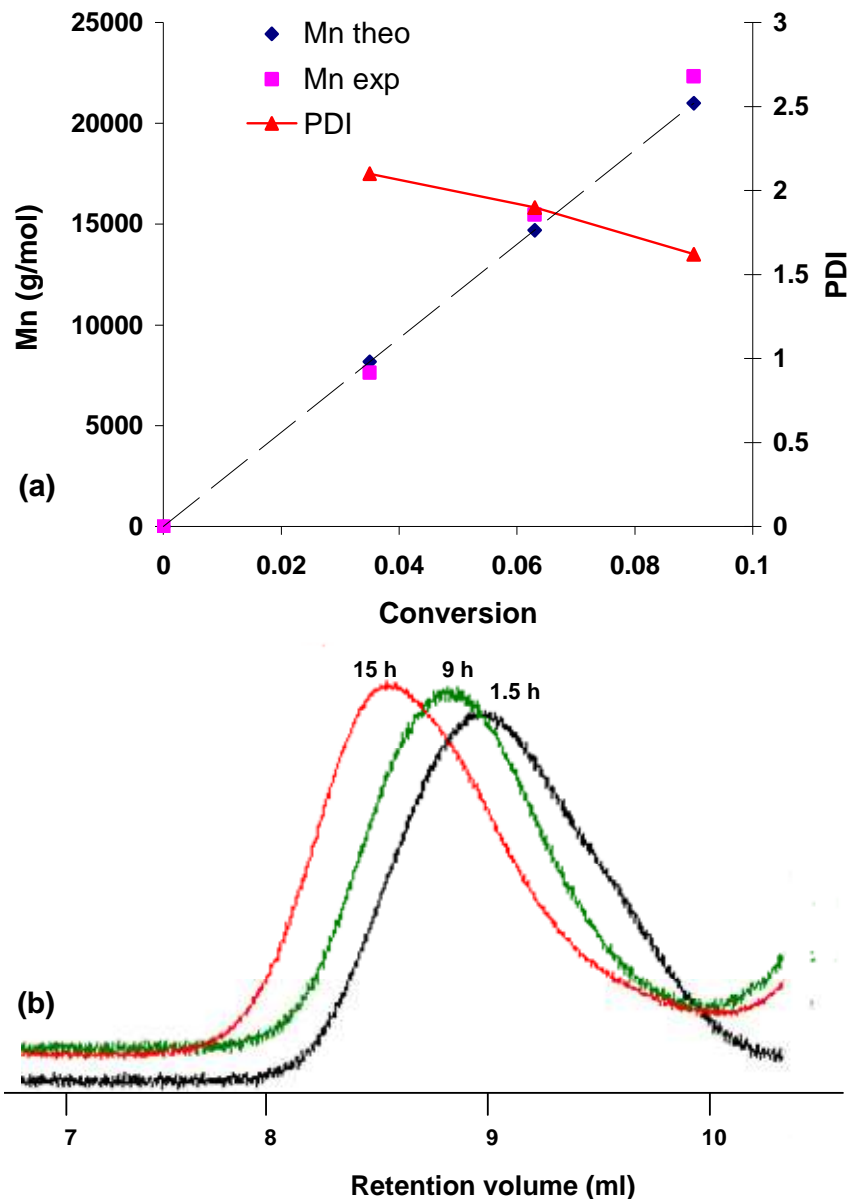
Figure 5. 13 (a) Molecular weight and PDI/conversion data for graft polymerization of MMA from n-TiO$_2$; Mn calculated with Eq. 5.7 (----), and (b) GPC elution profiles for graft polymerization of PMMA from n-TiO$_2$ surface for 1.5h (Mn = 7,629 g/mol, PDI= 2.1), 9 h (Mn = 15,471 g/mol, PDI= 1.9), 15h (M$_n$ = 22,320 g/mol, PDl = 1.62), via RAFT at 75-78°C and using low surface density (102 μ mol/g).

5.5. Conclusions

This research demonstrated that living polymerization initialized by AIBN in the solution and transferred to the functional groups on n-TiO$_2$ surfaces is promising to synthesize hybrid materials with an excellent dispersion of the nanofillers in the matrix. TiO$_2$ nanoparticles were functionalized by direct coordination with a RAFT agent, followed by living "grafting-from" polymerization using methyl methacrylate as the monomer, with resulting n-TiO$_2$/PMMA hybrid materials being synthesized. The coordination of the carboxylic group of the RAFT agent to the TiO$_2$ nanofiller was confirmed by IR spectra, XPS, and partitioning experiments in monomer-water bilayers. Electron microscopy images revealed the growth of the "graft-from" polymers around n-TiO$_2$, and the nanofillers were well separated and distributed throughout the polymer matrix. The effect of the concentration of RAFT agent on the rate of polymerization of MMA was investigated, with the experimental and theoretical molecular weights of PMMA from solution and graft polymerization compared. GPC results of cleaved polymer after various reaction times showed that the polymerization was still living, even after the RAFT agent was directly coordinated to n-TiO$_2$. The kinetics of graft polymerization of MMA from the surface of n-TiO$_2$ was studied with two different surface densities, and it was found that the rate of reaction decreased with increasing surface density of RAFT agent anchored to the nanoparticles.

CHAPTER 6

SYNTHESIS OF TiO_2/POLYMER NANOCOMPOSITES IN SUPERCRITICAL CO_2 VIA RAFT POLYMERIZATION

In this chapter polymer chains of PMMA were grown from n-TiO$_2$ by the RAFT polymerization process using the green solvent, supercritical carbon dioxide (scCO$_2$). The RAFT agent (**3**), 4-cyano-4-(dodecylsulf- anylthiocarbonyl) sulfanyl pentanoic acid, with an available carboxyl group was used to anchor onto the n-TiO$_2$ surface, with the S=C(SC$_{12}$H$_{25}$) moiety used for subsequent RAFT polymerization of MMA to form n-TiO$_2$/PMMA nanocomposites. The mechanism and kinetics of MMA polymerization from both solution and ''grafted from'' n-TiO$_2$ is investigated in scCO$_2$. The rate of polymerization and molecular weights at different pressures in scCO$_2$ and in high pressurized organic solvent (THF) were compared.

6.1.   Introduction

Recent progress in living radical/controlled polymerization (LCP) such as atom transfer radical polymerization (ATRP), stable free-radical polymerization (SFRP), and reversible addition fragmentation chain-transfer (RAFT) polymerization has opened new routes for the synthesis of polymers with controlled molecular weights, well-defined end-groups, and narrow polydispersities. As mentioned in section 2.3, "livingness" in living controlled polymerization is achieved by a balance between propagating and termination that maintains low concentrations of free-radicals until the rate of radical termination becomes negligibly small compared to that of propagation. The rate of reaction, R$_p$, in a living controlled polymerization can be calculated by Eq.5.2:

$$R_p = -\frac{d[M]}{dt} = k_p \cdot [P_n] \cdot [M] \qquad (5.2)$$

where $[P_n]$ is the concentration of propagating radicals, $[M]$ is the monomer concentration, and k_p is the rate coefficient for the propagation.

To increase the rate of reaction, R_p, one of the three parameters on the right-hand side of Eq.5.2 has to be increased. However, there are some limitations for increasing $[M]$ and $[P_n]$, such as the concentration of monomer is limited by the liquid bulk density, and in a living polymerization, $[P_n]$ has to be kept low throughout the polymerization to favor propagation vs. termination. Another parameter for accelerating the polymerization in Eq.5.2 is to increase the propagation rate coefficient, k_p, which is influenced by the nature of the monomer, and the solvent properties. As well, k_p can also be increased by increasing the temperature or pressure of the reaction media.[145]

Supercritical carbon dioxide (scCO$_2$) has emerged as a viable "green" alternative to organic solvents for several applications such as polymerizations,[146] and nanotechnology, as CO$_2$ is abundant, inexpensive, non-flammable, and non-toxic.[147] At supercritical conditions ($T_c = 31.1°C$, $P_c = 7.38MPa$), CO$_2$ has desirable properties of both liquids and gases including a liquid-like density, a gas-like diffusivity, and a "zero" surface tension.[148] Its liquid-like solubility parameter and density are easily "tunable" by varying the pressure and/or temperature according to the particular polymerization conditions required. Its zero surface tension and gas-like viscosity help facilitate transport, limiting diffusion control of the polymerization kinetics. In addition, the separation of CO$_2$ from the liquid or solid polymer product can be obtained simply by depressurizing.

Previously, DeSimone and coworkers have shown that scCO$_2$ is a promising alternative medium for free-radical, cationic, and step-growth polymerizations, and continuous processes.[147, 149, 150] Living radical polymerization has also been examined as McHale *et al.* polymerized styrene in scCO$_2$ via NMP,[151] Xia *et al.* polymerized

fluorinated acrylates in $scCO_2$ via ATRP,[152] while recently Gregory *et al.* polymerized methyl methacrylate via RAFT in $scCO_2$.[153] In addition, $scCO_2$ has been already used in many nanostructure processes, such as forming ZrO_2 modified TiO_2 nanotubes,[154] polymer nanocomposites,[155] filling nanotubes,[156] and functionalization of mesoporous silica.[157]

In this chapter, we report the first example of n-TiO_2/PMMA formation via RAFT polymerization in $scCO_2$ which provided significantly higher rates of polymerization (R_p's) and M_n's that increased with pressure and were significantly higher over solution polymerization, both at ambient and pressurized conditions. The bifunctional RAFT agent (**3**), was used to directly coordinate to n-TiO_2, while the $S=C(SC_{12}H_{25})$ moiety was used for subsequent RAFT polymerization of MMA in $scCO_2$.

6.2. Experimental

6.2.1. Materials

Titania nanospherical particles (99.5%, Sigma-Aldrich, avg. part. size D= 23.2 nm), 2,2′-Azobis (2-methylpropionitrile) (AIBN) initiator (Toronto Research Company), were used as received. Methyl methacrylate monomer (MMA) (99%, Sigma-Aldrich, inhibited with 200 ppm BHT) was passed through an inhibitor removal column before use. The RAFT agent 4-cyano-4-(dodecylsulfanylthiocarbonyl) sulfanyl pentanoic acid (**3**) was prepared as described elsewhere[126](for more detailed description see Appendix 3). High purity CO_2 (from BOC Gases, 99.99% with dip-tube) was used as received.

6.2.2. Functionalization of n-TiO_2

n-TiO_2 was functionalized with RAFT agent (**3**) based on the procedure described in section 4.2.2.

6.2.3. Synthesis of n-TiO$_2$/methyl methacrylate composites via RAFT in scCO$_2$ and high pressurized THF

Synthesis was conducted in a 100 mL high-pressure stainless steel autoclave (Parr 4842) coupled with a digital pressure transducer. The stirring speed was controlled at 171 rpm. In a typical polymerization, 1.2 g of functionalized n-TiO$_2$ and 0.006 g AIBN were first dispersed in 25 mL methyl methacrylate with the aid of sonication. Then the solution was transferred into the reactor, purging with a flow of argon, then pumping high purity CO$_2$ (from BOC Gases, 99.99% with dip-tube) into the autoclave by means of a syringe pump (Isco 260D). The reactor was then heated to 70°C, and pressurized to the desired pressure. In the case of using pressurized THF, 1.2 g of functionalized TiO$_2$, 25 mL methyl methacrylate, and 0.006 g AIBN were first dispersed in 40 mL THF. After transferring into the reactor, the solution was heated to 70°C and pressurized to 3600 psi using high purity N$_2$. After the reaction, CO$_2$ and/or N$_2$ were carefully vented leaving the formed nanocomposite sample in the autoclave.

As polymers may potentially grow in solution and not on the n-TiO$_2$ surface, the products were dissolved in THF to remove any PMMA homopolymer and/or un-reacted monomers using centrifugation at 7000 rpm for 10 min. The solid product was dried overnight under vacuum at 50 ^{o}C.

6.2.4. Cleaving Grafted Polymer from Particles

Grafted PMMA from n-TiO$_2$ nanoparticles was cleaved based on the procedure described in section 4.2.4.

6.3. Characterization

The molecular weight and PDIs of PMMA were measured by gel permeation chromatography (GPC) with a Viscotek instrument using triple detectors (RI, LS, and V) referenced to PMMA standards (1 ml/min, at 30 $^{\circ}$C). FT-IR spectra were collected using both KBr pellet on a Bruker IFS 55 FTIR instrument attached with a MCT detector, and an *in-situ* Fourier transform infrared monitoring of the solution concentration in the stirred 100 mL high-pressure autoclave performed using a high-pressure immersion probe (Sentinel-Mettler Toledo AutoChem). The DiComp ATR probe consists of a diamond wafer, a gold seal and a ZnSe support/focusing element, housed in alloy C-276. The probe was attached to an FT-IR spectrometer (Mettler Toledo AutoChem ReactIR 4000) via a mirrored optical conduit, connected to a computer, supported by ReactIR 2.21 software (MTAC). This system uses a 24-hour HgCdTe (MCT) photoconductive detector. The light source is a glow bar from which the interferometer analyzes the spectral region from 650 to 4000 cm^{-1}. The beam splitter inside the RIR4000 is ZnSe. The polymerization at 3000 psi and 4200 psi were carried out similarly. Scanning electron microscopy (SEM) images was recorded using a LEO 1530 instrument without gold coating at 10 kV, and thermogravimetric analysis were performed using a Mettler TGA Q500 at a heating rate of 10 °C/min under a nitrogen atmosphere. Dynamic light scattering was performed using a Malvern Zeta Sizer 3000HSA at room temperature.

6.4. Results and Discussion

The general synthesis route for synthesis of n-TiO$_2$/PMMA in scCO$_2$ via RAFT is described in Figure 6.1.
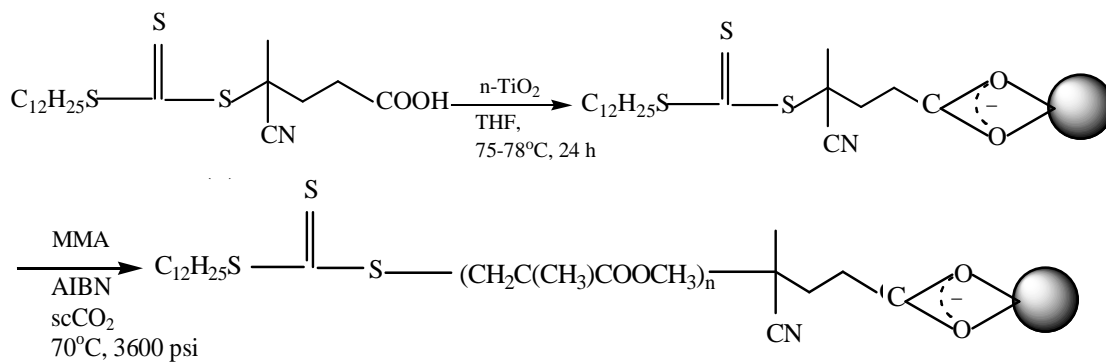
Figure 6. 1 Functionalization of n-TiO$_2$ using RAFT agent (3) and formation of n-TiO$_2$/ PMMA nanocomposite in scCO$_2$.

6.4.1. FTIR and XPS Study

Functionalization of n-TiO$_2$ with RAFT agent (**3**) was verified by FTIR and XPS analysis as reported in Ch.5.[62]

6.4.2. Solubility / Dispersity in scCO$_2$

In a typical experiment, RAFT agent (**3**) was placed in the view cell, followed by addition of CO$_2$ up to the desired temperature and pressure. A magnetic stirrer system was used for mixing the reaction mixture. The yellow transparent homogeneous phase formed at the specified temperature and pressure (Figure 6.2a), indicating that RAFT agent (**3**) is soluble in scCO$_2$. To show the behavior of nanoparticles in n-TiO$_2$/PMMA in scCO$_2$ media, the nanocomposite was also synthesized in a view cell reactor. As Figure 6.2b shows, a single opaque phase is observed in which the nanoparticles are dispersed homogeneously in scCO$_2$.
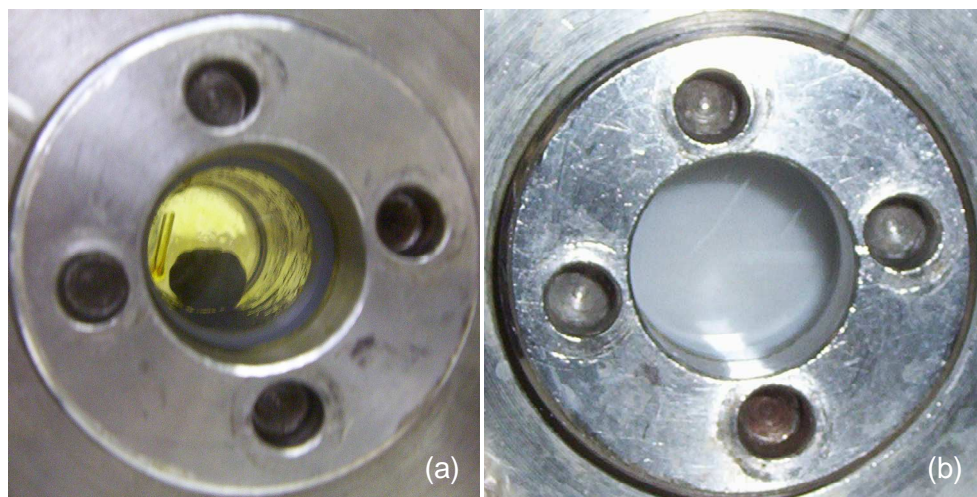
Figure 6. 2 Photographs following the reaction in the view cell: (a) RAFT agent (3); (b) n-TiO$_2$/ PMMA formation at 70 ^{o}C and 3600 psi in scCO$_2$.

6.4.3. Electron microscopy

SEM was used to study the morphology of the n-TiO$_2$ composites after polymerization in scCO$_2$. Figure 6.3a presents non-functionalized n-TiO$_2$, while Figure 6.3b-d shows the n-TiO$_2$ after "grafting from" polymerization with MMA at different times in scCO$_2$, but at the same magnification. As one can see, the diameter of particles is increasing with time. These are attributed to the polymer chains that can only grow from the RAFT agent attached to the n-TiO$_2$ surface, resulting in the formation of n-TiO$_2$/PMMA nanocomposite.
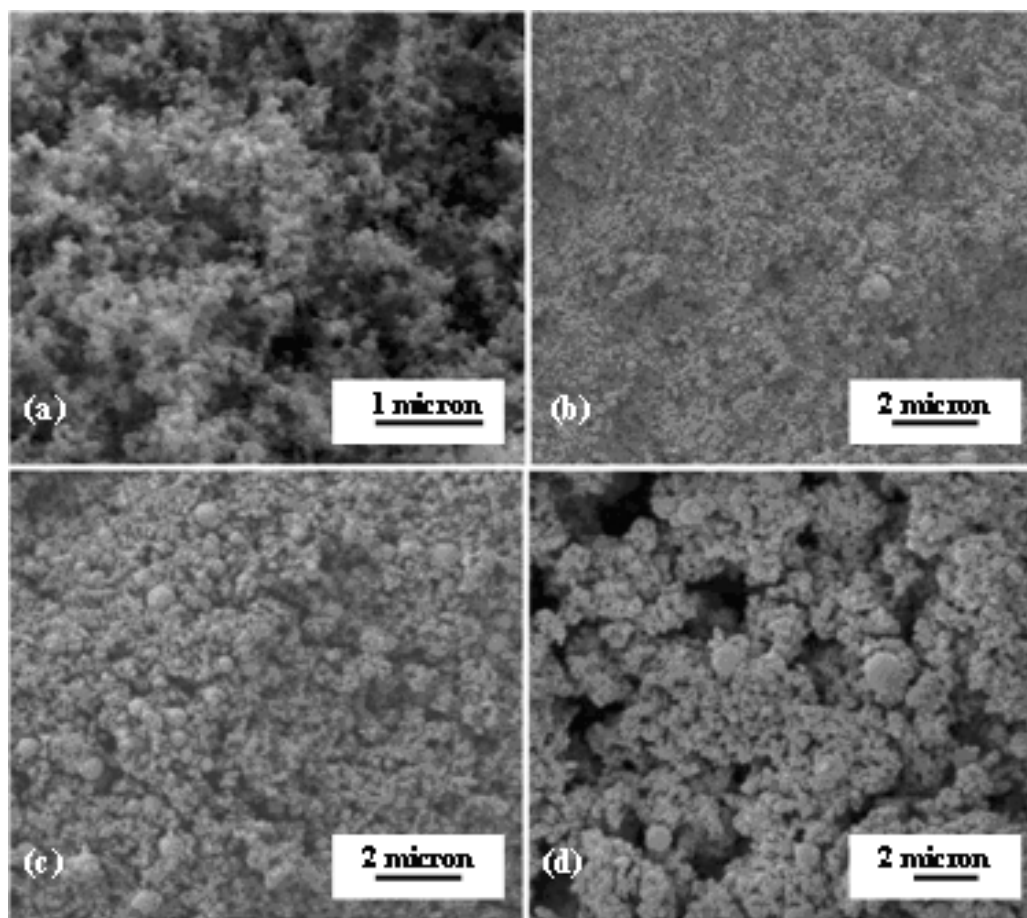
Figure 6. 3 SEM of (a) non-functionalized n-TiO$_2$, and of n-TiO$_2$/PMMA composite at 70 ^{o}C and 3600 psi in scCO$_2$ after (b) 5, (c) 15, and (d) 24 hour.

6.4.4. TGA analysis

The n-TiO$_2$/PMMA nanocomposites were dried and subjected to TGA (Figure 6.4). To investigate the livingness of n-TiO$_2$/PMMA, the samples prepared at 3600 psig were used. The TGA results show two obvious regions when the temperature was increased: the first region started from 30 °C and ended at 200 °C with a relatively small slope (due to evaporation of the entrapped water or solvent); while the second region started at 250 °C and ended at 450 °C with a large slope indicating more weight loss, and decomposition of some organic groups of the PMMA and RAFT agent components. It becomes flat again after the temperature increasing over 450 °C. Higher fractions of

110

PMMA were formed as the polymerization time increased; indicating the successful graft polymerization in $scCO_2$ of MMA from the RAFT functionalized n-TiO$_2$. The weight loss of n-TiO$_2$/PMMA at the region of 250-450 $^{\circ}$C gives further evidence regarding the content and species of polymer layers grafted onto n-TiO$_2$, since the polymer and TiO$_2$ components have distinct thermal stabilities.[136, 158]
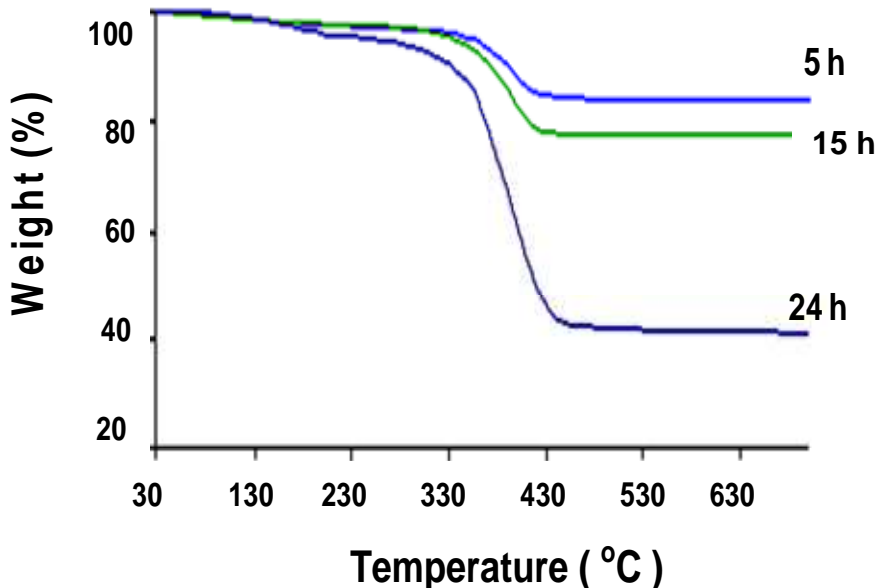
Figure 6. 4 TGA curves of the n-TIO$_2$/PMMA nanocomposites formed at 70 $^{\circ}$C and 3600 psi in scCO$_2$ at different polymerization times.

6.4.5. Molecular Weight Determination of Cleaved PMMA

As described previously, in an ideal living polymerization, all chains are initiated at the beginning of the reaction, grow at the same rate, and proceed with no termination step. As a result, the molecular weights increase linearly with conversion and the PDIs can be very narrow.[32] In order to determine whether the 'grafting from' polymerization was still living in scCO$_2$ when the RAFT agent had been attached to the n-TiO$_2$, the PMMA was cleaved after various polymerization times using acidic conditions based on the procedure described in Ch.4. The GPC results are presented in Table 6.1, which show

111

that the number average molecular weight increased directly with reaction time for all experimental conditions. As the $scCO_2$ pressure increased, the M_n's directly increased with pressure and significantly higher M_n's were obtained in $scCO_2$ compared to those synthesized in solution in THF at ambient pressure and at 3600 psi, pressurized using N_2. The PDIs of the cleaved PMMA polymerized in $scCO_2$ are similar to those obtained in THF (section 5.4.7). Table 6.1 also shows the monomer conversions that were obtained for the graft polymerizations of MMA from n-TiO$_2$ at the different pressures in $scCO_2$ and high pressurized THF. The conversions were determined by following the *in-situ* FTIR peaks (Figure 6.5). The decrease in height of the peak at 1638cm^{-1} (due to C=C stretching vibration) indicates the conversion of methyl methacrylate monomer to poly methyl methacrylate.
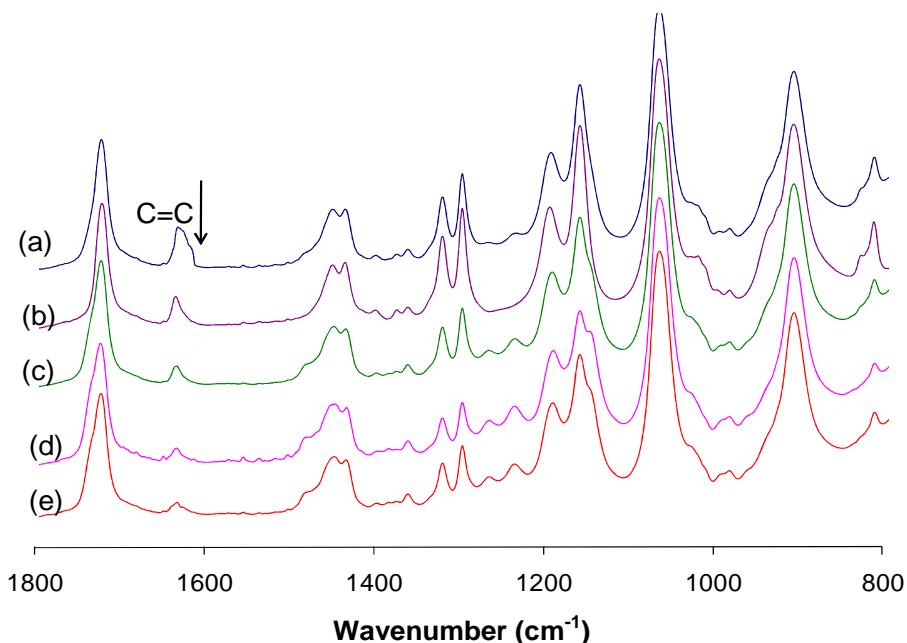
Figure 6. 5 *In-situ* **FTIR measurement of RAFT polymerization of the n-TiO$_2$/PMMA composites synthesized at 70 ^{o}C and 3600 psi in scCO$_2$. Reaction time: (a) 5 min; (b) 30 min; (c) 300 min; (d) 900 min; (e) 1440 min.**

Table 6. 1 Molecular weights, PDIs, and conversions of cleaved PMMA at different reaction times and different pressures. The speed of stirrer for all cases is 171 rpm except in THF.

Pressure (psi)	Time (h)	M_n (g/mol)	PDI	Conversion (%)
3000	1	-	-	3
	5	14,000	1.3	12
	15	29,000	1.6	20
3600	1	4,800	1.7	4
	5	25,000	1.5	17
	15	34,000	1.4	30
	24	80,000	1.5	60
4200	1	5,800	1.5	7
	5	32,000	1.5	28
	15	78,000	1.3	57
	24	120,000	1.5	70
THF[*]	1.5	7,600	2.1	3
	9	17,500	1.9	8
	15	23,500	1.6	14
THF[**]	5	16,000	1.6	7
	24	40,000	1.7	22

[*]: Ambient pressure, speed of stirrer: 100 rpm

[**]: High pressurized THF to 3600 psi using N_2

Based on the molecular weights summarized in Table 6.1, the rate of addition for each monomer of MMA to the chains of PMMA in the nanocomposite is ~ 1.5-2 per minute. In explanation, this slow rate can be attributed to the high local concentration of RAFT agent on the surface of n- TiO_2 which was determined by TGA (5.4%). In Ch.5, the effect of the concentration was studied which showed that the rate of reaction decreased when increasing the concentration of RAFT agent.[62] However, the molecular weights and PDIs in Table 6.1 are higher than those obtained by Gregory *et al.*[159] who polymerized MMA in $scCO_2$ at 4000 psi and 65 ^oC via the RAFT technique using dithiobenzoate compounds as RAFT agents. As mentioned in Ch.2, the RAFT agent where R = CH_2Ph (e.g. benzyl dithiobenzoate) does not function as a suitable chain-transfer agent in polymerization with methacrylyl propagating radicals, as the benzyl is a poor leaving group with respect to the methacrylyl propagating radical.[74]

6.4.6. Dynamic Light Scattering (DLS)

To more clearly examine the size of the synthesized n-TiO_2/PMMA nanocomposites using $scCO_2$ (at 70 ^oC and 3600 psi), dynamic light scattering (DLS) was utilized. The samples of nanocomposites at different times were dispersed in THF with the aid of sonication. Figure 6.6 shows the particle size evolution of n-TiO_2/PMMA nanocomposites with respect to polymerization time. As the polymerization time increased, the mean particle size of the nanocomposites also increases, which is consistent with the SEM images. The polydispersity index (PI) as well as the intensity of the mean particle size change only slightly, indicating the continuous growth of polymer chains of PMMA with polymerization time, confirming the livingness of polymerization. Chen *et al.* grafted four vinyl monomers, SStNa, NaVBA, DAM, and DEA from the

114

surface of silica via ATRP and they also found that the diameter of SiO_2 in the nanocomposites grew with the polymerization time.[160]
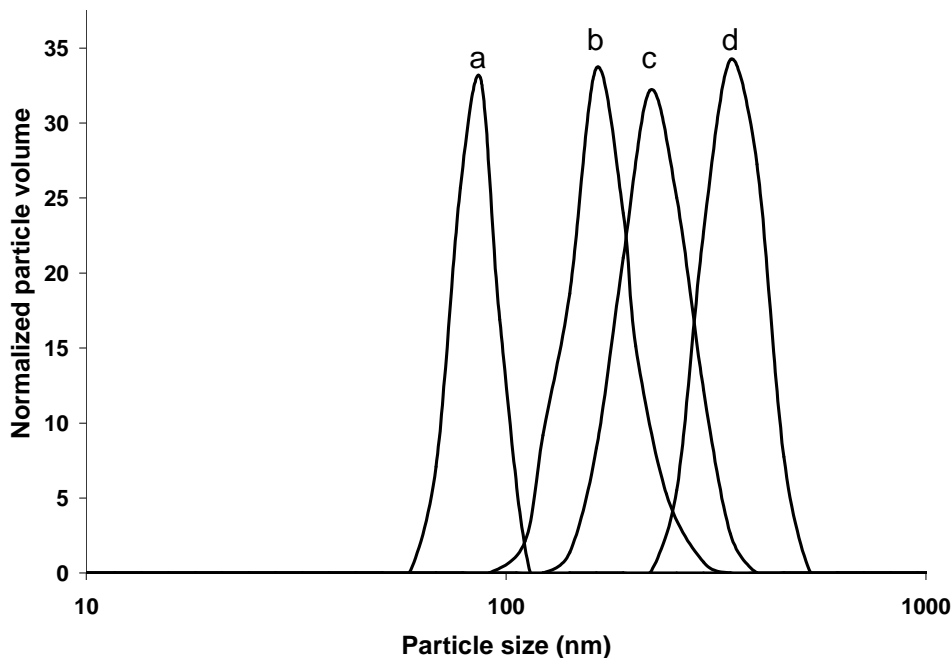
Figure 6. 6 Particle size distribution of the n-TiO$_2$/PMMA composites synthesized at 70 ^{o}C and 3600 psi in scCO$_2$ after (a) 1 hour (D$_{mean}$= 74 nm, PI = 0.31), (b) 5 hour (D$_{mean}$= 165 nm, PI = 0.40), (c) 15 hour (D$_{mean}$= 266 nm, PI = 0.32), and (d) 24 hour (D$_{mean}$= 338 nm, PI = 0.39) by DLS in THF and at room temperature.

6.4.7. Kinetic Analysis of Polymerization

Figure 6.7 plots the monomer conversion vs. time according to Eq.5.5, showing that the kinetics is first-order in regards to monomer consumption for polymerization in scCO$_2$. These plots also show that the rate of reaction increases directly with increasing pressure of scCO$_2$, and that significantly higher conversions were obtained in scCO$_2$ compared to high pressurized THF at constant temperature, initial RAFT agent

concentration, and speed of stirrer. Since more than one phase is present in this heterogeneous media, the movement of monomer from phase to phase must be considered. The R_p in general will incorporate mass transfer terms in addition to the usual chemical kinetic terms, in series. Thus the overall reaction rate can be affected by changing both the mass transfer coefficient and the reaction rate constants. If the two terms are of the same order of magnitude, the mass transfer coefficient affects the overall reaction rate. Referring to Table 6.1, the effect can be inferred by comparing the results obtained in THF at different pressure and speed of stirrer (100 rpm for ambient pressure and 171 rpm for high pressurized), while the other variables such as temperature and initial RAFT agent concentration were set aside at the same level for both experiments. Increasing pressure as well as the speed of stirrer in THF enhanced the conversion slightly. In the liquid phase, however, pressure has low influence on the mass transfer properties whereas the limitations can be reduced at higher speed of stirrer confirming the contribution of mass transfer on R_p in THF. In scCO$_2$, however, it was found that the R_p and conversions are higher than those in THF, which can be attributed to the lower viscosity and surface tension which could eliminate mass transfer limitations. As mentioned in section 6.4.5, the rate of addition for each monomer of MMA to the chains of polymer in n-TiO$_2$/PMMA was calculated to be ~ 1.5-2 per minute; hence the reaction kinetics can be assumed to control the R_p in scCO$_2$.

Without mass transfer limitations, the following Arrhenius-type expression is used to evaluate the rate constant, k, as a function of pressure (at constant temperature).[161]

$$k\left(T,p\right) = k\left(T,p_0\right)\exp\left(-\frac{\Delta V^{\#}}{RT}\left(p - p_0\right)\right) \qquad (6.1)$$

where p_0, T, R, and $\Delta V^{\#}$ are the reference pressure, the absolute temperature, universal gas constant, and the activation volume, respectively. $\Delta V^{\#}$ is the change in volume in going from the reactants to the transition states determined experimentally.[162] On the reaction path between the initial and final arrangements of atoms or molecules, there exists an intermediate configuration at which the potential energy has a maximum value. This state is referred to as the transition state, which has been used in many studies to investigate the effect of pressure on the rate of reaction in the system.[161, 163] The overall reaction rate would be increased or decreased by increasing the pressure depending on the sign of $\Delta V^{\#}$ in Eq.6.1.

The first step in the RAFT polymerization mechanism (Figure 2.9) is the decomposition of initiator (e.g. AIBN in this study). It was previously shown by DeSimone *et al.* that the decomposition rate of AIBN in scCO$_2$ is lower than that observed in organic solvents such as benzene at the same temperature and pressure.[163] Investigation on the pressure effects using scCO$_2$ showed that the decomposition rate and the initiation efficiency (*f*) of AIBN increased with increasing pressure, which increases R_p. In the propagation reaction, $\Delta V^{\#}_p$, is generally negative,[56] (the value of $\Delta V^{\#} = -16$ cm^{3}mol^{-1} is reported in the literature for MMA) resulting in R_p increasing with increasing pressure.[161] Hence, both these effects would increase the R_p with pressure, as observed experimentally.

scCO$_2$ is an effective diluent for increasing the free volume of polymer. It has useful advantages with a reduction of viscosity, surface tension and with an increase of diffusion into the polymer phase, so in a conventional free radical polymerization, termination reactions between two growing macroradicals may be expected to be

enhanced by the decreased viscosity. Arita *et al.* [164] showed that the overall polymerization rates were slower due to an enhanced termination between the growing micro radicals when using $scCO_2$ as the solvent in comparison to polymerization in toluene for free radical polymerization of styrene. However, it is well known that in an ideal RAFT polymerization (last step of the mechanism of RAFT polymerization in Figure 2.9), that the chemically controlled propagation reaction may be accelerated, whereas the diffusion controlled termination reaction would be negligible or proceed at lower rates.[165] In Figure 2.9, increasing pressure should have little effect on the reaction rate in the pre and core equilibrium steps, as all components are in the polymer phase. Increasing the overall rate of reaction, in general, would be anticipated by increasing the pressure of $scCO_2$ for living polymerization systems confirmed by our experimental results.
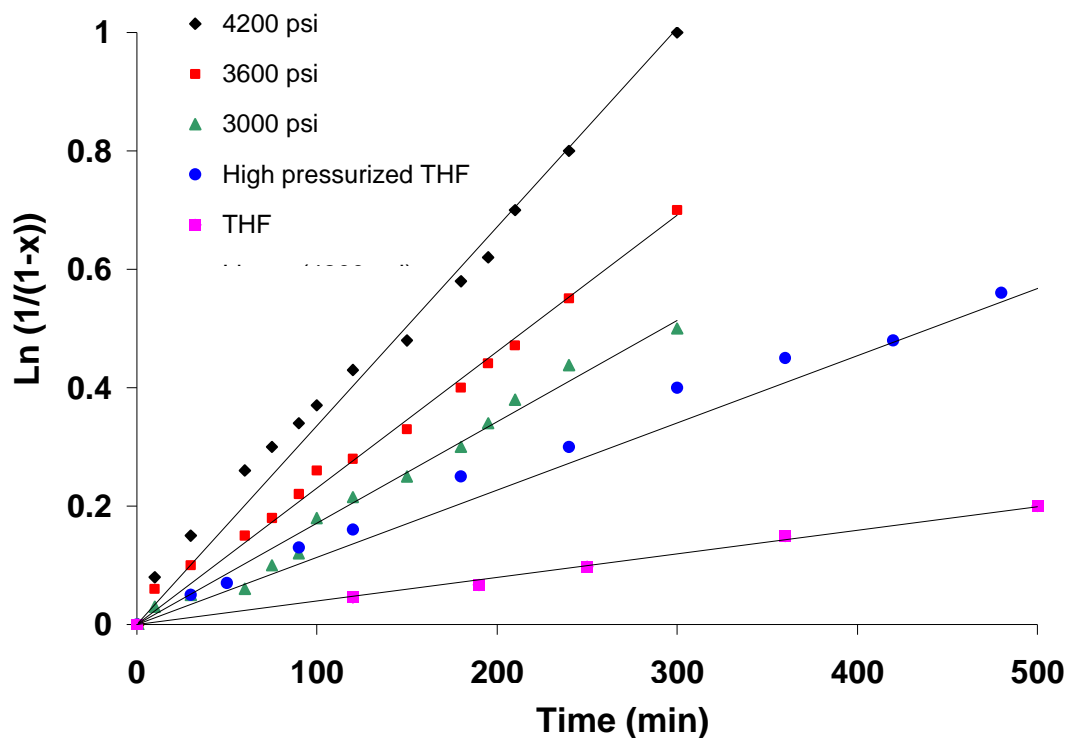
Figure 6. 7 First-order kinetic plot for the graft polymerization of MMA at 70°C with AIBN initiator mediated with functionalized n-TiO$_2$ at different pressures of scCO$_2$ and in high pressurized and ambient pressure of THF (3600 psi).

As shown in Ch.5, M$_n$ can be calculated by Eq.5.7: [71]

$$M_n = \frac{[M]_0 \cdot x \cdot M_{n,\,monomer}}{[RAFT]} \tag{5.7}$$

Figure 6.8 summarizes how M$_n$ (experimental and theoretical (Eq.5.7)) changes with time for polymerization at 3600 psi, 4200 psi, and in THF. It is clear that this direct coordination method for attaching the RAFT agent onto the n-TiO$_2$ surface provides a living polymerization with reasonably high molecular weights following first order kinetics.
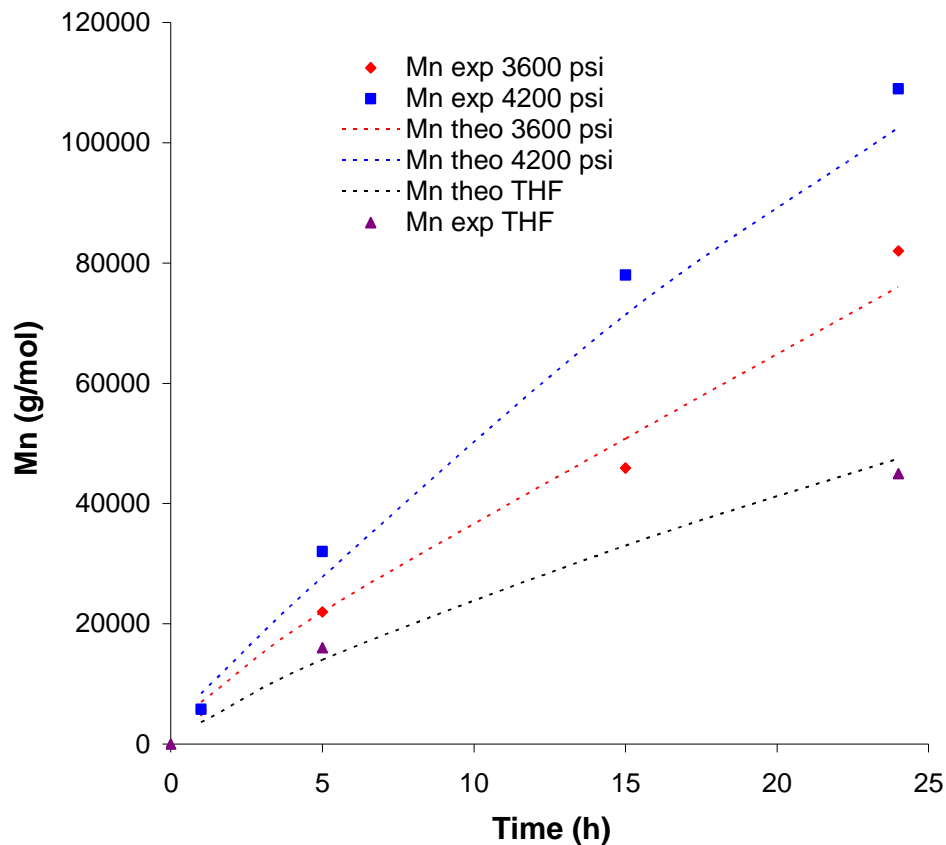
Figure 6. 8 Molecular weight vs. time data for graft polymerization of MMA from n-TiO$_2$ via RAFT at 70 ^{o}C and 3600 psi and 4200 psi in scCO$_2$ and in high pressurized THF at 70 ^{o}C and 3600 psi; M$_n$ theory calculated with Eq. 5.7 (----).

It can be clearly seen that Mn increases linearly with polymer reaction time both in high pressurized THF and in scCO$_2$, almost perfectly matching the theoretical Mn values, which are calculated via Eq.5.7.

6.5. Conclusions

For the first time, n-TiO$_2$ was functionalized with the RAFT agent, following living graft polymerization in supercritical carbon dioxide (scCO$_2$), and n-TiO$_2$/PMMA hybrid materials were synthesized. 4-cyano-4-(dodecylsulfanylthiocarbonyl) sulfanyl pentanoic acid served both as a functionalization and living polymerization agent in

scCO$_2$. SEM images, TGA, and DLS revealed the growth of the grafting polymers from n-TiO$_2$. GPC results confirmed the livingness of the grafted polymer after cleaving. The research demonstrated that living polymerization initialized from n-TiO$_2$ surface is promising to synthesize hybrid materials with high molecular weights. In addition, the kinetics of graft polymerization of MMA from the surface of n-TiO$_2$ in scCO$_2$ was studied and showed it was first-order in regards to monomer concentration.

CHAPTER 7

SYNTHESIS OF NiO/TiO$_2$ USING AMPHIPHILIC DIBLOCK COPOLYMER BRUSHES (PMMA-b-PAA) BY RAFT POLYMERIZATION

In this chapter, novel amphiphilic polymer brushes of PMMA-b-PAA were grown from n-TiO$_2$ by the RAFT polymerization process. The RAFT agent (**3**), 4-cyano-4-(dodecylsulfanylthiocarbonyl) sulfanyl pentanoic acid, with an available carboxyl group was used to anchor onto the n-TiO$_2$ surface, with the S=C(SC$_{12}$H$_{25}$) moiety used for subsequent RAFT polymerization of MMA and then copolymerization with AA to form n-TiO$_2$/PMMA-b-PAA nanocomposites. Ni^{+2} ions were subsequently attached to the n-TiO$_2$/PMMA-b-PAA polymer chains through the carboxyl moieties. After removing the copolymer chains by heat treatment, n-TiO$_2$ was decorated with NiO which was subsequently characterized for potential use as a nanocatalyst.
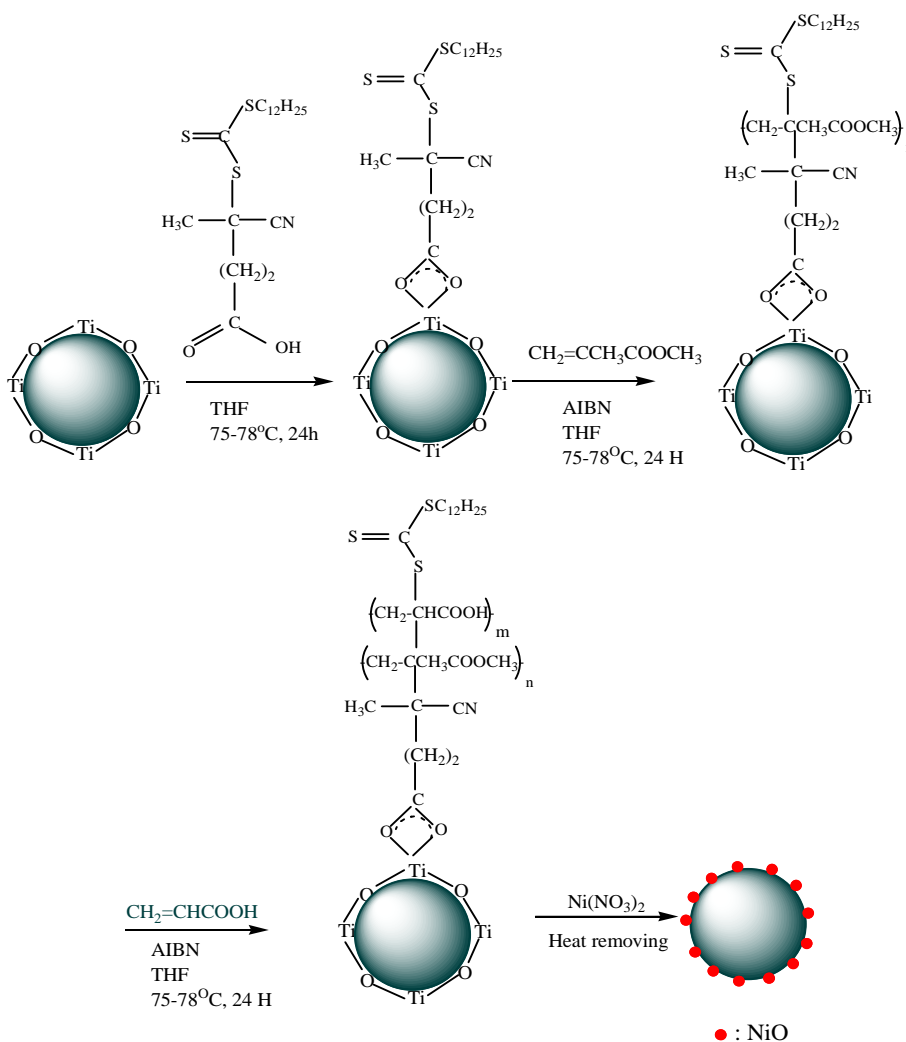
7.1. Introduction

Living radical/controlled polymerization (LCP) techniques provide the opportunity to prepare a variety of well-defined macromolecules with designed architectures, providing control of the molecular weight while maintaining low polydispersities.[166] Since the propagating chain spends a considerable amount of time in the dormant condition, free radical termination reactions such as coupling and disproportionation are effectively suppressed. When the available monomer has been consumed through propagation, the chains remain in the dormant capped state and are capable of being re-initiated using different monomers, thus, providing a route to the synthesis of block and multi-block copolymers.[167]

As mentioned in Ch.2, RAFT polymerization is recognized as one of the most versatile methods for block copolymer synthesis, with numerous examples of block synthesis now appearing in the literature.[86] This makes the RAFT technique very useful to synthesize block copolymers possessing various functional groups.[168] There is considerable interest in the RAFT technique has been for its ability to make amphiphilic block copolymers.[166] As mentioned in Ch.2, amphiphile is a term describing a chemical compound i.e. a polymer possessing both hydrophilic and hydrophobic properties. Recently, the controlled synthesis of complex amphiphilic nanostructures based on the living polymerization approach has received significant attention from both the scientific and technological communities.[169] Kong *et al.* grafted multi-walled carbon nanotubes (MWNTs) by amphiphilic polymer brushes of polystyrene-block-poly(acrylic acid) (PS-b-PAA), using atom transfer radical polymerization (ATRP).[170]Amphiphilic Poly(styrene-block-acrylamide)/organic montmorillonite nanocomposites were prepared

by Qu *et al.* via RAFT polymerization.[171] The block copolymer–nanoparticle hybrid materials combine the unique features of nanoparticles with the flexibility and solubility of polymeric materials, thus being promising for applications such as the next generation of catalysts, membranes and optoelectronic devices.[172]

During the last few years, attention has focused on the catalytic application of metal nanoparticles due to their unique physical and chemical properties including high surface areas and high metal dispersions. Because of their excellent catalytic activity, low cost and high availability, Ni-based catalysts are widely used in chemical processes such as hydrocarbon hydrogenation and dehydrogenation, steam reforming and catalytic partial oxidation of methane. Titania has attracted much interest as a support material for metals or metal oxides due to its ability to modify the catalytic properties of the supported phase.[173] As one example, NiO/TiO_2 catalysts are inexpensive and do not suffer as much from coking and poisoning, being an attractive industrial catalyst system. Conventionally, NiO/TiO_2 can potentially be synthesized via mixing Ni $(NO_3)_2$ and n-TiO_2 using a solvent, but the problem is reducing the surface area of the product because of penetrating of NiO into the n-TiO_2 pores.[174] This problem can be solved by using an intermediate component like polymer chains filling these pores.

The goal of this work is to demonstrate a novel approach for grafting amphiphilic diblock copolymers of PMMA-b-PAA onto n-TiO_2 particles following decoration with NiO for catalyst applications. The carboxylic group of RAFT agent, 4-cyano-4-(dodecylsulfanylthiocarbonyl) sulfanyl pentanoic acid (**3**), was directly coordinated to n-TiO_2, while the $S=C(SC_{12}H_{25})$ moiety was used for subsequent RAFT polymerization of MMA following PAA to form the amphiphilic copolymer brushes. As an example of the

functionality of this approach, Ni particles were attached to the surface of the spherical TiO$_2$ nanoparticles using the amphiphilic copolymer brushes of PMMA-b-PAA, as the carboxyl groups on PAA provide a site for attachment to the brushes. After removing the copolymer chains by heat treatment, n-TiO$_2$ decorated with NiO was obtained which can be used as a nanocatalyst for applications in alternative energy and biomedical devices. Based on our knowledge, grafting amphiphilic block PMMA-b-PAA from n-TiO$_2$ is reported for the first time.

To investigate the effect of chain length of blocks in nanocomposites on the attachment of Ni ion on the surface of n-TiO$_2$, n-TiO$_2$/PAA and n-TiO$_2$/PMMA-b-PAA with different chain length (after 5 and 24 hours) were used.

7.2.   Experimental

7.2.1. Materials

Titania nanospherical particles (99.5%, Sigma-Aldrich, avg. part. size D= 23.2 nm), 2, 2′-azobis (2-methylpropionitrile) (AIBN) initiator (Toronto Research Company), isopropanol (anhydrous, Sigma-Aldrich) were used as received. Methyl methacrylate (MMA) and Acrylic acid (AA) monomers (99%, Sigma-Aldrich, inhibited with 200 ppm BHT) were passed through an inhibitor removal column (Sigma-Aldrich) before use. The RAFT agent 4-cyano-4-(dodecylsulfanylthiocarbonyl) sulfanyl pentanoic acid (**3**) was prepared as described elsewhere[126](for more detailed description see Appendix 3). Ni (NO$_3$)$_2$ (99.999%, Sigma-Aldrich) was used as received.

7.2.2. Functionalization of n-TiO$_2$

n-TiO$_2$ was functionalized with RAFT agent (**3**) based on the procedure described in section 4.2.2.

7.2.3. Synthesis of n-TiO$_2$/PMMA

n-TiO$_2$/PMMA was synthesized based on the procedure described in section 5.2.3.

7.2.4. Synthesis of n-TiO$_2$/PMMA-b-PAA

14 mL of AA monomer, 0.7 g of n-TiO$_2$/PMMA (after 24 hours reaction), and 0.010 g of AIBN were dispersed in 120 mL THF with the aid of sonication. Then the solution was transferred to a 250 mL three-neck flask equipped with nitrogen supply, a thermometer, and a condenser under constant stirring for 24 hours at 75-78 ^{o}C. To ensure that no un-grafted polymer remained in the product, the particles were re-dissolved in THF and re-precipitated by centrifugation at 10,000 rpm for 10 min, with this process repeated until the solution was clear.

7.2.5. Cleaving Grafted Polymer from Particles

Grafted PMMA and/or PMMA-b-PAA from n-TiO$_2$ nanoparticles was cleaved based on the procedure described in section 4.2.4.

7.2.6. Synthesis of n-TiO$_2$/PMMA-b-PAA-NiO

0.3 g of n-TiO$_2$/PMMA-b-PAA and 0.4 g of Ni (NO$_3$)$_2$ were dispersed in 80 mL methanol using sonication. Then the solution was transferred to a 100 mL three-neck flask, a thermometer, and a condenser under constant stirring for 10 hours at 65-70 ^{o}C. To

ensure that no un-reacted Ni remained in the product, the particles were re-dissolved in methanol and re-precipitated by centrifugation at 10000 rpm for 15 min, with this process repeated until the solution was clear. The recovered material was dried under vacuum. After calcination of products at 600 ^{o}C for 2 h with a heating rate of 1.5 ^{o}C/ min to remove the block copolymer, NiO/TiO$_2$ was formed.

7.2.7. Conventional synthesis of NiO/TiO$_2$

NiO/TiO$_2$ was also made via a conventional wet incipient method with the resulting surface area of the approaches compared. 0.3 g of TiO$_2$ nanoparticle and 0.4 g of Ni (NO$_3$)$_2$ were dispersed in 80 mL methanol using sonication. Then the solution was transferred to a 100 mL three-neck flask, a thermometer, and a condenser under constant stirring for 10 hours at 65-70 ^{o}C. To ensure that no un-reacted Ni remained in the product, the particles were re-dissolved in methanol and re-precipitated by centrifugation at 10,000 rpm for 15 min, with this process repeated until the solution was clear. The recovered material was dried under vacuum.

7.3. Characterization

The molecular weight and PDIs of cleaved PMMA and/or PMMA-b-PAA were measured by gel permeation chromatography (GPC) with a Viscotek instrument using triple detectors (RI, LS, and V) referenced to PS standards (1 ml/min, at 30 ^{o}C). FTIR spectra were collected using a KBr pellet on a Bruker IFS 55 FTIR instrument attached with a MCT detector, with a resolution of 2 cm^{-1} and 128 scans for each sample. The X-ray Photoelectron Spectroscopy (XPS) analysis was carried out with a Kratos Axis Ultra spectrometer using a monochromatic Al Ka source (15mA, 14kV). The instrument work

function was calibrated to give a binding energy (BE) of 83.96 eV for the Au $4f_{7/2}$ line for metallic gold and the spectrometer dispersion was adjusted to give a BE of 932.62 eV for the Cu $2p_{3/2}$ line of metallic copper. X-ray diffraction (XRD) patterns were recorded for the finest powder samples on a Bruker D8 Discover Diffractometer and a Cu source. Scanning electron microscopy (SEM) images were recorded using a LEO 1530 instrument without gold coating at 10 kV, and transmission electron microscopy (TEM) was performed on a Phillips CM 10 electron microscope at 80 kV. Thermo gravimetric analysis was performed using a TGA Q500 at a heating rate of 10 °C/min under a nitrogen atmosphere. Temperature program reduction (TPR) was performed using an Autochem II ASAP 2920 analyzer (Micromeritics, USA). A gas stream of 10% hydrogen in argon was flowed through a bed containing approximately 150-200 mg of sample at a rate 50mL/min, the bed temperature was raised from ambient to 750 ^{o}C at a rate of 10 ^{o}C/min, and a thermal conductivity detector (TCD) was used to analyze the gas leaving the sample. Brunauer-Emmett-Teller (BET) surface area, pore size and distribution were obtained on Micromeritics ASAP 2010 at 77 K. Prior to the N_2 physisorption, a sample was degassed at 200 °C under vacuum. Dynamic light scattering was performed using a Malvern Zeta Sizer 3000HSA at room temperature.

7.4. Results and Discussion

The general synthesis route for growing amphiphilic polymer brushes from the n-TiO_2 surface via RAFT polymerization technique and subsequent Ni ion-exchange is described in Figure 7.1.
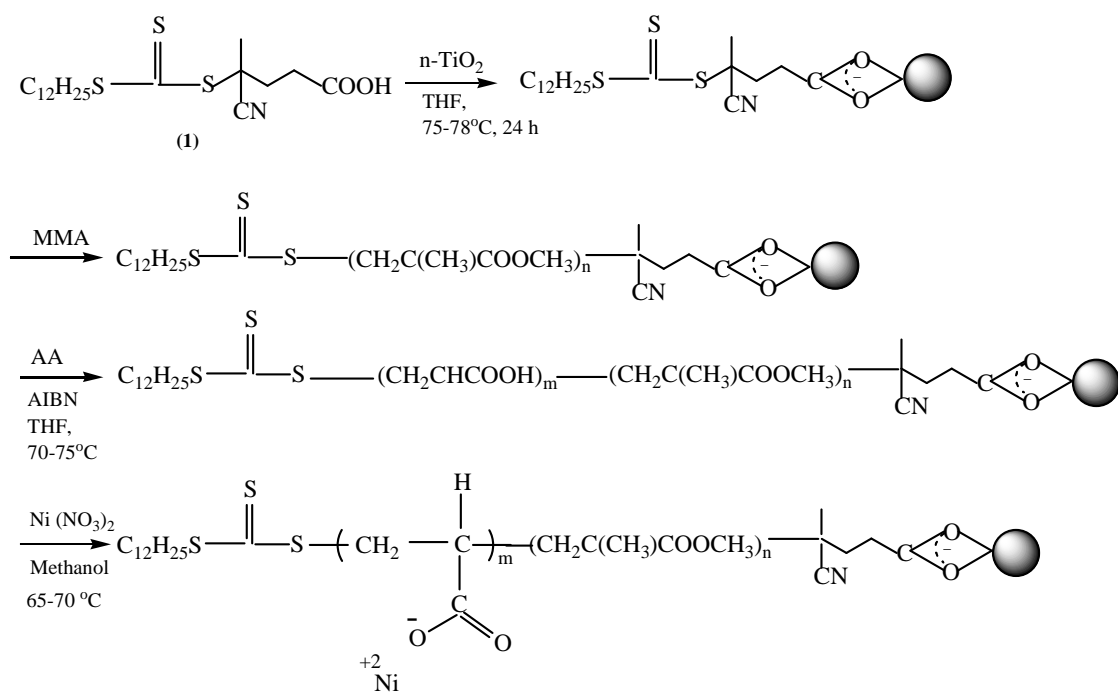
Figure 7. 1 Synthesis of NiO/TiO$_2$ advanced materials.

7.4.1. FTIR and XPS Study of functionalized n-TiO$_2$

Functionalization of n-TiO$_2$ with RAFT agent was verified by FTIR and XPS analysis as reported in Ch.5.[62]

7.4.2. FTIR Study of Polymer Nanocomposites

The chemical structure of the PMMA and PMMA-b-PAA moieties on the functionalized TiO$_2$ was determined by FTIR, which is an established technique for analyzing the complexes of metal carboxylate species.[123] In Figure 7.2a, the peaks at 1543 and 1646 cm^{-1} for n-TiO$_2$/RAFT agent are assigned to the bridging bidentate coordination between titanium atoms and the carboxyl group of the RAFT agent (Ti-carboxylate).[175] The absence of a peak at 1720 cm^{-1} (carboxylic group of RAFT agent) indicates that there is no free RAFT agent after functionalization. In Figure 7.2b, after MMA polymerization, the new peaks at 1731 cm^{-1} appeared due to the presence of an

ester carbonyl group stretching vibration for n-TiO$_2$/PMMA. After diblock formation when polymerizing AA, the stronger peaks at 1731 cm^{-1} and 1653 cm^{-1} in Figure 7.2c are attributed to the presence of the carboxylic group of PAA.[132]
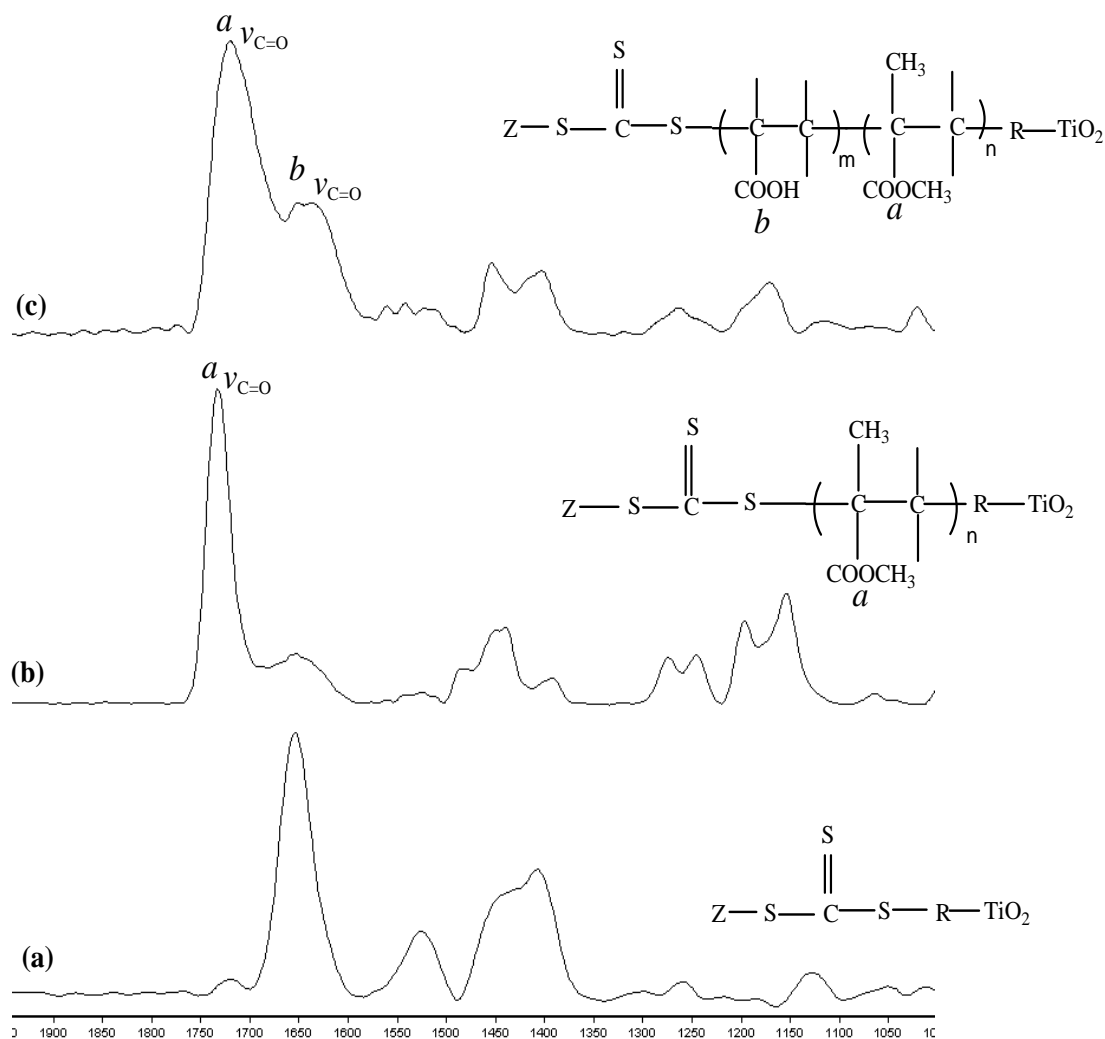
Figure 7. 2 FTIR Spectra of (a) functionalized n-TiO$_2$, (b) n-TiO$_2$/PMMA, and (c) n-TiO$_2$/PMMA-b-PAA.

7.4.3. Organic/Water Partitioning Study

The samples obtained in each step of TiO$_2$/diblock formation showed different solubilities or dispersibility in organic/water bilayers. As shown in Figure 7.3, n-

TiO$_2$/PMMA is dispersed in both the organic and water phases (Figure 7.3 A), because of the presence of both organic groups of RAFT agent and some un-functionalized n-TiO$_2$. On the other hand, as the end group of the nanocomposite is PAA which is hydrophilic, n-TiO$_2$/PMMA-b-PAA preferentially disperses in the water phase (Figure 7.3 B).
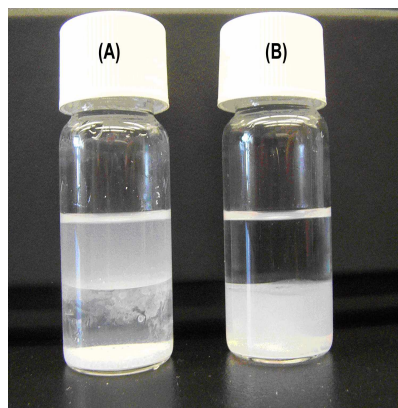
Figure 7. 3 In the vials, the upper layer is ether and the lower layer is the water phase. (A) The n-TiO$_2$/PMMA is well dispersed in both phases; (B) n-TiO$_2$/PMMA-b-PAA is suspended in the water phase.

7.4.4. TGA analysis

The functionalized TiO$_2$, n-TiO$_2$/PMMA, and n-TiO$_2$/PMMA-b-PAA nanocomposites were dried and subjected to TGA. In Figure 7.4a, the n-TiO$_2$-RAFT agent shows that the TGA curve can be divided into 2 sections. Below 200 °C, a small slope of weight loss is shown (~ 0.4 wt %), most likely due to evaporation of any remaining entrapped water and/or solvent. The slope becomes larger in the temperature range of 200 ~ 450 °C with the weight loss ~ 1.6 wt%, due to the decomposition of the RAFT agent groups and becomes flat again after the temperature is over 450 °C. The TGA results of the n-TiO$_2$/PMMA composite (Figure 7.4b) shows two obvious regions when the temperature was increased: the first region started from 25 °C and ended at 200

°C with a relatively small slope and weight loss ~ 0.4 wt%, again likely due to the evaporation of the entrapped water; while the second region started at 250 °C and ended at 450 °C with a large slope indicating more weight loss (ca.~ 5.6wt%) in this region and decomposition of some organic groups of PMMA and RAFT agent components. On the other hand, the TGA result of n-TiO$_2$/PMMA-b-PAA (Figure 7.4c) shows three regions; the first region is below 200 °C with a higher slope compared to Figure 7.4b (weight loss ~ 3 wt%). This can be explained by the evaporation of a larger amount of entrapped water as PAA is a superabsorbent polymer. The weight loss for the second region from 250 °C to 320 °C is ~ 2.5 wt% that can be attributed to the decomposition of organic groups of PAA in n-TiO$_2$/PMMA-b-PAA.[28] The slope becomes larger in the temperature range of 350 °C ~ 450 °C (with the weight loss ~ 3.5 wt%), which it can be assigned to the decomposition of PMMA in n-TiO$_2$/PMMA-b-PAA.[62] It becomes flat again after the temperature is over 450 °C.
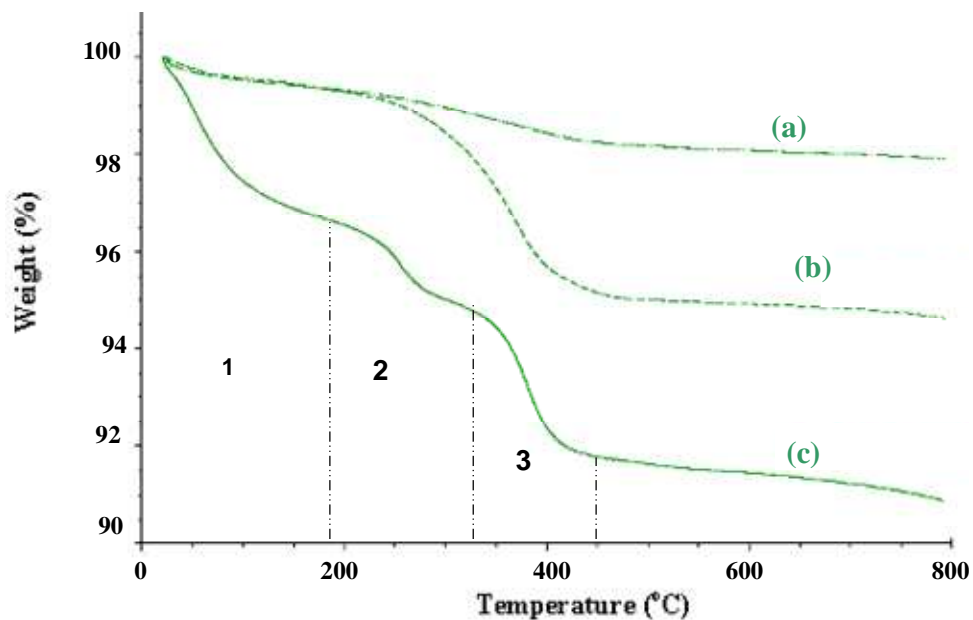
Figure 7. 4 TGA curves of (a) the functionalized n-TiO$_2$, (b) n-TiO$_2$/PMMA, and (c) n-TiO$_2$/PMMA-b-PAA.

7.4.5. Molecular weight and PDI of cleaved PMMA and PMMA-b-PAA

As described previously, in an ideal living polymerization, the molecular weights increase linearly with conversion/time and the PDIs can be very narrow.[32] In order to determine whether the 'grafting from' polymerization was still living when the RAFT agent had been attached to the n-TiO$_2$ surface, the PMMA and/or PMMA-b-PAA chains were cleaved after various polymerization times using acidic conditions based on the procedure described in Ch.4. GPC measurements show that the molecular weight of grafted PMMA and/or PMMA-b-PAA directly increases with time (Table 7.1). After 24 hours, the polymerization of PMMA from the functionalized n-TiO$_2$ was stopped (M$_n$=13,600 g/mol, and PDI=1.3), and PAA chains were subsequently grown from n-TiO$_2$/PMMA to produce n-TiO$_2$/PMMA-b-PAA by adding AA and a fresh amount of initiator (AIBN). The increasing molecular weight of the diblock copolymer with increasing polymerization time indicates that acrylic acid has been polymerized from n-TiO$_2$/PMMA. Figure 7.5 shows the GPC elution profiles of the diblock copolymer of PMMA-b-PAA obtained using solution polymerization with RAFT agent (**3**) for 5-24 h of polymerization time. The molecular weight distributions are relatively unimodal, with low PDIs.

Table 7. 1 Molecular weights and PDIs of cleaved PMMA and PMMA-b-PAA at different polymerization times.

Samples	Time (h)	M$_n$ (g/mol)	PDI
n-TiO$_2$/PMMA	15	9,100	1.4
n-TiO$_2$/PMMA	24	13,600	1.3
n-TiO$_2$/PMMA-b-PAA (1)	5	14,400	1.3
n-TiO$_2$/PMMA-b-PAA (2)	16	17,500	1.2
n-TiO$_2$/PMMA-b-PAA (3)	24	19,600	1.4
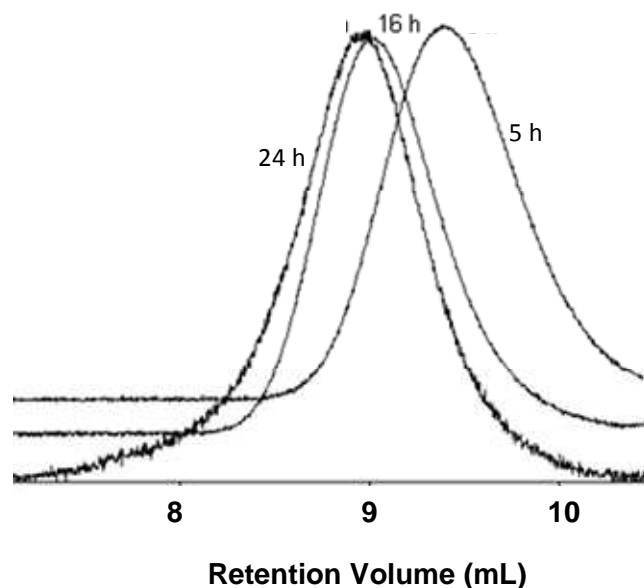
Figure 7. 5 GPC elution profiles for RAFT polymerization of PMMA-b-PAA from n-TiO$_2$ surface for 5 h (Mn = 14,400 g/ mol, PDI = 1.3), 16 h (Mn =17,500 g/mol, PDI =1.2), 24 h (Mn = 19,600 g/ mol, PDI =1.4).

Based on the molecular weights summarized in Table 7.1, the rate of addition for each monomer of AA to the chains of PMMA in heterogeneous media is more than 17 minutes, while this rate in solution (as will be discussed in Ch.8) is ~ 2.2 minutes. In explanation, this slower rate can be attributed to the high local concentration of PMMA-RAFT agent (macromolecule RAFT agent) on the surface of n-TiO$_2$ which was determined by TGA (6%). In Ch.5, the effect of the concentration was studied which showed that the rate of reaction decreased when increasing the concentration of RAFT agent.[62] Comparing with the previous reports by Chen *et al*. [176] and Peng *et al.,*[177] in solution media, the RAFT approach in homogeneous media produced PMMA-b-PAA with higher molecular weight and narrower PDIs in this work than the methods through hydrolysis of PMMA-*b*-P*t*BA via DPE and hydrolysis of poly(methoxymethyl acrylate)-b-PMMA via ATRP methods. Also in heterogeneous media, the molecular weights and

135

PDIs shown in Table 7.1 with those obtained by Lee *et al.*[178] and Pyun *et al.*[97] who grafted Poly (4-acetoxystyrene)-b-Polystyrene from carbon black, and Poly butyl acrylate-b-Polymethyl methacrylate, from the surface of silica nanoparticles, via SFRP and ATRP, respectively, shows the molecular weights and PDIs are almost in the same range, (M_n: 7729-17330 g/mol and PDI: 1.28-1.45 for each block).

7.4.6. Electron Microscopy

TEM and SEM were used to study the morphology of the formed nanocomposites (Figure 7.6). Figure 7.6a shows the TEM image of n-TiO_2/PMMA, while Figure 7.6b exhibits the n-TiO_2/PMMA-b-PAA structure. Some agglomeration of n-TiO_2 still exists, although the generally excellent separation of n-TiO_2 particles is attributed to the growing of ''grafting from'' PMMA and/or PMMA-b-PAA chains, which separates the previously agglomerated TiO_2 nanoparticles.

Figure 7.6c shows the SEM image of the n-TiO_2/PMMA while Figure 7.6d presents the SEM image of n-TiO_2/PMMA-b-PAA. One can see that as the n-TiO_2/PMMA-b-PAA was made from further polymerization of AA from n-TiO_2/PMMA, the thickness of its copolymer layers is larger than that of the homopolymer.
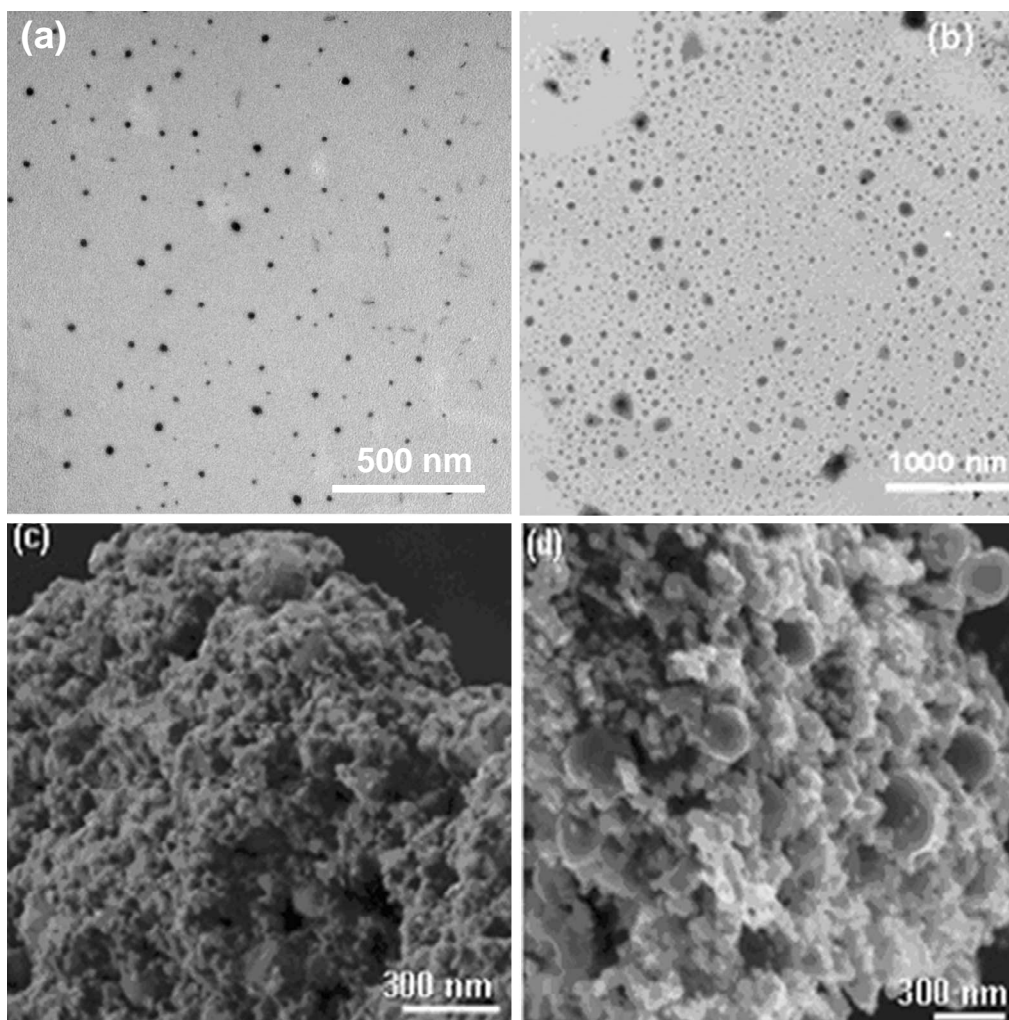
Figure 7. 6 TEM images of (a) n-TiO$_2$/PMMA, (b) n-TiO$_2$/PMMA-b-PAA, (c) SEM images of n-TiO$_2$/PMMA, and (d) n-TiO$_2$/PMMA-b-PAA composites.

7.4.7. Dynamic Light Scattering (DLS)

The size of the TiO$_2$ nanocomposites in THF solution was investigated by dynamic light scattering (DLS) measurements. Figure 7.7 shows the particle size evolution of n-TiO$_2$/PMMA and n-TiO$_2$/PMMA-b-PAA nanocomposites with respect to the polymerization time. As the polymerization time increases, the mean particle size of the nanocomposites also increases, which is consistent with the SEM images (Figure 7.6). This is due to the growing polymer chains of PMMA and/or PAA with time, providing

further evidence of the living nature of the polymerization. The polydispersity index (PI) as well as the intensity of the mean particle size change only slightly, indicating the continuous growth of polymer chains of PMMA-b-PAA with polymerization time, confirming the livingness of polymerization.
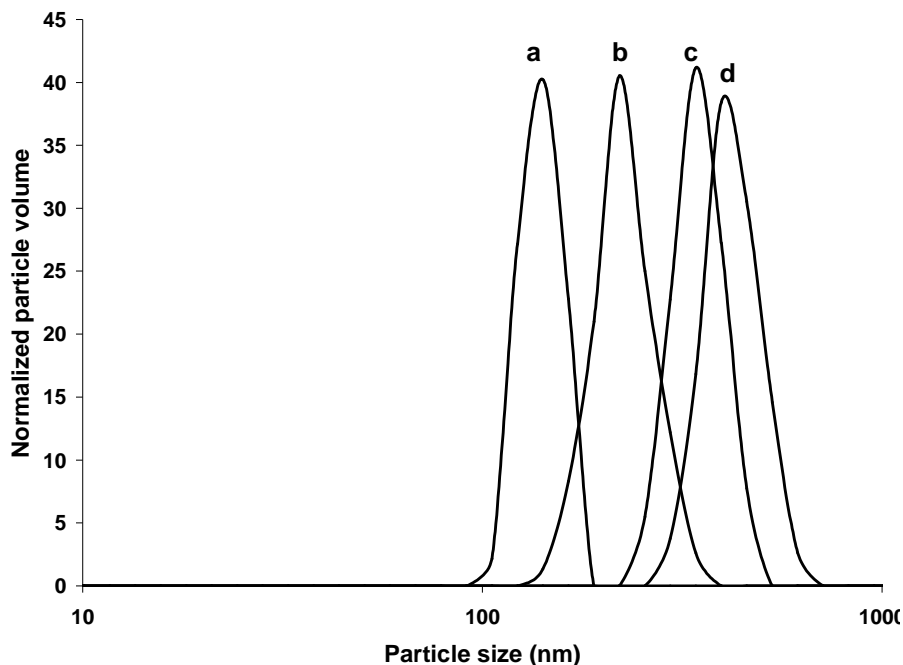
Figure 7. 7 Particle size distribution of the (a) n-TiO$_2$/PMMA after 24 h (D$_{mean}$= 140 nm, PI= 0.3), and n-TiO$_2$/PMMA-b-PAA after (b) 5h (D$_{mean}$= 226 nm, PI= 0.33), (c) 16 h (D$_{mean}$= 350 nm, PI= 0.34), and (d) 24 h (D$_{mean}$= 460 nm, PI= 0.4) by DLS in THF and at room temperature.

Figure 7.7 shows the size distributions becoming slightly broader as the polymerization time increases, which attributed to the electrostatic force between the PAA chains increasing with chain length, that likely result in complex chain interactions from both association electrostatic repulsion effects.

7.4.8. XPS Study

As shown in Figure 7.1, once the amphiphilic copolymer brushes of n-TiO$_2$/PMMA-b-PAA were formed, various metal ions such as Ag$^+$ or Ni^{++} can be

attached by ion-exchange to facilitate the formation of advanced materials. To investigate this reaction (bottom reaction of Figure 7.1) the block copolymers attached to TiO_2 were ion-exchanged with Ni^{++} in methanol. The chemical composition of the resulting advanced materials were studied using XPS, with the full spectrum of the n-TiO_2/PMMA-b-PAA-Ni showing the existence of S, N, C, Ni elements beside O and Ti (Figure 7.8a). A high resolution XPS scan of the Ni 2p region (Figure 7.8b) shows five major sources of nickel peaks, as expected from the literature.[179] The peaks commonly appeared at 855.25 or 855.35 eV with related satellite peaks at 860-865 eV (Ni $2p_{3/2}$).[180] The high resolution XPS of the O 1s region (Figure 7.8c) shows peaks at ~ 529.9 eV, 531.1 eV and 533 eV which are assigned to the O atom in n-TiO_2 and/or NiO, the carbonyl group and adsorbed water, respectively.[181, 182] The shoulder at ca. 854.5 eV in Ni 2p and an intense peak at ca. 529.9 eV in O 1s can be assigned to NiO.[183] The content of Ni is about 2% with respect to Ti.

NiO/TiO_2 was also synthesized via a conventional approach (heating up a mixture of $Ni(NO_3)_2$ and n-TiO_2 in methanol to 65-70 ^{o}C) and subsequently investigated by XPS showing that 0.2% Ni with respect to Ti was present on the n-TiO_2. Hence, a larger amount of Ni was attached to the n-TiO_2 surface using the amphiphilic diblock copolymer approach compared with the conventional wet incipient approach (XPS full spectrum of NiO/TiO_2 is shown in Appendix 6).
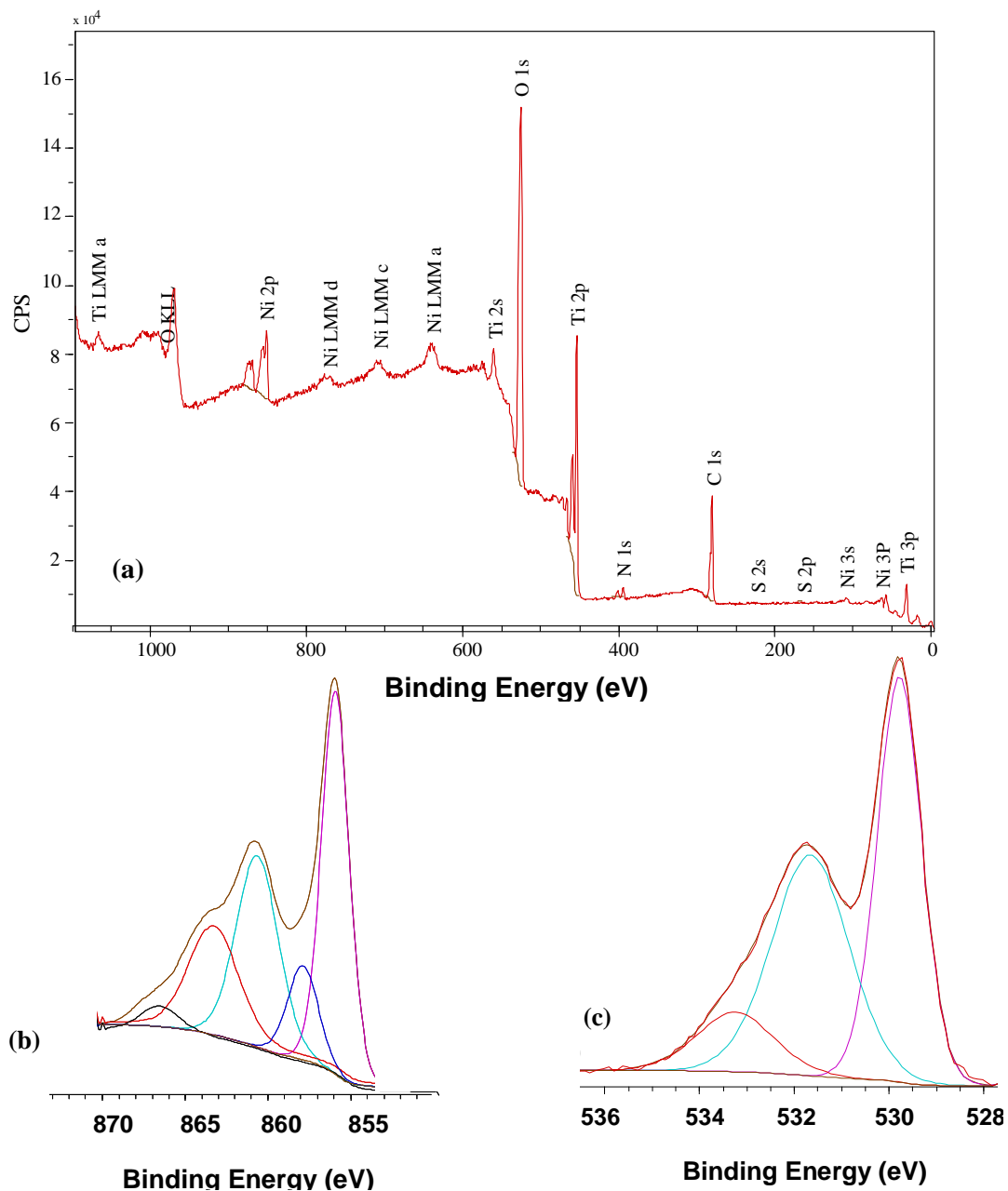
Figure 7. 8. XPS full-scan spectrum of the (a) n-TiO$_2$/PMMA-b-PAA-Ni, and high resolution spectrum of (b) Ni, and (c) O.

7.4.9. EDX and XRD Study

These n-TiO$_2$/PMMA-b-PAA-Ni complexes were subsequently calcined at 600°C to form NiO/TiO$_2$ structures. Figure 7.9a-c shows the EDX Ni mapping of TiO$_2$/NiO, using n-TiO$_2$/PAA, n-TiO$_2$/PMMA-b-PAA (1), and n-TiO$_2$/PMMA-b-PAA (3) as

templates, which indicates the amount of Ni as 0.5%, 0.7%, and 2% with respect to Ti, respectively, while Figure 7.9d presents the EDX spectra of NiO/TiO_2 synthesized using n-TiO_2/PMMA-b-PAA after 24 hours, showing that well-distributed nickel decorated the nanomaterials (for more detailed description see Appendix 5). These results show that as the chain length of PAA in the diblock copolymer increases, more Ni is decorated on the surface of n-TiO_2. In the n-TiO_2/PAA nanocomposites, all carboxylic groups of PAA are not available to react with Ni ions, as some of them are interacting with n-TiO_2 particles. On the other hand, using the n-TiO_2/PMMA-b-PAA nanocomposites, the carboxylic groups of PAA are kept farther away from the surface of n-TiO_2 particles using PMMA, so the carboxylic groups are available for reacting with Ni ions. As the chain length of PAA is increasing with the time of copolymerization, the availability of these carboxylic groups are increasing.
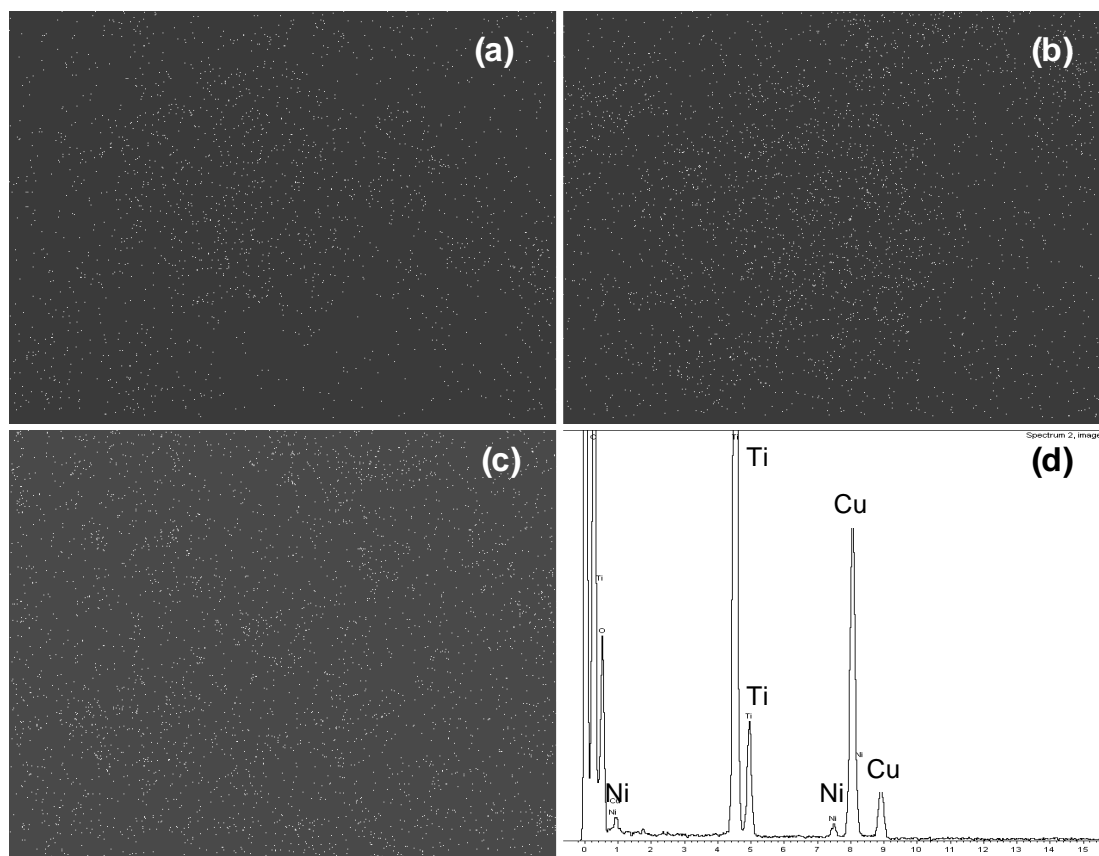
Figure 7. 9 EDX Ni mapping of NiO/TiO$_2$ using (a) n-TiO$_2$/PAA, (b) n-TiO$_2$/PMMA-b-PAA (5 h), (c) n-TiO$_2$/PMMA-b-PAA (24 h) as templates, and (d) spectra of NiO/TiO$_2$ (using n-TiO$_2$/PMMA-b-PAA (24 h) as a template).

The crystal structure of the NiO/TiO$_2$ composite was also examined by XRD, with the spectra given in Figure 7.10. This figure shows that the calcined components consist of anatase and rutile,[184] while three peaks at 2θ at 38, 62.5, and 75.4 degrees are attributed to nickel oxide,[185,186] confirming that that nickel oxide was attached to the surface of the TiO$_2$ nanoparticles.
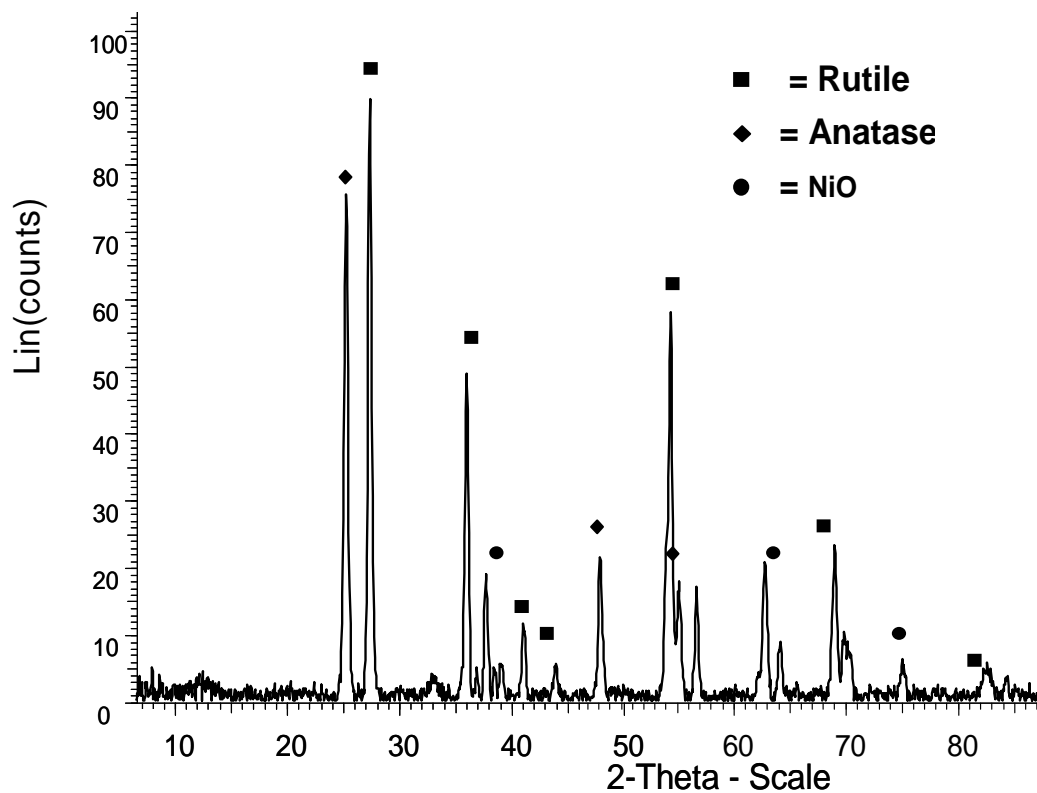
Figure 7. 10 XRD patterns of NiO/TiO$_2$ using n-TiO$_2$/PMMA-b-PAA after 24 hours.

7.4.10. Nitrogen Adsorption/Desorption Analysis

The textural properties such as surface area, the single point adsorption total pore volume per gram, and adsorption average pore diameters (4V/A BET) of samples were measured using nitrogen adsorption/desorption techniques. From the BJH analysis, an average pore size and pore volume were calculated using data points from the desorption branch of the isotherm. The properties of the as received n-TiO$_2$ and synthesized NiO on n-TiO$_2$ by conventional and amphiphilic copolymer method are summarized in Table 7.2.

Table 7. 2 Physical properties of synthesized samples.

Sample	S_{BET}	D_{pore}	V_{pore}
	(m^2/g)	(A)	(cm^3/g)
n-TiO$_2$	32	75	0.062
NiO/TiO$_2$*	18	120	0.069
n-TiO$_2$-PMMA	25	125	0.077
n-TiO$_2$-PMMA-b-PAA (24 h)	24	121	0.075
NiO/TiO$_2$	**27**	**108**	**0.074**

*: NiO/TiO$_2$ was made using conventional method.

S_{BET}: BET surface area; D_{pore}: Adsorption average pore diameter (4V/A); V_{pore}: Single-point adsorption total pore volume per gram.

It can be seen that the surface area decreases with nickel loading by both methods, as the added metal covers the pore-walls and eventually fills up the pores. It should be noted that the surface area is much lower using the conventional method compared to the block copolymer method i.e. 18 vs.27 m^2/g. This can be explained in two different ways: a) in the conventional method islands of metal or metallic oxide clusters form that may block micro and macro pores, and b) in our copolymer method, n-TiO$_2$ was de-agglomerated by brushes of PMMA-b-PAA resulting in better separation of the nanoparticles, which provides more sites for Ni ions to be adsorbed to the surface and pore walls. The increase of average pore diameter and pore volume is due to macro pore formation caused by adsorbed inter-metallic oxide particles on the support surface. Functionalizing n-TiO$_2$ by PMMA or PMMA-b-PAA also reduces the specific surface

area by pore blocking. The surface area again increases by removing the polymer chains from pores by calcination.

The samples exhibited IUPAC type III adsorption-desorption isotherms with hysteresis loops at higher relative pressures (Figure 7.11). This phenomenon is typically associated with capillary condensation within mesopores.[187] Single, well defined step, and a clear hysteresis loop in the desorption branch are attributed to some diffusion bottlenecking in the mesoporous structure.[188]
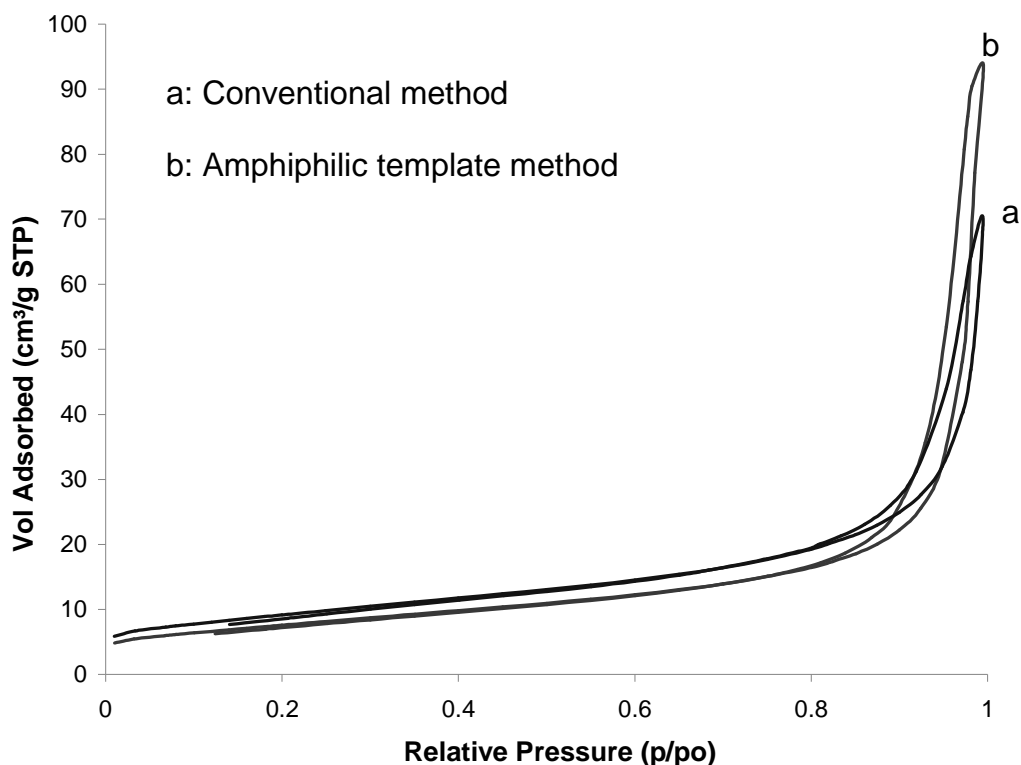
Figure 7. 11 N$_2$ adsorption and desorption isotherm.

7.4.11. Temperature program reduction (TPR)

To further examine the formed NiO/TiO$_2$ species, temperature program reduction (TPR) was applied to measure the available amount of reducible species. Figure 7.12 shows the TPR spectra of NiO/TiO$_2$ synthesized using the amphiphilic templating

method compared to the conventional approach, which indicates that larger numbers of reducible species of NiO were observed for the amphiphilic template vs. conventional approach. As one can see the peaks are formed after 570 $^{\circ}$C with a hump around 460 $^{\circ}$C. The peak near 600 $^{\circ}$C is attributed to the reduction of dispersed NiO which is strongly adsorbed to n-TiO$_2$.[189] The higher dispersion by the amphiphilic approach was also confirmed by EDX and XPS analysis. The reduction at 460 $^{\circ}$C is attributed to a secondary NiO layer that does not strongly adsorb to the n-TiO$_2$ support.[190] In the conventional method the secondary NiO layer is prominent, while this is absent when using the amphiphilic brush approach. This confirms higher nickel adsorption when using the polymer brush method and better decoration illustrating the potential utility of this approach for development of catalysts.
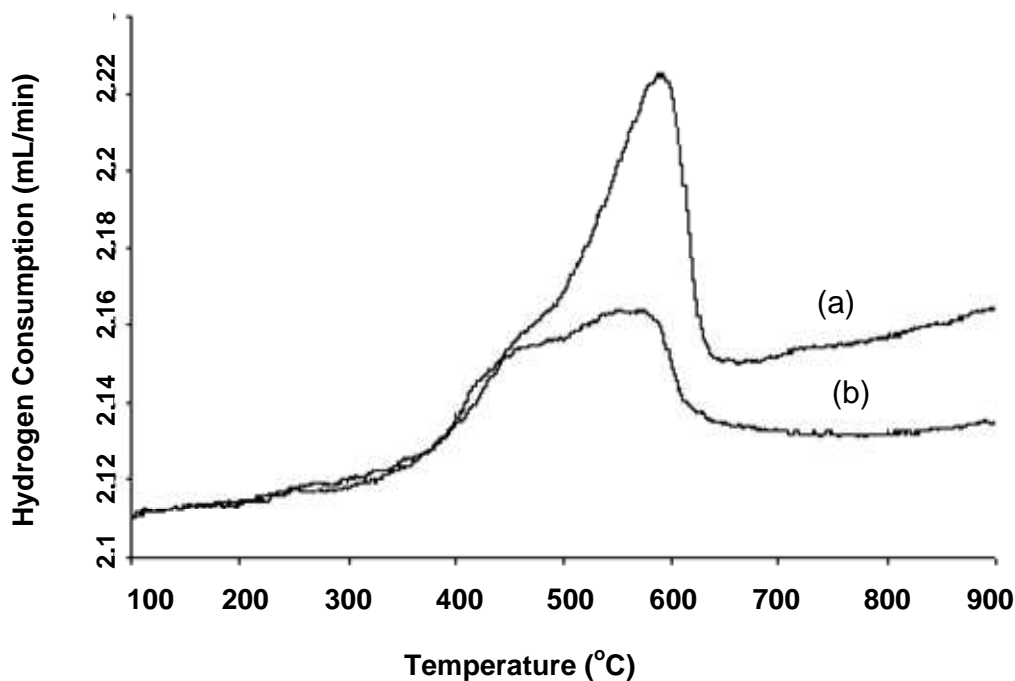
Figure 7. 12 TPR spectra of NiO loaded TiO$_2$ prepared using (a) amphiphilic polymer brush and (b) conventional approaches.

7.5. Conclusions

Novel n-TiO$_2$-based amphiphilic polymer brushes have been prepared via the RAFT technique. The related covalent functionalization was confirmed by TEM, SEM and TGA characterization. The n-TiO$_2$/PMMA-b-PAA nanocomposites and precursors exhibited different dispersibilities in water/organic bilayers. The results showed that living polymerization of both MMA and then AA initialized in the solution from AIBN and transferred to the functional groups on the n-TiO$_2$ surfaces, which is promising to synthesize hybrid materials possessing excellent dispersion of the fillers within the matrix. The coordination of the carboxylic group of the RAFT agent to the TiO$_2$ nanofiller was confirmed by FTIR spectra, and XPS. Electron microscopy images revealed the growth of the "grafting from" polymers around n-TiO$_2$, and the nanofillers were well separated and distributed throughout the polymer matrix. GPC results of cleaved polymer after various reaction times showed that the polymerization was still living, even after the RAFT agent was directly coordinated to n-TiO$_2$. As one example of potential application, Ni was reacted with the brushes with heat treatment to remove the polymer chains providing NiO decorated n-TiO$_2$ advanced materials with superior decoration compared to a conventional method for preparing NiO/TiO$_2$.

CHAPTER 8

SYNTHESIS OF MESOPOROUS TiO$_2$ USING AMPHIPHILIC DIBLOCK COPOLYMER (PMMA-b-PAA) AS A SELF-ASSEMBLY AGENT BY RAFT POLYMERIZATION

In this chapter, we attempted a new approach for synthesizing ordered mesoporous TiO$_2$ by using a polycarboxylic acid, i.e., polyacrylic acid in diblock copolymer of PMMA-b-PAA, as a self-assembling agent, via a sol-gel process in isopropanol. The synthesis involves coordination of metal alkoxides to the carboxylate group of the diblock copolymer template, sol-gel condensation, and then removal of the organic groups by subsequent heat treatment, forming ordered TiO$_2$ structures.
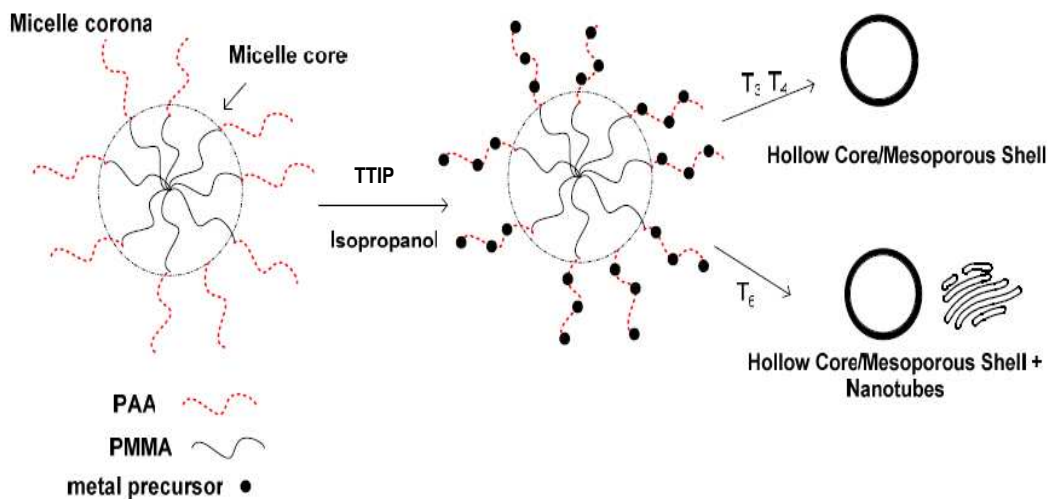
8.1. Introduction

TiO$_2$ nanomaterials have been extensively studied in the past two decades due to their application for photocatalysts, semiconductors and catalyst supports.[191, 192] Three-dimensional (3-D) semiconductors such as TiO$_2$ nanowires and nanotubes are of immense interest for solar cells[193] and electronic devices.[194] Among the methods that manipulate the morphology of metal oxides, sol-gel reactions with the aid of a template is promising, because of the mild synthesis condition and the high conversion.[195,196] For example, TiO$_2$ nanotube arrays have been prepared using anodic alumina membrane as a template, in which sol-gel reactions take place in the nanochannels of the alumina template. The TiO$_2$ nanotubes were obtained after removal of the alumina by corrosion, and calcination of the resulting TiO$_2$ materials. This method involves both anodization and corrosion of the alumina membrane, and the procedures are complicated and energy intensive, thus less appealing for commercialization. Soft templates such as carbon fibers and natural membrane have also been used as inexpensive templates for sol-gel synthesis of micrometer size TiO$_2$ tubes,[197, 198] in which the soft template is conveniently removed through thermal decomposition during the calcination process to crystallize TiO$_2$. For preparing nanotubes or other shapes of a desired size, however, the limited source of existing templates makes the synthesized organic materials more attractive. For instance, cationic colloidal particles have been used to prepare hollow TiO$_2$ nanospheres by thermal condensation of the TiO$_2$ shell on the template, followed by calcination to remove the polystyrene core.[195] Also poly (styrene-block-2-vinylpyridiane) diblock copolymers have been used to synthesize highly dense arrays in a regular pattern of TiO$_2$ nanoparticles through a sol-gel process.[199, 200]

In the past years, living radical/controlled polymerization (LCP) techniques provide the synthesis of block copolymers with well-defined architectures.[201] Among the LCP techniques, the reversible addition-fragmentation chain transfer technique offers exceptional versatility in providing polymers of predetermined molecular weight and very narrow polydispersity and it is recognized as one of the most versatile methods for block copolymer synthesis, with numerous examples reported.[71] The usual procedure for synthesizing diblock copolymers via RAFT consists in the synthesis of a macro RAFT agent, which will then be used for the polymerization of the second monomer.

Recently, amphiphilic block copolymers have been increasingly used to organize mesostructured composite solids, because the architectures of the these copolymers can be used to control the morphology and interactions between the inorganic and organic species.[202, 203] As mentioned in Ch.2, the amphiphilic block copolymers have the ability to self-assemble into supramolecular architectures.[204] Park *et al.* reported the preparation of metal nanoparticles at the PEtOz shell by using poly(2-ethyl-2-oxazoline)- poly(ε-carprolactone) (PEtOz-PCL) micelle as a template in an aqueous phase.[205] Also microporous zeolites are templated by single molecules, while mesoporous zeolites are templated by assemblies of molecules like block copolymers.[206]

Metal alkoxides or salts are widely used as the precursors for synthesizing metal oxides with various morphologies via a sol-gel route. This synthetic method generally allows control of the texture, chemical, and morphological properties of the solid. Carboxylic acid is known to react with titanium alkoxide to form a Ti-bridging carboxylate complex.[207] The coordination chemistry of metal ions with the carboxylate group has been previously well studied by single crystal X-ray diffraction and FTIR,[124,]

151

[207-209] and it has been used to synthesize a number of metal oxides with different morphologies.[154, 210-213]

In this study, the amphiphilic diblock copolymer, polymethyl methacrylate-block-polyacrylic acid (PMMA-b-PAA), was synthesized via RAFT polymerization and was used as a template to synthesize TiO_2 with different morphologies. The PMMA moiety was used to form the micelle core structure in the polar solvent, while the polar PAA tail was used to interact with Ti complexes via coordination bonding. The TiO_2 anatase nanoarchitectures were obtained after calcination to remove the polymer template. It was found that the TiO_2 morphology was a function of the size of PAA moiety in the block copolymers: short PAA chains facilitated formation of a polymer core-TiO_2 shell structure, while longer PAA chains are feasible for nanotube structures.

8.2. Experimental

8.2.1. Materials

Titanium tetraisopropoxide (TTIP, Sigma-Aldrich), 2, 2′-azobis (2-methylpropionitrile) (AIBN) initiator (Toronto Research Company), and isopropanol (anhydrous, Sigma-Aldrich) were used as received. Methyl methacrylate (MMA) and Acrylic acid (AA) monomers (99%, Sigma-Aldrich, inhibited with 200 ppm BHT) were passed through an inhibitor removal column (Sigma-Aldrich) before use. The RAFT agent 4-cyano-4-(dodecylsulfanylthiocarbonyl) sulfanyl pentanoic acid (**3**) was prepared as described elsewhere (for more detailed description see Appendix 3).[126]

8.2.2. Synthesis of PMMA in THF

Methyl methacrylate was polymerized in solution via the RAFT technique based on the procedure in Ch.5. The polymerization was stopped after 5 hours and the product was used for the next step without adding an inhibitor.

8.2.3. Synthesis of PMMA-b-PAA in THF

14 mL of AA monomer, 0.7 g of PMMA, and 0.010 g of AIBN were dissolved in 120 mL THF. The solution was transferred to a 250 mL three-neck flask equipped with nitrogen supply, a thermometer, and a condenser under constant stirring at 70 °C. At various time intervals during the polymerization, samples were taken for GPC analysis. The polymerization was stopped at the reaction time of 6 hours. In the clear solution 200 mL of methanol was added, which resulted in precipitation of the block copolymers. The polymer was separated through filtration and was dried in vacuum at 50 °C for 12 hours. Figure 8.1 summarizes the synthesis of PMMA-b-PAA.
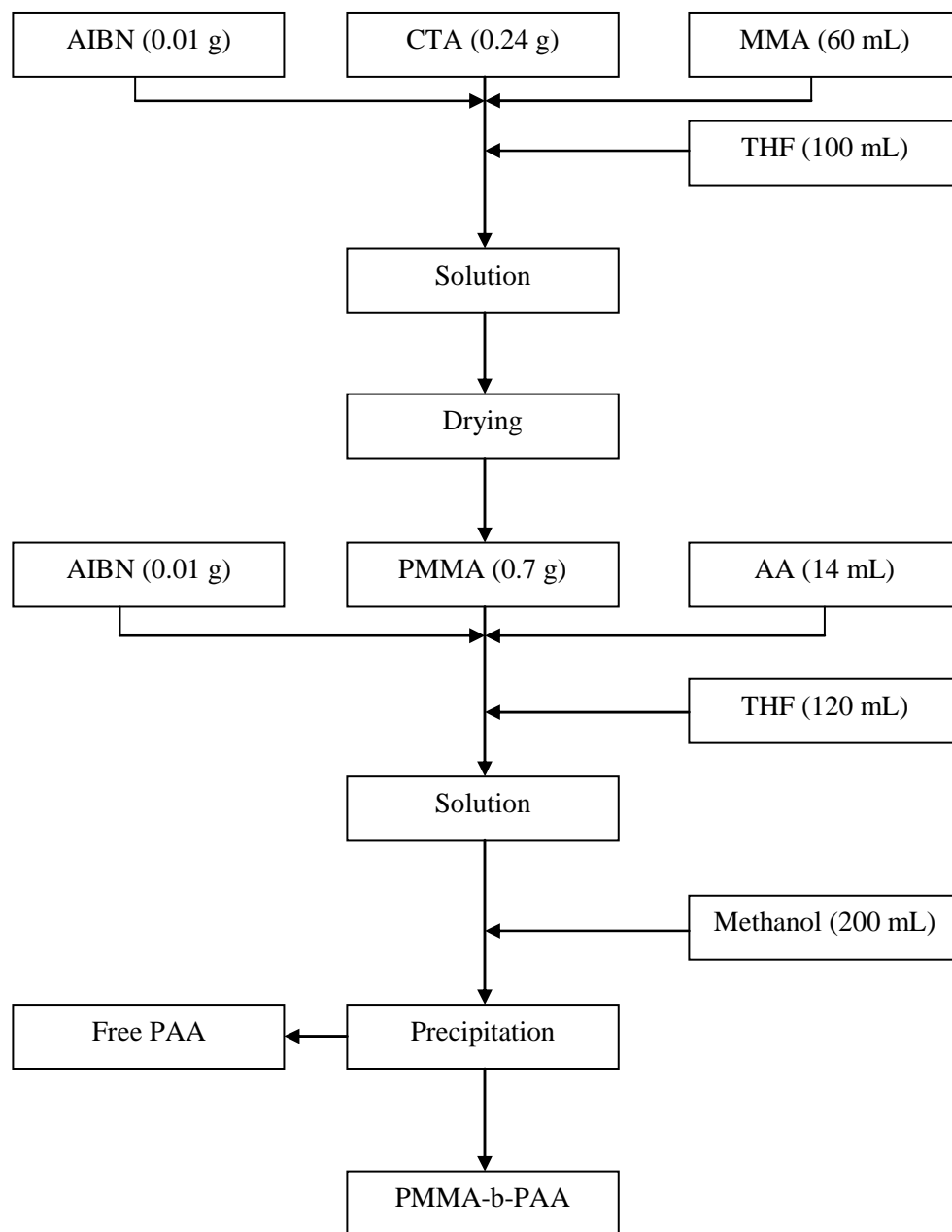
Figure 8. 1 Preparation scheme for PMMA-b-PAA via RAFT polymerization.

8.2.4. Synthesis of mesoporous TiO₂

As mentioned in section 8.1, in this step, the carboxylic groups of PAA were needed, so a good solvent for PAA such as isopropanol was used. After dispersion of 0.5 g PMMA-b-PAA in 50 mL isopropanol at room temperature, 10 mL of TTIP were

transferred to the reactor equipped with FTIR probe. The reactor was heated to and maintained at 65 °C for 48 h. The obtained solid product was separated from the solution by centrifugation, which was followed by calcination at 600 °C for 2 h with a heating rate of 1.5 °C/min to remove the polymer template. Figure 8.2 summarizes the synthesis of mesoporous TiO_2.
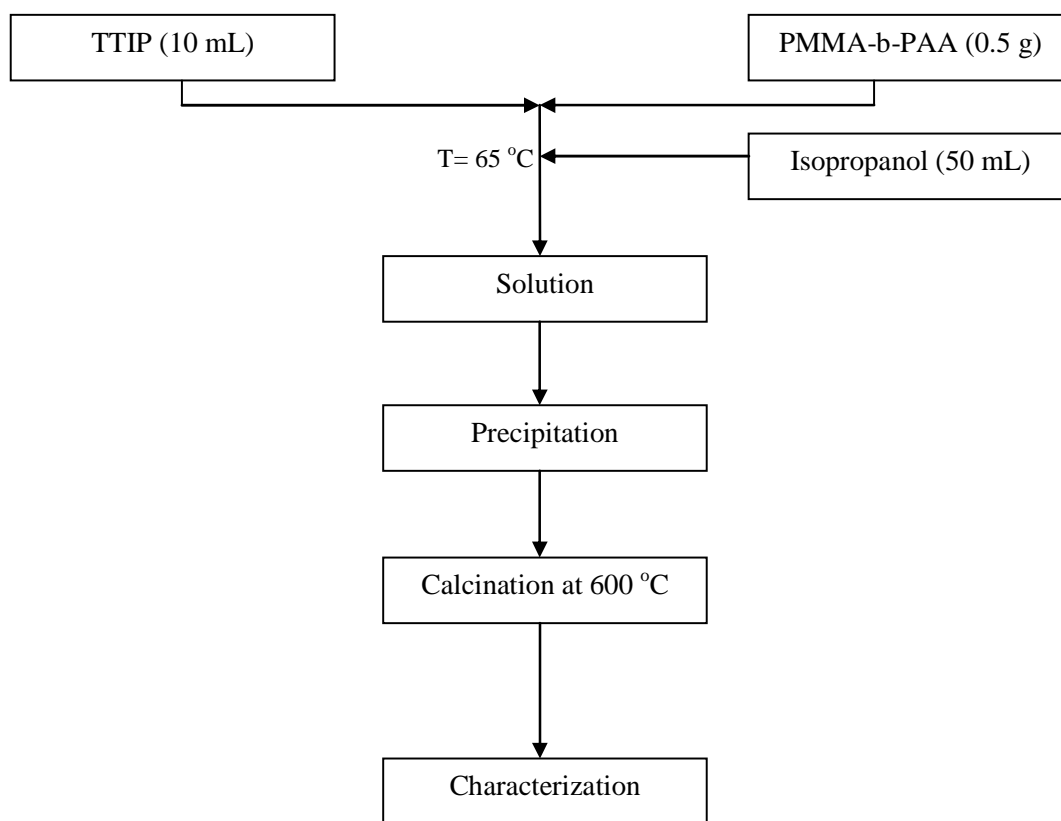
Figure 8. 2 Preparation scheme for mesoporous TiO$_2$ by sol-gel process.

8.3. Characterization

The molecular weights and PDIs of PMMA and/or novel PMMA-b-PAA were amphiphilic copolymer measured by gel permeation chromatography (GPC) with a Viscotek instrument using triple detectors (RI, LS, and V) referenced to PS standards (1

ml/min, at 30 $^{\circ}$C). In-situ FTIR monitoring of solution concentration in the stirred autoclave was performed using a diamond immersion probe (Sentinel-ASI Applied Systems). The probe is attached to an ATR-FTIR spectrometer (ASI Applied System ReactIR 4000). The spectra were collected automatically with a resolution of 2 cm^{-1} and 128 scans for each sample. Powder XRD was performed on Bruker D8 Discover Diffractometer with GADDS employing CuKα radiation for the crystalline analysis. The samples were finely ground and spread on a glass substrate. Scanning electron microscopy (SEM) images were recorded using a LEO 1530 instrument without gold coating at 10 kV, and transmission electron microscopy (TEM) was performed using either a JEOL 2010 operated at 200 kV or Philips CM 10 at 80 kV a Phillips CM 10 electron microscope at 80 kV, with dispersed samples in hexane. Brunauer-Emmett-Teller (BET) surface area, pore size and distribution were obtained on Micromeritics ASAP 2010 at 77 K. Prior to the N_2 physisorption, a sample was degassed at 200 °C under vacuum.

8.4. Results and Discussions

The novel PMMA-b-PAA copolymers were synthesized according to the scheme as given in Figure 8.3.

The reaction scheme shows:

$$Z\text{-}S\text{—}\underset{\|}{\overset{S}{C}}\text{—}S\text{—}R \xrightarrow[\substack{\text{AIBN,THF} \\ 75\text{-}78\,^\circ\text{C, 24 h}}]{\text{MMA}} Z\text{-}S\text{—}\underset{\|}{\overset{S}{C}}\text{—}S\text{—}(CH_2C(CH_3)COOCH_3)_n\text{—}R$$

(3)

$$\xrightarrow[\substack{\text{AIBN, THF} \\ 70\text{-}75\,^\circ\text{C}}]{\text{AA}} Z\text{-}S\text{—}\underset{\|}{\overset{S}{C}}\text{—}S\text{—}(CH_2CHCOOH)_m\text{—}(CH_2C(CH_3)COOCH_3)_n\text{—}R$$

$R = CH_3CCNCH_2CH_2CO_2H$

$Z = SCH_3(CH_2)_{11}$
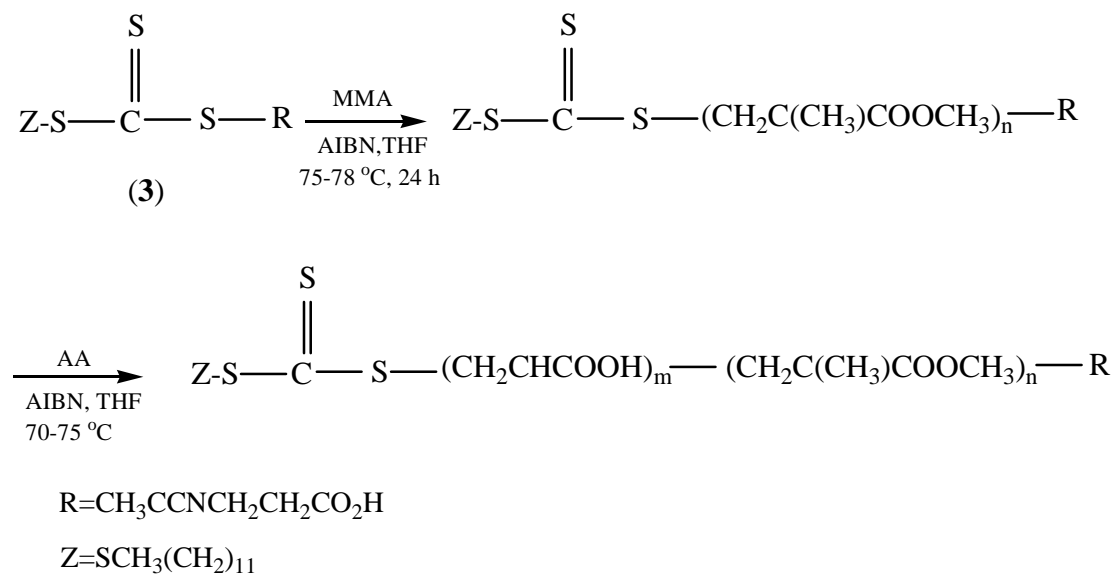
Figure 8. 3 Synthesis of PMMA-b-PAA.

8.4.1. Molecular Weight Determination

Figure 8.4 shows the GPC elution profiles of the PMMA-b-PAA obtained using solution polymerization with RAFT agent (**3**) at the reaction time of 1-6 hours, in which the molecular weight distributions can be observed to be unimodal. Living polymerization is known to show the characteristics of a linear increase of the molecular weight with conversion and reaction time, and a narrow molecular weight distribution, as indicated by the polydispersity index (PDI) approaching 1. Table 8.1 summarizes how the M_n of PMMA and PMMA-b-PAA change with conversion or time, where the conversions were determined gravimetrically. It can be observed that M_n was proportional to the reaction time. The low PDIs indicate that a living polymerization took place. Comparing with the previous reports by Chen *et al.* [176] and Peng *et al.,* [177] the RAFT approach used in this research produced PMMA-b-PAA with higher molecular

weight and narrower PDIs than the methods through hydrolysis of PMMA-*b*-P*t*BA via DPE and hydrolysis of poly(methoxymethyl acrylate)-b-PMMA via ATRP methods.

Table 8. 1 Molecular weight, PDIs, and conversions of PMMA and PMMA-b-PAA at different reaction times.

Samples	Time (h)	M_n (g/mol)	PDI	Conversion (%)
PMMA	1	5,760	1.3	15
PMMA	5	9,200	1.2	60
PMMA-b-PAA (T_1)	1	10,200	1.5	7
PMMA-b-PAA (T_2)	2	14,000	1.4	20
PMMA-b-PAA (T_3)	3	16,000	1.3	30
PMMA-b-PAA (T_4)	4	17,600	1.4	42
PMMA-b-PAA (T_6)	6	22,900	1.4	55
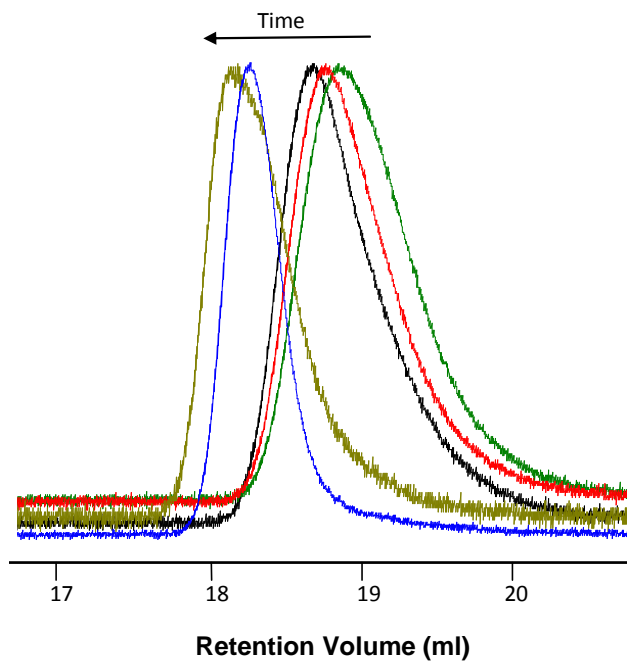
Figure 8. 4 GPC elution profiles of PMMA-b-PAA for 1h (Mn = 10,200 g/mol, PDI= 1.5), 2 h (Mn = 14,000 g/mol, PDI= 1.4), 3h (M_n = 16,000 g/mol, PDI = 1.3), 4h (M_n = 17,600 g/mol, PDI = 1.4), and 6h (M_n = 22,900 g/mol, PDI = 1.4).

8.4.2. ^{1}H NMR

Evidence in the support of the overall RAFT reaction is the retention of the RAFT agent end groups, which can be demonstrated by NMR.[86] The dissolved PMMA and PMMA-b-PAA in DMSO-d$_6$ were examined using ^{1}H NMR (Figure 8.5); however, end group signals were not evident in ^{1}H NMR spectra for block copolymer samples. This is typical for high molecular weight of polymers. The ^{1}H NMR spectra of PMMA and PMMA-b-PAA are shown in Figure 8.5a-b, respectively, which confirms that the RAFT copolymerization reaction occurred.

PMMA (DMSO-d$_6$): 0.7, 0.9, 1.2 (3H, C**H**$_3$), 1.7 (2H, C**H**$_2$), 3.5 (3H, COOC**H**$_3$)

PMMA-b-PAA (DMSO-d$_6$): 0.7, 0.9 (3H, C**H**$_3$), 1.5 (2H, C**H**$_2$), 1.7 (2H, C**H**$_2$), 2.2 (1H, C**H**COOH), 3.5 (3H, COOC**H**$_3$), 12.3 (1H, COO**H**)
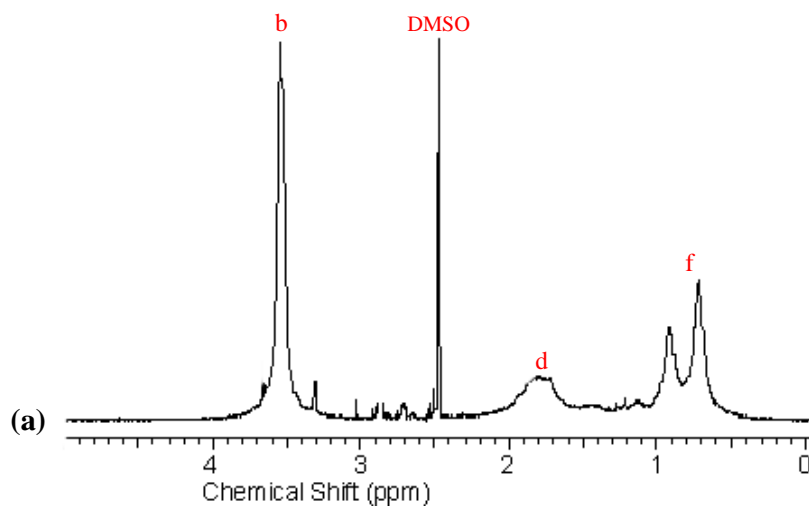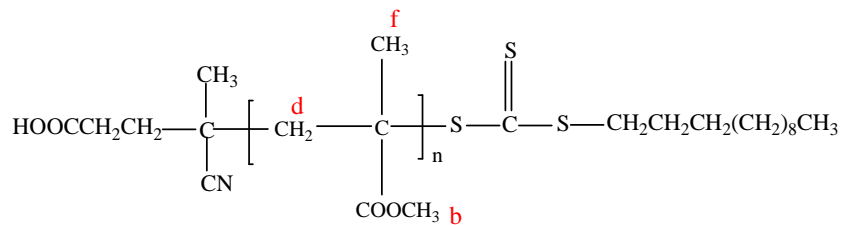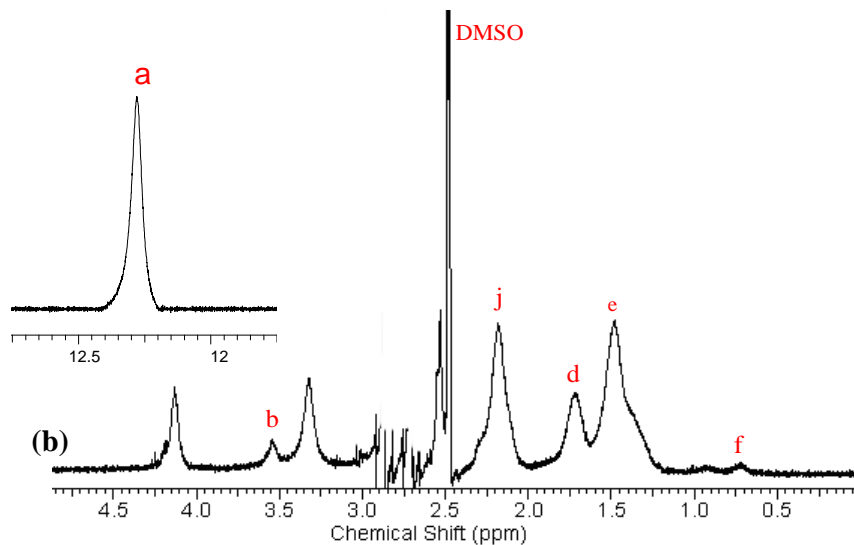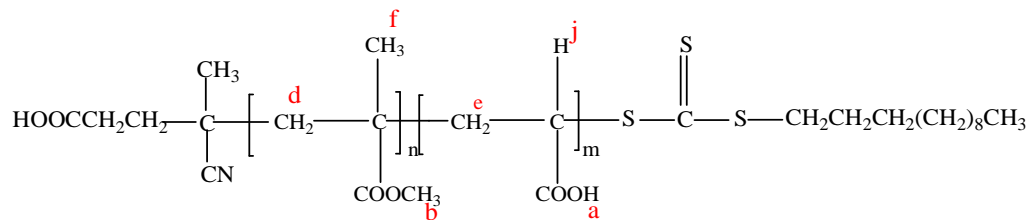
Figure 8. 5 ^{1}H NMR spectra of (a) PMMA, and (b) PMMA-b-PAA.

160

8.4.3. Electron microscopy

To investigate the morphology of PMMA-b-PAA, the polymers at different stages of polymerization were dissolved in methanol and deposited on the TEM grids (Cu-200 FC) and examined with TEM. Methanol has a strong interaction with PAA but is a poor solvent for PMMA, so the block copolymers form micelles with PMMA cores surrounded by PAA corona. Figure 8.6a shows that round micelles were formed in the PMMA-b-PAA$_1$ sample, which can be attributed to the strong PMMA-PMMA interaction; the PAA blocks are not long enough to be easily recognized. As the length of the PAA block increased from PMMA-b-PAA$_2$ to PMMA-b-PAA$_6$, the micelles grew and cross-linked into networks (Figure 8.6b-d). The strong interaction between PAA chains in the corona facilitates the network self-assembly,[94] and the PMMA cores located at the intersections. As previously mentioned in Ch.2, the amphiphilic nature of many block copolymers is manifested by the tendency to phase separate and promote self-assembly or micelle formation in different solvents. This self-assembly of the amphiphilic block copolymers can be explained by the strong supramolecular force between PAA blocks such as hydrogen bonding and electrostatic forces, and the solvophobic effects between the PMMA and the solvent. In self-assembled structures, these temporal intermolecular forces connect the molecular scale building blocks in a reversible, controllable and specific way.
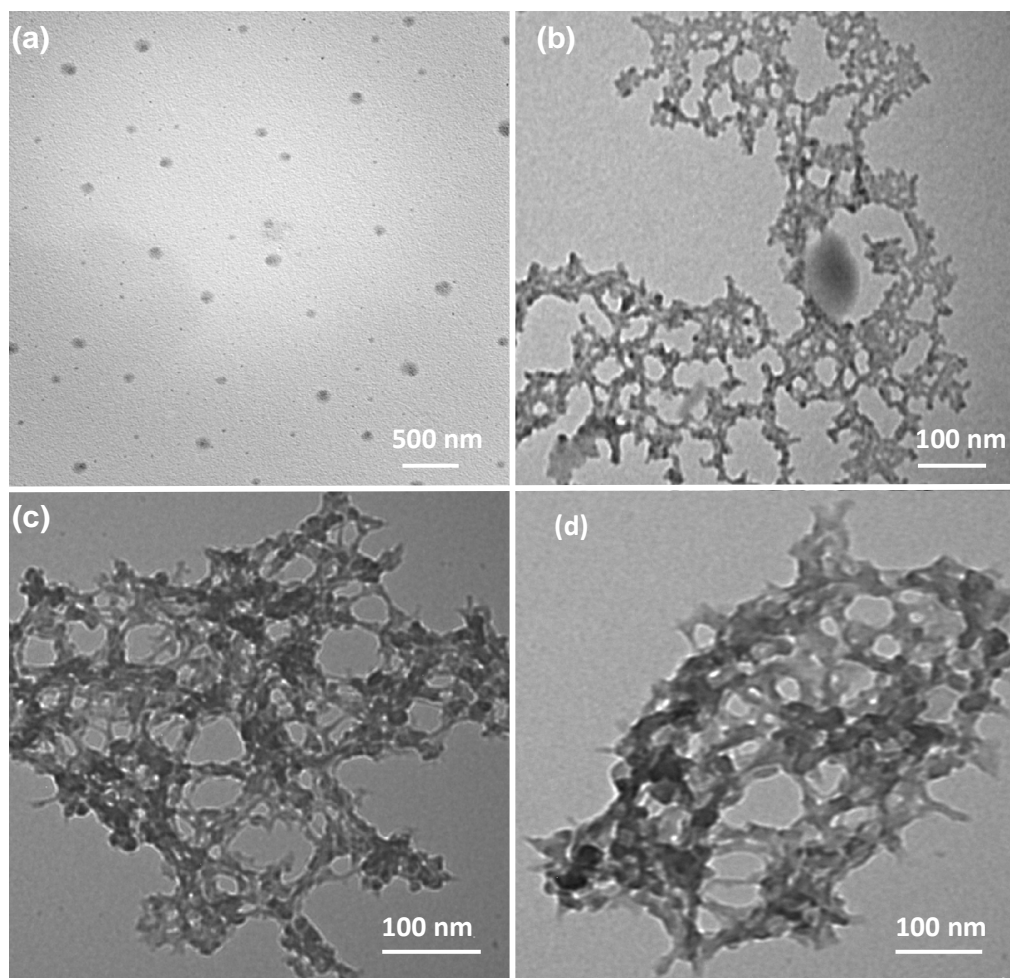
Figure 8. 6 TEM images of (a) PMMA-b-PAA$_1$, (b) PMMA-b-PAA$_2$, (c) PMMA-b-PAA$_3$, and (d) PMMA-b-PAA$_6$.

8.4.4. *In-situ* FTIR

In-situ FTIR has been an established technique for studying the reaction mechanism and reaction kinetics of the sol-gel reactions between TTIP and carboxylic acids.[130, 212] In this research, it was used to investigate the polycondensation reactions of TTIP reacting with the PAA of the block copolymers. As shown in Figure 8.7, the IR spectra were collected from 60-4320 min, and various reaction chemistries including formation of the Ti-carboxylate complex, polycondensation products, and consumption of the carboxylic acid group of PAA and titanium alkoxide is apparent. Consumption of

162

COOH⁻ of PAA can be observed from the decreasing peak at 1715 cm^{-1}, while the consumption of TTIP alkoxide precursor can only be observed from the peak at 1320 cm^{1}, as the other strong peaks of TTIP from 950 to 1120 cm^{-1} are in the fingerprint region of isopropanol and propyl carboxylate, hence being obscured. In Figure 8.7a, the new peaks at 1670 and 1480 cm^{-1} are assigned to the asymmetric (v_{asym}) and symmetric (v_{sym}) stretching modes of Ti-carboxylate monodentate, respectively.[123] This is an important observation providing direct evidence of coordination. These Ti-carboxylate monodentate peaks disappeared after the reaction time of 300 min, and transformed into Ti-carboxylate bidentates which show peaks at 1580 and ~1450 cm^{-1} (Figure 8.7b-d). The progressive increasing of the peaks at 760 cm^{-1} in spectra (Figure 8.7b-d) indicates the formation of μ_2-oxo bridging bonds, suggesting the polycondensation of the Ti precursors and/or Ti complexes presumed around the PAA chains.
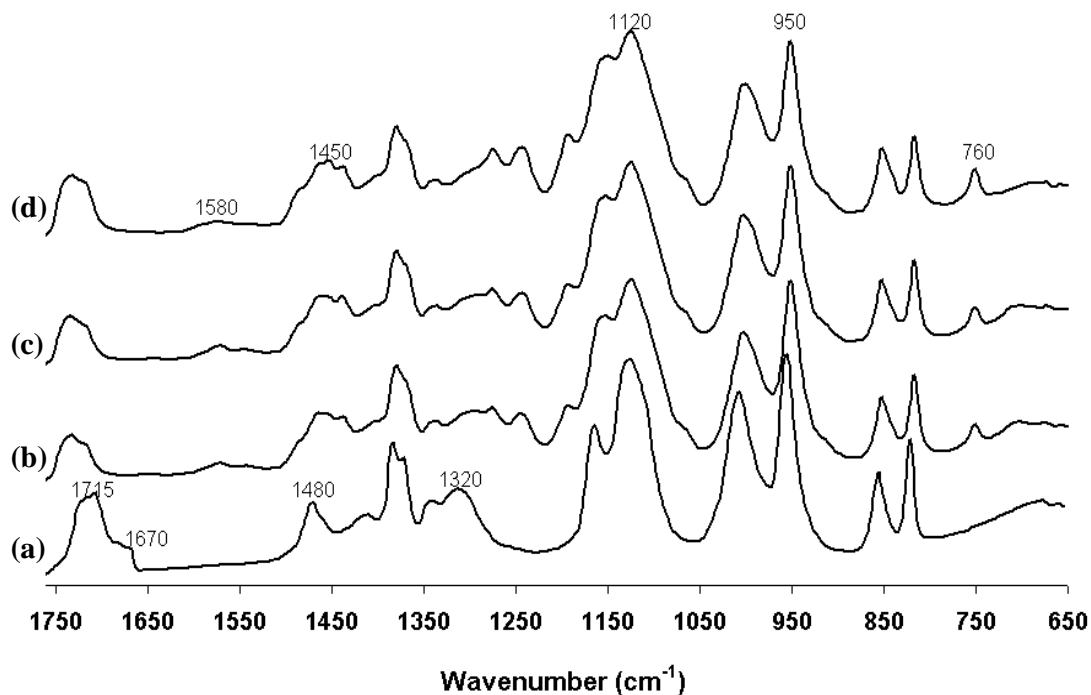
Figure 8. 7 In situ FTIR spectra of polymerization of TTIP with PMMA-b-PAA (T$_4$) in isopropanol at 60 °C. Reaction time: (a) 60 min; (b) 300 min; (c) 900 min; (d) 4320 min.

8.4.5. Electron microscopy

The effects of the chain length of PAA in PMMA-b-PAA on the TiO_2 morphology were studied using SEM and TEM analysis after removal of the polymer templates (T_1-T_6) at 600 °C.

The SEM micrograph (Figure 8.8a) shows that the short PAA chain in diblock copolymer template (T_1) produced agglomerated TiO_2 spherical particles with diameters in the range of 10-80 nm. When T_2 was used as templates, there were rods with diameter 40-300 nm and length of 200-4000 nm besides the TiO_2 spherical particles (Figure 8.8b). Figure 8.8b inset shows the top view of the rod particles. By increasing the chain length of PAA, interactions between the carboxylic groups of PAA and RAFT agent produce a self-assembly phenomena (Figure 8.6c-d). Reaction of titanium isopropoxide with the carboxylic groups in this network creates large spherical particles. However, after heat removal of the block copolymer, the morphology of these particles is changed to hollow core/shell structures, having a wall thickness ~ 110 nm (Figure 8.8c-d). Figure 8.8c inset shows the thichness of the wall (~ 110 nm). As the time of the block copolymerization increased from 4 to 6 hours, the cluster size of PAA (chain length) is increasing, which means the ratio of PAA/TTIP is increasing. The reaction between titania alkoxide and carboxylic groups of these long chains produces some hollow core/shell and nanotubular structures with diameters 10-25 nm as well (Figure 8.8e-f). This can be explained by the hydrogen bonding between the long chains resulting in breaking some supramolecules after heat removal, as it is well known that the morphology of mesoporous materials depend significantly on the synthesis conditions, such as solvent,[202] calcination temperature,[214] and template concentration.[215]
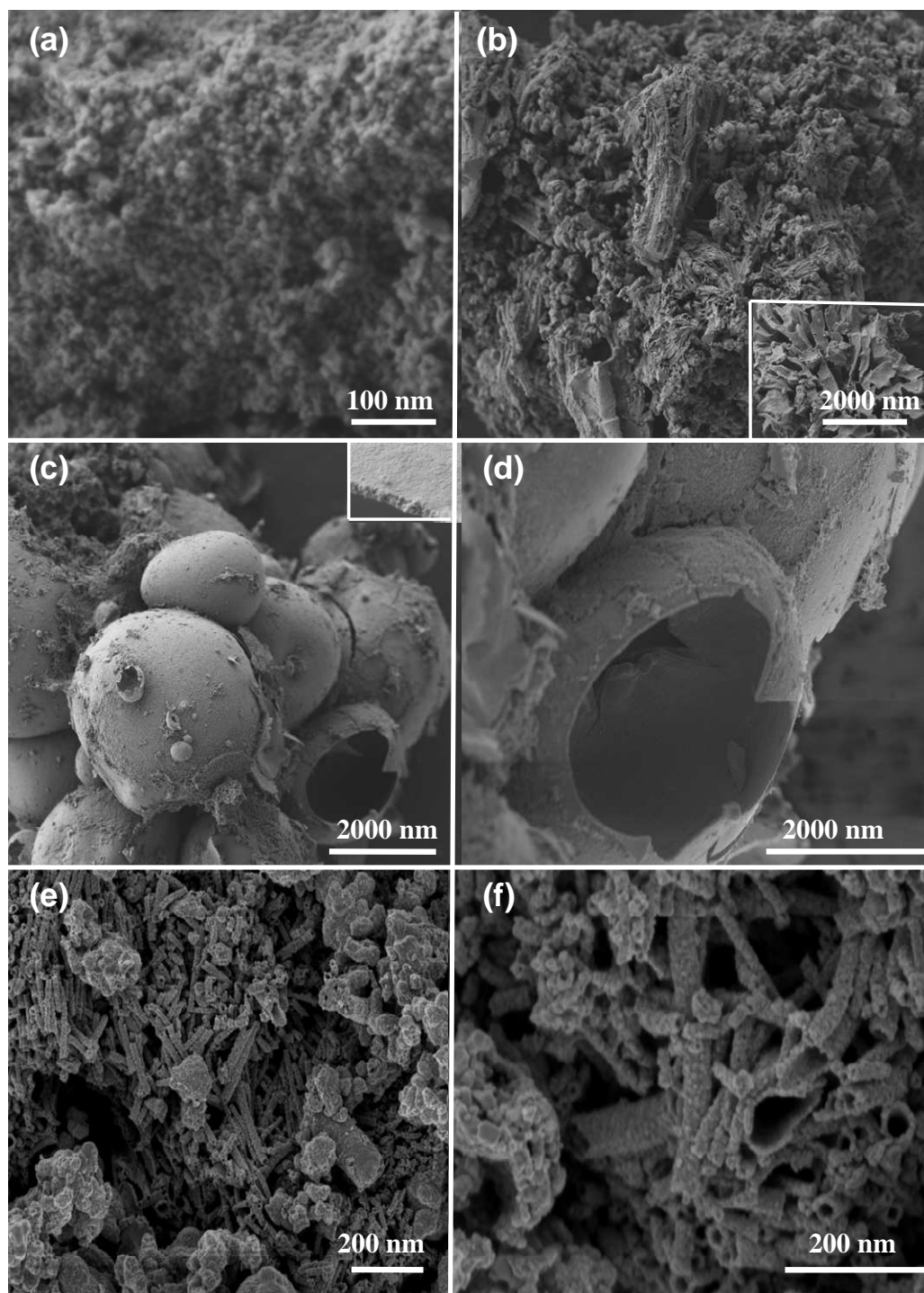
Figure 8. 8 SEM images of mesoporous TiO$_2$ using TTIP (0.68 M) and (a) T$_1$, (b) T$_2$, (c-d) T$_3$, and (e-f) T$_4$ and T$_6$ as templates.

165

Different from SEM images that "scan" the specimen and only provide surface information on the nanomaterials, TEM images can provide more details about the microstructure underneath the surface, and as important, crystal information. Figure 8.9 shows the TEM image of mesoporous TiO_2 calcined at 600 °C for 2 hours. Using the short chain length of PAA (T_1 and T_2) (Figure 8.9a) both the crystalline and amorphous phases can be observed. Selected area electron diffraction patterns recorded on mesoporous TiO_2 show the wall of these materials are comprised of nano crystalline oxides with characteristic diffuse electron diffraction rings (Figure 8.9a inset), which is consistent with the XRD measurement (Figure 8.12). The TEM image in Figure 8.9b indicates that the morphology of synthesized TiO_2 after increasing the chain length of PAA in diblock copolymer template (T_3 and T_4) was changed to a hollow core/mesoporous shell. However, because of the thickness of the shell wall (~110 nm) and the agglomeration of TiO_2 particles, electron beams cannot pass through the shell which results in a dark image of the core. Upon increasing the PAA chain length, the morphology of TiO_2 is changed to hollow core/mesoporous shells and nanotubes having length ca. 500-750 nm as shown in Figure 8.9c-d. These images are consistent with the SEM images (Figure 8.8e-f). It has been shown that not only the type of template but also the template agent concentration in the initial gel has a strong impact on the morphology and crystal size of mesoporous metal oxides.[216] HRTEM of the sample provides the reflection pattern of the crystalline phase (Figure 8.9e-f). The d-spacing of 0.35 nm indicates that the (101) lattice plane of anatase is present.[217]
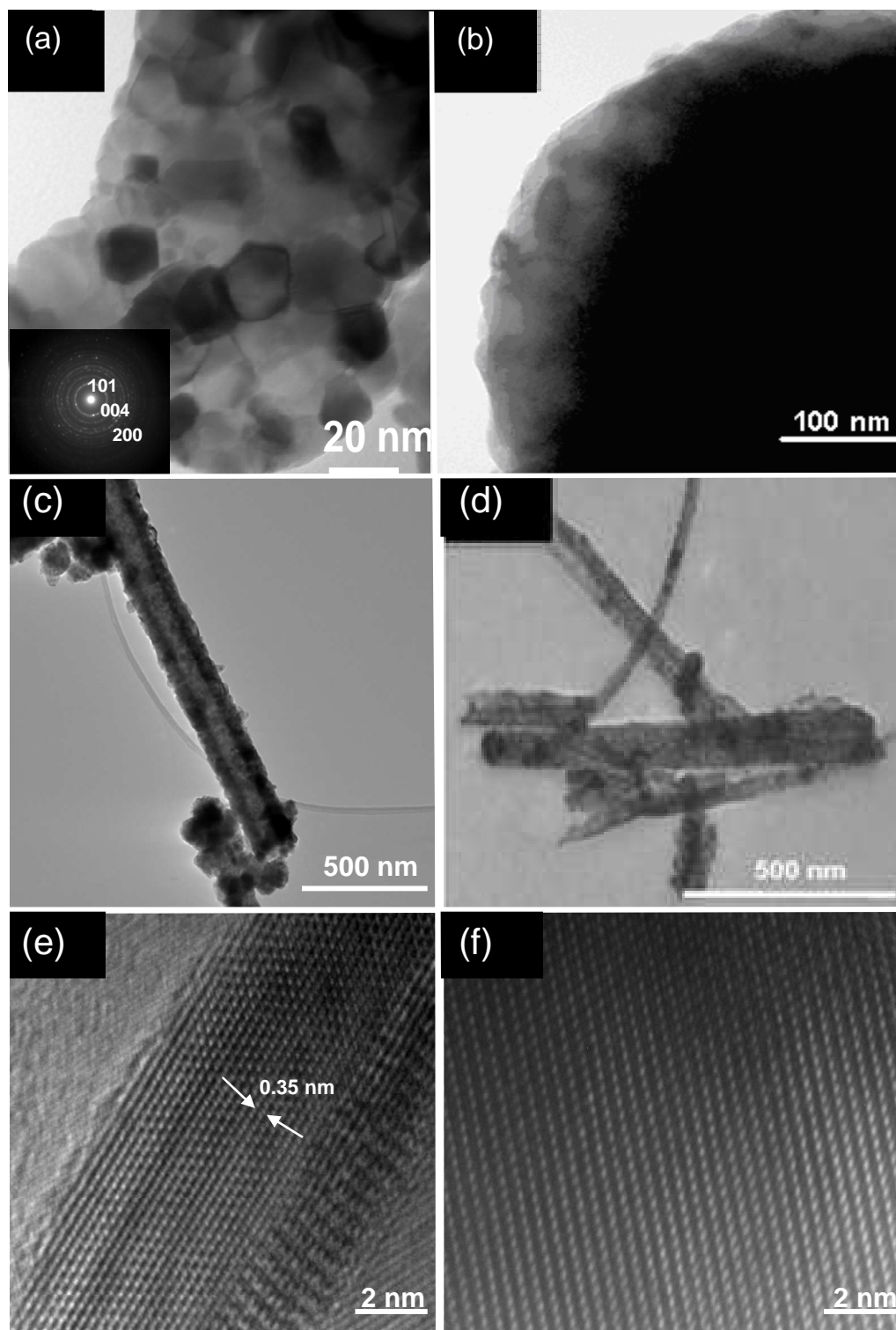
Figure 8. 9 TEM images TiO$_2$ using polycondensation of TTIP on templates of (a) T$_1$ and T$_2$, (b) T$_3$ and T$_4$, (c-d) T$_6$, and (e-f) HRTEM images of TiO$_2$ nanotubes followed by calcination at 600 °C.

167

From the above electron microscopy analysis results, the TiO_2 morphology is a function of the chain length of PAA block. When the PAA chains were short such as T_1 and T_2, no obvious templating effects were observed. We hypothesize that there were not enough COO^- groups in the block copolymers that manipulate the assembly of the metal complexs to form well-defined nanostructures around the polymer micelle. With the PAA chain length increasing, there were more COO^- groups that can coordinate to the Ti complexes. The Ti complexes attached to the PAA chains will polycondensate with other Ti complexes, forming Ti-O-Ti oxo bonds eventually resulting in a core-shell structure. The polymers are cores and the Ti complexes are shells. When the PAA chains were not very long, e.g., T_3 and T_4; the Ti complexes surround the micelle structures, and TiO_2 hollow spheres are formed after calcination. When the PAA chains were long enough (e.g., T_6), as described in Figure 8.10, the Ti complexes could surround both the micelle and the long PAA chains to form core-shell structure, and calcination of these structures results in hollow spheres and nanotubes, respectively.
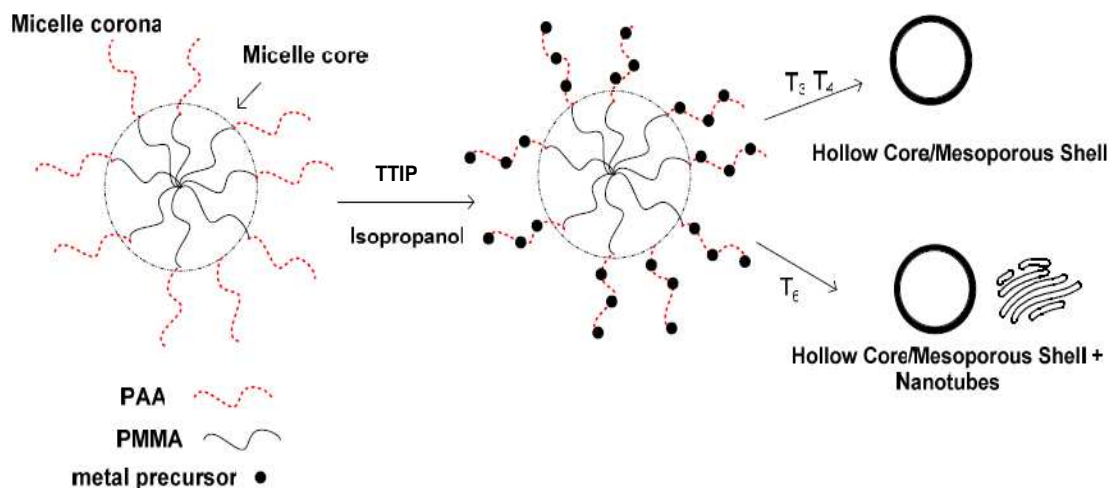
Figure 8. 10. Schematic formation of TiO_2 hollow spheres and nanotubes.

8.4.6. N_2 physisorption

N_2 physisorption was used to study the surface area and the mesopore structures of the TiO_2 materials (Figure 8.11). The N_2 isotherms of the resulting TiO_2 after calcination show type-IV curves with H3 loops according to the IUPAC definition, suggesting the existence of mesopores (2-50 nm in diameter).[218] The mesopore structures can be observed from the hysteresis loops (Figure 8.11a) and the pore size distribution (Figure 8.11b). A narrow hysteresis loop and pore size distribution was observed for TiO_2 spheres and rods (prepared using T_1 and T_2 templates), attributed to the relatively small void space between the particles. A larger pore size distribution was observed for TiO_2 hollow spheres and nanotubes, because of the irregular shape and size of the void space between the TiO_2 structures. It should be pointed out that N_2 physisorption is not able to detect macropores (>50 nm) that exist in the TiO_2 hollow spheres and between the nanotube bundles.
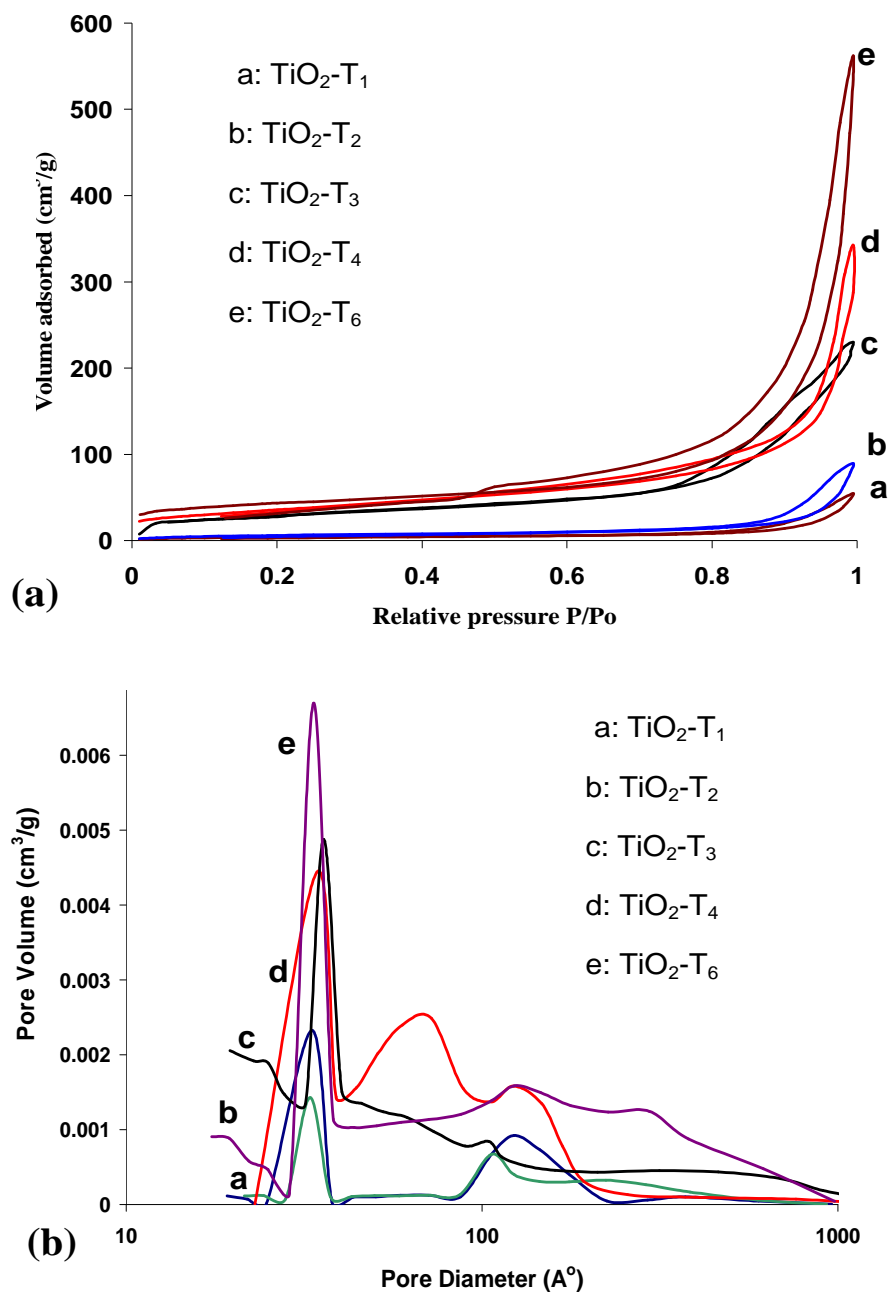
Figure 8. 11 (a) Isotherm plots and (b) pore size distributions of the mesoporous TiO₂ prepared using different templates.

BET surface area calculated from the N$_2$ adsorption reveals that the specific surface area of the synthesized mesoporous TiO$_2$ increased progressively with increased chain length of PAA (Table 8.2). For instance, the BET surface areas increased from 15

to 153 m^2/g when T_6 template was used instead of T_1, which is partially attributed to the morphological change from spherical to hollow core/shell structure.

Table 8. 2 Surface area, pore volume, pore diameter and morphology of the calcined TiO$_2$ using different templates.

Template	BET (m^2/g)	Pore Vol. (cm^3/g)	Pore Dia. (nm)	Morphology
T_1	15	0.05	14	Spherical
T_2	28	0.08	12	Rod/Cylinder
T_3	105	0.2	11.4	Hollow Core/Shell
T_4	129	0.35	9.1	Hollow Core/Shell
T_6	153	0.5	13	Hollow Core/Shell + nanotubes

8.4.7. XRD

The XRD patterns of the as-prepared and calcined mesoporous TiO$_2$ particles are presented in Figure 8.12. Figure 8.12a shows that the as-prepared sample is amorphous because of the absence of any peaks. After calcination at 600°C, five crystal peaks at 25.28^o, 37.80^o, 48°, 53.89^o, and 62.7^o appeared (Figure 8.12b), which can be assigned to diffraction from (1 0 1), (0 0 4), (2 0 0), (1 0 5), and (2 0 4) planes of anatase TiO$_2$, respectively (JCPDS No. 21-1272, 1988).[219] This figure shows that a pure anatase phase could be obtained, as it has been shown that titanium alkoxide, such as titanium ethoxide, titanium isopropoxide, or titanium butoxide usually create anatase TiO$_2$.[220]
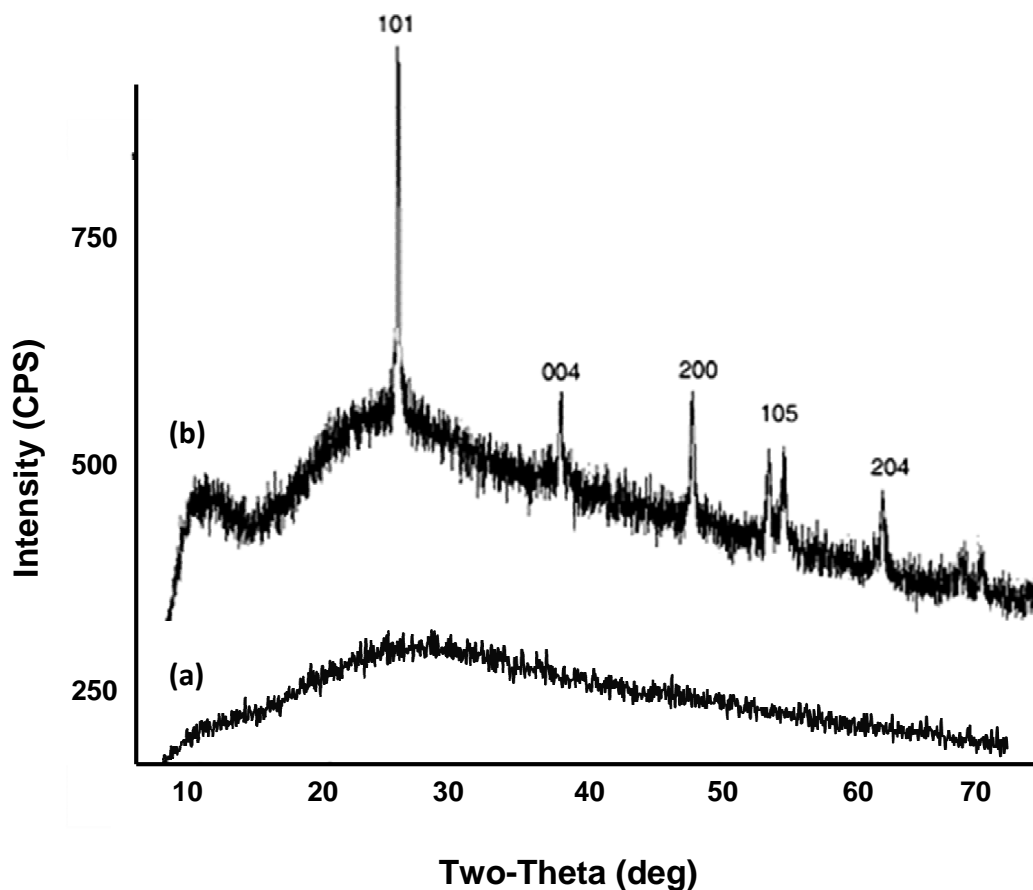
Figure 8. 12 X-ray diffraction (XRD) patterns of (a) as-prepared TiO$_2$, and (b) after calcination at 600°C.

8.5. Conclusions

The self-assembly and structural organization of the amphiphilic copolymer of PMMA-b-PAA were used to synthesize different morphologies of TiO$_2$ with relatively high surface area, via a sol-gel process in nonaqueous solvents. The in situ IR analysis showed the coordination of Ti precursors with PAA chains that was followed by polycondensations and formation of Ti-μ_2-oxo-Ti bonds. By varying the chain lengths of PAA, the morphology of the resulting materials was changed from spherical to hollow core/shell structures. Future work will be controlling the orientation of the amphiphilic

172

polymers and consequently the arrangement of TiO_2 nanotubes by using liquid-liquid interface or growing TiO_2 nanotubes from the surface of conductive glass substrates.

CHAPTER 9

CONCLUSIONS AND RECOMMENDATIONS

Surface functionalization of inorganic fillers with polymer chains (through covalent bonding) is attracting significant attention as the polymers alter the interfacial properties of these modified particles. In addition, the mechanical and thermal properties of the matrix polymers in hybrid systems can be improved by enhanced compatibility of the nanoparticles with the matrix. The main challenge in dispersing nanoparticles lies in controlling the inter-particle aggregation. It is necessary to stabilize these particles to prevent aggregation, which is done by either grafting polymer chains to the particle surface or growing them from the surface. These long polymer chains control the nanoparticle aggregation by steric repulsion. Another advantage of grafting polymer chains is that it improves the compatibility of the matrix with the particle surface.

In this research, a comprehensive study was conducted on developing a new method for controlling grafting of polymers from the surface of TiO_2 nanoparticles using an emerging living radical polymerization technique, reversible addition fragmentation chain-transfer (RAFT).[1] This approach allows the synthesis of advanced polymeric substrates for use in potential applications in catalysis, biomedical, and dye sensitized solar cells.

The study of livingness of polymerization with RAFT agents was the most important issue in this thesis which was examined using the analytical technique, GPC. RAFT agents were chosen not only for their living polymerization ability but also for having free carboxylic groups to functionalize TiO_2 nanoparticles. FTIR analysis, XPS, and organic phase/water phase partitioning studies provided the evidence of the functionalization of n-TiO_2 by the RAFT agent. TGA also was employed to calculate the surface density of RAFT agent on the surface of TiO_2 which was important for a kinetic

investigation. GPC results of cleaved polymer after various reaction times showed that the polymerization was still living, even after the RAFT agent was directly coordinated to n-TiO$_2$. Electron microscopy images revealed the growth of the "grafting from" polymers around n-TiO$_2$, and the nanofillers were well separated and distributed in the polymer matrix.

During solution polymerization, the effect of the concentration of RAFT agent on the rate of polymerization of MMA was investigated, with the experimental and theoretical molecular weights of PMMA compared. In the heterogonous phase, the kinetics of graft polymerization of MMA from the surface of n-TiO$_2$ was studied with two different surface densities, and it was found that the rate of reaction decreased with increasing the surface density of RAFT agent anchored to the nanoparticles. The kinetic studies were studied using *in-situ* ATR-FTIR.

With supercritical carbon dioxide (scCO$_2$) being considered as a viable alternative to organic solvents in various chemical processes, the RAFT technique was examined for grafting MMA onto the surface of functionalized n-TiO$_2$. The resulting polymers had a linear first-order kinetic plot with the molecular weight increasing linearly with conversion. The polymers had a PDI of between 1.2 and 1.5, with this broadening caused by the heterogeneous surface of the TiO$_2$ nanoparticles and incomplete separation of polymer chains from nanoparticles after cleaving. In addition, it was found that the rate of reaction and molecular weights increased with increasing pressure.

Further to this, amphiphilic brush copolymers of PMMA-b-PAA were produced through the RAFT system and also grafted from the functionalized TiO$_2$ nanoparticles. The attractive amphiphile and its precursors exhibited different self-assembly in solvents.

176

The results showed that living polymerization of both MMA and then AA initialized in the solution from AIBN and transferred to the functional groups on n-TiO$_2$ surfaces, which is promising to synthesize hybrid materials with excellent dispersion of the nanofillers in the matrix.

For several decades, much attention has focused on nano- or macroscopic metal oxides because of their specific chemical and physical properties which are distinct from those of bulk metal oxides. Research on these metal oxides is composed mainly of two aspects, preparation and application. Application of metal oxides in catalysis is regarded as an active research field. In this study, the amphiphilic copolymer of PMMA-b-PAA, which was grafted from TiO$_2$ nanoparticles, was used to produce NiO decorated TiO$_2$ by coordination of Ni to amphiphilic diblock copolymer following calcination to produce NiO/TiO$_2$. XRD and XPS confirmed the presence of NiO. This approach gave higher surface area and better metal dispersion than a conventional metal technique due to the steric stabilization of the nanoparticles allowing better decoration.

The amphiphilic copolymer of PMMA-b-PAA was also synthesized in solution and was used to produce mesoporous TiO$_2$ through a sol-gel method. Titanium isopropoxide (TTIP) was used as a starting material and the morphology of mesoporous materials was studied with different chain lengths of PAA in the diblock copolymer. This study showed different morphologies, from spherical to hollow core, can be obtained with increasing chain length. Also the surface area was increased from15 to105 m^2/g.

Recommendations

The application of the methodologies in this thesis are already being utilized by new graduate students in Charpentier's lab studying several applications, however there

is still much more work to be done in the development of controlled "grafting from" polymerization from surfaces. In particular, RAFT grafting from surfaces offers the advantage over other methods in that no chemical modification of the surface is required to conduct this grafting. However, a significant amount of work still needs to be done to fully realize the potential of this method, both in theory and in application.

Recommendations for future work include:

- In this study, the kinetics study including the effects of pressure (in $scCO_2$ case), the graft density of RAFT agent on the TiO_2 surface, and the concentration of RAFT agent in the solution polymerization were investigated. To better understanding this area, more kinetic investigations should be performed, such as the effect of temperature, the concentration of initiator (AIBN) and RAFT agents, and investigating other cosolvents.

- The kinetic study of graft polymerization from the functionalized TiO_2 in the presence of free RAFT agent would be interesting, and grafting thicknesses can be measured and compared.

- Different initiator should be employed to graft polymerization and the molecular weight and rate of reactions may be compared.

- "Grafting to" technique can be employed to synthesize polymer nanocomposites and the rate of reaction and thicknesses of polymer chains on the nanoparticles may be investigated.

- Although self-assembly of amphiphilic molecules in fluid media is one of the oldest topics of colloid science, it has gone through remarkable progress in the past decade. Block copolymers containing acrylic acid segments have been

extensively investigated during the last decade in terms of the synthetic methodologies for novel architectures, characteristic bulk and solution properties related with the self-organization process and a wide range of applications, with the knowledge increasing.[54] However, the well-controlled synthesis of complex macromolecules, such as branched and star polymers is still a challenging subject, and more information is required.

- One main goal of this study was to create a grafting method which could allow one to grow a wide range of polymers from nanoparticle surfaces. To this end, grafting reactions should be performed from substrates other than titania. The successful synthesis of the TiO_2-based nanocatalysts materials is encouraging to extend this method for synthesizing other oxide nanostructures, such as Al_2O_3 and ZnO, which are of interest in catalysis and photovoltaics.

- In the last couple of decades in scientific fields, the use of radiation grafting methods has been dramatically increased. Synthesis of polymer nanocomposites using γ-radiation controlled graft polymerization via the RAFT technique would be interesting.

BIBLIOGRAPHY

1.   Borisch.J; Pilkenton.S; Miller.M.L; Raftery.D; Francisco.J.S. *J Phys Chem B* **2004,** 108, 5640.
2.   Byl.O; Yates.J.T. *J. Phys. Chem. B* **2006,** 110, 22966.
3.   Schultz. E. *J Chem Educ* **2005,** 82, 1649.
4.   Mitchell, D. T.; Lee, S. B.; Trofin, L.; Li, N.; Nevanen, T. K.; Soderlund, H.; Martin, C. R. *J Am Chem Soc* **2002,** 124, 11864.
5.   Lee, S. B.; Mitchell, D. T.; Trofin, L.; Nevanen, T. K.; Soderlund, H.; Martin, C. R. *Science* **2002,** 296, 2198.
6.   Martin, C. R.; Kohli, P. *Nat Rev Drug Discovery* **2003,** 2, 29.
7.   Frisch, H. L.; Mark, J. E. *Chem Mater* **1996,** 8, 1735.
8.   Lu, M.-D.; Yang, S.-M. *Synthetic Metals* **2005,** 154, 73.
9.   Teo, B. K.; Li, C. P.; Sun, X. H.; Wong, N. B.; Lee, S. T. *Inorg. Chem.* **2003,** 42, 6723.
10.   Petrella, A.; Tamborra, M.; Curri, M. L.; Cosma, P.; Striccoli, M.; Cozzoli, P. D.; Agostiano, A. *J Phys Chem B* **2005,** 109, 1554.
11.   Kocher, M.; Daubler, T. K.; Harth, E.; Scherf, U.; Gugel, A.; Neher, D. *Appl Phys Lett* **1998,** 72, 650.
12.   Bisquert, J.; Cahen, D.; Hodes, G.; Ruhle, S.; Zaban, A. *J. Phys. Chem. B* **2003,** 108, 8106.
13.   Tokuhisa, H.; Hammond, P. T. *Advanced Functional Materials* **2003,** 13, 831.
14.   Zhu.J; Zhu.X; Cheng.Z; Zhang, Z. *Macromol. Symp.* **2008,** 261, 46.
15.   Lott, J. R. Reversible Addition-Fragmentation Chain-Transfer (RAFT) Polymerization in Grafting Polymer Chains from TiO2 Nanoparticles. Rochester Institute of Technology, Rochester, New York, 2006.
16.   Currie, E. P. K.; Norde, W.; Cohen Stuart, M. A. *Advances in Colloid and Interface Science* **2003,** 100, 205.
17.   Chieffari, J.; Chong, Y. K.; Ercole, F.; Krstina, J.; Jeffery, J.; Le, T.; Mayadunne, R.; Meijs, G. F.; Moad, C.; Moad, G.; Rizzardo, E.; Thang, S. H. *Macromolecules* **1998,** 31, 5559.
18.   Rong;, M. Z.; Zhang;, M. Q.; Zheng;, Y. X.; Zeng;, H. M.; Walter, K. F. *Polymer* **2001,** 42, 167.
19.   Husseman, M.; Malmstrom, E. E.; McNamara, M.; Mate, M.; Mecerreyes, D.; Benoit, D. G.; Hedrick, J. L.; Mansky, P.; Huang, E. R., T. P.; Hawker, C. J. *Macromolecules* **1999,** 32, 1424.
20.   Xie, S.; Zhang, S.; Wang, F. *J Appl Polym Sci* **2004,** 94, 1018.
21.   Minko, S.; Muller, M.; Motornov, M.; Mitschke, M.; Grundke, K.; Stamm, M. *J. Am. Chem. Soc.* **2003,** 125, 3896.
22.   Yosikawa, S.; Tsubokawa, N. *Polym. J.* **1996,** 28, 317.
23.   Binder.W.H; Sachsenhofer.R. *Macromol. Rapid Commun.* **2007,** 28, 15.
24.   Guerrero-Sanchez.C; Paulus.R.M; Fijten.M.W.M; Mar.M.J; Hoogenboom.R; Schubert.U.S *Applied Surface Science* **2006,** 252, 2555.
25.   Kunitake.N; Fujikawa.S. *Aust.J.Chem.* **2003,** 56, 1001.
26.   Lee, T. W.; Park, O. O.; Yoon, J.; Kim, J. J. *Advanced Materials* **2001,** 13, 211.

27.	McEuen P L; Bockrath M; Cobden D H; Lu J G. *Microelectronic Engineering* **1999,** 47, 417.
28.	Hojjati.B; Sui.R; Charpentier.P.A. *Polymer* **2007,** 48 5850.
29.	Wypych, F.; Satyanarayana, K. G. *J Colloid Interface Sci* **2005,** 285, 532.
30.	Katz.D.A. *Polymer* **2002,** 4, 13.
31.	Mikitaev.A.K; Ligidov.M.K; Zaikov.G.E, *Polymers, Polymer Blends, Polymer Composites and Filled Polymers. Synthesis, Properties, Application*. Nova Science Publishers.Inc.: Moscow, 2006.
32.	Moad.G; Solomon.D.H. *Polymer International* **1995,** 42, 346.
33.	Gilbert, R. G., *Emulsion Polymerization: A mechanistic approach*. London; Academic Press: 1995.
34.	Moad, G.; Rizzardo, E.; Thang, S. H. *Aus.J.Chem* **2005,** 58, 379.
35.	Szwarc.M.L; Milkovich.R. *Nature* **1956,** 178, 1168.
36.	Cazzniga.L.C.R.E. *Macromolecules* **1991,** 24, 5817.
37.	Fieser;, L. F.; M. Fieser. *Organic Chemistry; D.C. Heath and Company: Boston,* **1944**.
38.	O.W.Webster. *Science* **1991,** 251, 887.
39.	J.M.G.Cowie. *Polymers Chemistn' and Physics of Modern Materials; Blackie Academic and Professional: London,* **1991**.
40.	Otsu.T; Yoshida.M. *Makromol.Chem.Rapid Commun.* **1982,** 3, 4391.
41.	T.Otsu; M.Yoshida. *Macromolecular Chemistry: Rapid Communications* **1982,** 3, 127.
42.	S.R.Turner;; R.W. Blevins. *Macromolecules* **1990,** 23, 1856.
43.	N.A.A.Zwaneveld. Surface grafting of polymers via living radical polymerization techniques; polymeric supports for combinatorial chemistry. University of New South Wales, Sydney, Australia, 2006.
44.	G. Moad; J. Chiefari; J. Krstina; A. Postma; R. T. A. Mayadunne; E. Rizzardo; S. H. Thang. *Polym. Int.* **2000,** 49, 993.
45.	J.H.Xia; X. Zhang; K. Matyjaszewski. *Macromolecules* **1999,** 32, 4484.
46.	K.L.Beers; A.Kern; K.Matyjaszewski. *Polim Pepr. (Aim Chem. Soc. Div. Polym. Chem.)* **1997,** 38, 695.
47.	S.Angot; N.Ayres; S.A.Bon; D.M.Haddleton. *Macromolecules* **2001,** 34, 768.
48.	Kricheldorf.H.R; Nuyken.O; Swift.G, *Handbook of Polymer Synthesis*. Marcel Dekker: New York, 2005.
49.	Georges, M. K.; Veregin, R. P. N.; Kzamaier, P. M.; Hamer, G. K. *Macromolecules* **1995,** 28, 4391.
50.	Harwood, H. J. A., L.D,; Greuel, M. P. P. *Am.Chem.Soc.Div.Polym.Chem.* **1994,** 116, 7943.
51.	Benoit, D.; Grimaldi, S.; Finet, J. P.; Tordo, P.; Fontanille, M.; Gnanou, Y. *Polym.Prepr* **1997,** 38, 729.
52.	Yu, E.; Ritcher, M.; Chen, P.; Wang, X.; Zhang, Z.; Tavlarides, L. L. *Industrial and Engineering Chemistry Research* **1995,** 34, 340.
53.	M.Sawamoto; M.Kato; M. Kamigatto; Higashimura., T. *Macromolecules* **1995,** 28, 1721.
54.	ISO 13220:1999 Particle Size Analysis - Laser Diffraction Methods; ISO, G., Switzerland., In press.

55.   Pyun. J; Matyjaszewski. K. *Chem. Mater.* **2001,** 13, 3436.
56.   Odian.G, *Principles of polymerization*. John Wiley & Sons, Inc,Chapter 3: New York, 1981.
57.   Hu.B; Fuchs.A; Huseyin.S; Gordaninejad.F; Evrensel.C. *Polymer* **2006,** 47, 7653.
58.   Chiefari.J; Mayadunne.R.T.A; Moad.C.L; Moad.G; Rizzardo.E; Postma.A; Skidmore.M.A; Thang.S.H. *Macromolecules* **2003,** 36, 2273.
59.   Barner-Kowollik. C; Davis.T. P; Heuts.J. P. A; Stenzel.M. H; Vana.P; Whittaker. M. *J. Polym. Sci., Part A: Polym. Chem.* **2003,** 41, 365.
60.   Boyer.C; Bulmus.V; Davis.T.P; Ladmiral.V; Liu.J; Perrier.S. *Chem. Rev.* **2009,** 109, 5402.
61.   Le, T. P. T.; Moad, G.; Rizzardo, E.; Thang, S. H. *Chem. Abstr.* **1998,** 128, 115390.
62.   Hojjati.B; Charpentier.P.A. *Polym.Sci. part A: Polym Chem* **2008,** 46, 3926.
63.   Cacioli.P; Hawthorne.D.G; Laslett.R.L; Rizzardo.E; Solomon.D.H. *J Macromol. Sci.: Chem.A* **1986,** 23.
64.   Meijs.G.F; Rizzardo.E; Thang.S.H. *Macromolecules* **1988,** 21, 3122.
65.   Meijs.G.E; Rizzardo.E; Thang.S.H. *Polym. Bull. (Berlin)* **1990,** 24, 501.
66.   Meijs.G.E; Rizzardo.E; Thang.S.H. *Polym. Prepi* **1992,** 33, 893.
67.   Meij s.G.E; Rizzardo.E; Le.T.P.T; Chen.Y.C. *Macromol. Chem. Phvs.* **1992,** 193, 369.
68.   Mitsukami, Y.; Donovan, M.; Lowe, A.; McCormick, C. *Macromolecules* **2001,** 34, 2248.
69.   Stange, T. G.; Mathew, R.; Evans, D. F. *Langmuir.* **1992,** 8, 920.
70.   Barner-Kowolik.C. *Macromolecules* **2001,** 34, 7849.
71.   Chong.Y.K; Le.T.P.T; Moad.G; Rizzardo.E; Thang.S.H. *Macromolecules* **1999,** 32, 2071.
72.   Vana, P.; Davis, T. P.; Barner-Kowolik, C. *Macromolecular Theory and Simulations* **2002,** 11, 823.
73.   Kiang, C.-H.; Goddard, W. A., III; Beyers, R.; Bethune, D. S. *Carbon* **1995,** 33, 903.
74.   Moad.G; Rizzardo.E; Thang.S.H. *Polymer* **2008,** 49, 1079.
75.   Chong.Y. K; Krstina.J; Le.T. P. T; Moad.G; Postma.A; Rizzardo.E; Thang.S. H. *Macromolecules* **2003,** 36, 2256.
76.   Hawthorne.D.G; Moad.G; Rizzardo.E; Thang.S.H. *Macromolecules* **1999,** 32, 5457.
77.   Barner-Kowollik.C; Buback.M; Charleux.B; Coote.M.L; Drache.M; Fukuda.T; Goto.A; Klumperman.B; Lowe.A.B; Mcleary.J.B; Moad.G; Monteiro.M.J; Sanderson.R.D; Tonge.M.P; Vana.P. *Polym.sci.Part A: Polym.chem* **2006,** 44, 5809.
78.   Drache.M; Schmidt-Naake.G; Buback.M; Vana.P. *Polymer* **2005,** 46, 8483.
79.   Arita.T; Beuermann.S; Buback.M; Vana.P. *Macromol.Mater.Eng.* **2005,** 290, 283.
80.   Bozˇovic´-Vukic´.J; Man H.T; Meuldijk.J; Koning.C; Klumperman.B. *Macromolecules* **2007,** 40, 7132.
81.   Jian Zhu; Xiulin Zhu; Zhenping Cheng; Zhang, Z. *Macromol. Symp.* **2008,** 261, 46.
82.   Hua.F.J; Yang.Y.L. *Polymer* **2001,** 42, 1361.

83.   Suna.X; Hailiang Zhanga.H; Huanga.X; Wanga.X; Zhouc.Q. *Polymer* **2005,** 46, 5251.
84.   Guang-Qiang Chen; Zhi-Qiang Wu; Jian-Ru Wu; Zi-Chen Li; Li, F.M. *Macromolecules* **2000,** 33, 232.
85.   Cianga.L; Yagci.Y; Fernandes.E.G; Galli.G. *Designed Monomers and Polymers* **2003,** 6, 145.
86.   Moad.G; Rizzardo.E; Thang.S.H. *Polymer* **2008,** 49, 1079.
87.   Rizzardo. E; Mayadunne. R; Moad. G; Thang.S.H. *Macromol Symp* **2001,** 174, 209.
88.   (Bill) Y. K. Chong; Tam P. T. Le; Graeme Moad; Ezio Rizzardo; Thang, S. H. *Macromolecules* **1999,** 32, 2071.
89.   Tsujii.Y; Ejaz.M; Sato.K; Goto.A; Fukuda.T. *Macromolecules* **2001,** 34, 8872.
90.   Riess, G. *Prog. Polym. Sci.* **2003,** 28, 1107.
91.   Discher.D.E; Eisenberg.A. *Science* **2002,** 297, 967.
92.   Mecke.A; Dittrich.C; Meier.W. *Soft Matter.* **2006,** 2, 751.
93.   http://en.wikipedia.org/wiki/Micelle.
94.   Angew.H.I; Ed. *Chem. Int.Ed* **2003,** 42, 1692.
95.   Ruhe.J. *Nachr.Chem.Technol.Lab* **1994,** 42, 1237.
96.   Werne, T. V.; Patten, T. E. *Am.Chem.Soc* **2001,** 123, 7497.
97.   Pyun, J.; Jia, S.; Kowalewski, T.; Patterson, G. D.; Matyjaszewski, K. *Macromolecules* **2003,** 36, 5094.
98.   Ejas M; Yamamoto S; Ohno K; Tsujii Y; Fukuda T. *Macromolecules* **1998,** 31, 5934.
99.   Baum, M.; Brittain, W. J. *Macromolecules* **2002,** 35, 610.
100.   Nguyen.D; Vana. P. *Polym. Adv. Technol.* **2006,** 17, 625.
101.   Hong. C.Y; You.Y.Z; Pan.C, Y. *Journal of Polymer Science: Part A: Polymer Chemistry* **2006,** 44, 2419.
102.   Cui, J.; Wang, W.; You, Y.; Liu, C.; Wang, P. *Polymer* **2004,** 45, 8717.
103.   Chen.Y; Sun.W; Deng.Q; Chen.L. *Journal of Polymer Science: Part A: Polymer Chemistry* **2006,** 44, 3071.
104.   Barner. L; Perera.S; Sandanayake.S; Davis.T.P. *Journal of Polymer Science: Part A: Polymer Chemistry* **2006,** 44, 857.
105.   Mintmire, J. W.; White, C. T. *Carbon* **1995,** 33, 893.
106.   Nguyen. T.L.Uyen; Farrugia. B; Davis.T.P; Barner-Kowollik. C; Stenzel. M.H. *Journal of Polymer Science: Part A: Polymer Chemistry* **2007,** 45, 3256.
107.   Yang.Y; Liu.L; Zhang.J; Li.C; Zhao.H. *Langmuir* **2007,** 23, 2867.
108.   http://www.viscotek.com/theory.htm.
109.   http://www.nuance.northwestern.edu/keckii/ftir1.asp.
110.   Yamahara, K.; Sholklapper, T. Z.; Jacobson, C. P.; Visco, S. J.; De Jonghe, L. C. *Solid State Ionics* **2005,** 176, 1359.
111.   Jordan, J.; Jacob, K. I.; Tannenbaum, R.; Sharaf, M. A.; Jasiuk, I. *Mater Sci Eng, A* **2005,** A393, 1.
112.   Cai.R; Kubota.Y; ShunT; Sakai.H; Hashimoto.K; Fujishima.A. *Cancer Res.* **1992,** 52, 2346.
113.   Cai.R; Hashimoto.K; Fujishima.A. *J. Electron. Chem.* **1992,** 326, 345.
114.   Hirakawa.K; Hirano.T. *Chem. Lett.* **2006,** 35, 832.

115.   Chen.C; Lv.G; Pan.C; Song.M; Wu.C; Guo.D; Wang.X; Chen.B; Gu.Z. *Biomed. Mater.* **2007,** 2, 1.

116.   Kanehira.K ; Banzai.T; Ogino.C; Shimizu.N; Kubota.Y; Sonezaki.S. *Colloids and Surfaces B: Biointerfaces* **2008,** 64, 10.

117.   R. Ackroyd. *Photochem. Photobiol* **2001,** 74, 656.

118.   Chibowski.S; Paszliewicz.M. *Adv. Sci. Technol.* **2001,** 19, 397.

119.   Deiss.J.L; Anizan.P; Hadigui.S.E; Wecker.C. *Colloids Surf.A* **1996,** 106, 59.

120.   Liufu.S; Xiao.H; Li.Y. *J. Colloid Interface Sci.* **2005,** 281, 155.

121.   Bohmer.M.R; Sofi.Y.E.A; Foissy.A. *J. Colloid Interface Sci.* **1994,** 164, 126.

122.   Tatsuma.T; Takada.K; Miyazaki.T. *Adv. Mater.* **2007,** 19, 1249.

123.   Nakamoto, K., *Infrared and Raman Spectra of Inorganic and Coordination Compounds*. A Wiley-Interscience Publication: New York, 1997; Vol. Part B, p 59.

124.   Deacon, G. B.; Phillips, R. J. *Coord Chem Rev* **1980,** 33, 227.

125.   Hernandez-Guerrero, M.; Davis, T. P.; Barner-Kowollik, C.; Stenzel, M. H. *Eur Polym J* **2005,** 41, 2264.

126.   Ferguson, C. J.; Hughes, R. J.; Pham, B. T. T.; Hawkett, B. S.; Gilbert, R. G.; Serelis, A. K.; Such, C. H. *Macromolecules* **2002,** 35, 9243.

127.   Ferguson, C. J.; Hughes, R. J.; Nguyen, D.; Pham, B. T. T.; Gilbert, R. G.; Serelis, A. K.; Such, C. H.; Hawkett, B. S. *Macromolecules* **2005,** 38, 2191.

128.   Miquelard-Garnier, G.; Demoures, S.; Creton, C.; Hourdet, D. *Macromolecules* **2006,** 39, 8128.

129.   Ladaviere C; Dorr N; Claverie JP. *Macromolecules* **2001,** 34, 5370.

130.   Sui, R.; Rizkalla, A. S.; Charpentier, P. A. *J. Phys. Chem. B* **2006,** 110, 16212.

131.   Heijman, S. G. J.; Stein, H. N. *Langmuir* **1995,** 11, 422.

132.   Chen.J; Chen.N; Huang.J; Wang.J; Huang.M. *Inorganic Chemistry Communications* **2006,** 9, 313.

133.   Loiseau, J.; Doerr, N.; Suau, J. M.; Egraz, J. B.; Llauro, M. F.; Ladaviere, C.; Claverie, J. *Macromolecules* **2003,** 36, 3066.

134.   Li C; Benicewicz B C. *Macromolecules* **2005,** 38, 5929.

135.   Gang.G; Jianjun.C; Xiaoping.D. *Modern Chemical Industry* **2004,** 24, 38.

136.   Khaled, S. M.; Sui, R.; Charpentier, P. A.; Rizkalla, A. S. *Langmuir* **2007,** 23, 3988.

137.   Ling.Z; Zhongshi.L; Wenjun.F; Tianyou.P. *Wuhan University Journal of Natural Sciences* **2006,** 11, 415.

138.   Pelet.J.M; Putnam.D. *Macromolecules* **2009,** 42, 1494.

139.   Li. D; Luo. Y; Li. B.G; Zhu. S. *Journal of Polymer Science: Part A: Polymer Chemistry* **2008,** 46, 970.

140.   Arita.T; Buback.M; Vana.P. *Macromolecules* **2005,** 38, 7935.

141.   Kwak.Y; Goto.A; Tsujii Y; Murata.Y; Komatsu.K; T, F. *Macromolecules* **2002,** 35, 3026.

142.   Xuedong Wu; Dapu Wang; Shengrong Yangy. *Journal of Colloid and Interface Science* **2000,** 222, 37.

143.   Wagner. C.D; Muilenberg.G.E, *Handbook of X-ray photoelectron spectroscopy* 1979.

144.   Hammond.J.S; Holubka.J.W; Devries.J.E; Duckie.R.A. *Corros Sci* **1981,** 21, 239.

145.   Sawada.H, *Thermodynamics of polymerization*. M.Dekker: New York, 1976.

146.   Charpentier.P.A; DeSimone.J.M; Roberts.G.W. *Chemical Engineering Science* **2000,** 55, 5341.

147.   Kendall, J. L.; Canelas, D. A.; Young, J. L.; DeSimone, J. M. *Chem.Rev.* **1999,** 99, 543.

148.   McHugh, M. A.; Krukonis, V. J., *Supercritical Fluid Extraction : Principles and Practice*. Second ed.; Butterworth-Heinemann: Boston, 1994.

149.   DeSimone, J. M.; Tumas, W., *Green Chemistry Using Liquid and Supercritical Carbon Dioxide*. Oxford University Press, Inc.: New York, N.Y., 2003; p 259.

150.   Charpentier, P. A.; Kennedy, K.; DeSimone, J. M.; Roberts, G. W. *Macromolecules* **1999,** 32, 5973.

151.   McHale.R; Aldabbagh.F; ZetterlundP.B; Okubo.M. *Macromol. Chem. Phys.* **2007,** 208, 1813.

152.   Xia.J; Johnson.T; Gaynor.S.G; Matyjaszewski.K; DeSimone.J.M. *Macromolecules* **1999,** 32, 4802.

153.   Gregory.A.M; Thurecht.K.J; Howdle.S.M. *Macromolecules* **2008,** 41, 1215.

154.   Lucky.R.A; Charpentier.P.A. *Advanced Materials* **2008,** 20, 1755.

155.   Charpentier, P. A.; Xu, W. Z.; Li, X. *Green Chemistry* **2007,** 9, 768.

156.   Britz. D.A; Khlobystov.A.N; Wang.J; O'Neil.A.S; Poliakoff.M; Ardavan.A; Briggs.A.D. *Chem. Commun* **2004**, 176.

157.   Zemanian.T.S; Fryxell.G.E; Liu.J; Mattigod.S; Franz.J.A; Z. Nie.Z. *Langmuir* **2001,** 17, 8172.

158.   Wanjale.S. D; Jog.J. P. *Journal of Polymer Science Part B: Polymer Physics* **2003,** 41, 1014.

159.   Gregory.A.M; Thurecht.K.J; Howdle.S.M. *Macromolecules* **2008,** 41, 1215.

160.   Chen.X; Randall.D.P; Perruchot.C; Watts.J.F; Patten.T.E; Werne.T; Armes.S.P. *Journal of Colloid and Interface Science* **2003,** 257, 56.

161.   Kemmere.M.F; Meyer.T, *Supercritical Carbon Dioxide in Polymer Reaction Engineering*. WILLEY-VCH: Weinheim, Germany, 2005.

162.   Asano, T.; LeNoble, W. J. *J. Chem. Rev.* **1978,** 78, 407.

163.   Guan, Z.; Combes, J. R.; Menceloglu, Y. Z.; DeSimone, J. M. *Macromolecules* **1993,** 26, 2663.

164.   Arita.T; Beuermann.S; Buback.M; Vana.P. *e-Polymers* **2004,** no. 003.

165.   Arita.T; Buback.M; Janssen.O; Vana.P. *Macromol.Rapid Commun.* **2004,** 25, 1376.

166.   Strube.O.I; Schmidt-Naake.G. *Macromol. Symp.* **2009,** 275, 13.

167.   Brauneckera.W.A; Matyjaszewski.K. *Progress in Polymer Science* **2007,** 32, 93.

168.   Fan.D; He.J; Xu.J; Tang.W; Liu.Y; Yang.Y. *Journal of Polymer Science: Part A: Polymer Chemistry,* **2006,** 44, 2260.

169.   R. Erhardt; M. Zhang; A. Bo¨ ker; H. Zettl; C. Abetz; P. Frederik; G. Krausch; V. Abetz; A. H. E. Mu¨ ller. *J. Am.Chem. Soc.* **2003,** 125, 3260.

170.   Hao Kong, C. G., Deyue Yan. *Macromolecules* **2004,** 37, 4022.

171.   Yuan-Zhi Qu; Yi-Nao Su; Jin-Sheng Sun; Kui-Cai Wang. *Journal of Applied Polymer Science,* **2008,** 110, 387.

172.   Gutierrez.J; Tercjak.A; Garcia.I; Peponi.L; Mondragon.I. *Nanotechnology* **2008,** 19, 155607.

173.   van de Loosdrecht, J.; van der Kraan, A. M.; van Dillen, A. J.; Geus, J. W. *J.Catal.* **1997,** 170, 217.
174.   Jothimurugesan.K; Gangwal.S.K. *Ind. Eng. Chem. Res.* **1998,** 37, 1181.
175.   Jankovic´.I.A; Saponjic´.Z.V; Comor.M.I; Nedeljkovic.J.M. *J. Phys. Chem. C* **2009,** 113, 12645.
176.   Chen.D; Fu.Z; Shi.Y. *Polymer Bulletin* **2008,** 60, 259.
177.   Peng.D; Zhang.X; Feng.C; Lu.G; Zhang.S; Huang.X. *Polymer* **2007,** 48, 5250.
178.   Lee.C.F; Yang.C.C; Wang.L.Y; Chiu.W.Y. *Polymer* **2005,** 46, 5514.
179.   Ferna´ndez-Garcı´a.M; Martı´nez-Arias.A; Hanson.J.C; Rodriguez.J.A. *Chem. Rev.* **2004,** 104, 4063.
180.   Enkviste.C; Vardsson.D; Lunell.S. *International Journal of Quantum Chemistry* **1998,** 63, 189.
181.   Luo.P.F; Kuwana.T. *Anal. Chem.* **1996,** 68, 3330.
182.   Wu.X; Wang.D; Yangy.S. *Journal of Colloid and Interface Science* **2000,** 222, 37.
183.   Chigane.M; Ishikawa.M. *J. Chem. Soc., Faraday T rans.* **1998,** 94, 3665.
184.   Zhang.W.J; He.Y.Q; Qi.Q. *Materials Chemistry and Physics* **2005,** 93, 508.
185.   Sookman.C; Kongkachuiychay.P. *Journal of Materials Online* **2006,** 2, 1.
186.   Parada.C; Mora´n.E. *Chem. Mater.* **2006,** 18, 2719.
187.   Thammanoon Sreethawong; Yoshikazu Suzuki; Susumu Yoshikawa. *International Journal of Hydrogen Energy* **2005,** 30, 1053.
188.   Sreethawong.T; Suzuki.Y; Yoshikawa.S. *Catalysis Communications* **2005**, 119, 124.
189.   Ho, S. W.; Chu, C. Y.; Chen, S. G. *J. Catal.* **1998,** 178, 34.
190.   Loc.L.C; Huan.N.M; Dung.N.K; Phuc.N.H.H; Thoang.H.S. *Advances in Natural Sciences* **2006,** 7, 91.
191.   Chen, X.; Mao, S. S. *Chem. Rev.* **2007,** 107, 2891.
192.   Linsebigler.A.L; Lu.G; Yates.J.T. *Chem. Rev.* **1995,** 95, 735.
193.   Hochbaum, A. I.; Yang, P. *Chem. Rev.* **2009**, 14, 721.
194.   Kolmakov.A; Moskovits.M. *Annu. Rev. Mater. Res.* **2004,** 34, 151.
195.   Kim, T. H.; Kang, J. P.; Kwon, Y. K. *Polymer Preprints* **2005,** 46, 566.
196.   Iwasaki, M.; Davis, S. A.; Mann, S. *J Sol-Gel Sci Techn* **2004,** 32, 99.
197.   Wakayama, H.; Itahara, H.; Tatsuda, N.; Inagaki, S.; Fukushima, Y. *Chem Mater* **2001,** 13, 2392.
198.   Zeng, J.; Zhang, M.; Song, Z.; Wang, L.; Li, J.; Li, K.; Lin, C. *Applied Surface Science* **1999,** 148, 137.
199.   Wei, M.; Zhou, H.; Konishi, Y.; Ichihara, M.; Sugiha, H.; Arakawa, H. *Inorg. Chem.* **2006,** 45, 5684.
200.   Kresge, C. T.; Leonowicz, M. E.; Roth, W. J.; Vartuli, J. C.; Beck, J. S. *Nature* **1992,** 359, 710.
201.   Matyjaszewski.K; Davis.T. P, *Handbook of Radical Polymerization*. Wiley-Interscience: Hoboken, 2002.
202.   Yang.P; Zhao.D; Margolese.D.I; Chmelka.B.F; Stucky.G.D. *Chem.Mater.* **2008,** 11, 2813.
203.   Förster.S. *Top Curr Chem* **2003,** 226, 1.

204.   Boisse.S; Rieger.J; Di-Cicco.A; Albouy.P.A; Bui.C; Li.M.H; Charleux.B. *Macromolecules* **2009,** 42, 8688.
205.   Park.C; Rhue.M; Lim.J; Kim.C. *Macromolecular Research* **2007,** 15, 39.
206.   Ozin. G. A; Arsenault. A.C, Nanochemistry. In The Royal Society of Chemistry, Thomas Graham House: 2005.
207.   Boyle, T. J.; Tyner, R. P.; Alam, T. M.; Scott, B. L.; Ziller, J. W.; Potter, B. G., Jr. *J Am Chem Soc* **1999,** 121, 12104.
208.   Rammal, A.; Brisach, F.; Henry, M. *Comptes Rendus Chimie* **2002,** 5, 59.
209.   Steinhuebel, D. P.; Fuhrmann, P.; Lippard, S. J. *Inorganica Chimica Acta* **1998,** 270, 527.
210.   Loy, D. A.; Russick, E. M.; Yamanaka, S. A.; Baugher, B. M. *Chem. Mater.* **1997,** 9, 2264.
211.   Moner-Girona, M.; Roig, A.; Molins, E. *J Sol-Gel Sci Techn* **2003,** 26, 645.
212.   Sui.R; Rizkalla.A.S; Charpentier.P.A. *Cryst. Growth Des.* **2008,** 8, 3024.
213.   Chowdhury.M.B.I; Sui.R; Lucky.R.A; Charpentier.P.A. *Langmuir* **2009,** In print.
214.   Smarsly.B; Antonientti.M. *Eur. J. Inorg. Chem.* **2006,** 2006, 1111.
215.   Yun.H; Miyazawa.K; Zhou.H; Honma.I; Kuwabara.M. *Adv.Mater.* **2001,** 13, 1377.
216.   Camblor. M.A; Corma.A; Valencia.S. *Microporous Mesoporous Mater.* **1998,** 25, 89.
217.   Wu.P.G; Ma.C.H; Shang.J.K. *Appl Phys A* **2005,** 81, 1411.
218.   Gregg, S. J.; Sing, K. S. W., *Adsorption, surface area, and porosity*. 2nd ed.; Academic Press: London ; Toronto, 1982; p xi, 303 p.
219.   Haung.D; Luo.G; Yang.L; Wang.Y. *China particulogy* **2005,** 3, 176.
220.   Luo, H.; Wang, C.; Yan, Y. *Chem Mater* **2003,** 15, 3841.
221.   Ladavie` re.C; Dorr.N; Claverie.J.P. *Macromolecules* **2001,** 34, 5370.

APPENDICES

Appendix 1. Synthesis of 2-{[(butylsulfanyl)carbonothioyl]sulfanyl}propanoic acid (1)

Acetone (700 mL) and tetrapropylammonium bromide (5.58 g, 21.0 mmol) were added with stirring to a solution of sodium hydroxide (10.5 g, 0.263 mol) in water (36 mL), followed by 1-butanethiol (23.7 g, 0.263 mol). After 20 min, carbon disulfide (17 mL, 21.7 g, 0.285 mol) was added and stirring was continued for 15 min, after which 2-bromopropanoic acid (40.14 g, 0.263 mol) was added. The reaction was stirred overnight, then acidified to pH<1 with 2 M hydrochloric acid (100 mL). The acetone was removed under reduced pressure and the remaining mixture was extracted with ether (400 mL). The extract was washed with water (2x100 mL), saturated sodium chloride solution (200 mL), dried (sodium sulfate), and evaporated. The oily residue was crystallized by the addition of ice (500 g), the crystals were collected by filtration and washed with water (5x100 mL) and then dried in a vacuum oven at room temperature. The resulting impure product was redissolved in ether (400 mL) and extracted with saturated sodium bicarbonate (5x150 mL). The combined aqueous extracts were acidified to pH<1 with concentrated hydrochloric acid and extracted with ether (400 mL). The organic extract was washed with saturated sodium chloride (200 mL), dried (sodium sulfate), and evaporated under reduced pressure. The residue was crystallized by the addition of ice (500 g) and the solid was collected and washed with water (5x150 mL), then dried in a vacuum oven to give the title compound (15, $R^3 = C_4H_9$) as a yellow solid (39.0 g, 62%).
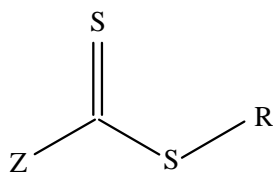
$R = CH(CH_3)CO_2H$

$Z = C_4H_9S$

189

Appendix 2. Synthesis of Diethyl 2-[(Ethoxythiocarbonyl)thio]-2-methyl malonate) (2)[221]

8.82 g of potassium O-ethyl dithiocarbonate, 8.82 g of diethyl-2 bromo-2-methyl malonate, 0.5 g of Aliquat 336, and 55 mL of water were combined and the yellow mixture was stirred vigorously at 15 °C until yellow oil was formed on the bottom and the aqueous solution became colorless. Then 2.24 g of potassium O-ethyl dithiocarbonate were added and stirring was continued for 20 minutes. Ether (2x60 ml) was added and the combined organic extracts were washed with water (3x10 ml), dried over $MgSO_4$, and filtered over a small layer of silica gel (ϕ5 cm x 1.5 cm), using ether as eluent. The solvent was removed to give yellow oil.

$$\underset{Z}{\overset{\displaystyle \overset{S}{\|}}{\diagdown}}\underset{S}{\diagup}\diagdown_{R}$$
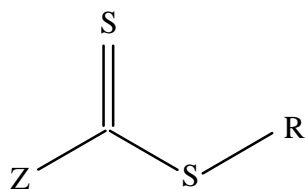
Z = OEt

R = C(CH$_3$)(CO$_2$Et)$_2$

Appendix 3. 4-cyano-4-(dodecylsulfanylthiocarbonyl) sulfanyl pentanoic acid (3)[86]

N-Dodecylthiol (15.4 g, 76 mmol) was added over 10 min to a stirred suspension of sodium hydride (60% in oil) (3.15 g, 79 mmol) in diethyl ether (150 mL) at a temperature between 5 and 10 $^{\circ}$C. A vigorous evolution of hydrogen was observed and the greyish sodium hydride was transformed to thick white slurry of sodium thiododecylate. The reaction mixture was cooled to 0 $^{\circ}$C and carbon disulfide (6.0 g, 79 mmol) added to pr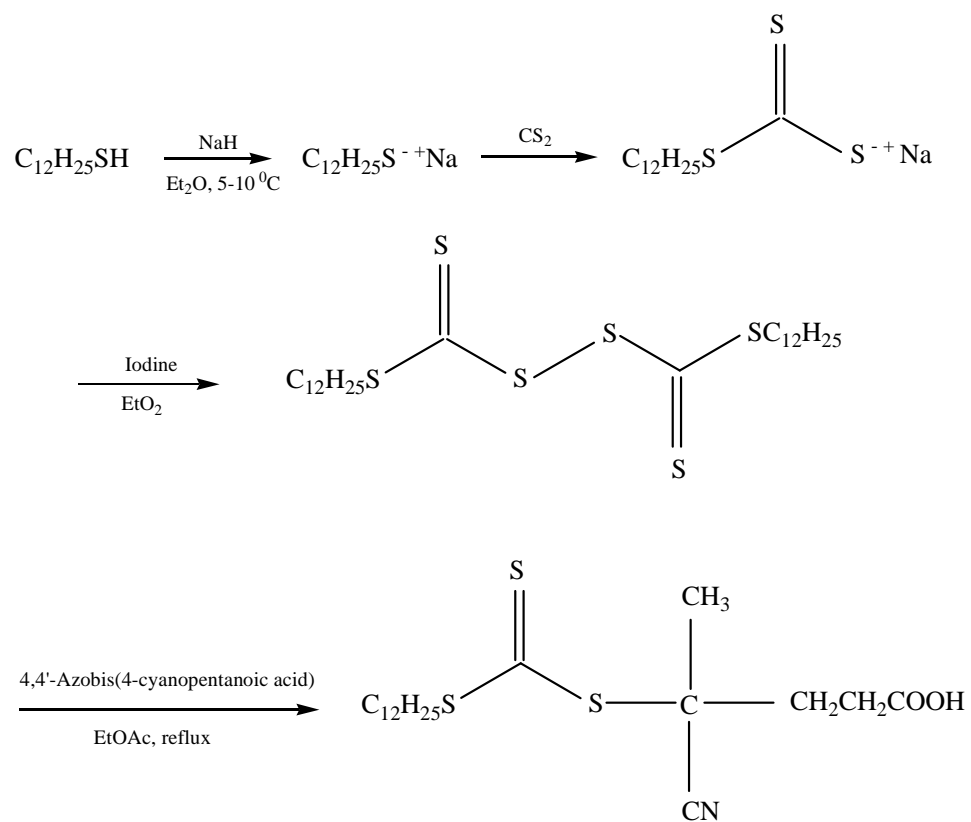ovide a thick yellow precipitate of sodium S-dodecyl trithiocarbonate which was collected by filtration and used in the next step without purification.

A suspension of sodium S-dodecyl trithiocarbonate (14.6 g, 0.049 mol) in diethyl ether (100 mL) was treated by portion-wise addition of solid iodine (6.3 g, 0.025 mol). The reaction mixture was then stirred at room temperature for 1 h when the white sodium iodide which settled was removed by filtration. The yellow–brown filtrate was washed with an aqueous solution of sodium thiosulfate to remove excess iodine and water and dried over sodium sulfate and evaporated to leave a residue of bis-(dodecylsulfanylthiocarbonyl) disulfide (13.6 g, quantitative), mp 33–35 $^{\circ}$C.

1H NMR (CDCl$_3$): d 0.89, t, 6H; 1.30, br s, 36H; 1.71, m, 4H; 3.29, t, 4H.

A solution of 4,4$^{'}$-azobis(4-cyanopentanoic acid) (2.10 g, 0.0075 mol) and the above bis-(dodecylsulfanylthiocarbonyl) disulfide (2.77 g, 0.005 mol) in ethyl acetate (50 mL) was heated at reflux for 18 h. After removal of the volatiles in vacuo, the crude product was extracted with water (5x100 mL) to afford 4-cyano-4-(dodecylsulfanylthiocarbonyl) sulfanyl pentanoic acid as a pale yellow solid (3.65 g, 87% yield), mp 58–59 $^{\circ}$C, after recrystallization from hexane.

$$C_{12}H_{25}SH \xrightarrow[\text{Et}_2\text{O, 5-10}\,^0\text{C}]{\text{NaH}} C_{12}H_{25}S^{-\,+}Na \xrightarrow{\text{CS}_2} C_{12}H_{25}S\text{-C}(=S)\text{-S}^{-\,+}Na$$

$$\xrightarrow[\text{EtO}_2]{\text{Iodine}}$$

4,4'-Azobis(4-cyanopentanoic acid), EtOAc, reflux

1H NMR (CDCl$_3$): d 0.89 (t, 3H, CH$_3$); 1.28 (br s, 18H); 1.72 (m, 2H); 1.89 (s, 3H, CH$_3$); 2.40–2.80 (m, 4H, CH$_2$CH$_2$); 3.38 (t, 2H, CH$_2$S).
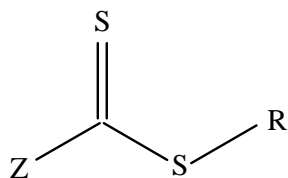
$$Z = SCH_3(CH_2)_{11}$$

$$R = CH_3CCNCH_2CH_2CO_2H$$

192

Appendix 4. Calculation of the amount of RAFT agent anchored to nanoparticles

Basis: 100 g of sample (TiO_2 + RAFT gent)

Part A:

Based of TGA results (5.4%), we have,

Mass of TiO_2: 94.6 g

Mass of RAFT agent **3**: 5.4 g

Molecular weight of RAFT agent **3** is 403 g/gmol, thus:

Mole of RAFT agent/100 g of sample = 5.4 / 403 = 0.0134 mol/100 g sample

or

134 μ mol/g of sample

Part B:

Based on the BET results, we have,

Average particle size of TiO_2 nanoparticles (D) = 23.2 nm

Assuming spherical shape for the particle results in:

The volume of one nanoparticle: $V = 4/3 \; \pi r^3 = 6.54 \times 10^{-18} \; cm^3$

The surface area of one nanoparticle: $S = 4 \pi r^2 = 1690.9 \; nm^2$

The density of RAFT agent/n-TiO_2 can be assumed to be comparable with the density of

n-TiO_2. Thus

$\rho = 4.26 \; g/cm^3$

Mass of one nanoparticle of TiO_2: $\rho \times V = 2.78 \times 10^{-17} \; g$

Number of TiO_2 in the sample: $94.6 / (2.78 \times 10^{-17}) = 3.4 \times 10^{18}$

Total area of the sample: $1690.9 \text{ nm}^2 \times (3.4 \times 10^{18}) = 5.75 \times 10^{21}$

Avogadro number: $N_A = 6.022 \times 10^{23} \text{ mol}^{-1}$

Therefore, the amount of RAFT agent anchored to the nanoparticles is:

$[(134 \times 10^{-4}) \times (6.022 \times 10^{23})] / (5.75 \times 10^{21}) = 1.4 \text{ \# RAFT agent/ nm}^2$

The calculation is the same for the other graft density (TGA results, 4.1%).

Appendix 5. EDX spectrum of NiO/TiO$_2$ components using n-TiO$_2$/PAA and n-TiO$_2$/PMMA-b-PAA

Standard:
C   CaCO3   1-Jun-1999 12:00 AM
O   SiO2   1-Jun-1999 12:00 AM
Ti   Ti   1-Jun-1999 12:00 AM
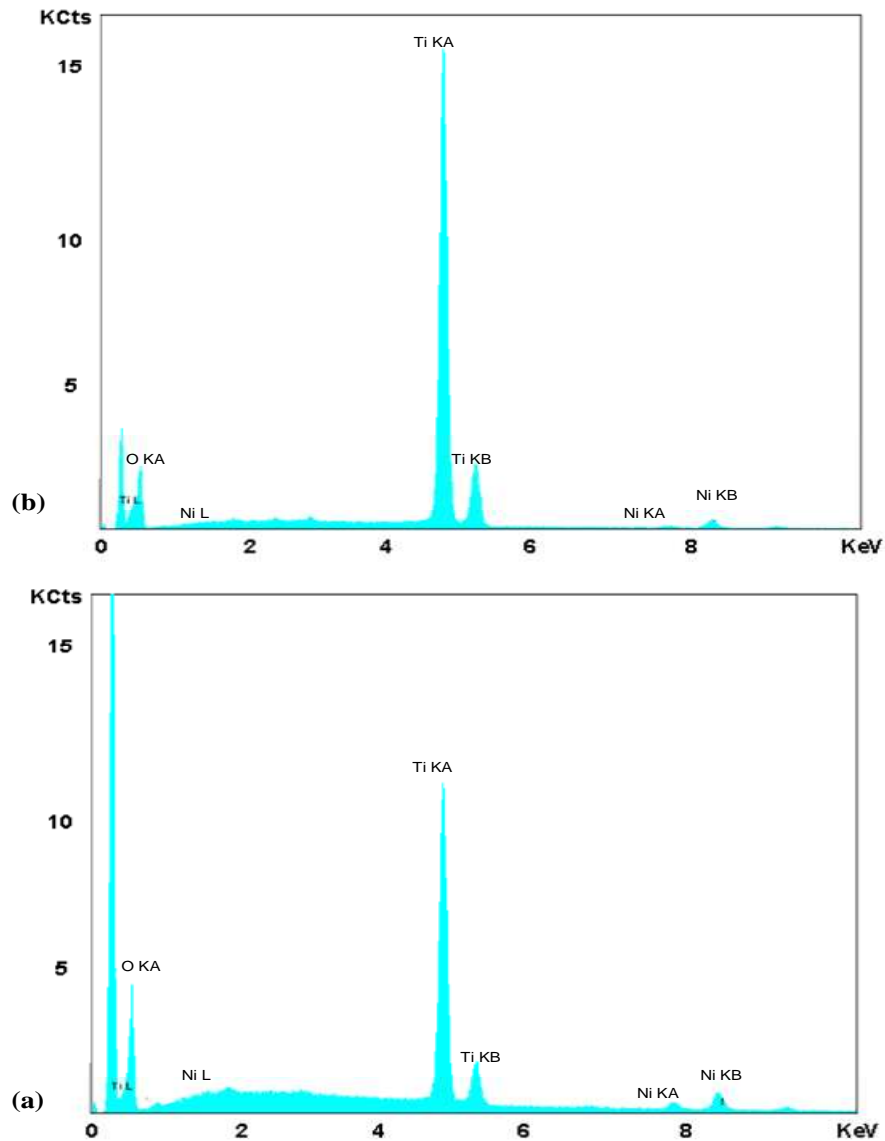Ni   Ni   1-Jun-1999 12:00 AM

Figure A. 11 EDX spectrum of NiO/TiO$_2$ components using (a) n-TiO$_2$/PAA and (b) n-TiO$_2$/PMMA-b-PAA as a template

Appendix 6. XPS spectrum of NiO/TiO₂ synthesized via template and conventional methods
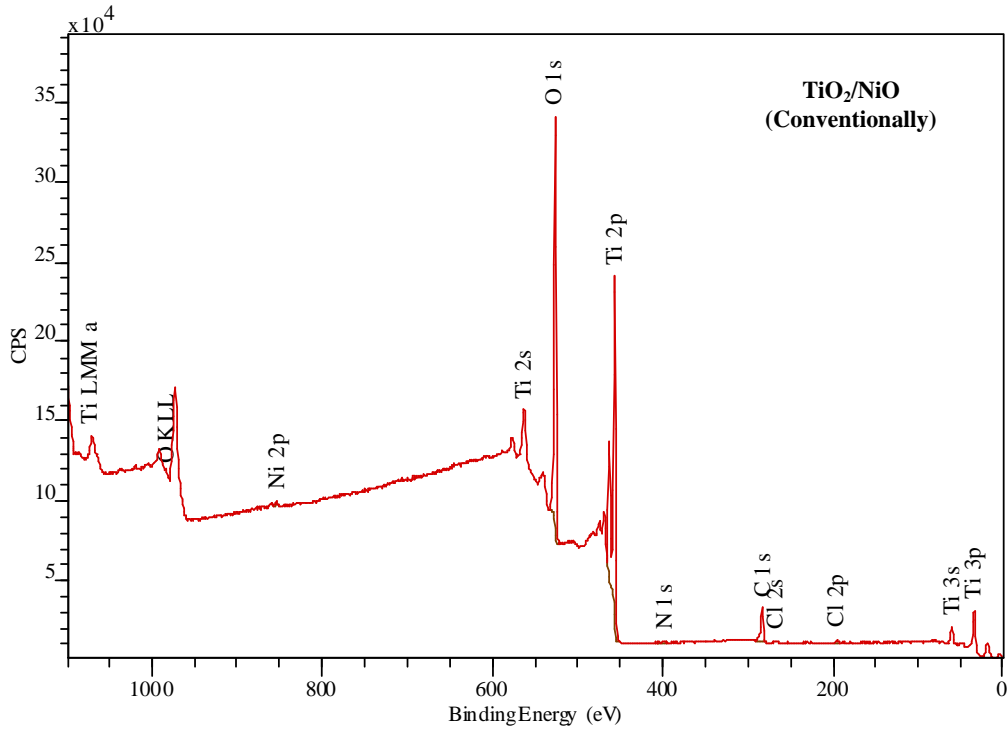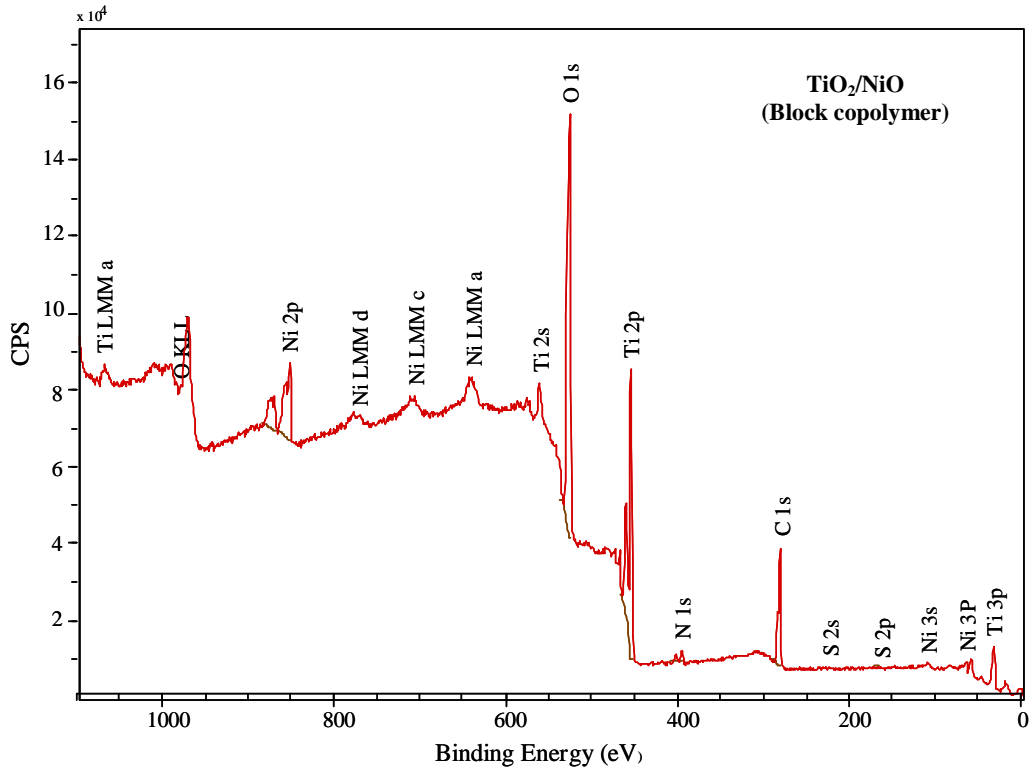
Appendix 7. Powder XRD Analysis Conditions

Experimental parameters for Bruker D8 Discover diffractometer

Type of radiation	CuKα1+Kα2 = 1.54184 Å
Power	40 kV x 40 mA
Type of scan	Coupled
Number of frames	3 (merged)
Beam Diameter	500 µm
2θ range	7°-107 °
Number of samples analyzed	6

Angle 2-Theta °	d value Angstrom	Intensity Count	Intensity %
25.35	3.51	75.70	84.10
27.50	3.24	90.00	100.00
36.14	2.48	49.00	54.40
37.84	2.38	19.00	21.10
39.19	2.30	5.64	6.30
41.24	2.19	10.50	11.70
44.07	2.05	5.81	6.50
48.05	1.89	21.40	23.80
54.32	1.69	58.10	64.50
55.05	1.67	17.80	19.70
56.67	1.62	17.00	18.90
62.77	1.48	20.80	23.10
64.11	1.45	8.91	9.90
68.98	1.36	23.20	25.80

Appendix 8. License Agreement with Elsevier Limited

ELS	0032-3861			false
printablelicense		quickprice	3337	/App/Includes/Pri
/App/PrintableLic	/App/Includes/No	1240328600561	iLxp5SCs1ZOCK	unknown
unknown				

<div align="center">

ELSEVIER LICENSE
TERMS AND CONDITIONS

</div>

Apr 21, 2009

This is a License Agreement between Behnaz Hojjati ("You") and Elsevier ("Elsevier") provided by Copyright Clearance Center ("CCC"). The license consists of your order details, the terms and conditions provided by Elsevier, and the payment terms and conditions.

All payments must be made in full to CCC. For payment instructions, please see information listed at the bottom of this form.

Supplier	Elsevier Limited The Boulevard,Langford Lane Kidlington,Oxford,OX5 1GB,UK
Registered Company Number	1982084
Customer name	Behnaz Hojjati
License Number	2173701039859
License date	Apr 21, 2009
Licensed content publisher	Elsevier
Licensed content publication	Polymer
Licensed content title	Synthesis of TiO_2/PAA nanocomposite by RAFT polymerization
Licensed content author	Behnaz Hojjati, Ruohong Sui and Paul A. Charpentier
Licensed content date	21 September 2007
Volume number	48
Issue number	20
Pages	9
Type of Use	Thesis / Dissertation
Portion	Full article
Format	Electronic
You are an author of the Elsevier article	Yes
Are you translating?	No
Order Reference Number	

Expected publication date	Jul 2009
Elsevier VAT number	GB 494 6272 12
Permissions price	0.00 USD
Value added tax 0.0%	0.00 USD
Total	0.00 USD

Terms and Conditions

INTRODUCTION

1. The publisher for this copyrighted material is Elsevier. By clicking "accept" in connection with completing this licensing transaction, you agree that the following terms and conditions apply to this transaction (along with the Billing and Payment terms and conditions established by Copyright Clearance Center, Inc. ("CCC"), at the time that you opened your Rightslink account and that are available at any time at http://myaccount.copyright.com).

GENERAL TERMS

2. Elsevier hereby grants you permission to reproduce the aforementioned material subject to the terms and conditions indicated.

3. Acknowledgement: If any part of the material to be used (for example, figures) has appeared in our publication with credit or acknowledgement to another source, permission must also be sought from that source. If such permission is not obtained then that material may not be included in your publication/copies. Suitable acknowledgement to the source must be made, either as a footnote or in a reference list at the end of your publication, as follows:

"Reprinted from Publication title, Vol /edition number, Author(s), Title of article / title of chapter, Pages No., Copyright (Year), with permission from Elsevier [OR APPLICABLE SOCIETY COPYRIGHT OWNER]." Also Lancet special credit - "Reprinted from The Lancet, Vol. number, Author(s), Title of article, Pages No., Copyright (Year), with permission from Elsevier."

4. Reproduction of this material is confined to the purpose and/or media for which permission is hereby given.

5. Altering/Modifying Material: Not Permitted. However figures and illustrations may be altered/adapted minimally to serve your work. Any other abbreviations, additions, deletions and/or any other alterations shall be made only with prior written authorization of Elsevier Ltd. (Please contact Elsevier at permissions@elsevier.com)

6. If the permission fee for the requested use of our material is waived in this instance,

please be advised that your future requests for Elsevier materials may attract a fee.

7. Reservation of Rights: Publisher reserves all rights not specifically granted in the combination of (i) the license details provided by you and accepted in the course of this licensing transaction, (ii) these terms and conditions and [73] CCC's Billing and Payment terms and conditions.

8. License Contingent Upon Payment: While you may exercise the rights licensed immediately upon issuance of the license at the end of the licensing process for the transaction, provided that you have disclosed complete and accurate details of your proposed use, no license is finally effective unless and until full payment is received from you (either by publisher or by CCC) as provided in CCC's Billing and Payment terms and conditions. If full payment is not received on a timely basis, then any license preliminarily granted shall be deemed automatically revoked and shall be void as if never granted. Further, in the event that you breach any of these terms and conditions or any of CCC's Billing and Payment terms and conditions, the license is automatically revoked and shall be void as if never granted. Use of materials as described in a revoked license, as well as any use of the materials beyond the scope of an unrevoked license, may constitute copyright infringement and publisher reserves the right to take any and all action to protect its copyright in the materials.

9. Warranties: Publisher makes no representations or warranties with respect to the licensed material.

10. Indemnity: You hereby indemnify and agree to hold harmless publisher and CCC, and their respective officers, directors, employees and agents, from and against any and all claims arising out of your use of the licensed material other than as specifically authorized pursuant to this license.

11. No Transfer of License: This license is personal to you and may not be sublicensed, assigned, or transferred by you to any other person without publisher's written permission.

12. No Amendment Except in Writing: This license may not be amended except in a writing signed by both parties (or, in the case of publisher, by CCC on publisher's behalf).

13. Objection to Contrary Terms: Publisher hereby objects to any terms contained in any purchase order, acknowledgment, check endorsement or other writing prepared by you, which terms are inconsistent with these terms and conditions or CCC's Billing and Payment terms and conditions. These terms and conditions, together with CCC's Billing and Payment terms and conditions (which are incorporated herein), comprise the entire agreement between you and publisher (and CCC) concerning this licensing transaction. In the event of any conflict between your obligations established by these terms and conditions and those established by CCC's Billing and Payment terms and conditions, these terms and conditions shall control.

14. Revocation: Elsevier or Copyright Clearance Center may deny the permissions

described in this License at their sole discretion, for any reason or no reason, with a full refund payable to you. Notice of such denial will be made using the contact information provided by you. Failure to receive such notice will not alter or invalidate the denial. In no event will Elsevier or Copyright Clearance Center be responsible or liable for any costs, expenses or damage incurred by you as a result of a denial of your permission request, other than a refund of the amount(s) paid by you to Elsevier and/or Copyright Clearance Center for denied permissions.

LIMITED LICENSE

The following terms and conditions apply to specific license types:

15. **Translation**: This permission is granted for non-exclusive world **English** rights only unless your license was granted for translation rights. If you licensed translation rights you may only translate this content into the languages you requested. A professional translator must perform all translations and reproduce the content word for word preserving the integrity of the article. If this license is to re-use 1 or 2 figures then permission is granted for non-exclusive world rights in all languages.

16. **Website**: The following terms and conditions apply to electronic reserve and author websites:
Electronic reserve: If licensed material is to be posted to website, the web site is to be password-protected and made available only to bona fide students registered on a relevant course if:
This license was made in connection with a course,
This permission is granted for 1 year only. You may obtain a license for future website posting,
All content posted to the web site must maintain the copyright information line on the bottom of each image,
A hyper-text must be included to the Homepage of the journal from which you are licensing at http://www.sciencedirect.com/science/journal/xxxxx or, for books, to the Elsevier homepage at http://www.elsevier.com,
Central Storage: This license does not include permission for a scanned version of the material to be stored in a central repository such as that provided by Heron/XanEdu.

17. **Author website** for journals with the following additional clauses:

All content posted to the web site must maintain the copyright information line on the bottom of each image, and
The permission granted is limited to the personal version of your paper. You are not allowed to download and post the published electronic version of your article (whether PDF or HTML, proof or final version), nor may you scan the printed edition to create an electronic version,
A hyper-text must be included to the Homepage of the journal from which you are licensing at http://www.sciencedirect.com/science/journal/xxxxx,
Central Storage: This license does not include permission for a scanned version of the

material to be stored in a central repository such as that provided by Heron/XanEdu.

18. **Author website** for books with the following additional clauses:
Authors are permitted to place a brief summary of their work online only.
A hyper-text must be included to the Elsevier homepage at http://www.elsevier.com.
All content posted to the web site must maintain the copyright information line on the bottom of each image
You are not allowed to download and post the published electronic version of your chapter, nor may you scan the printed edition to create an electronic version.
Central Storage: This license does not include permission for a scanned version of the material to be stored in a central repository such as that provided by Heron/XanEdu.

19. **Website** (regular and for author): A hyper-text must be included to the Homepage of the journal from which you are licensing at http://www.sciencedirect.com/science/journal/xxxxx or, for books, to the Elsevier homepage at http://www.elsevier.com.

20. **Thesis/Dissertation**: If your license is for use in a thesis/dissertation your thesis may be submitted to your institution in either print or electronic form. Should your thesis be published commercially, please reapply for permission. These requirements include permission for the Library and Archives of Canada to supply single copies, on demand, of the complete thesis and include permission for UMI to supply single copies, on demand, of the complete thesis. Should your thesis be published commercially, please reapply for permission.

21. **Other conditions:** None

v1.5

cancel, please contact us referencing this license number 2173701039859 and noting the reason for cancellation.

Questions? customercare@copyright.com or +1-877-622-5543 (toll free in the US) or +1-978-646-2777.

Curriculum Vitae

Name	Behnaz Hojjati

Post-secondary Education and Degrees:

Sharif University of Technology
Tehran, Iran
1984-1989

The University of Western Ontario
London, Ontario, Canada
2002-2007

Honors and Awards:

American Chemical Society
Green Chemistry Summer School Scholarship
2006

Ontario Centers of Excellence (OCE)
Professional Outreach Award
2008

Ontario Graduate Scholarship in Science and Technology
(OGSST)
2008-2009

Ross & Jean Clark Scholarship
2008-2009

As-approved candidate for Industrial R & D Fellowships
from Natural Science and Engineering research Council

Related Work Experience:

Process Engineer
Pars Tahrir Co., Kermanshah, Iran.
2000-2001

Laboratory supervisor and quality control engineer
Bakhtar Flour Production Co., Kermanshsh, Iran
1998-2000

Production and quality control manager
Nazboyeh Food Industries, Kermanshsh, Iran
1995-1998

Publications:

1. **Behnaz Hojjati**, Paul.A. Charpentier, (2008), "Synthesis and kinetics of RAFT-Mediated Graft Polymerization of Methyl methacrylate on a surface of n-TiO$_2$" Polymer Science Part A: Polymer Chemistry, 46, 3926-3937

2. **Behnaz Hojjati**, Ruohong Sui., Paul.A. Charpentier, (2007), "Functionalization of TiO$_2$ Nanocomposites by Reversible Addition Fragmentation Chain-Transfer Polymerization" Polymer, 48, 5850-5858

3. **Behnaz Hojjati**, Paul.A.Charpentier, (2008) "Synthesis of TiO$_2$/PMMA nanocomposites in Supercritical CO$_2$ via Reversible Addition Fragmentation Chain-Transfer polymerization" Polymer preprints, 48 (2), 349-350

4. **Behnaz Hojjati**, Paul.A.Charpentier, (2009) "Synthesis of NiO/TiO$_2$ using Amphiphilic Diblock Copolymer brushes by RAFT polymerization", Polymer preprint, Polymer preprint, 50 (2), 418.

5. **Behnaz Hojjati**, Paul A. Charpentier, (2008) "Synthesis of TiO$_2$-Polymer Nano-Composite in Supercritical CO$_2$ via RAFT Polymerization" Submitted to polymer Journal.

6. **Behnaz Hojjati**, Muhammad Choudhury, Jeffrey M. Gribbon, Paul A. Charpentier, (2009) "Synthesis of NiO/TiO$_2$ using Amphiphilic Diblock Copolymer brushes (PMMA-b-PAA) by RAFT Polymerization" Submitted to Langmuir Journal

7. .**Behnaz Hojjati**, Ruohong Sui, Paul A. Charpentier, "Synthesis of TiO$_2$ Nanotubes and Hollow Spheres Using PMMA-b-PAA Block Copolymer as Templates" Submitted to Chemistry of Materials Journal.

Conferences:

1. **Behnaz Hojjati**, Paul.A.Charpentier, (2008) "Synthesis of TiO$_2$/PMM nanocomposites in scCO$_2$ by Reversible Addition Fragmentation Chain-Transfer polymerization (RAFT)"Poster presentation, 236th ACS National Meeting, Philadelphia, PA, United States, August 17-21, 2008

2. **Behnaz Hojjati**, Paul.A.Charpentier, (2009) "Synthesis of NiO/TiO$_2$ using Amphiphilic Diblock Copolymer brushes (PMMA-b-PAA) by RAFT polymerization", Oral presentation in 238th ACS National Meeting, August 16-21, 2009; Washington DC USA.

3. **Behnaz Hojjati**, Paul.A.Charpentier," Synthesis of Mesoporous TiO$_2$ using Amphiphilic Diblock copolymer (PMMA-b-PAA) as a Self-Assembling

Agent by RAFT Polymerization", Oral presentation in the fall annual conference of American Institute of Chemical Engineers (AIChE), November 8-13, 2009; Nashville, USA.